Halogen Bonding Supramolecular Hosts for Fluorescence Sensing

Andrew J. Taylor

Magdalen College



A thesis submitted for the degree of Doctor of Philosophy.

Michaelmas Term 2024

Halogen Bonding Supramolecular Hosts for Fluorescence Sensing of Charged and Neutral Species

Andrew J. Taylor, Magdalen College

Abstract of Thesis Submitted for the Degree of Doctor of Philosophy

Michaelmas Term 2024

This thesis describes the development of various supramolecular host systems employing halogen bonding interactions for guest recognition, primarily, but not exclusively, for the purpose of fluorescence sensing in both organic and aqueous-containing media.

Chapter One introduces the field of host-guest chemistry within the wider domain of supramolecular chemistry, with a particular focus on the design of hosts for anions, ion-pairs and neutral species, and the non-covalent interactions which they employ. The various methods of optical sensing are discussed and the design principles of supramolecular optical sensors are considered through surveying prior examples.

Chapter Two describes the synthesis and characterisation of a family of six halogen (XB) and hydrogen bonding (HB), redox-active ferrocene anion sensors, which contain BODIPY fluorescent reporter groups. Fluorescence anion titration, fluorescence lifetime and electrochemical experiments elucidate the various anion binding-induced mechanisms of fluorescence modulation active in each of the sensors, including photo-induced electron transfer (PET). Finally, the exciting, novel ability of the redox-active fluorescent sensors to enable spectroelectrochemical anion sensing, which combines the advantages of electrochemical and fluorescence sensing, is demonstrated in a proof-of-concept study.

Chapter Three presents a series of three red-shifted, XB anion sensors employing the aza-BODIPY fluorophore, which operate in the biologically-relevant near-IR window. The relationship between the structure and sensing function of the first generation sensors is explored and a second generation mixed BODIPY/aza-BODIPY sensor is developed, which enables ratiometric halide anion sensing. The unprecedented ability of one of the sensors to display anion binding-modulated singlet oxygen generation is demonstrated, with possible utility in improving the selectivity of photodynamic therapy agents

Chapter Four demonstrates the general applicability of the XB BODIPY sensing motif developed in Chapter Two and uses it to construct two classes of sensor by appending the motif to contrasting guest recognition pillar[5]arene and diaza-crown ether macrocycles. The use of a hydrophobic pillar[5]arene guest binding domain enables the sensing of both dicarboxylates and a simulant of the chemical warfare agent, sulfur mustard, with impressive selectivity and affinity in aqueous-containing media, by formation of interpenetrated pseudo[2]rotaxane host-guest assemblies. By employing a diaza-crown ether as the central guest binding macrocycle, a sensor for both inorganic and organic ion-pairs is constructed, which demonstrates the ability to selectively sense K^+ over Na^+ and the HCl salt of dopamine over other closely related phenethylamine compounds.

Chapter Five summarises the conclusions of the thesis and highlights the main themes running through all three research chapters. Suggestions for future work are also discussed.

Chapter Six contains the experimental procedures used in the preparation of this thesis and presents the full characterisation of all novel compounds.

Acknowledgements

To start, I would like to extend my heartfelt gratitude to Professor Paul Beer for all that he has done for me, from the beginning of my Part II in the midst of the pandemic through to the end of my DPhil four years later. I am grateful for so much: that he took me on as a Part II, despite the fact that I only met him on the application deadline day; his interesting and exciting research ideas, as well as the space to pursue my own; his assistance in preparing manuscripts and reports, from which I have learned so much in the skill of technical communication; and most fundamentally his unwavering support over the past four years, no matter what I have asked of him. It is an honour to be the last full-time student of the Beer group and it is testament to Paul's excellence as a supervisor that I will be number 101 on such an illustrious list of past members.

A large part of Paul's success is the excellent group culture which he fostered and in which individuals brought the best out of each other. I'd like to thank some group members in particular: Dr Andrew Docker, for introducing me to the field of host-guest chemistry and for teaching me so much about the synthetic and practical skills it demands; Dr Robert Hein, for his excellent and exciting research ideas which we collaborated on; Dr Jamie Wilmore, for also being a great collaborator and a close friend, having worked together particularly closely in the past two years; and Dr Arya Arun, Dr Hui Min Tay and Dr Richard Tse for inspiring me so much with their amazing synthetic feats. I must also thank members of other groups with whom I have worked closely: Dr Sophie Patrick, for teaching me all I know about electrochemistry and for persisting with difficult experiments which took a long time to come to fruition; Professor Jason Davis for his incisive assistance in preparing the manuscript we published together; and Professor

Matthew Langton and all the members of his group who I have increasingly worked alongside in recent years.

Before starting my research in the Beer group, I was lucky enough to receive an excellent education in chemistry and science generally for which I will always be hugely grateful. I would particularly like to thank in chronological order: Mr Collins and Mr Seymour for letting me burn the ceiling with the exploding soap bubbles demonstration as a 9-year-old – a formative experience in my practical chemistry career; Ms. Carroll and Dr Worrall for continuing to encourage and support my increasing interest in chemistry throughout secondary school; Mr Dunbar, for doing the same and also acting as a great mentor both academically and otherwise throughout my teenage years; and Professors Stuart Mackenzie and Tim Donohoe and Drs Robert Jacobs, Ai Fletcher, Dean Sheppard and Jack Rowbotham for the exceptional teaching I received during my undergraduate studies at Magdalen.

Seven years in Oxford has had a huge impact on my life outside of my academic work as well. I would like to thank all the friends I have been lucky to meet along the way, particularly those made at Magdalen, Vinnies and from my time rowing with MCBC and OUBC. Truly, I think you are the greatest gift Oxford has given me and I look forward to staying friends for life.

Above all, I must thank my family and Luiza for their love, kindness, sacrifice and support that has let me get this far. I am more grateful to you all than I could ever put into words.

A.J.T, Oxford, MT 2024

Abbreviations

[2.2.2]-crypt	4,7,13,16,21,24-Hexaoxa-1,10-diazabicyclo[8.8.8]hexacosane
°	Degrees
° C	Degrees Celsius
1-D	One dimensional
2-D	Two dimensional
3-D	Three dimensional
A^-	Anion
ACN	Acetonitrile
App	Apparent
ATP	Adenosine triphosphate
a.u.	Arbitrary units
Aza-BODIPY	Aza-boron-dipyrromethene
$BAr^F{}_4^-$	Tetrakis(3,5-bis(trifluoromethyl)phenyl)borate
Bn	Benzyl
BODIPY	Boron-dipyrromethene (4,4-difluoro-4-bora-3a,4a-diaza-s-indacene)
Bu	Butyl
c.	*circa*
CEES	2-Chloroethyl ethyl sulfide
conc.	Concentrated
CuAAC	Copper(I)-catalysed azide-alkyne cycloaddition
CV	Cyclic voltammogram
CWA	Chemical warfare agent
d	Doublet

d	Deuterated
DCA	Dicarboxylic Acid
DCB	Dicarboxylate
DCE	1,2-Dichloroethane
DCM	Dichloromethane
dd	Doublet of doublets
DDT	Dichlorodiphenyltrichloroethane
DDQ	2,3-Dichloro-5,6-dicyano-1,4-benzoquinone
DIPEA	*N*,*N*-Diisopropylethylamine
DIPY	Dipyrromethene
DMAP	4-Dimethylaminopyridine
DMF	*N*,*N*-Dimethylformamide
DMSO	Dimethyl sulfoxide
DNA	Deoxyribonucleic acid
DPBF	Diphenylisobenzofuran
e^-	Electron
$E_{1/2}$	Half-wave potential
EDTA	Ethylenediaminetetraacetic acid
e.g.	*Exempli gratia*
Eq	Equivalents
ESI-MS	Electrospray ionisation mass spectrometry
Et	Ethyl
et al.	*Et alia*
EtOAc	Ethyl acetate

ex	Excitation
Fc	Ferrocene
Fc^+	Ferrocenium
FI	Fluorescence Intensity
FLP	Frustrated Lewis pair
FRET	Förster resonance energy transfer
g	Gram
G	Gibbs' free energy
GC	Glassy carbon
h	Planck constant
h	Hour
HB	Hydrogen bonding
HEPES	*N*-(2-hydroxyethyl)piperazine-*N*'-(2-ethanesulfonic acid)
Hex.	Hexane
HOMO	Highest occupied molecular orbital
HPTS	8-Hydroxypyrene-1,3,6-trisulfonic acid
HRMS	High resolution mass spectrometry
Hz	Hertz (s^{-1})
I	Emission intensity
I_{Ox}	Emission intensity of the oxidised form of a redox-active molecule
I_{Red}	Emission intensity of the reduced form of a redox-active molecule
i.e.	*Id est*
IR	Infra-red
J	Joule

J	Coupling constant
k	Kilo (10^3)
k	Rate constant
K	Kelvin
K_a	Association constant
K_{App}	Apparent association constant
K_{Ox}	Association constant with the oxidised form of a redox-active receptor
K_{Red}	Association constant with the reduced form of a redox-active receptor
LoD	Limit of detection
LUMO	Lowest unoccupied molecular orbital
M	Molar (mol dm^{-3}), molecular ion
m	*meta*
m	Multiplet, metre
Max	Maximum
MALDI-ToF	Matrix-assisted laser desorption/ionisation-time of flight
MCH	Methylcyclohexane
Me	Methyl
MeOH	Methanol
Mes	Mesityl (2,4,6-trimethylphenyl)
MLCT	Metal-to-ligand charge transfer
mol	Mole
Ms	Methanesulfonyl
MS	Mass spectrometry
m/z	Mass-to-charge ratio

n	Nano (10^{-9})
NDI	Naphthalene diimide
NHC	*N*-Heterocyclic carbene
NIR	Near infra-red
NIS	*N*-Iodosuccinimide
NMR	Nuclear Magnetic Resonance
o	*ortho*
OAc	Acetate
O/N	Overnight
p	Pico (10^{-12})
p	*para*
P[*n*]A	Pillar[*n*]arene
P5A	Pillar[5]arene
P6A	Pillar[6]arene
PDT	Photodynamic therapy
PET	Photo-induced electron transfer
PFA	Paraformaldehyde
pH	$-\log_{10}[H^+]$
Ph	Phenyl
pK_a	$-\log_{10}[K_a]$
ppm	Parts per million
Py	Pyridine
R	Chemical substituent, gas constant
R_f	Retention factor

ROS	Reactive oxygen species
RNA	Ribonucleic acid
rt	Room temperature
s	Singlet, second
SEM	Scanning electron microscopy
SWV	Square wave voltammogram
T	Tesla
t, *tert*	*Tertiary*
TBA	Tetra-*n*-butylammonium
TBTA	Tris[(1 benzyl-1*H*-1,2,3-triazol-4-yl)methyl]amine
^{t}Bu	*Tert*-butyl
TCSPC	Time-correlated single photon counting
TEM	Transmission electron microscopy
TFA	Trifluoroacetic acid
TFSI	Bis(trifluoromethane)sulfonimide
THF	Tetrahydrofuran
TLC	Thin layer chromatography
TMS	Trimethylsilyl
Tolyl	-$C_6H_4CH_3$
Ts, tosyl	*p*-Toluenesulfonyl
UV	Ultraviolet
v/v	Volume-to-volume ratio
Vis.	Visible
vs.	Versus

wrt.	With respect to
X	Halogen atom/halide
XB	Halogen bonding
XRD	X-ray diffraction
δ	Chemical shift
Δ	Change in [physical quantity]
ΔE_{Max}	Maximum voltammetric shift
λ	Wavelength
λ_{ex}	Excitation wavelength
λ_{max}	Wavelength of maximum intensity
µ	Micro (10^{-6})
µW	Microwave irradiation
$\Phi_{(\mathrm{F})}$	Fluorescence quantum yield

Previously Published Work

Anti-Hofmeister Anion Selectivity via a Mechanical Bond Effect in Neutral Halogen-Bonding [2] Rotaxanes.

A. Docker, Y. C. Tse, H. M. Tay, **A. J. Taylor**, Z. Zhang, P. D. Beer.

Angew. Chem. Int. Ed. **2022**, 61, e202214523.

Allosteric and Electrostatic Cooperativity in a Heteroditopic Halogen Bonding Receptor System

A. J. Taylor, A. Docker, P. D. Beer.

Chem. Asian J. **2023**, 18, e202201170.

Cyaphide-Azide 1, 3-Dipolar Cycloaddition Reactions: Scope and Applicability

E. S. Yang, A. Mapp, **A. J. Taylor**, P. D. Beer, J. M. Goicoechea.

Chem. Eur. J. **2023**, 29, e202301648.

Anion Sensing through Redox-Modulated Fluorescent Halogen Bonding and Hydrogen Bonding Hosts

A. J. Taylor, R. Hein, S. C. Patrick, J. J. Davis, P. D. Beer.

Angew. Chem. Int. Ed. **2024**, 63, e202315959.

Halogen bonding aza-BODIPYs for anion sensing and anion binding-modulated singlet oxygen generation

A. J. Taylor, P. D. Beer

Chem. Commun., **2024**, 60, 7983-7986.

A Halogen Bonding [2] Rotaxane Shuttle for Chloride-Selective Optical Sensing

H. M. Tay, A. Docker, **A. J. Taylor**, P. D. Beer.

Chem. Eur. J., **2024,** 30, e202400952.

Halogen bonding BODIPY-appended pillar [5] arene for the optical sensing of dicarboxylates and a chemical warfare agent simulant

A. J. Taylor, J. T. Wilmore, P. D. Beer.

Chem. Commun., **2024**, 60, 11916-11919.

Table of Contents

Abstract ..... **i**

Acknowledgements ..... **iii**

Abbreviations ..... **v**

Previously Published Work ..... **xii**

Table of Contents ..... **xiv**

1 Introduction **1**

1.1 Supramolecular Chemistry **2**

1.1.1 Supramolecular Chemistry and Host-Guest Chemistry 2

1.1.2 Principles of Host Design 4

1.1.2.1 Chelate Effect, Macrocyclic Effect and Pre-Organisation 5

1.1.2.2 Complementarity 9

1.1.2.3 Exploiting the Relative Solvation of Host and Guest 10

1.2 Supramolecular Recognition of Anions and Neutral Species **14**

1.2.1 The Importance of Anions and Neutral Species 14

1.2.1.1 The Importance of Anions 14

1.2.1.2 The Importance of Neutral Species 16

1.2.2 The Challenges of Designing Hosts for Anions and Neutral Species 17

1.2.2.1 The Challenges of Designing Hosts for Anions 17

1.2.2.2 The Challenges of Designing Hosts for Neutral Species 20

1.2.3 Supramolecular Interactions for the Recognition of Anions and Neutral Species 21

1.2.3.1 Electrostatic Interactions 22

1.2.3.2 Hydrogen Bonding 23

1.2.3.3 Halogen Bonding 25

1.2.3.4 π Interactions 28

1.2.4 Synthetic Hosts for Anions 31

1.2.4.1 Positively Charged Anion Hosts 31

1.2.4.2 Neutral Hydrogen Bonding Anion Hosts 34

1.2.4.3 Neutral Halogen Bonding Anion Hosts 37

1.2.5 Synthetic Hosts for Neutral Molecules 39

1.2.6 Synthetic Hosts for Ion-Pairs 41
1.3 Supramolecular Sensing of Anions and Neutral Species 45
1.3.1 Optical Sensing Approaches 45
1.3.2 Absorbance-Based Optical Sensors for Anions and Neutral Species 47
1.3.3 Emission-Based Optical Sensors for Anions and Neutral Species 52
1.4 Thesis Aims 59
1.6 References for Chapter One 61

2 Halogen Bonding BODIPY Hosts for Redox-Modulated Fluorescent Anion Sensing 67
2.1 Introduction 68
2.1.1 Mechanisms of Fluorescence Modulation in Anion Sensors 68
2.1.2 Photo-Induced Electron Transfer in Ferrocene-BODIPY Dyads 71
2.1.3 Electrochemical Anion Sensing with Ferrocene Derivatives 73
2.1.4 Spectroelectrochemical Anion Sensing 74
2.1.5 Chapter Aims 75
2.2 Synthesis and Optical Characterisation of Target Anion Sensors 77
2.2.1 Synthesis of Target Anion Sensors 77
2.2.2 Optical Characterisation of Target Anion Sensors 83
2.3 Anion Binding Studies 87
2.3.1 Fluorescence Titration Studies 87
2.3.2 Fluorescence Lifetime Studies 91
2.3.3 Electrochemical Studies 96
2.4 Spectroelectrochemical Anion Sensing 103
2.4.1 Influence of Ferrocene Oxidation State on BODIPY Fluorescence 103
2.4.2 Spectroelectrochemical Anion Sensing 110
2.5 Chapter Conclusions and Future Work 115
2.6 References for Chapter Two 119

3 Aza-BODIPY Hosts for Ratiometric Anion Sensing and Tuneable Singlet Oxygen Generation 121
3.1 Introduction 122
3.1.1 Red-Shifted Fluorophores and the Near Infra-Red Window 122

3.1.2 Oxygen Sensitisation and Photodynamic Therapy....127
3.1.3 Ratiometric Sensing....130
3.1.4 Chapter Aims....132
3.2 First Generation Aza-BODIPY Sensors.... 135
3.2.1 Synthesis and Characterisation....135
3.2.2 Anion Sensing Studies....141
3.2.3 Ion-Pair Sensing Studies....146
3.2.4 Singlet Oxygen Generation Studies....150
3.3 Second Generation Ratiometric (Aza)-BODIPY Anion Sensor.... 157
3.3.1 Synthesis and Characterisation....157
3.3.2 Anion Binding Studies....162
2.5 Chapter Conclusions and Future Work.... 167
2.6 References for Chapter Three.... 171

4 Halogen Bonding, BODIPY-Functionalised Pillararene and Aza-Crown Ether Host Systems for Fluorescence Sensing of Anions, Neutral Species and Ion-Pairs.... 173
4.1 Introduction.... 174
4.1.1 The Pillararene Macrocycle....174
4.1.2 Sensing of Dicarboxylates....178
4.1.3 Sensing of Sulfur Mustard....179
4.1.4 Aza-Crown Ether Macrocycles....181
4.1.5 Ion-Pair Sensors....183
4.1.6 Chapter Aims....183
4.2 Sensing of Dicarboxylates and a Sulfur Mustard Simulant using a Halogen Bonding BODIPY-Appended P5A.... 186
4.2.1 Synthesis and Characterisation....186
4.2.2 Fluorescence Sensing Studies in Organic Media....189
4.2.3 Fluorescence Sensing Studies in Aqueous-Containing Media....194
4.3 Sensing of Ion-Pairs Using a Halogen Bonding BODIPY-Appended Aza-Crown Ether.... 200
4.3.1 Synthesis and Characterisation....200
4.3.2 Alkali Metal and Ammonium Halide Ion-Pair Sensing Studies....205

4.3.3 Hydrogen Bonding-Assisted Sensing of Biological Ammonium Compounds 213
4.4 Chapter Conclusions and Future Work 218
4.5 References for Chapter Four 223

5 Conclusions 225
5.1 Conclusions 226
5.2 References for Chapter Five 233

6 Experimental Details 234
6.1 General Information 235
6.1.1 Instruments and Reagents 235
6.1.2 General Method for Optical Titrations 236
6.1.3 General Method for ^{1}H NMR Titrations 236
6.2 Experimental Details for Chapter Two 238
6.2.1 Determination of Quantum Yields 238
6.2.2 Electrochemical Measurements 238
6.2.3 Spectroelectrochemical Measurements 239
6.2.4 Gibbs Free Energy of Electron Transfer Calculations 240
6.2.5 Synthesis and Characterisation of Novel Compounds 242
6.3 Experimental Details for Chapter Three 252
6.3.1 Synthesis and Characterisation of Novel Compounds 252
6.4 Experimental Details for Chapter Four 264
6.4.1 Synthesis and Characterisation of Novel Compounds 264
6.5 References for Chapter Six 273

Chapter 1

Introduction

1 Introduction

1.1 Supramolecular Chemistry

1.1.1 Supramolecular Chemistry and Host-Guest Chemistry

Supramolecular non-covalent interactions mediate a vast variety of biotic and abiotic processes necessary for life. The nerve impulses which allow this thesis to be read are relayed across the synapses in the brain by neurotransmitters, which interact in a supramolecular fashion with receptors on the surface of the next neuron.[1] The DNA which encodes the structure of those receptors is itself a supramolecular assembly, held together by hydrogen-bonding interactions between complementary Watson-Crick nucleotide base pairs.[2] In an abiotic setting, reversible, supramolecular interactions are the basis of the solvent-extraction/electrowinning process for the refinement of copper ore,[3] responsible for 20% of global copper production in 2022,[4] in which copper ions are selectively extracted into an organic phase before being electrochemically reduced to copper metal. Clearly therefore, the study of supramolecular chemistry is critical for both understanding life and improving our lives.

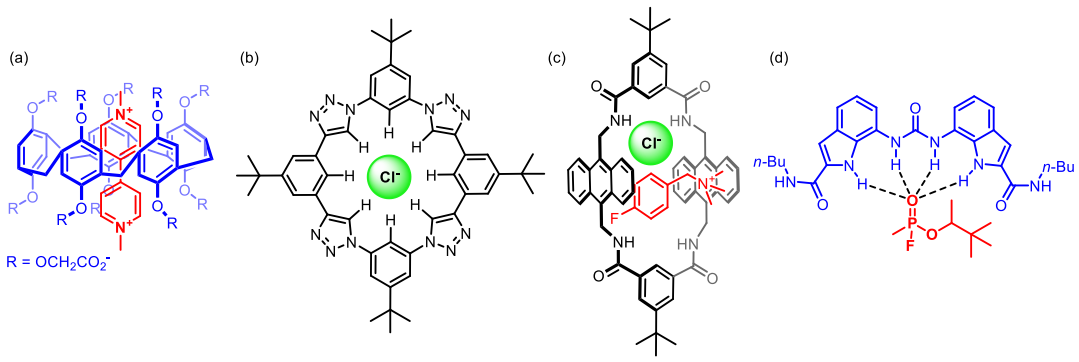


Fig. 1.1 Modern examples of host systems: (a) Ogoshi's pillar[5]arene cation receptor;[5] (b) Flood's triazolophane anion receptor;[6] (c) Smith's quaternary ammonium chloride ion-pair receptor;[7] (d) Gale's urea-based receptor for the neutral chemical warfare agent soman.[8]

The term supramolecular chemistry, first coined by the 1987 Chemistry Nobel Laureate Jean-Marie Lehn,[9] refers to *"the chemistry of the intermolecular bond, covering the structures and functions of the entities formed by the association of two or more chemical species"*,[9] or, more succinctly: 'chemistry beyond the molecule'.[9] Within this broad field, supramolecular host-guest chemistry in particular is concerned with the design of molecular hosts, engineered to bind specific guest species through non-covalent interactions. Since its inception in the mid-20th century, host-guest chemistry has developed into a cross-disciplinary field with many applications. To highlight just a few recent examples, hosts capable of binding cations,[5, 10] anions,[6, 11-12] ion-pairs,[13-15] and neutral species[8, 16-17] have been reported (Fig. 1.1), which in turn have facilitated the development of optical and electrochemical sensors for charged[18-22] and neutral species,[23-25] catalysts,[26-28] trans-membrane transporters,[29-31] salt solubilising agents for organic synthesis,[32] and ion extractants,[33-35] all of which are based on supramolecular host-guest interactions (Fig. 1.2).

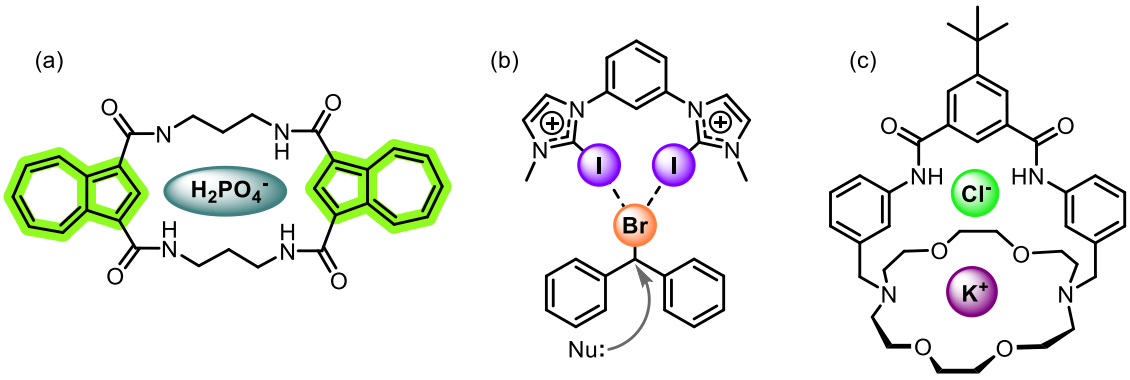


Fig. 1.2 Uses of modern host systems: (a) Jurczak's optical dihydrogen phosphate sensor;[22] (b) Huber's supramolecular halide abstraction catalyst;[28] (c) Smith's ion-pair membrane transporter.[31]

Given the broad applicability and utility of host-guest chemistry, this thesis aims to use supramolecular host-guest recognition primarily as a means of optically sensing anionic and neutral species. In particular, it explores the influence of guest binding on the

photochemical properties of host molecules and how this influence may be exploited for other applications, including multichannel modes of sensing and switchable generation of singlet oxygen for potential therapeutic use.

This introductory chapter will first provide an overview of the principles of host design required to achieve strong and selective guest binding through surveying seminal examples, followed by an account of the field of anion, neutral species and ion-pair recognition. The supramolecular sensing of anionic and neutral analytes will also be discussed and the aims of this thesis will be outlined.

1.1.2 Principles of Host Design

The 1987 Nobel Prize in Chemistry was awarded to Charles Pedersen, Donald Cram and Jean-Marie Lehn "for their development and use of molecules with structure-specific interactions of high selectivity",[36] which recognised the beginnings of the rapidly expanding field of host-guest chemistry. Pedersen's seminal contributions concerned the development of crown ethers, reported in the 1960s (Fig. 1.3a).[37] Crown ethers were the first class of macrocyclic compound to exhibit high affinity and selectivity for alkali metal cations, and implement key host design principles: chelation, host-guest size complementarity and pre-organisation (*vide infra*).

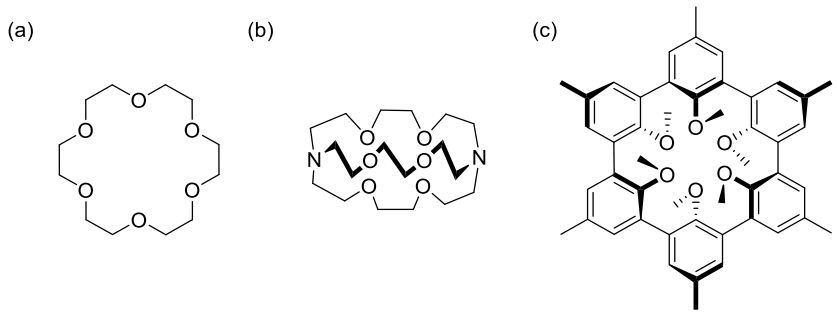


Fig. 1.3 A representative example of each class of cation binding ligands recognised by the 1987 Nobel Prize: (a) Pedersen's crown ethers; (b) Lehn's cryptands; (c) Cram's spherands.

Exploiting these principles further, Lehn and Cram,[38-42] developed cryptands and spherands respectively, which offered improved alkali metal cation guest recognition (Fig. 1.3b-c). This section seeks to illustrate how the key host design principles, first pioneered by Pedersen, Lehn and Cram, have been applied to all types of hosts.

1.1.2.1 Chelate Effect, Macrocyclic Effect and Pre-Organisation

The *chelate effect*, first coined in relation to the tellurium (II) complexes of acetylacetone,[43] describes the increased affinity of polydentate ligands for metal ions over analogous monodentate ligands.[44]

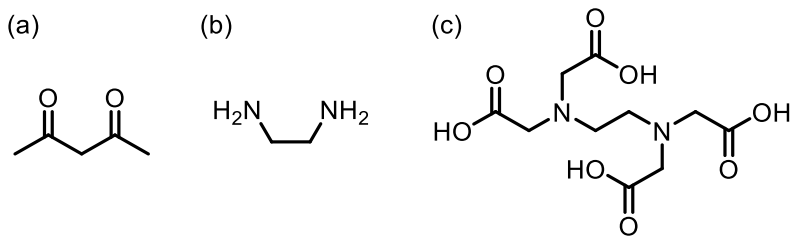


Fig. 1.4 Polydentate, chelating ligands for metal ions: (a) acetylacetone; (b) ethylenediamine; (c) ethylenediaminetetraacetic acid (EDTA).

The main contribution to the chelate effect is entropic in nature.[45] Upon binding a metal ion, a single chelating ligand displaces multiple metal-coordinated solvent molecules, thus increasing the number of free molecules in solution and causing a positive entropy change. There is also an additional enthalpic contribution, which is due to the fact that the enthalpic penalty of bringing together the Lewis basic oxygen and nitrogen donor groups, present in each of the ligands in Fig. 1.4, which arises from the electrostatic repulsion between the electron lone pairs, has been partially surmounted in the synthesis of the ligand itself. Thus, the additional repulsion between the groups upon binding to a metal ion is correspondingly reduced compared to the case of multiple monodentate ligands.

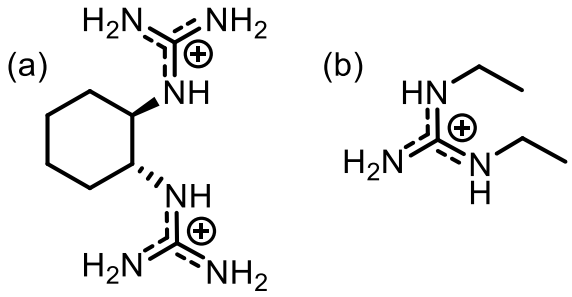


Fig. 1.5 Guanidinium anion hosts reported by Lehn. The bidentate ligand (a) displayed enhanced affinity for PO_4^{3-} over the monodentate ligand (b).

The chelate effect was also demonstrated for anions by Lehn and co-workers in 1979.[46] The bidentate, cyclohexane-based bis-guanidinium host shown in Fig. 1.5a displayed an affinity for PO_4^{3-} in unbuffered water which was approximately 100-fold greater than the affinity displayed by diethylguanidinium (Fig. 1.5b). Since then, the anion chelate effect has been commonly deployed in modern anion hosts, such as those reported by Bowman-James and co-workers in 2015,[47] in which the 8-coordinate hydrogen bond donating receptor shown in Fig. 1.6b exhibited a 25-fold higher affinity for SO_4^{2-} in H_2O : DMSO 1:3 (*v/v*) than the equivalent tetradentate ligand (Fig. 1.6a).

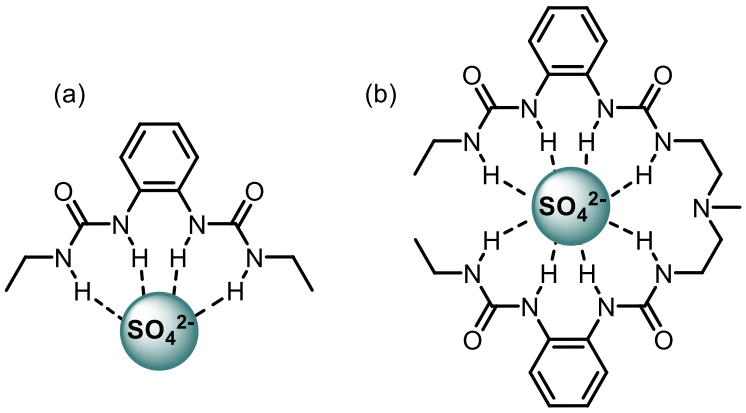


Fig. 1.6. Structures of (a) tetradentate and (b) 8-coordinate anion hosts reported by Bowman-James.

The additional stability of complexes formed by macrocyclic ligands, such as crown ethers, over their acyclic open-chain analogues is known as the *macrocyclic effect*

(Fig. 1.7).[45] Like the chelate effect, the macrocyclic effect has both enthalpic and entropic contributions, both of which are related to Cram's concept of *pre-organisation*.[48-49]

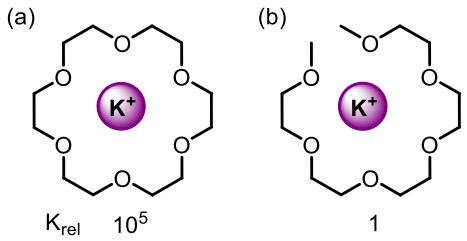


Fig. 1.7 K^+ complexes of (a) 18-crown-6 and (b) its acyclic analogue, showing the enhancement in association constant K_a due to the macrocyclic effect. (K_a determined in water).[41]

Pre-organisation refers to the structure of the free host molecule being well-arranged for guest binding prior to complexation, such that a highly pre-organised host undergoes only minimal changes to its conformation upon guest binding.[50] Indeed, Cram's completely pre-organised hosts, the spherands (Fig. 1.3c), exhibited no conformational changes upon complexation of Li^+ or Na^+, demonstrated by solid state crystal structures of the alkali metal cation complexes.[38] This remarkable degree of pre-organisation results in the highly impressive association constant $K_a(Li^+) > 10^{16}$ M^{-1} in $CDCl_3$ saturated with D_2O.[39]

Part of the enthalpic contribution to the macrocyclic effect arises from the fact that because they are more pre-organised than their acyclic analogues, macrocyclic hosts experience little additional enthalpic conformational strain upon guest binding. A further enthalpic contribution can be attributed to the cavities of macrocyclic ligands being poorly solvated,[49] such that the enthalpic cost of de-solvating the host upon guest binding is reduced relative to acyclic analogues.

As a consequence of pre-organisation, the loss of conformational entropy upon guest binding for macrocyclic hosts is smaller in comparison to their acyclic analogues,[38, 48, 51] which constitutes the entropic contribution to the macrocyclic effect.

The principle of pre-organisation can be applied to improve the recognition properties of acyclic hosts too, which is desirable due to the synthetic challenges associated with preparing macrocycles. In 2024, Langton and co-workers reported two related anion hosts:[52] one containing phenolic groups, capable of forming intramolecular hydrogen bonds to the proximal amide moieties, thus pre-organising the host for anion binding in the amide cleft (Fig. 1.8b); and an analogous compound lacking the phenolic groups and consequent pre-organisation (Fig. 1.8a). Chloride anion association constants were determined in acetonitrile-d_3, revealing the marked improvement in affinity afforded by pre-organisation: the phenolic receptor (Fig. 1.8b) exhibited an association constant $K_a(Cl^-)$ = 25400 M^{-1}, compared to $K_a(Cl^-)$ = 530 M^{-1} for the conformationally flexible analogue (Fig. 1.8a). Interestingly, the pre-organised host exhibited excellent chloride anion membrane transport properties, in stark contrast to the flexible host which proved to be completely inactive for transport.

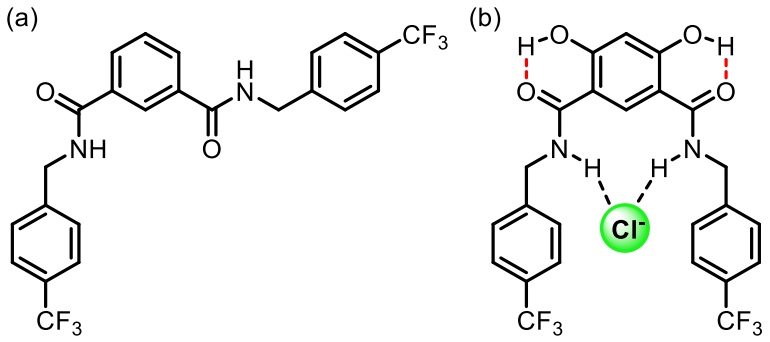


Fig. 1.8 Anion hosts reported by Langton, showing the increased pre-organisation of the intramolecularly hydrogen-bonded (shown in red) analogue.

1.1.2.2 Complementarity

Possessing a complementary size and shape to their target guest is a powerful means by which host molecules can exhibit high affinities and good selectivity. This method of achieving high affinity and selectivity is inspired by nature, which makes use of highly complementary binding sites in a variety of biological functions,[53-54] as first noted by Fischer in his 1894 lock-and-key hypothesis of enzyme activity.[55] Notable biological examples are found in the antibody-antigen interactions involved in immune responses (Fig. 1.9).[56] Antibodies contain a variable region which is highly complementary to its target antigen, such that discrimination between the *R* and *S* enantiomers of the same molecule can be routinely achieved.[57]

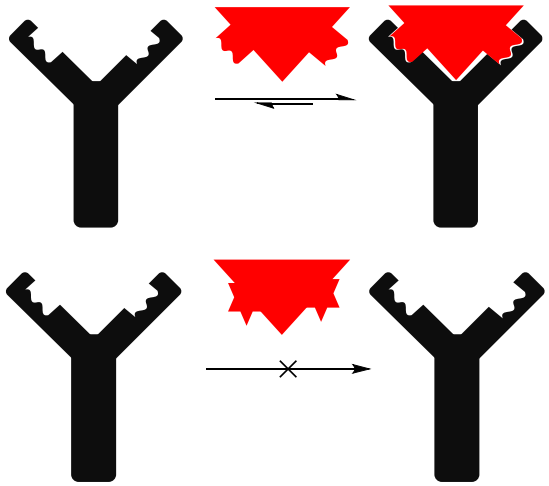


Fig. 1.9 Cartoon showing the selectivity conferred by a high degree of complementarity in antibodies.

Complementarity can also be deployed in synthetic receptors to achieve impressive levels of selectivity and high binding affinities. Lehn's early investigations into cryptands powerfully demonstrated the impressive size discrimination offered by these ligands, which could selectively bind different alkali metal cations on the basis of their ionic radii (Fig. 1.3b). More recently, Bencini and co-workers reported a chiral BINOL-

based polyammonium anion host capable of enantiomeric discrimination between the optical isomers of tartrate in aqueous buffer (Fig. 1.10).[58] Impressively, the host showed high selectivity for (*S*,*S*)-tartrate (K_a = 1.3 × 10^6 M^{-1}) over (*R*,*R*)-tartrate or *meso*-tartrate, both of which were bound approximately three orders of magnitude more weakly. This selectivity was ascribed to the shape of the host being complementary for (*S*,*S*)-tartrate, allowing for hydrogen bonding interactions between the hydroxyl groups of the guest and the tertiary amine of the host, in addition to the electrostatic interactions between the polyammonium macrocycles and carboxylate groups. In contrast, (*R*,*R*)-tartrate could not form these additional hydrogen bonds and consequently was bound much more weakly.

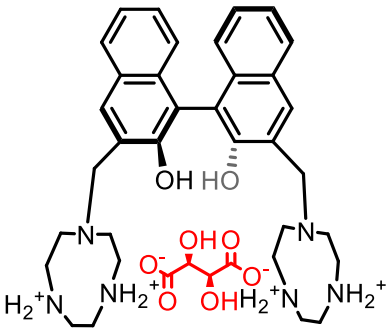


Fig. 1.10 Bencini's enantioselective BINOL-based host for tartrate.

1.1.2.3 Exploiting the Relative Solvation of Host and Guest

As noted above in relation to the chelate and macrocyclic effects, the binding of a host by a guest involves the (at least partial) de-solvation of both the host and the guest.[59] Therefore, the interactions of both the host and guest with the surrounding solvent have significant impacts on host-guest recognition. Whilst this presents challenges for the recognition of strongly-solvated guests,[59] in other settings the relative solvation of the host and guest can be exploited to effect strong and selective recognition. For example, hydrophobic effects are often harnessed to facilitate the strong binding of non-polar guests in aqueous media. Classically, the propensity of hydrophobic molecules to

aggregate in water is described as an entropic phenomenon. Non-polar molecules cannot participate in hydrogen bonding with water and therefore their introduction disrupts the hydrogen bonded network of water molecules, such that the network reorientates to form a solvent cage around the hydrophobic molecule, thus restricting the mobility of the proximal water molecules and decreasing their translational and rotational entropy.[59-61] Upon the association of two hydrophobic molecules, the exposed non-polar surface area is reduced and the disruption of the hydrogen bonding water network is correspondingly decreased, leading to a positive entropy change.

Such an effect was exploited to give rise to the very strong inclusion complex formed between a cationic pillar[5]arene derivative and octyl-sulfonate (K_a = 4.8 × 10^7 M^{-1} in water), reported by Mejuto and co-workers (Fig 1.11).[62] Upon binding the alkyl sulfonate, a positive entropy change was observed in isothermal titration calorimetry (ITC) experiments, which was ascribed to the release of ordered water molecules from the pillar[5]arene cavity and the alkyl chain of the alkyl sulfonate.

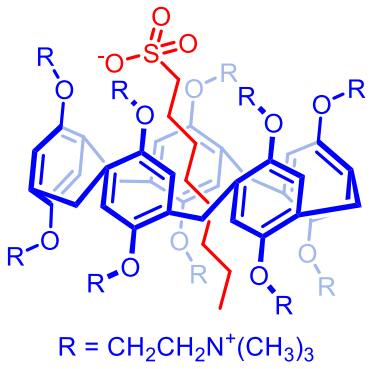


Fig. 1.11. The highly stable complex between a cationic pillar[5]arene derivative and octyl-sulfonate reported by Mejuto and co-workers.

In some cases, the solvophobicity of the host alone is sufficient to drive strong binding of well-hydrated guest species *via* the classical hydrophobic effect. Such an effect

has been harnessed to allow the binding of sulfate in water, a very strongly hydrated anion. In 2017, Kubik and co-workers reported a neutral water-soluble bis(cyclopeptide) which exhibited an impressive 1:1 stoichiometric host-guest association constant with sulfate ($K_a(SO_4^{2-})$ = 2040 M^{-1} in H_2O buffered with 35 mM phosphate) (Fig. 1.12).[63] Importantly, ITC experiments revealed that the binding of sulfate (and other anions) was associated with a large, positive entropy change, ascribed to the release of ordered water molecules into the bulk solution from the bis(cyclopeptide) host as it collapsed into its clam-like binding conformation, which drastically reduces the exposed hydrophobic surface area (Fig. 1.12b).

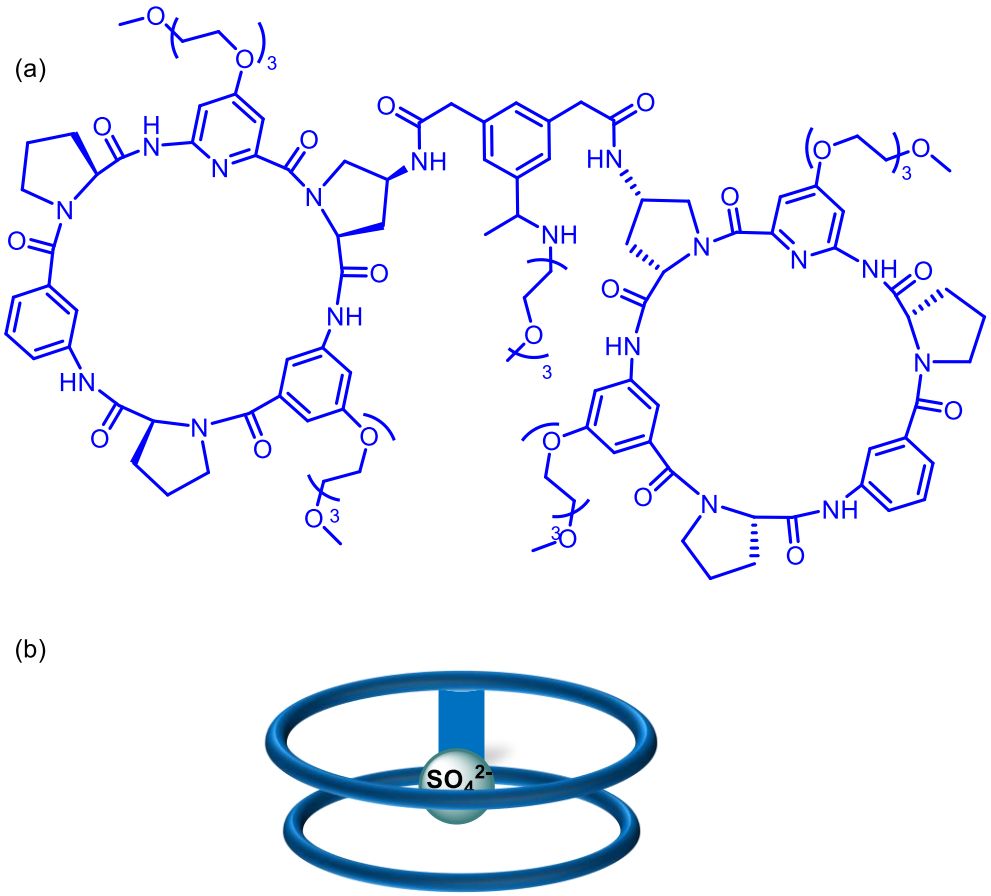


Fig. 1.12. (a) Sulfate binding bis(cyclopeptide) reported by Kubik and co-workers and (b) a cartoon representation of its clam-like binding mode.

More recently, non-classical hydrophobic effects have also been reported, in which *enthalpy* changes are the driving force for the association between a hydrophobic host and guest.[64] These arise from the increased number and strength of hydrogen bonds that water molecules can form in the bulk solution, relative to the hydrogen bonds they can form when confined in the host cavity. This effect was ascribed as the cause of the unprecedently high iodide binding constant measured for the bambusuril host in water ($K_a(I^-) = 3.2 \times 10^7\ M^{-1}$), reported by Sindelar and co-workers in 2018 (Fig. 1.13).[65] The authors described the highly favourable enthalpic gain upon anion binding to the release of high energy, 'frustrated' water molecules from the binding cavity into the bulk solution, where they can form stronger hydrogen bonds.

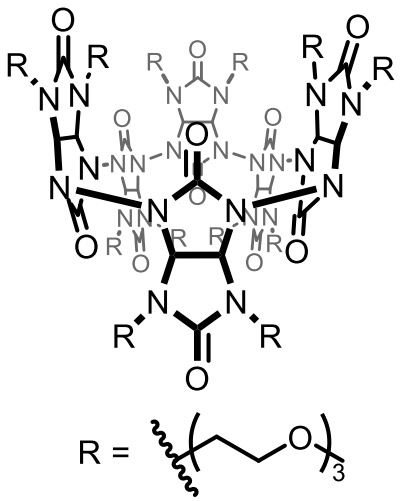


Fig. 1.13. Sindelar's bambusuril iodide binding host which displayed a non-classical hydrophobic effect.

1.2 Supramolecular Recognition of Anions and Neutral Species

Having introduced the field of host-guest chemistry within supramolecular chemistry and discussed the principles of host-design common to all types of hosts, this section seeks to review the recognition of anions and neutral species in more detail. Initially, their importance and challenges inherent to their recognition will be highlighted, followed by discussion of the types of non-covalent interactions used in the recognition of anions and neutral species. Finally, seminal examples of synthetic hosts for anions, neutral species and ion-pairs will be reviewed.

1.2.1 The Importance of Anions and Neutral Species

1.2.1.1 The Importance of Anions

In 1968, Park and Simmons reported the first anion host,[52] a macrobicyclic ammonium compound capable of encapsulating chloride and bromide anions within its internal cavity in aqueous TFA solution (Fig. 1.14).

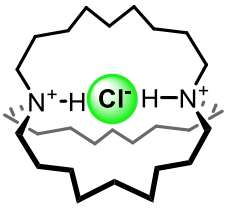


Fig. 1.14 Park and Simmons' seminal macrobicyclic anion host.

Despite this early report, the field of anion host chemistry remained overlooked in comparison to cation coordination chemistry until the late 1970s, when reports of polycationic quaternary ammonium cages were published by Schmidtchen and Lehn (Fig. 1.15).[66-67] The renewed interest in anion host chemistry was driven by the recognition of the importance of anions, particularly in biology. Indeed, reporting the quaternary

ammonium cage shown in Fig. 1.15a, Schmidtchen wrote: *"since at least two thirds of all enzymes act on negatively charged substrates or cofactors, the construction and complexation behavior of abiotic receptors for anions should provide interesting comparisons with substrate binding to enzyme pockets and to cell wall receptors"*.[66]

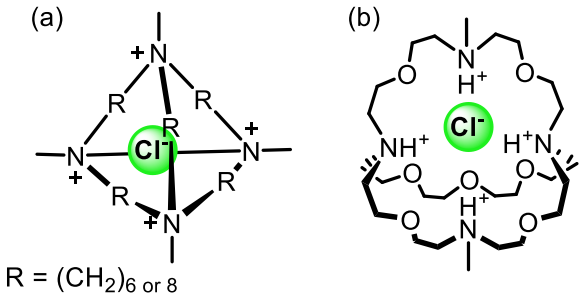


Fig. 1.15. (a) Schmidtchen's quaternary ammonium cages binding a chloride anion. (b) Lehn's polyammonium cage binding a chloride anion.

In addition to the enzyme substrates mentioned by Schmidtchen, other crucial biologically-relevant anions include: DNA, a polyanionic polymer;[2] ATP, the polyphosphate-based biological energy transducer and signalling molecule;[68] and citrate, malate and fumarate, organic carboxylates all involved in the Krebs cycle of metabolism.[69] Simple inorganic anions are also highly important for the regulation and function of biological processes: chloride transport mis-regulation is implicated in cystic fibrosis,[70] iodide is required for correct thyroid function,[71] and bicarbonate is the primary means through which CO_2 is excreted from the body.[72] The design of anion hosts is therefore essential to aid our understanding of biological processes, to monitor the production of anions in the body, and to correct any imbalances in anion concentration that may arise due to disease.

Anions also have significant agricultural and environmental roles. Highlighting the former, 195 million tonnes of ubiquitous NPK* fertilisers containing nitrogen in the form of nitrate and phosphorus in the form of phosphate were used globally in 2021,[73] and their excessive use is associated with detrimental environmental impacts such as the pollution and eutrophication of water sources.[74] Furthermore, toxic anions in the environment can pose a direct threat to life, which has been highlighted by the recent spill of cyanide into a canal in Walsall by a metal processing company.[75] Radioactive anions such as pertechnetate, a component of nuclear waste streams, are also very dangerous and long-lasting.[76] Clearly therefore, it is of paramount importance to monitor and remediate the presence of damaging anions in the environment, which further strengthens the case for the design of strong and selective anion hosts.

1.2.1.2 The Importance of Neutral Species

Neutral inorganic and organic compounds are enormously important in modern life. Due to their cell membrane permeability, neutral compounds are commonly found as signalling molecules in biology and medicine, with the small molecule nitric oxide being identified as a powerful vasodilator in work which won the Nobel Prize in Medicine in 1998.[77] Other small molecules such as H_2S and CO have been identified as signalling agents implicated in the response to hypoxia and angiogenesis.[78]

Perhaps more important in recent times is the impact of anthropogenic neutral pollutants on the environment. Plasticisers, such as phthalates, are ubiquitous in modern products and have been classified as potential endocrine disruptors (Fig. 1.16a).[79] The infamous insecticide dichlorodiphenyltrichloroethane (DDT), which is remarkably

* Nitrogen, phosphorus, potassium.

persistent in the environment and accumulates in ecosystems,[80] has been shown to have devasting ecological impacts, particularly on birds (Fig. 1.16b).[81] Dicarboxylic acids, such as malonic acid and succinic acid, have recently been found to be key constituents of the particulate pollution responsible for visibility degradation in cities, amongst other negative environmental impacts (Fig. 1.16c).[82] Furthermore, many highly toxic and extremely dangerous chemical warfare agents (CWAs) are neutral molecules. These include the organophosphate G-series of nerve agents (Fig. 1.16d) and the blistering agent sulfur mustard.[24, 83]

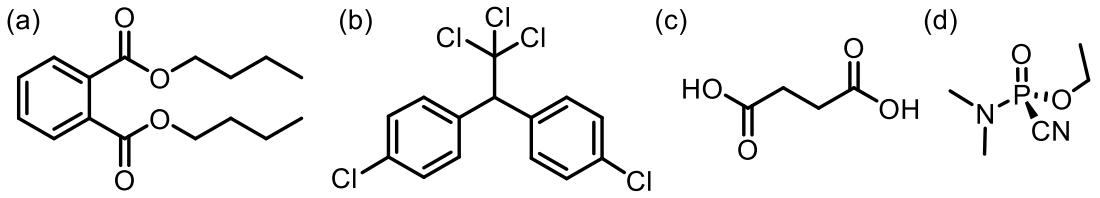


Fig. 1.16. Neutral molecules with dangerous environmental effects: (a) Di-*n*-butyl phthalate, a plasticizer, (b) DDT, a banned pesticide, (c) Succinic acid, implicated in particulate pollution, (d) tabun, a G-series nerve agent CWA.

Clearly, the development of host systems which can selectively bind neutral molecules for the detection and elimination of pollutants in the environment are highly desirable.

1.2.2 The Challenges of Designing Hosts for Anions and Neutral Species

1.2.2.1 The Challenges of Designing Hosts for Anions

Relative to cations, the design of hosts for anions is significantly more challenging, due to their inherent properties. These properties include: geometric variation, pH dependence, charge density, and solvation. The implications of each of these fundamental properties on the binding of anions are discussed below.

Geometric variation: In contrast to cations, which are typically spherical, anions adopt a much broader range of geometries,[84] including linear (N_3^-), bent (NO_2^-), trigonal planar (NO_3^-), tetrahedral (PO_4^{3-}), square planar ($AuCl_4^-$) and octahedral (PF_6^-). Although this structural diversity makes the design of hosts for anions more challenging, it also offers supramolecular chemists an opportunity to construct selective host systems with complementary sized and shaped cavities.[20, 85-86]

pH dependence: Anions can often also exist in multiple states of protonation and can become neutral at low pH; for example phosphate has four protonation states and is neutral below pH = 2 (Fig. 1.17).[87] Therefore, hosts for anions must ideally be themselves pH independent, such that they can operate in a pH window in which their target guest exists in the correct protonation state. Early macrocyclic polyammonium anion hosts, such as those reported by Hosseini and Lehn,[67, 88] suffer from being deprotonated and therefore incapable of anion recognition at high pH values.[66-67] A further complication is that highly basic anions, such as fluoride, may deprotonate a host and therefore receptors for these species must be designed without acidic sites.

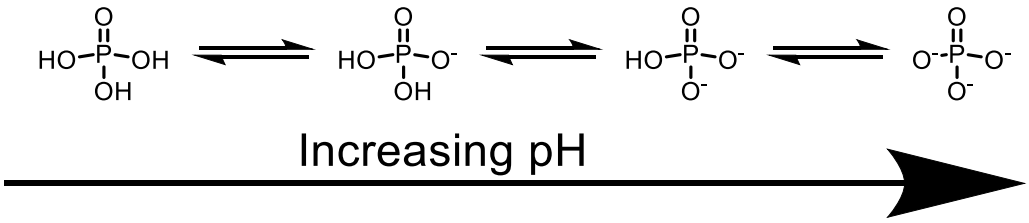


Fig. 1.17. The variable protonation states of the phosphate anion.

Charge density: Non-covalent supramolecular interactions (*vide infra*) used in the binding of an anionic guest by a host all have at least some electrostatic contribution and therefore are stronger when formed with guest species of higher charge density. Hence, due to their larger radii relative to isoelectronic cations, host-anion non-covalent

interactions are typically weaker than analogous interactions formed with cations (Table 1.1).[89]

Solvation: As mentioned in Section 1.1.2.3, host-guest complexation involves the (partial) de-solvation of the guest, which creates significant challenges in the context of anion recognition. First, anions of a given radius typically display larger energies of solvation than equivalent cations,[89] which increases the enthalpic barrier to binding and therefore suppresses the affinity of hosts for anionic guests (Table 1.1).

Table 1.1. 6-Coordinate ionic radii and Gibb's free energies of hydration of halide anions and isoelectronic alkali metal cations. [90-92]

Anion	Ionic Radius (Å)	ΔG_{hyd} (kJ mol^{-1})	Cation	Ionic Radius (Å)	ΔG_{hyd} (kJ mol^{-1})
F^-	1.33	-465	Na^+	1.02	-365
Cl^-	1.81	-340	K^+	1.38	-295
Br^-	1.96	-315	Rb^+	1.57	-275
I^-	2.20	-275	Cs^+	1.67	-250

Second, in aqueous media, the selectivity of anion hosts is frequently dictated by the relative solvation of different anions, rather than by the innate recognition characteristics of the host itself. Specifically, smaller, more charge dense and hence more strongly hydrated anions, such as chloride, are bound more weakly than larger, less-charge dense and hence poorly hydrated anions such as iodide, due to the enthalpic penalty of de-solvation (Fig. 1.18).[59, 93-94] This commonly observed selectivity trend is known as the "Hofmeister bias" in anion binding strengths, in recognition of Franz Hofmeister who first classified the relative solvation of various anions in the context of their influence on the structure of water: charge-dense anions interact strongly with water

molecules and induce structure in their local environment (kosmotropes), whereas less charge-dense anions disrupt the structure of water (chaotropes).[95] This has important implications for the solubility of hydrophobic proteins, which Hofmeister studied.



Less charge dense
Weakly hydrated
Chaotropic

More charge dense
Strongly hydrated
Kosmotropic

$$ClO_4^- > I^- > SCN^- > ClO_3^- > Br^- > Cl^- > F^- > CO_3^{2-} > HPO_4^{2-} > SO_4^{2-} > citrate^{3-}$$

Fig. 1.18. The Hofmeister series of anion hydration.[96]

1.2.2.2 The Challenges of Designing Hosts for Neutral Species

The recognition of neutral species is also more challenging than cation recognition, but for different reasons.

Charge neutrality: Due to their lack of charge, the strength of non-covalent supramolecular interactions formed with neutral species is dramatically reduced, which therefore requires the use of notably different recognition strategies. In particular, in competitive solvent media, such as water, neutral molecules are typically poorly solvated, which is frequently exploited by well-designed hosts using solvophobic effects. This strategy alone is poorly suited to conferring selectivity to a host however, as it is not based on any complementarity between the host and guest but rather their mutual hydrophobicity. Hence, hydrophobic effects must be employed alongside directional supramolecular interactions formed with specific functional groups on the neutral guest to effect the selective recognition of neutral species.[97]

Geometric variation: In a similar manner to anions but to a greater degree, neutral compounds, particularly organics, exhibit a hugely varied set of geometries which requires careful complementary host design.

pH dependence: Although many neutral compounds do not possess any ionisable groups, a number of environmentally and medically relevant species do have variable protonation states. For example, the neurotransmitter GABA exists as a neutral zwitterion at physiological pH, but is cationic and anionic at low and high pH respectively (Fig. 1.19).[98] Basic neutral guests, such as amines, may also deprotonate acidic hosts, in analogy to the problems posed by basic anions such as fluoride.

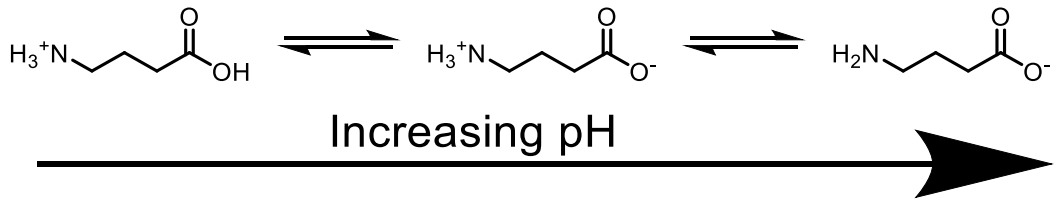


Fig. 1.19. The variable protonation states of (a) the neurotransmitter GABA

1.2.3 Supramolecular Interactions for the Recognition of Anions and Neutral Species

Supramolecular host-guest assemblies are held together through reversible, non-covalent interactions which allow dynamic guest binding and release.[96] Due to the aforementioned difficulties inherent to recognising anionic and neutral species, the judicious application of a wide toolkit of supramolecular interactions is required in the design of effective hosts. Supramolecular chemists have deployed a variety of interactions for this purpose, including electrostatic interactions, hydrogen bonding, σ-hole interactions and π interactions and this section seeks to survey these non-covalent interactions.

1.2.3.1 Electrostatic Interactions

The most fundamental interaction used to bind anions is simple Coulombic electrostatic attraction to a positively charged host. Such very strong ion-ion interactions were indeed employed by the early anion hosts, for anion binding in competitive solvents such as water (Figs. 1.14 & 1.15).[46, 66-67, 99-100] However, they are non-directional,[101] which means they are poorly suited to conferring selectivity to a host and commonly the most highly charged anion is bound the strongest. In addition, positively charged hosts necessitate counter-anions, which can compete with the target anion guest.

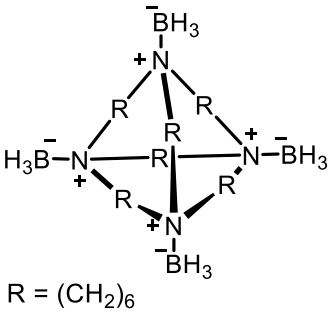


Fig. 1.20. Schmidtchen's 2nd generation electronically neutral anion host.

An important improvement on Schmidtchen's first generation quaternary ammonium cage (Fig. 1.15a) was the development of the zwitterionic compound shown in Fig. 1.20.[102] This electronically neutral host employed electrostatic ion-*dipole* interactions for anion binding and therefore exhibited better recognition selectivity characteristics because it does not suffer from the counterion competing with the target guest. Additionally, ion-dipole interactions have a higher degree of directionality.[103] However, the electronically neutral host did show reduced anion binding strengths relative to the *tetra*-cationic first generation quaternary ammonium cage, which highlights the reduced strength of ion-dipole interactions relative to ion-ion interactions. A further disadvantage of ion-dipole interactions is that they display a stronger distance dependence than ion-ion

interactions ($E \propto r^{-2}$ and $E \propto r^{-1}$, respectively),[104] and thus quickly weaken at increased interaction distances.

1.2.3.2 Hydrogen Bonding

Hydrogen bonding (HB) interactions can form when a hydrogen atom is bonded to an electronegative atom, R (R = N, O, F and occasionally C), and thus develops a partial positive charge. This hydrogen atom (known as the hydrogen bond donor) can subsequently interact with a Lewis basic species (E) to form a hydrogen bond. HB interactions are essentially ion-dipole interactions, but the possibility of further orbital overlap contributions is a disputed topic.[105-106] Regardless of their exact nature, empirically HB interactions display some degree of directionality and are strongest when the R−H···E bond angle approaches 180°.[107]

Due to their relatively low strength (< 50 kJ mol^{-1}),[108] HB donor hosts normally employ multiple HB interactions to effect guest binding.[109-110] This is the approach seen in nature, which makes extensive use of HB interactions in protein structure, enzyme catalysis and DNA structure.[111] For example, the iron binding site of the iron-transport protein transferrin contains a carbonate anion (known as a synergistic ligand) to complete the coordination sphere of the Fe^{3+} cation (Fig. 1.21).[112] This carbonate anion is held in place by two convergent HB interactions from a nearby arginine (guanidinium) residue, in a manner typical of the way nature employs HB interactions.

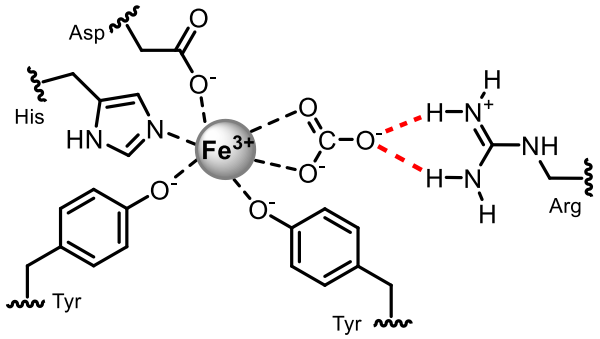


Fig. 1.21. The structure of the iron (III) binding site of transferrin. HB interactions highlighted in red.

Supramolecular chemists have employed HB interactions in synthetic hosts for anions and neutral molecules from the inception of the field of host-guest chemistry. For example, in 1993, Zimmermann and Murray reported a series of complementary HB donor/acceptor (D/A) pairs, forming arrays held together by HB interactions (Fig. 1.22).[113] The ADA·DAD pair, shown in Fig. 1.22a, exhibited an association constant K_a of 78 M^{-1} in $CDCl_3$, whereas the AAA·DDD array, shown in Fig.1.22b, displayed a dramatically enhanced K_a of > 10^5 M^{-1}, due to the pre-organising influence of the additional HB interactions between the ester and amine groups of the HB donor. HB interactions continue to be commonly employed in the recognition of anions and neutral molecules and examples of such hosts will be surveyed in a later section.

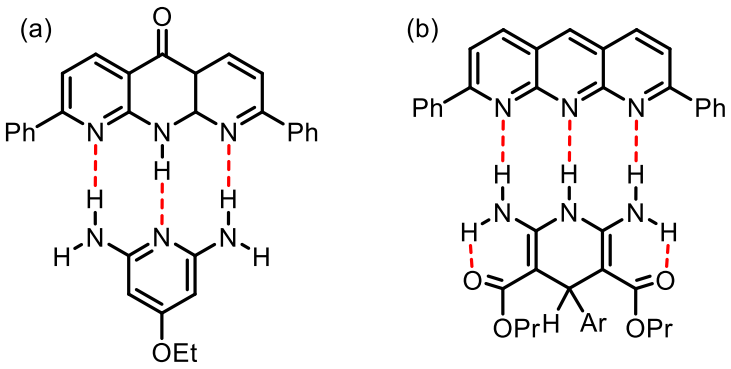


Fig. 1.22. Zimmermann and Murray's HB arrays.

1.2.3.3 Halogen Bonding

According to IUPAC, halogen bonding (XB) is a form of sigma-hole interaction that *"occurs when there is evidence of a net attractive interaction between an electrophilic region associated with a halogen atom in a molecular entity and a nucleophilic region in another, or the same, molecular entity."*[114] The existence of an electrophilic region, which is known as a σ-hole, on an electronegative halogen atom is initially counterintuitive, but is rationalised by consideration of the anisotropic electron distribution around a polarisable halogen atom which occurs when it is covalently bonded to an electron-withdrawing substituent (R).

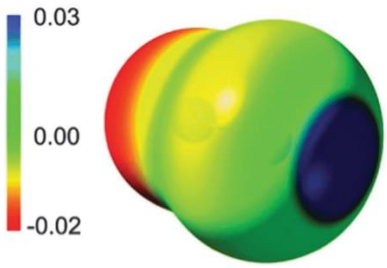


Fig. 1.23. Calculated molecular electrostatic potential, in Hartrees, at the 0.001 electrons Bohr^{-3} iso-density surface of BrF showing the sigma hole on the bromine atom. Copyright RSC, 2015, reproduced with permission.[115]

The σ-hole is located along the extension of the R-X bond and is an area of depleted electron density with electrophilic character.[†116] Molecular electrostatic potential surfaces enable this σ-hole to be visualised, as in Fig. 1.23.[115] The depth of the σ-hole is increased in more polarisable halogen atoms and hence the majority of XB hosts use iodine as the XB donor. Additionally, as the depth of the σ-hole is increased by attaching the halogen atom

[†] This region aligns with the location of the sigma antibonding orbital, and therefore XB and HB interactions can be considered to involve this unoccupied molecular orbital.

to a highly electron-withdrawing neutral or positively charged substituent, most modern XB hosts employ one of the motifs displayed in Fig 1.24.

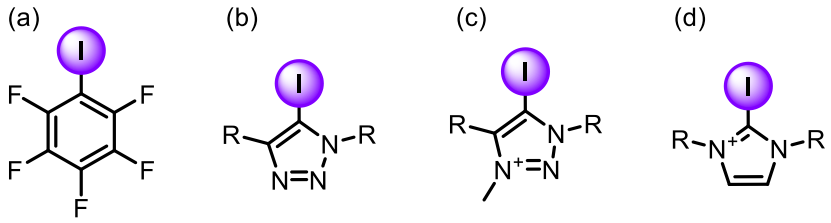


Fig. 1.24. Commonly employed XB donor motifs, showing the electron-withdrawing nature of the halogen substituent: (a) iodoperfluoroarene, (b) iodotriazole, (c) iodotriazolium and (d) iodoimidazolium.

The first crystallographic evidence of XB interactions was reported by Hassel and Hvoslef in 1954 in the structure of the 1:1 adduct of 1,4-dioxane and bromine.[117] Infinite chains containing linear O···Br–Br···O units were observed in which the Br···O distance was less than the sum of the van der Waal's radii of the two atoms and where the Br–Br bond was elongated relative to its length in the gas phase. Around the same time, Mulliken reported the observation of charge-transfer bands in the UV spectra of I_2 complexed with various ethers and alcohols.[118] Taken together, these observations suggested that XB interactions have a degree of covalency, which explains the close contacts of the crystal structure and the elongation of the Br–Br bond (due to electron donation into the Br–Br sigma antibonding orbital), as well as the charge transfer band.[119] Incidentally, these observations also presaged the utility of XB interactions in binding neutral guests.

The covalency of XB interactions in a supramolecular context was probed by Kennepohl, Beer and co-workers by X-ray absorption spectroscopy (XAS) measurements on the chloride and bromide complexes of a XB bis-iodotriazole-pyridinium receptor (Fig. 1.25).[120] These studies revealed the presence of pre-edge features in the XAS spectra of the chloride and bromide complexes of the XB host, which correspond to excitations

from the Cl_{1s} to the Cl_{3p} (Br_{1s} to Br_{4p}) orbitals. As the halide anions are closed shell species, these transitions are not observed in ionic salts containing halide ions and therefore this observation was taken as evidence of charge transfer between the halide anions and XB donor host, which was quantified at 6% – analogous to the degree of covalency in a chloro-metal ion such as $[CuCl_4]^{2-}$. Importantly, no evidence of charge transfer was observed in the HB analogue of the host.

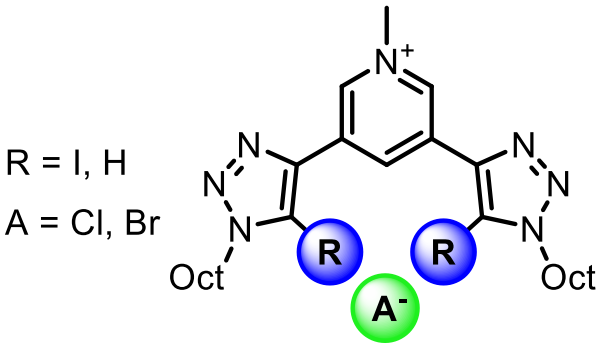


Fig. 1.25. Beer's XB and HB anion receptors, studied by XAS.

XB interactions also have electrostatic and solvophobic contributions.[121] However the notable covalent contribution gives rise to many of the benefits that XB hosts exhibit over their HB analogues. Importantly, XB hosts consistently show greater anion guest binding potency than HB host analogues,[13, 122] particularly in aqueous media,[123-124] where they are less severely attenuated by the increased dielectric constant of the polar protic solvent.[125] This solvent-resistance was demonstrated in a systematic study by Perutz and Hunter, which reported the effect of increasing solvent polarity on the strength of complexes formed by an HB donor and an XB donor with neutral organic acceptors.[126] In *n*-octane, the HB donor (Fig. 1.26a) exhibited an association constant with tetramethyl-thiourea (Fig. 1.26c) of 370 M^{-1}, compared to an association constant value of K_a = 8800 M^{-1} for the XB donor (I_2, Fig. 1.26b). However, in DCM, a more polar solvent, the association constant for the HB donor was reduced to 9 M^{-1}, whereas the XB donor's guest affinity was

increased to 58,000 M^{-1}. In methanol, the HB donor exhibited no association with the thiourea guest, but the XB donor maintained an impressive K_a = 2700 M^{-1}. This insensitivity of the XB donor's guest affinity to the nature of the solvent was attributed to charge transfer contributions to the XB interaction.

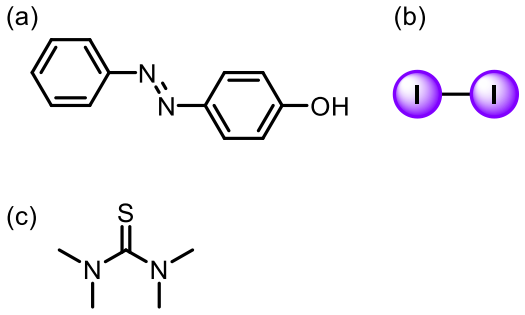


Fig. 1.26. (a) The HB donor used in Perutz and Hunter's systematic study, (b) the XB donor, I_2, and (c) the tetramethyl-thiourea guest.[126]

Furthermore, due to the highly localised nature of the σ-hole, XB interactions have a stricter preference for linearity than HB interactions,[127] which allows the design of more selective hosts.[128] Additionally, the hydrophobic nature of XB donors, which reduces the host de-solvation enthalpic penalty of guest binding, and the pH independence of the XB donor motifs, render XB particularly attractive for host-guest applications in aqueous media.[123]

1.2.3.4 π Interactions

π interactions are a class of non-covalent interactions formed between the surfaces of two aromatic systems or an aromatic surface and an ion. They are dominated by polarisation of the π electron cloud of the aromatic moiety, giving rise to electrostatic attraction between the two interacting species. These interactions are relatively weak (< 20 kJ mol^{-1})[90] compared to other non-covalent interactions and therefore are normally

used in concert with other interactions in a supramolecular context. For example, Ghosh and co-workers reported an anion host based on a bis-phenanthroline Ru (II) centre,[129] which used ion-ion electrostatic attraction and an XB donor in combination with an assisting anion-π interaction formed to an electron-deficient perfluorobenzene moiety to bind $H_2PO_4^-$ with an impressive association constant of 2.76 x 10^6 M^{-1} in acetonitrile (Fig. 1.27).

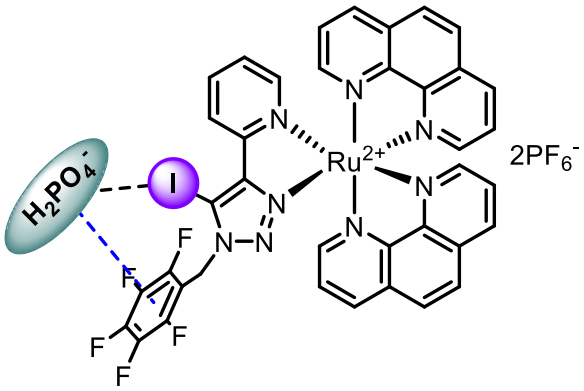


Fig. 1.27. Ghosh's $H_2PO_4^-$ host, showing the anion-π interaction (in blue) acting in concert with the primary XB interaction (in black) and electrostatic forces.

Electron-rich aromatic surfaces can form attractive interactions to cations,[130-131] which was demonstrated in a 2009 report by Rathore and co-workers concerning terphenyl crown-ethers, which formed strong (K_a > 10^5 M^{-1}) complexes with potassium cations in acetone-d_6 (Fig. 1.28).[132] The formation of cation-π interactions between the central benzene ring and the co-bound K^+ cation was indicated by downfield shifts in the aromatic signals and confirmed by the solid state XRD-determined structure, which showed close separation between the K^+ cation and the aromatic surface.

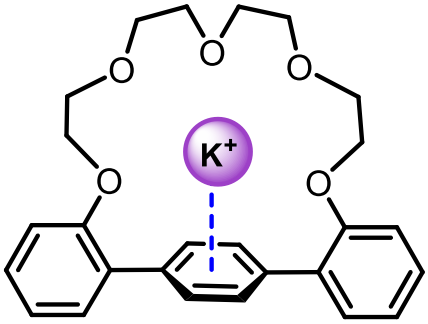


Fig. 1.28. Rathore's K^+ host with the cation-π interaction shown in blue.

The recognition of neutral molecules can also be mediated by π interactions,[133] which generally form between complementary pairs of electron-rich and electron-poor aromatic surfaces, as illustrated by the triphenylene – hexaazatriphenylene triimide donor-acceptor pair reported by Chai and Liu, which exhibited an impressive association constant K_a = 2.6 × 10^4 M^{-1} in DCM, attributed to the almost identical size and shape of the constituents of the donor-acceptor pair (Fig. 1.29).[134]

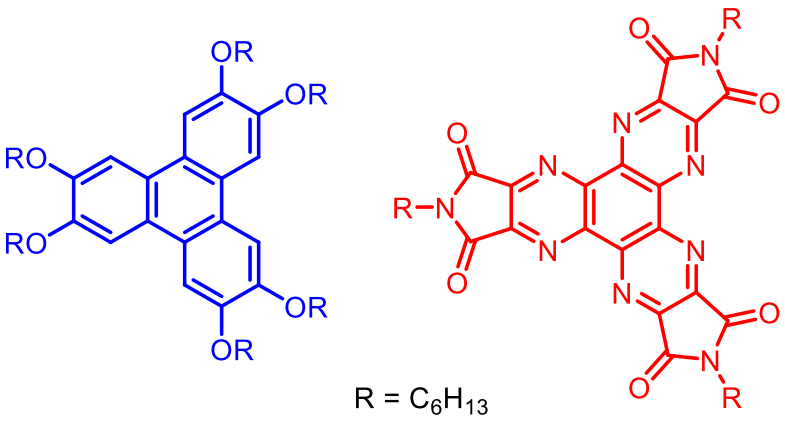


Fig. 1.29. Chai and Liu's triphenylene – hexaazatriphenylene triimide donor-acceptor pair (shown in blue and red respectively)

1.2.4 Synthetic Hosts for Anions

Supramolecular chemists have used the interactions surveyed above, often in combination, to design a plethora of hosts for anions and this section seeks to provide an overview of particularly notable examples.

1.2.4.1 Positively Charged Anion Hosts

As mentioned above, the early history of the field of anion host-guest chemistry was dominated by highly positively charged macrocyclic hosts capable of anion binding in water or water/methanol mixtures – the pioneering hosts reported by Park and Simmons, Lehn and Schmidtchen all fall into this category (Figs. 1.14 & 1.15). The recognition strategy employed by these receptors proved to be a powerful method for anion binding and many related positively charged systems have been reported in the ensuing five decades. For example, in 2014 Amendola and co-workers reported a hexa-cationic polyammonium aza-cryptand host,[135] capable of selective recognition of the radioactive pertechnetate $^{99}TcO_4^-$ anion in water (buffered to pH = 2 with 0.1 M CF_3SO_3Na) (Fig. 1.30). The ammonium cage host bound $^{99}TcO_4^-$ strongly with an association constant $K_a = 3.1 \times 10^5\ M^{-1}$, compared to $K_a(Cl^-) < 100\ M^{-1}$, demonstrating excellent selectivity. This was attributed to size match of the cryptand allowing the formation of multiple HB interactions with all four of the tetrahedral $^{99}TcO_4^-$ oxygen atoms simultaneously, as revealed by the XRD-determined solid state structure. Interestingly, anion-π interactions were also evident in the crystal structure between the oxo-anion and the anthracenyl moiety. The host was also capable of *sensing* $^{99}TcO_4^-$, through changes to the anthracene emission spectrum upon anion binding.

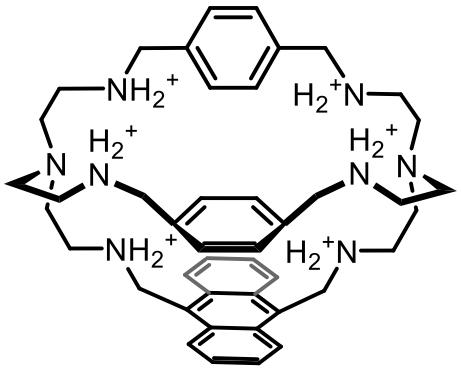


Fig. 1.30. Amendola's pertechnetate-selective polyammonium cryptand host.

Positively charged acyclic guanidinium hosts also demonstrated early promise, such as the receptors reported by Lehn in 1979 (Fig. 1.5a).[46] Due to the high pKa of the guanidium motif (pK_a = 13.8),[136] it has proved to be able to function in a much wider pH range than polyammonium hosts, and therefore continues to be deployed in more recent anion receptors. For example, Anslyn and co-workers reported a citrate-selective polyguanidinium host,[137] which exhibited an association constant for citrate of $K_a = 6.9 \times 10^3$ M^{-1} in water buffered to pH = 7.4 (Fig. 1.31). Impressively, due to the steric pre-organisation offered by the ethyl groups, the receptor exhibited a preference for citrate over the more highly charged ATP anion, indicating that the increased electrostatic attraction to the ATP anion could be outweighed by the selective influence of the directional HB interactions.

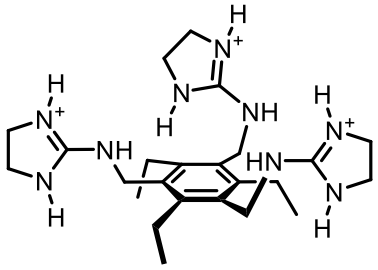


Fig. 1.31. Anslyn's citrate-selective polyguanidinium host.

Charge-assisted XB donor interactions have also been deployed to augment the binding properties of positively charged anion receptors. A distinct advantage of such hosts is that the XB interaction is particularly sensitive to through-bond polarisation;[138] the positive charge not only augments the electrostatic attraction of the host to the anionic guest, but also dramatically increases the XB donor strength by deepening the sigma hole. An elegant example was reported by Berryman and co-workers in 2018,[139-140] concerning a family of XB and HB 1,3-bis(4-ethynylpyridinium) receptors (Fig. 1.32). The XB host shown in Fig. 1.32a displayed a bromide association constant of $K_a(Br^-)$ = 4690 M^{-1} recorded in $CDCl_3$: CD_3NO_2 2:3 (*v/v*), whereas its HB analogue (Fig. 1.32c) exhibited $K_a(Br^-)$ = 1150 M^{-1} in the same solvent mixture, highlighting the potency of XB interactions to improve anion affinity. Interestingly, the XB host containing an aniline ring (Fig. 1.32b) exhibited a significantly higher chloride association constant ($K_a(Cl^-)$ = 23,700 M^{-1}) than both its HB analogue (Fig. 1.32d) and the related XB host lacking the amine group (Fig. 1.28a) ($K_a(Cl^-)$ = 2500 M^{-1} and ($K_a(Cl^-)$ = 2630 M^{-1} respectively). This enhanced anion affinity for the host containing the aniline group was attributed to intramolecular HB interactions formed between the aniline protons and the electron-rich central belt of the iodine XB donor atom (shown in red in Fig. 1.32b), both pre-organising the host and further polarising the XB donor atom for stronger XB anion binding. This strategy has been termed hydrogen bonding enhanced halogen bonding (HBeXB).[141]

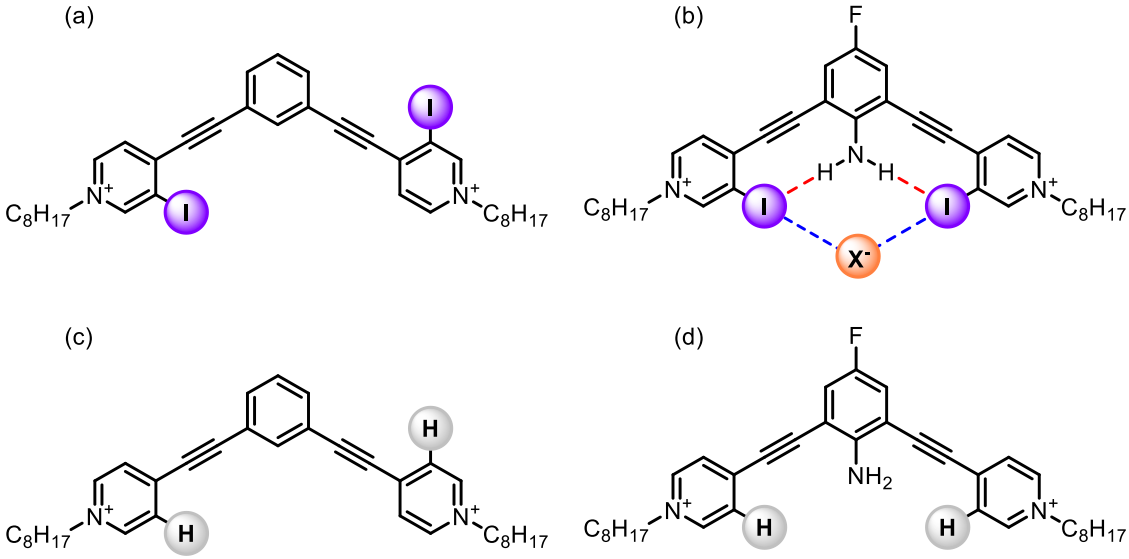


Fig. 1.32. Berryman's charged anion hosts: (a) conventional XB host, (b) pre-organised HBeXB host (XB interaction shown in blue, HB interaction shown in red), (c) and (d) the HB analogues of the XB receptors.

1.2.4.2 Neutral Hydrogen Bonding Anion Hosts

A key development in the progression of anion binding hosts was the construction of neutral receptors which offer improved selectivity, do not suffer from counter-anion competition and were originally designed to function in organic solvent media. The vast majority of the early examples relied on multiple convergent HB donor interactions for recognition.

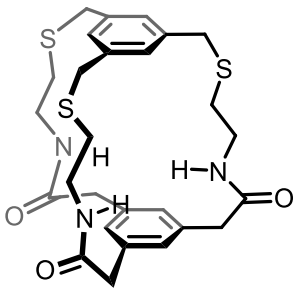


Fig. 1.33. Pascal's seminal amide-based anion host.

A seminal example of a neutral anion host based on HB interactions was reported by Pascal in 1986 (Fig. 1.33).[142] The cyclophane host proved capable of associating with

fluoride in DMSO-d_6, and the solid state XRD-determined structure revealed that the macrobicyclic cavity was of the right size to accommodate small anions, such as hydroxide and fluoride.

A drawback of notably acidic amide and related urea HB donors is that they are pH sensitive and can undergo deprotonation with basic anions such as fluoride in polar organic solvent media.[143] For example, in 2004 Fabbrizzi and co-workers reported a urea-based host, which bound carboxylates such as acetate strongly in acetonitrile ($K_a(CH_3COO^-) = 4.1 \times 10^6\ M^{-1}$) (Fig. 1.34). However, the acyclic receptor was not capable of reversibly binding fluoride, due to the halide's higher basicity. Analysis of the discontinuous isotherms obtained from UV-visible absorption and ^{1}H NMR experiments revealed that, upon addition of more than one equivalent of fluoride, the urea moiety was deprotonated and the highly stable, hydrogen-bonded anion HF_2^- was formed.

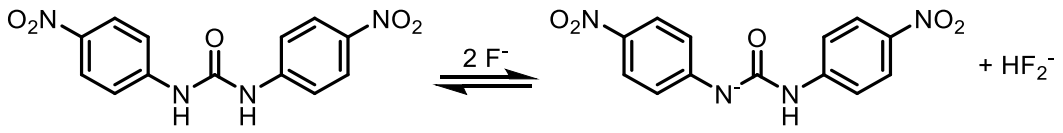


Fig. 1.34. Deprotonation of Fabbrizzi's urea anion host by the basic fluoride anion.

The use of CH HB donors, which are far less acidic than OH or NH donors, can overcome the issue of pH sensitivity.[144] The first report of a CH donor host for anion recognition was published by Farnham, Dixon and co-workers in 1990,[145] concerning a fluorinated macrocycle binding fluoride in THF through four concerted HB interactions from non-aromatic CH units, themselves polarised by adjacent CF_2 groups (Fig. 1.35).

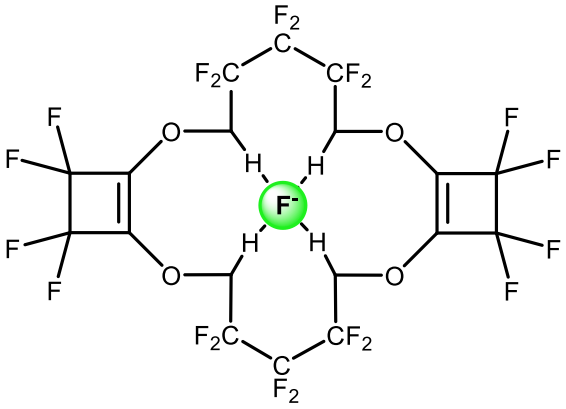
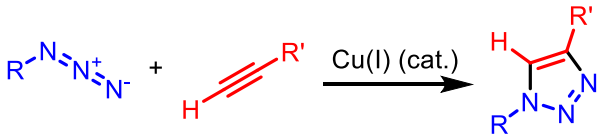


Fig. 1.35. Farnham and Dixon's fluorinated macrocycle, the first CH HB donor anion host.

Since then, a variety of aryl and heterocycle-based CH donor hosts have emerged, with 1,2,3-triazoles becoming particularly popular as a consequence of the facile Cu(I)-catalysed azide-alkyne cycloaddition (CuAAC) 'click' reaction (Scheme 1.1).[146-147]



Scheme 1.1. The CuAAC 'click' reaction, a convenient method for the generation of the 1,2,3-triazole CH HB donor motif.

A seminal example of a 1,2,3-triazole based anion receptor was reported by Li and Flood in 2008[148] – a highly pre-organised and rigid macrocyclic receptor which demonstrated a very strong affinity for chloride ($K_a(Cl^-)$ = 130,000 M^{-1}, DCM), a remarkable association constant value for a neutral host using only CH donor HB interactions, which highlights the potency of judiciously applying the aforementioned principles of good host design (Fig. 1.36a). In 2019, Flood built upon this work to achieve the important goal of anti-Hofmeister anion extraction from water. A related macrobicyclic anion binding 'cage' demonstrated the ability to extract NaCl from water into dichloromethane at an efficiency (relative to the concentration of host) of 18% (Fig. 1.36b).[149] In contrast, no extraction of

NaI was observed, despite its lower hydration enthalpy, which was ascribed to the cavity of the cage being of complementary size for chloride, but too small for iodide.

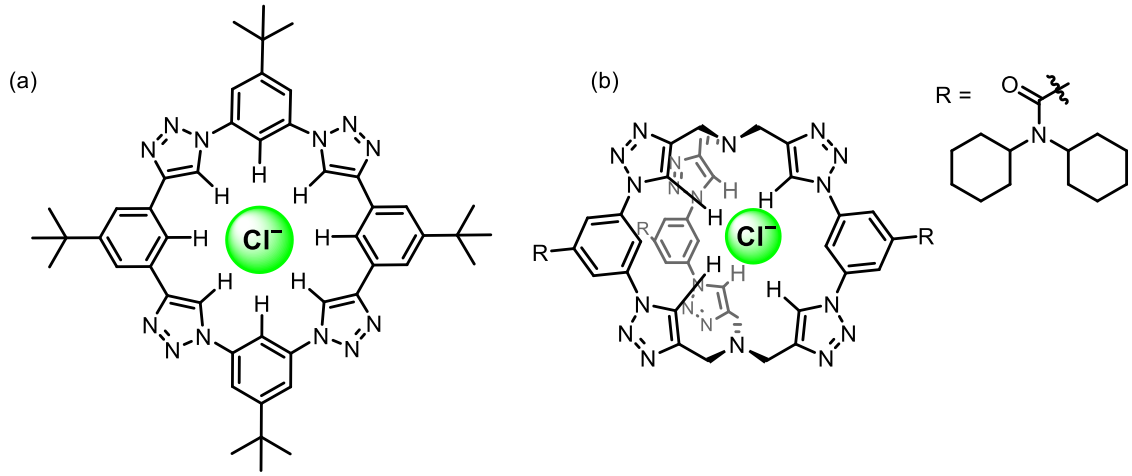


Fig. 1.36. Flood's (a) macrocyclic chloride host, using 1,2,3-triazole CH HB donor moieties and (b) chloride binding 'cage', capable of anti-Hofmeister liquid-liquid extraction.

1.2.4.3 Neutral Halogen Bonding Anion Hosts

Due to the advantages of XB interactions over more conventionally employed HB interactions, most importantly their enhanced anion binding strength, more stringent directionality and greater hydrophobicity, in recent times XB hosts have increased in popularity. The first example of an XB anion receptor, reported by Metrangolo, Resnati and co-workers in 2005, employed iodoperfluoroarene XB donor motifs (Fig. 1.37a).[150] In $CDCl_3$ solution, this heteroditopic receptor bound a sodium cation through the polyether region and an iodide anion *via* one XB interaction (the geometry of the host precluded convergent XB interactions with multiple XB donors simultaneously).

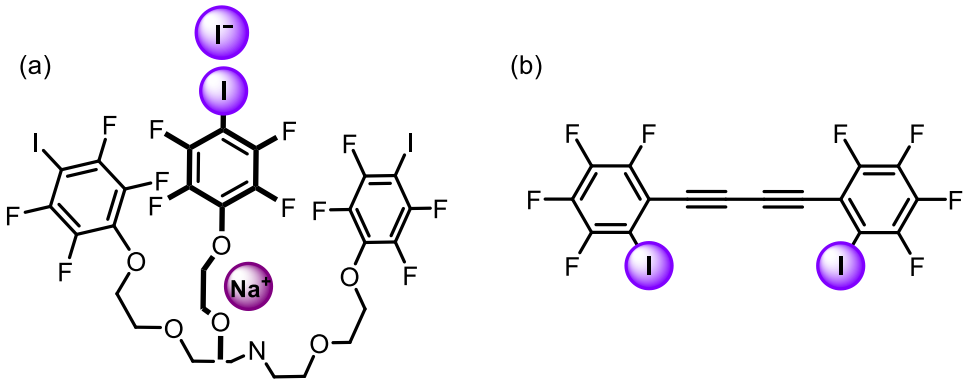


Fig. 1.37. (a) Metrangolo and Resnati's XB anion receptor and (b) an example of the iodoperfluoroarene anion hosts reported by Taylor.

This pioneering work was built on by Taylor and co-workers, who described a large family of polydentate XB anion hosts using iodoperfluoroarene XB donor motifs.[151-153] The host shown in Fig. 1.37b,[151] reported in 2013, demonstrated the frequently observed preference of XB donors for halide anions over oxo-anions,[154] exhibiting $K_a(Cl^-) = 1.2 \times 10^3\ M^{-1}$ and $K_a(NO_3^-)$, $K_a(HSO_4^-) < 50\ M^{-1}$, determined in acetone by ^{19}F NMR titration experiments.

In 2005, the preparation of 5-iodo-1,2,3-triazole (iodotriazole) derivatives by a copper(I)-catalysis methodology was reported,[155] which, alongside subsequent refinements to this synthetic procedure,[156-158] paved the way for the multitude of supramolecular hosts built around this powerful XB donor motif which would follow,[122] facilitated by the convenient and high-yielding 'click' methodology. A pair of such receptors was reported by Schubert and co-workers in 2015 (Fig. 1.38a-b).[159] The carbazole-based host shown in Fig. 1.38a, pre-organised for anion binding through the formation of intramolecular HB interactions between the triazole *N*-atom and the nearby phenolic groups, displayed a significantly enhanced affinity for chloride ($K_a(Cl^-) = 7.1 \times 10^4\ M^{-1}$), in comparison to the conformationally flexible receptor analogue

shown in Fig. 1.38b, lacking this pre-organisation ($K_a(Cl^-)$ = 2.3 × 10^3 M^{-1}), both measured in THF *via* ITC experiments. Interestingly, the entropy change upon anion binding was positive for the pre-organised host (+34 J K^{-1} mol^{-1}), reflecting the release of solvent molecules from the host and guest, whereas it was negative for the conformationally flexible host (-18 J K^{-1} mol^{-1}), due to the loss of conformational freedom upon anion binding. In 2017, Kubik and co-workers incorporated XB donors into a pseudopeptide macrocyclic host (Fig. 1.38c),[160] which demonstrated superior anion affinity in aqueous-containing media, $K_a(Cl^-)$ = 1.9 × 10^3 M^{-1} in DMSO-d_6 : H_2O 195:5 (*v*/*v*), compared with the HB analogue which displayed no detectable binding in the same solvent mixture.[161]

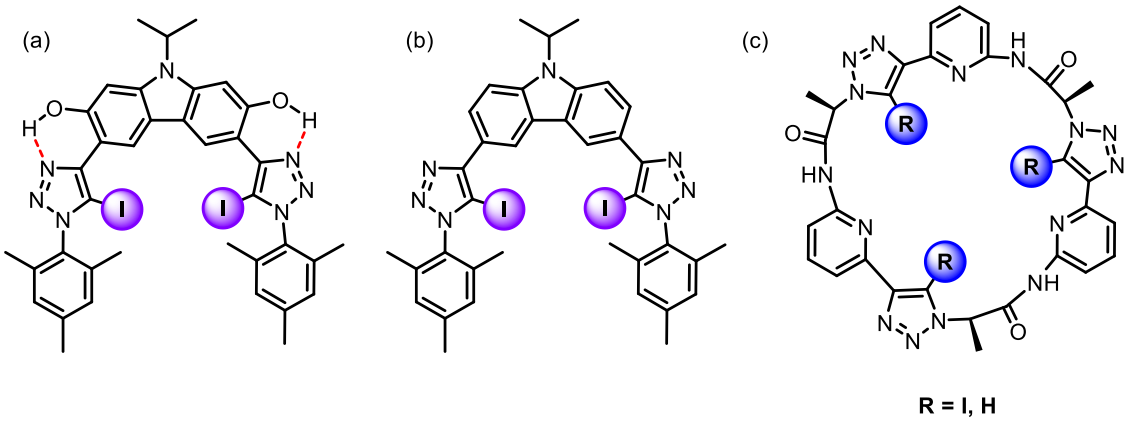


Fig. 1.38. Schubert's XB anion hosts: (a) pre-organised through intramolecular HB interaction (shown in red) and (b) conformationally flexible. (c) Kubik's XB and HB cyclopseudopeptide anion hosts.

1.2.5 Synthetic Hosts for Neutral Molecules

The effective recognition of neutral species, particularly in aqueous media, requires a different approach to that taken in respect of anion recognition. Typically, hydrophobic effects are harnessed as the main driving force for guest binding, with secondary interactions such as hydrogen bonding also being deployed to confer selectivity.[97] An example of such an approach was reported by Davis and co-workers in 2020,[162] who

synthesised a host for purine nucleotide base derivatives (Fig. 1.39). Whilst overall the receptor was anionic, due to the peripheral polycarboxylate water-solubilising groups, the central host cavity, containing hydrophobic aromatic surfaces, was uncharged and thus able to leverage hydrophobic effects to assist in the binding of the organic guest, giving rise to an impressive association constant value K_a = 8.7 × 10^6 M^{-1} for the purine derivative hypoxanthine (water buffered to pH 7.4 with 10 mM phosphate).

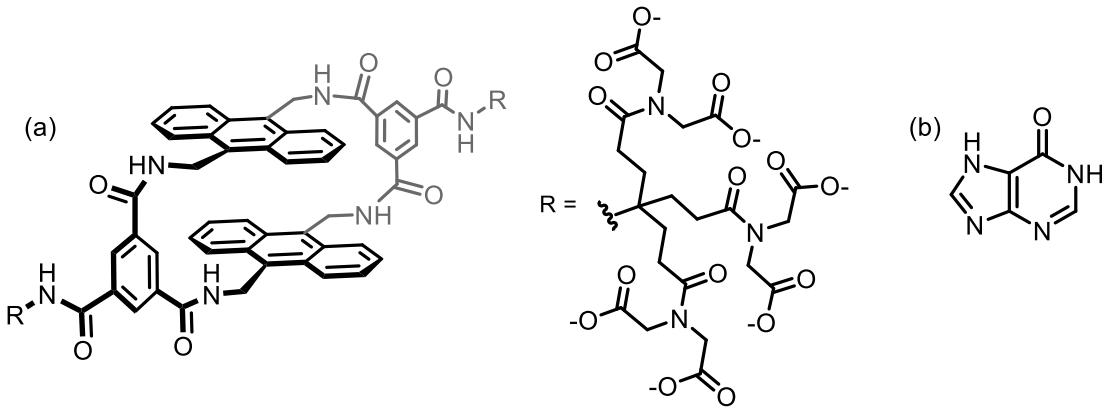


Fig. 1.39. (a) Davis's anthracene-based macrocyclic receptor for purine derivatives such as (b) hypoxanthine.

The use of halogen bonding for the binding of neutral guests has received much less interest than the related field of XB anion hosts. However, employing XB interactions for association with neutral species has been probed for a number of systematic studies.[126, 152] For example, in 2010, Taylor and co-workers investigated the interaction between two monodentate XB donors and a variety of neutral Lewis-basic molecules,[152] observing relatively weak association constants in the highly non-competitive organic solvent cyclohexane (e.g. $K_a(Bu_3PO)$ = 18 M^{-1} for iodoperfluorooctane) (Fig. 1.40). The observation of association with Bu_3PO was particularly interesting, given the ubiquity of chemical warfare agents containing P=O double bonds. XB hosts have also found use as organo-catalysts,[28, 163-164] for which the substrates are normally neutral haloalkanes (see Fig. 1.2b),

however binding of the neutral substrate, whilst implied by the mechanism of catalyst, is not normally directly observed or quantified.[165]

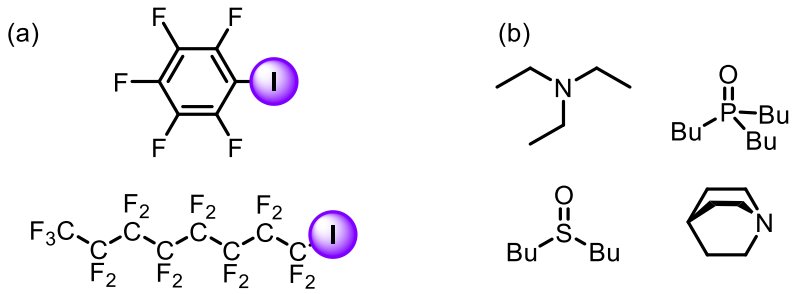


Fig. 1.40. (a) Monodentate XB donors investigated by Taylor for the binding of (b) neutral species.

1.2.6 Synthetic Hosts for Ion-pairs

Heteroditopic ion-pair receptors, which feature two distinct binding sites for the simultaneous recognition of oppositely charged species, have attracted considerable interest as a class of supramolecular hosts despite their more intricate structures and synthetic complexity.[166] This interest largely stems from their superior affinity and selectivity towards charged species when compared to their monotopic receptor counterparts, particularly anion hosts.[15, 31, 33-35, 167] Moreover, the ability to bind both a cation and an anion simultaneously is better suited to the practical applications of supramolecular hosts, wherein an ion will always be found together with its counterion, which is highly likely to be coordinating.[168] For example, ion-pair hosts have been used as membrane transporters,[31] for salt extraction,[33, 169] and as salt solubilisation agents.[170]

Ion-pair receptors may be classified by the binding mode by which they recognise an ion-pair, which is either as a *contact ion-pair*, in which the co-bound ions are in direct contact with each other or as a *separated ion-pair*, wherein either the host itself or a solvent molecule lies in between the constituent ions of the ion-pair (Fig. 1.41).

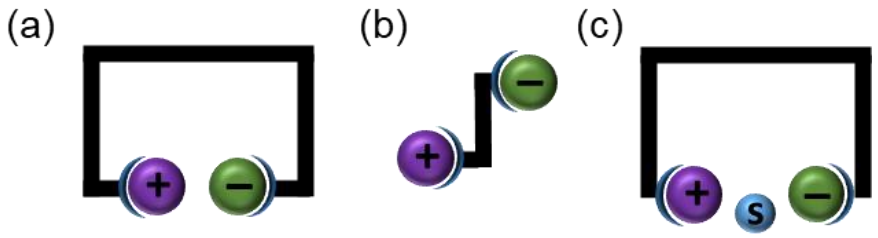


Fig. 1.41. Schematic cartoons representing (a) a contact ion-pair, (b) a host separated ion-pair and (c) a solvent separated ion-pair.

The superior binding properties exhibited by heteroditopic ion-pair receptors in comparison to monotopic host analogues are normally as a result of *positive cooperativity*, which refers to the mutual beneficial influence of the co-bound species on each other's binding affinity, attributable to a combination of proximal favourable electrostatic interactions, through-bond polarisation and/or conformational allosteric effects. The latter is elegantly demonstrated in nature by the O_2-transport protein haemoglobin, for which the binding of one molecule of O_2 improves its affinity for subsequent O_2 binding by a factor of up to 300.[171]

Electrostatic positive cooperativity was demonstrated by the lithium halide ion-pair host reported by Sessler, Kim and co-workers in 2024,[172] which consisted of a calix[4]pyrrole anion binding site, strapped with a phenanthroline lithium cation binding motif (Fig. 1.42a). Whilst the host exhibited very weak binding (< 5 M^{-1}) of lithium cations and chloride anions independently, it proved capable of strongly binding LiCl (K_a(Cl) > 10^5 M^{-1} in the presence of one equivalent of Li^+ and *vice versa*) and also was able to extract the LiCl ion-pair into DCM from water. Crystal structures revealed the formation of a contact ion-pair with strong electrostatic attraction between the cation and co-bound anion. In 2017, Schubert and co-workers reported a crown ether-embedded (iodo)triazole ion-pair receptor, which bound NaI in a host-separated manner (Fig. 1.42b).[173] A

significant enhancement in the iodide affinity of the XB host was observed in the presence of one equivalent of sodium cations ($K_a(I^-)$ increased from < 5 M^{-1} to 135 M^{-1} in CD_2Cl_2 : CD_3CN 3 : 1 (*v*/*v*)), which was attributed to both electrostatic attraction between the oppositely charged ions and also polarisation of the XB donor, leading to a stronger interaction with the anion. It is noteworthy that the HB analogue did not exhibit iodide binding in either the presence or absence of sodium cations in this solvent mixture.

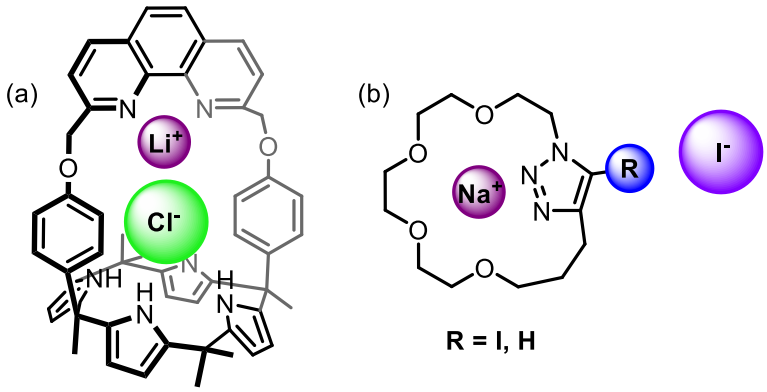


Fig. 1.42. (a) Sessler and Kim's heteroditopic lithium halide ion-pair receptor. (b) Schubert's XB NaI ion-pair receptor and its HB analogue.

Halogen bonding has exhibited a significant advantage over hydrogen bonding in achieving positive cooperativity, as it has consistently proved to be more sensitive to through-bond polarisation, presumably due to its greater covalent contribution.[13, 138, 174] This advantage was utilised by Docker *et al.* in 2021 to effect the highly cooperative binding of sodium halide ion-pairs by an XB heteroditopic receptor (Fig. 1.43a).[174] The binding of halides by both the XB and HB hosts was weak in the absence of co-bound Na^+ cations, with $K_a(Br^-)$ < 50 M^{-1} for both hosts in DMSO-d_6 : $CDCl_3$ 1:9 (*v*/*v*). However, upon complexation with two equivalents of Na^+, the bromide association constant was increased by a factor of 130 for the XB receptor, compared to a modest factor of 20 for the HB host. The increases in anion association constants were a consequence of electrostatic

attraction between the co-bound constituents of the ion-pair, with the larger enhancement for the XB host attributed to an additional increase in the strength of the XB interaction due to the through-bond polarisation of the XB donor induced by cation binding – an effect not replicated in the HB analogue.

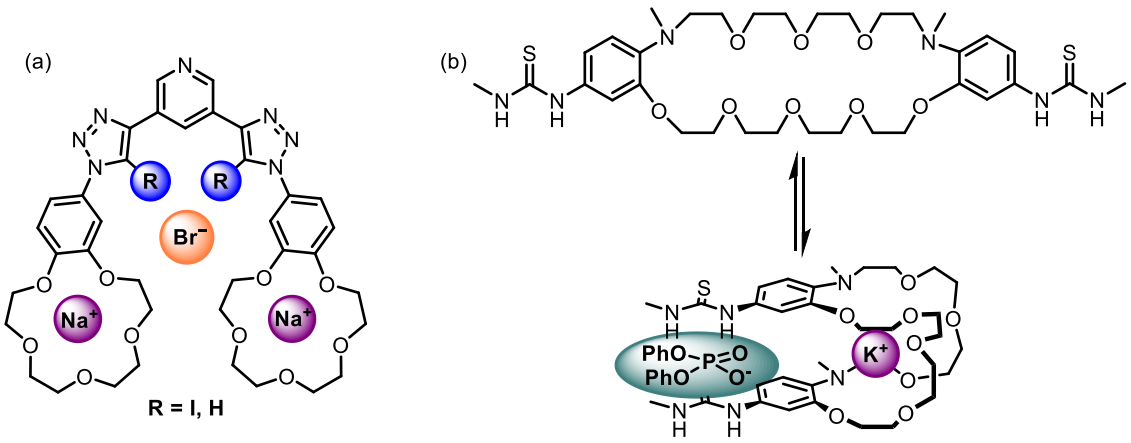


Fig. 1.43. (a) Docker *et al.*'s heteroditopic ion-pair receptor demonstrating through-bond polarisation effects. (b) Kubo's allosterically cooperative ion-pair receptor based on conformational changes in the crown-ether upon cation binding.

Allosteric positive cooperativity was shown by Kubo's bis(thiourea)-substituted dibenzo-diaza-30-crown-10 receptor,[175] which underwent a large conformational change upon potassium cation complexation which served to pre-organise the bis(thiourea) binding site for diphenylphosphate anion recognition (Fig. 1.43b). The affinity of the receptor for the diphenylphosphate anion was improved by a factor of 19 by potassium cation pre-complexation in CD_3CN.

1.3 Supramolecular Sensing of Anions and Neutral Species

Having covered the principles that underpin effective host design, the non-covalent interactions frequently employed by hosts for anions and neutral molecules, and having surveyed the various categories of previously developed hosts, this section explores one of the main uses of host systems: supramolecular sensing. This is a highly active area of research within the field of supramolecular chemistry, because the sensing of anions and neutral species is of crucial importance for environmental monitoring and medical applications,[176-179] including in the implementation of responsive treatments for diseases such as diabetes.[180]

A *sensor* is a system which can indicate the presence and concentration of a target analyte *via* a macroscopic, observable response.[178, 181-182] Typically, this measurable response (or signal) is either optical or electrochemical – modalities which readily lend themselves to incorporation into compact devices suitable for real-world applications.[176] This thesis focuses on optical methods for sensing and this section first outlines the various approaches to optical sensing and then surveys important prior examples of supramolecular optical sensors for anions and neutral species.

1.3.1 Optical Sensing Approaches

Whilst a supramolecular approach to optical sensing is appealing for a variety of reasons, it is one amongst many methods of optical chemical sensing, which notably also include chemidosimeters and displacement assays (Fig. 1.41). This section provides a brief overview of these alternative sensing modalities and the advantages that a supramolecular approach has over each of them.

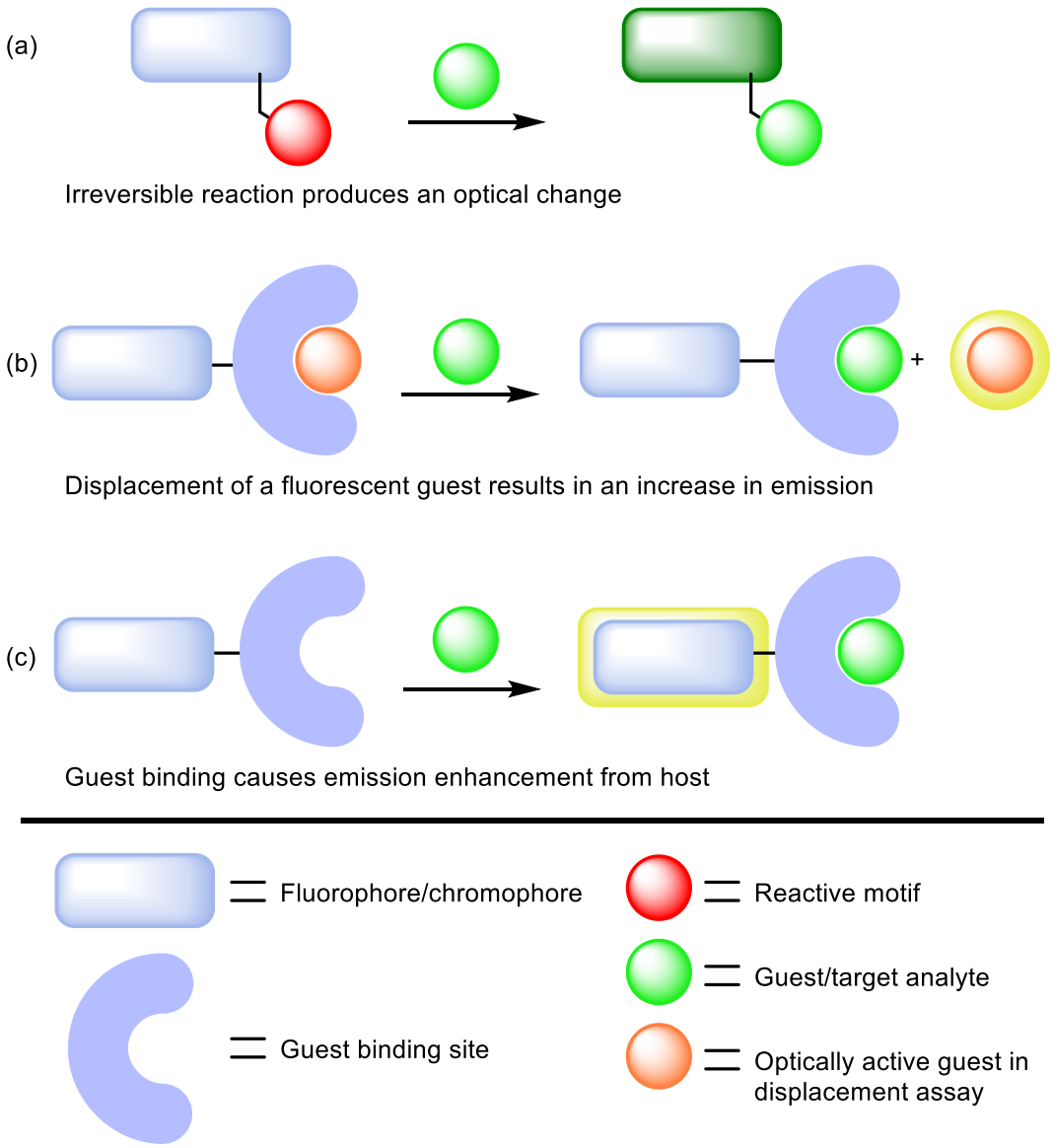


Fig. 1.44. Schematic representations of general methods of chemical sensing: (a) a chemidosimeter, (b) a displacement assay and (c) a supramolecular sensor.

Chemidosimeters: An optical chemidosimeter is a molecule which irreversibly reacts with its target analyte, changing the optical properties of the molecule and producing the sensing signal (Fig. 1.44a).[183] Chemidosimeters can be designed to be highly specific for their target, but as the sensing process relies on an irreversible reaction, they cannot be used repeatedly or for continuous monitoring.

Displacement Assays: A displacement assay is a multiple component system, generally consisting of a host pre-complexed to an optically active guest.[184] In the presence of the target analyte, the optically active guest is displaced from the host, resulting in a detectable optical change (Fig. 1.44b). Displacement assays are a useful method of adding sensing capability to an optically-inactive host, but are complex and fickle systems, which are not suitable for continuous operation in flowing analyte streams.

Supramolecular Sensing: A supramolecular optical sensor first acts as a host by binding its target analyte but then additionally relays this binding event through a discernible change in its optical properties (Fig. 1.44c). In contrast to the other methods, due to its reversibility, supramolecular sensing allows the construction of continuous monitoring devices[124] and reusable sensors[18] and therefore only requires a very small amount of sensor to be prepared. For this reason, they are a very attractive sensing solution.

1.3.2 Absorbance-Based Optical Sensors for Anions and Neutral Species

Supramolecular optical sensors can be split into two categories: absorbance-based sensors, in which guest complexation perturbs the ground state of the host, thus inducing a change in the host's absorbance spectrum; and fluorescent emission-based sensors, in which the excited state of the sensor is perturbed by guest binding and changes to the host's emission spectrum are induced.

Absorbance-based sensors have a key advantage of offering naked-eye detectable colourimetric changes in the presence of their target analyte, which renders them exceedingly easy to incorporate into a useful sensing device. An example of a naked-eye detectable colourimetric sensor was reported by Sessler and co-workers in 2000, which consisted of a calix[4]pyrrole anion binding motif conjugated to an anthraquinone optical

reporter group (Fig. 1.45).[185] Addition of a variety of anions to a DCM solution of the receptor caused visible changes in the colour of the solution, which differed according to the identity of the anion, allowing discrimination between different anionic species. These spectral changes were tentatively attributed to charge transfer processes between the bound anion and the anthraquinone unit.

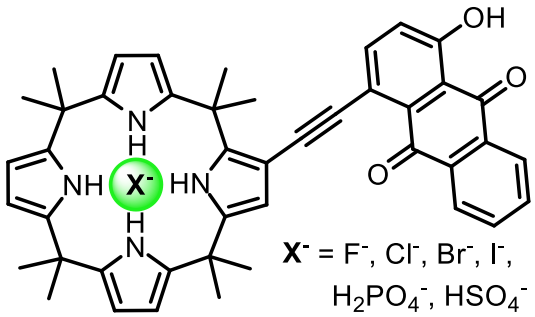


Fig. 1.45. Sessler's colourimetric anion sensor.

In addition to their benefits for guest recognition, XB interactions have also demonstrated superior signal transduction for anion sensing – specifically, XB sensors have shown relatively larger magnitude sensing responses in comparison to their HB analogues. A large magnitude sensing response is desirable for real-world applications,[176] as it improves the signal-to-noise ratio of a sensor,[186] and therefore optical XB anion sensors are an active area of research within supramolecular chemistry. For instance, in 2018, Lim and Beer reported a pyrrole-containing XB anion sensor, capable of sensing of halides and oxo-anions in aqueous-containing media (Fig. 1.46).[187] Upon addition of chloride and nitrate to a H_2O : ACN 1:9 (*v/v*) solution of the sensors, both the XB and the HB receptors showed changes in the pyrrole absorption band, centred at 315 nm. Notably, the XB sensor exhibited significantly greater magnitude responses, with a 30% increase and a 44% decrease in absorbance for chloride and nitrate respectively, compared to a 15% increase and a 34% decrease recorded for the HB analogue. These larger magnitude

sensing responses, combined with its enhanced anion binding affinity ($K_a^{XB}(Cl^-)$ = 1400 M^{-1}, $K_a^{HB}(Cl^-)$ = 630 M^{-1}) rendered the XB sensor considerably more sensitive and potent than its HB congener.

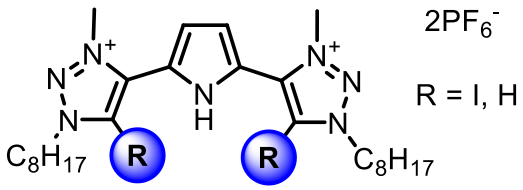


Fig. 1.46. Lim and Beer's pyrrole-based anion sensor.

Selectivity towards a particular analyte is a crucial property of an optimal sensor. Supramolecular optical sensors can achieve selective sensing responses by either employing a selective binding domain (improving the selectivity of the host component of the sensor) or by engineering the sensing mechanism to be selective for a target analyte. The former approach was utilised in 2013 report by Boyle *et al.*,[188] with a Tröger's base scaffold appended with thiourea HB donor sites for colourimetric sensing of AcO^- and $H_2PO_4^-$ (Fig. 1.47). Upon addition of AcO^- or $H_2PO_4^-$ anions to a DMSO solution of the host, a significant increase in absorbance at 480 nm was observed, however, minimal changes to the UV-visible spectrum were observed upon addition of SO_4^{2-}. ^{1}H NMR titrations in DMSO-d_6 confirmed that whilst AcO^- and $H_2PO_4^-$ interacted with the thiourea protons through HB interactions, SO_4^{2-} did not bind to the host and therefore did not produce a colourimetric response.

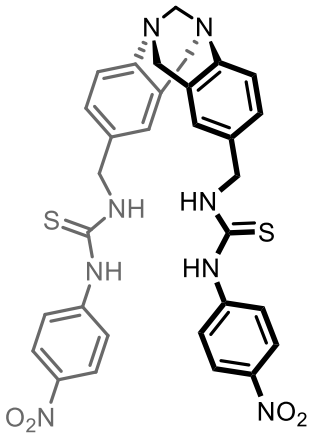


Fig. 1.47. Boyle *et al.*'s colourimetric sensor for AcO^- and $H_2PO_4^-$.

The latter approach was demonstrated in a 2024 report by Tay *et al.*,[19] which concerned an XB chloride-selective [2]rotaxane sensor using an naphthalene diimide (NDI) chromophore (Fig. 1.48a). Although the rotaxane bound both chloride and iodide with comparable association constants ($K_a(Cl^-)$ = 3250 M^{-1}, $K_a(I^-)$ = 2720 M^{-1}, measured in D_2O : acetone-d_6 5:195 (*v/v*) *via* ^1H NMR titration experiments), the sensor only responded optically to chloride binding. This was attributed to the different binding mode of the two anions – only chloride binding induced shuttling of the macrocycle away from the NDI unit on the axle (Fig. 1.48c), because the other halide anions were too large to be bound endotopically by both the axle and macrocycle components of the rotaxane. Therefore, only chloride caused changes to the NDI absorption spectrum, *via* loss of charge-transfer interactions between the NDI unit and macrocycle-based hydroquinone moieties (Fig. 1.48b).

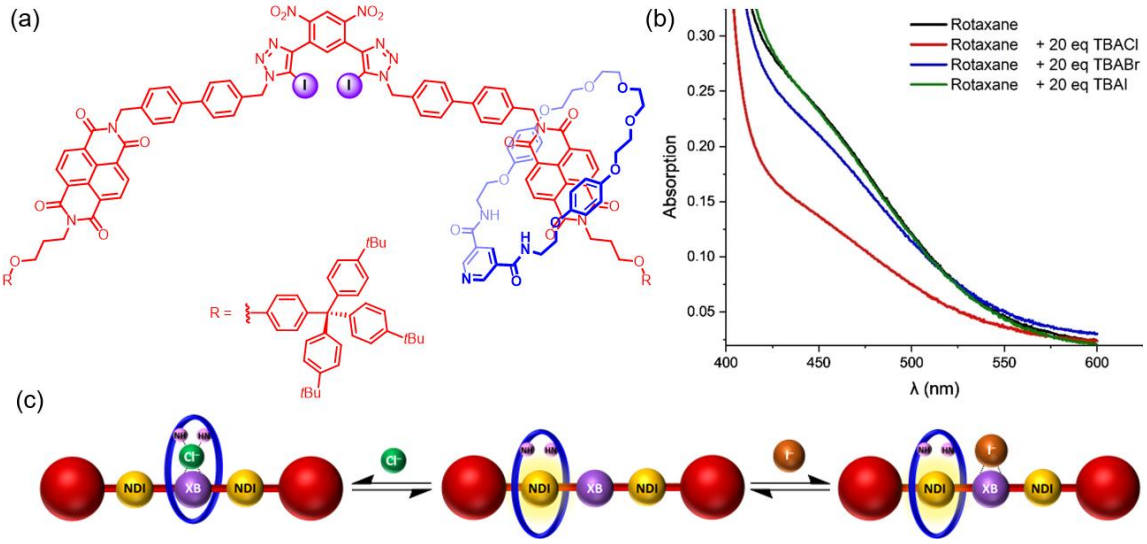


Fig. 1.48. (a) Tay *et al.*'s chloride selective rotaxane sensor, (b) its absorption spectrum in the presence of various anions, showing the selective response to chloride, and (c) the proposed mechanism giving rise to the observed selectivity.

Absorbance-based sensors for neutral species are rarer, possibly due to the weaker interactions that characterise host-guest complexes with neutral species being unable to significantly perturb the absorbance spectra of host chromophores. Nonetheless, Würthner and co-workers have reported perylene-based absorbance sensors for the HB-mediated sensing of melamine (Fig. 1.49).[189] The absorbance spectrum of the perylene imide host underwent significant changes upon binding of the melamine guest through concerted HB interactions in methylcyclohexane (MCH) and carbon tetrachloride. Fitting of these spectral changes to a 1:1 stoichiometric host-guest binding model allowed association constants of 54,000 M^{-1} and 4,080 M^{-1} to be determined in MCH and CCl_4 respectively. Interestingly, an analogue of the perylene imide host, lacking the alkyl group on the non-binding imide *N*-atom, proved capable of forming supramolecular polymers with melamine derivatives, as shown by TEM and SEM studies.

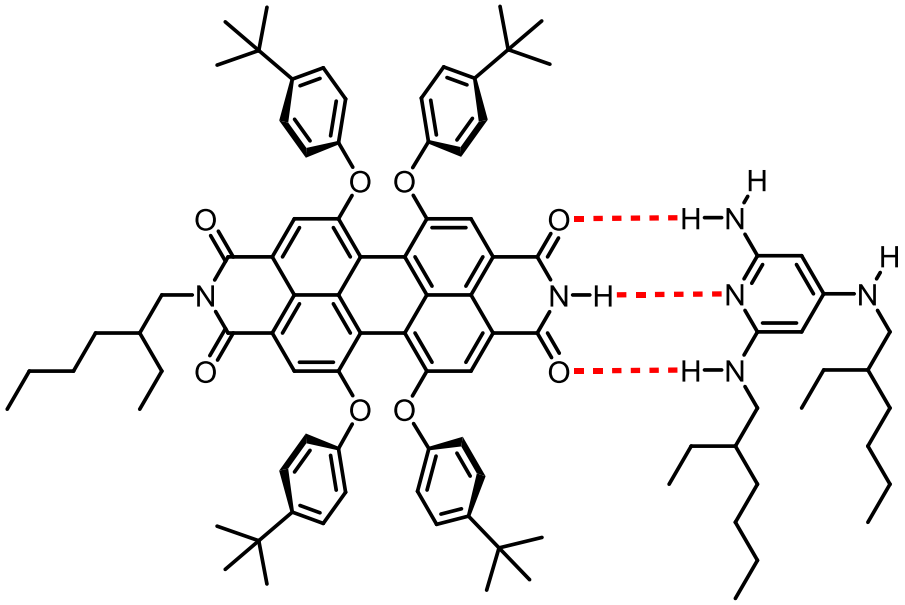


Fig. 1.49. Würthner's HB perylene hosts for neutral species with HB interactions shown in red.

1.3.3 Emission-Based Optical Sensors for Anions and Neutral Species

In comparison to absorbance-based sensing, emission-based sensing offers much improved sensitivity, as fluorescence spectroscopy is a far more sensitive technique than absorption spectroscopy, and acquisition times are also significantly reduced.[190] Emission-based sensors also offer increased structural flexibility and diversity, as the fluorescent reporter group need not be directly appended or even covalently linked to the guest recognition site,[191-192] due to the myriad ways in which guest binding can influence the emission spectrum of the fluorophore, which include: photo-induced electron transfer (PET),[192-193] vibronic relaxation,[194-195] rigidification,[196] aggregation,[25, 197] and excimer formation.[198-199] For example, in 2003 Gunnlaugsson and co-workers reported a thiourea-based anion host appended with NDI fluorescent reporter groups (Fig. 1.50).[200] Upon addition of $H_2PO_4^-$ in DMSO, significant quenching of the NDI emission was observed, which allowed sensing of $H_2PO_4^-$ with K_a = 790 M^{-1}. However, no significant changes to the UV-visible spectrum of the receptor were noted – indicating the superior sensitivity of the

fluorescence technique to remote anion binding. The quenching of the NDI emission was attributed to enhanced PET from the thiourea moiety to the NDI fluorophore in the presence of a bound anion.

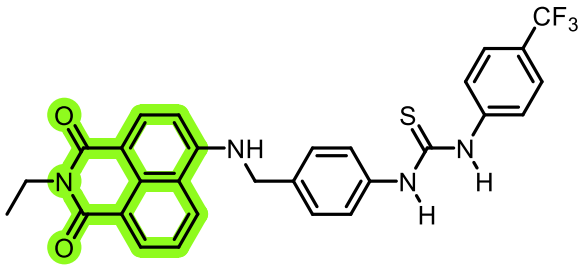


Fig. 1.50. Gunnlaugsson's thiourea-based anion sensor, with the NDI fluorescent reporter group highlighted in green.

In the context of fluorescence sensing, XB interactions have also demonstrated superior signal transduction characteristics, relative to their HB counterparts. In 2016, Ghosh and co-workers reported a pair of Ru(II) based hosts,[201] capable of selective MLCT emission sensing of $H_2PO_4^-$ and $HP_2O_7^{3-}$ in acetonitrile (Fig. 1.51). An impressive 17-fold increase in emission intensity response to $H_2PO_4^-$ binding was shown for the XB sensor, whereas the HB analogue showed only a 6-fold emission enhancement. Only for the XB sensor did this impressive emission intensity enhancement persist in aqueous-containing media, with a 3-fold turn-on response to $H_2PO_4^-$ binding observed in H_2O : ACN 1:4 (*v*/*v*), whereas the HB counterpart showed no response to $H_2PO_4^-$ in the same solvent medium. This highlights the ability of hydrophobic XB interactions to continue to exhibit good signal transduction in aqueous media, whereas conventionally employed HB interactions often prove to be more severely attenuated in the presence of water.

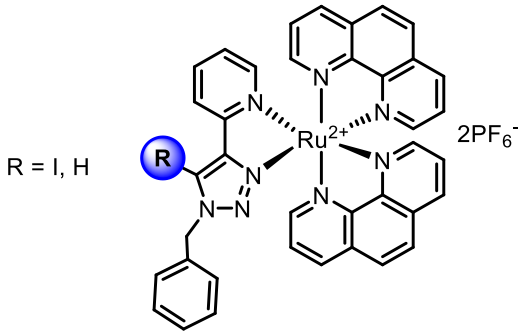


Fig. 1.51. Ghosh's Ru(II) based sensor for $H_2PO_4^-$ and $HP_2O_7^{3-}$.

As for absorbance-based sensors, selectivity towards a particular analyte can be engineered through either the binding selectivity of the host or *via* careful design of the sensing mechanism. A particularly impressive example of sensing mechanism-induced selectivity was reported by Caballero, Molina and co-workers in 2016.[202] An anthracene-appended acyclic XB bromo-imidazolium receptor and its HB analogue were reported (Fig. 1.52a). In acetonitrile, the XB sensor exhibited no changes in the anthracene emission spectrum when exposed to chloride, bromide, iodide, and certain oxoanions, including HSO_4^- and NO_3^-. However, F^- and SO_4^{2-} caused significant fluorescence quenching, attributed to a PET mechanism. Notably, the addition of $H_2PO_4^-$ resulted in the emergence of a higher-wavelength emission band due to the intramolecular formation of an anthracene excimer, which was attributed to the unique binding mode of this anion and allows the XB probe to selectively detect dihydrogen phosphate. Interestingly, no anion triggered an increase in excimer emission from the HB sensor, rendering it incapable of selective sensing. Similar sensing mechanism-derived selectivity was demonstrated by a report from Curiel and co-workers in the same year, when they reported a biscarbazole-based dicarboxylate sensor which exhibited a selective, naked-eye detectable fluorescence response to glutarate over other dicarboxylates (Fig 1.52b).[203] ^{1}H NMR titration experiments in DMSO-d_6 indicated that the host displayed similar affinities for a

variety of dicarboxylate anions (K_a(glutarate) = 3600 M^{-1}, K_a(adipate) = 2700 M^{-1}). However, addition of glutarate caused a change in the colour of fluorescence emission from blue to green, which was not observed for other anions. This was attributed to the size complementarity of the host for glutarate enhancing the emission of charge transfer bands in the host-guest complex and allowed selective detection of glutarate, which is implicated in glutaric aciduria, a metabolic disease.[204]

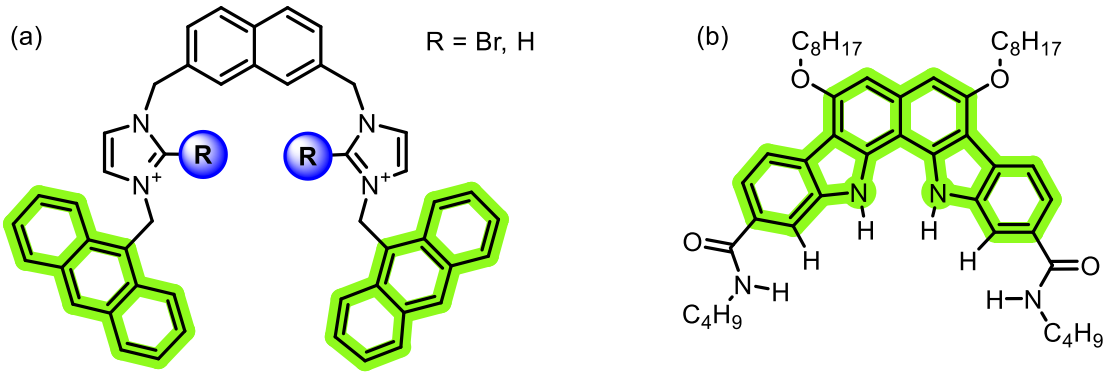


Fig. 1.52. (a) Caballero and Molina's anthracene-based (highlighted in green) anion sensor, capable of selective dihydrogen phosphate sensing. (b) Curiel's carbazole-based (highlighted in green) selective glutarate sensor.

Sensors capable of detecting the presence of ion-pairs have also been developed. For instance in 2018, Caballero and Molina reported an XB tetraphenylethylene (TPE) sensor capable of detecting HSO_4^-,[205] but only in the presence of co-bound Zn^{2+} cations (Fig. 1.53). Addition of Zn^{2+} cations to an acetonitrile solution of the XB receptor increased the fluorescence emission intensity from the TPE fluorophore 18-fold, binding in a 1:2 host-guest stoichiometry through the imidazole *N*-atoms. Addition of a wide variety of anions (as their TBA salts) did not provoke an emission response from either receptor, showing that the sensors could detect Zn^{2+} but not anions alone. However, if HSO_4^- anions were added to an acetonitrile solution containing either sensor pre-complexed with two

equivalents of Zn^{2+}, anion binding was observed, with marked fluorescence changes – HSO_4^- caused an increase in emission intensity of over 100% for the XB sensor and was bound strongly with a 1:2 host-guest stoichiometry (K_1= 2.2 × 10^5 M^{-1} and K_2 = 3.4 × 10^4 M^{-1}).

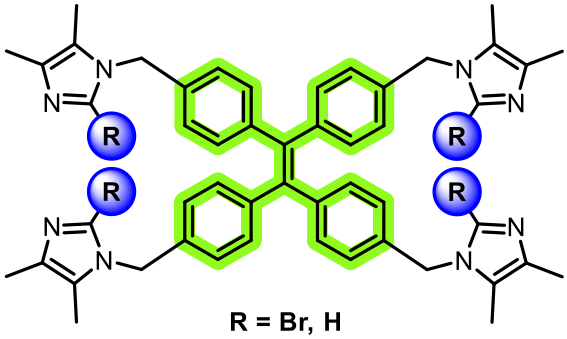


Fig. 1.53. Caballero and Molina's TPE ion-pair sensor

Fluorescent supramolecular sensors for neutral species are rarer than for anions, but are known.[206] For example, the anthracene-based receptor reported by Davis and co-workers (Fig. 1.39a), exhibited an approximately three-fold increase in anthracene emission intensity upon addition of hypoxanthine in 10 mM phosphate buffer (pH 7.4).[162] A further example was reported in 2023 by Dar and co-workers,[207] which related to the use of XB anils for the detection of nitroaromatic compounds, which are commonly used in explosives.[208] This work exploited a phenomenon known as aggregation-induced emission (AIE), in which a fluorophore only becomes emissive once it has formed into aggregates, to give rise to very large sensing responses.[209] Three halogenated anils were reported (Fig. 1.54), which showed a marked increase in emission intensity in THF upon addition of increasing fractions of water. DLS studies confirmed that maximum emission intensity occurred at the same water fraction at which the maximum particle size was observed, confirming the proposed AIE mechanism, which itself was attributed to the hydrophobicity of the halogen-appended anils. These aggregates were subsequently used for the sensitive detection of nitroaromatic compounds, in particular picric acid. Addition

of picric acid and other nitroaromatic compounds to organo-aqueous solutions of various compositions (H_2O : THF 9:1 (*v/v*) to H_2O : THF 3:2 (*v/v*)) of the receptors led to dramatic emission quenching (greater than 100-fold). The mechanism of this quenching was not investigated further, although it is conceivable that the coordination of picric acid to the molecular aggregates led to their dissociation and hence fluorescence quenching. Importantly, the doubly iodinated anil showed the largest association constant with picric acid compared to the other compounds, which contained one iodine atom each, highlighting the importance of the polarizable iodine atom, acting as a strong XB donor, in mediating the recognition of picric acid.

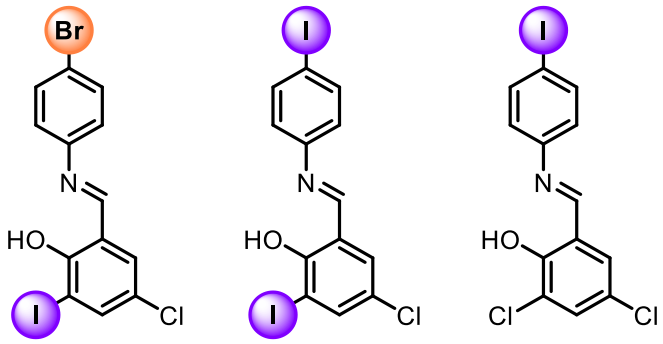


Fig. 1.54. Dar's XB anils for the detection of nitroaromatics *via* an AIE mechanism.

Although displacement assays have their disadvantages, they have been effectively deployed to allow highly sensitive sensing of neutral analytes of biological interest.[210] In 2020, Pischel and Ballester reported an elegant approach to sensing creatinine using a calix[4]pyrrole appended to a dansyl fluorescent reporter group (Fig. 1.55a).[211] The displacement assay consisted of the calix[4]pyrrole host bound to a pyridine *N*-oxide quencher molecule through HB interactions (Fig. 1.55b), which suppressed the fluorescence of the pendant dansyl group *via* Förster resonance energy transfer (FRET).[212] Upon binding of creatinine in $CHCl_3$, through concerted HB interactions with the pyrrole moieties and the phosphonate group (Fig. 1.55a), the quencher molecule

was displaced and the fluorescence of the dansyl group restored, leading to a five-fold increase in emission intensity and facilitating highly sensitive detection of creatinine with a limit of detection on the order of 110 nM.

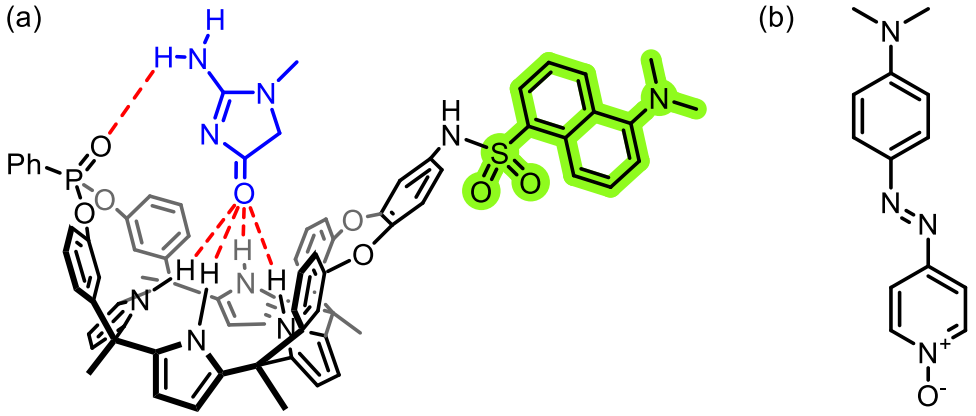


Fig. 1.55. (a) Pischel and Ballester's calix[4]pyrrole-based host binding creatine, shown in blue, *via* concerted HB interactions, shown in red, with the dansyl fluorophore highlighted in green and (b) the quencher molecule used in the displacement assay.

1.4 Thesis Aims

This thesis aims to develop XB emission-based optical sensors for anions, ion-pairs and neutral species. Evidently, great progress has been made in integrating halogen bonding interactions into optical sensors, yielding promising results. However, there are still a number of outstanding challenges that this thesis seeks to address: (i) the mechanisms of fluorescence modulation in sensors are poorly understood and further investigation is required to gain predictable control over the magnitude and direction of the fluorescence response; (ii) fluorescent XB sensors operating at the long wavelengths required for biological or medical applications are very rare and need development; (iii) XB-mediated fluorescence sensing of neutral guests is unprecedented and thus the benefits of XB interactions have not yet been brought to the field of neutral species sensing.

Chapter Two describes the synthesis of a family of six redox-active ferrocene-appended XB and HB BODIPY-functionalised optical anion sensors. Detailed anion binding studies involving measurements of the fluorescence emission, fluorescence lifetime and electrochemical responses to anion binding enable the various mechanisms of fluorescence modulation at play in these sensors, including rigidification and PET, to be elucidated. The exciting prospect of combining the advantages of optical and electrochemical methods of sensing is also explored in a study of spectroelectrochemical anion sensing.

Chapter Three describes the development of long-wavelength optical XB anion sensors employing the aza-BODIPY fluorophore. The sensing properties of a first-generation pair of sensors are tested and a second generation mixed aza-BODIPY/BODIPY ratiometric anion sensor is developed. Finally, the possibility of supramolecular

host-guest anion binding-modulated singlet oxygen generation is explored, with exciting potential application in the improvement of selective photodynamic therapy agents.

Chapter Four returns to BODIPY-based systems and describes the construction of two classes of sensors aimed at detecting environmentally and medically relevant species through the formation of interpenetrated host-guest complex assemblies. A powerful BODIPY-based sensing synthon, developed in Chapter Two, is appended to a either a hydrophobic pillar[5]arene or a diaza-crown ether central macrocyclic guest binding motif to allow the selective sensing of both environmental pollutants and ion-pairs. Specifically, a pillar[5]arene-based host for the sensing of dicarboxylates and a chemical warfare agent simulant is described alongside a crown ether-based host for the detection of ion-pairs and the neurotransmitter dopamine.

1.5 References for Chapter One

1. W. M. Cowan, T. C. Südhof, C. F. Stevens, *Synapses*, JHU Press, **2003**.
2. F. H. C. Crick, J. D. Watson, *Proc. R. Soc. London, Ser. A* **1954**, *223*, 80-96.
3. M. S. Prasad, V. P. Kenyen, D. N. Assar, *Miner. Process. Extr. Metall. Rev.* **1992**, *8*, 95-118.
4. *World Copper Factbook*, The International Copper Study Group, Lisbon, **2023**.
5. T. Ogoshi, M. Hashizume, T.-A. Yamagishi, Y. Nakamoto, *Chem. Commun.* **2010**, *46*, 3708.
6. Y. Li, A. H. Flood, *J. Am. Chem. Soc.* **2008**, *130*, 12111-12122.
7. D.-H. Li, B. D. Smith, *J. Org. Chem.* **2019**, *84*, 2808-2816.
8. M. R. Sambrook, J. R. Hiscock, A. Cook, A. C. Green, I. Holden, J. C. Vincent, P. A. Gale, *Chem. Commun.* **2012**, *48*, 5605-5607.
9. J. M. Lehn, *Angew. Chem. Int. Ed. Engl.* **1988**, *27*, 89-112.
10. G. W. Gokel, J. L. Atwood, *Comprehensive supramolecular chemistry. 1. Molecular recognition: receptors for cationic guests*, Pergamon Press, **1996**.
11. P. D. Beer, P. A. Gale, *Angew. Chem. Int. Ed.* **2001**, *40*, 486-516.
12. A. Docker, Y. C. Tse, H. M. Tay, A. J. Taylor, Z. Zhang, P. D. Beer, *Angew. Chem. Int. Ed.* **2022**, *61*, e202214523.
13. A. J. Taylor, A. Docker, P. D. Beer, *Chem. Asian J.* **2023**, *18*, e202201170.
14. S. K. Kim, J. L. Sessler, *Chem. Soc. Rev.* **2010**, *39*, 3784-3809.
15. V. K. Munasinghe, H. M. Tay, D. Manawadu, J. Pancholi, Z. Zhang, P. D. Beer, *Dalton Trans.* **2024**.
16. D. Ajami, J. Rebek Jr, *Acc. Chem. Res.* **2013**, *46*, 990-999.
17. Y.-D. Yang, X.-L. Chen, J. L. Sessler, H.-Y. Gong, *J. Am. Chem. Soc.* **2020**, *143*, 2315-2324.
18. J. T. Wilmore, Y. Cheong Tse, A. Docker, C. Whitehead, C. K. Williams, P. D. Beer, *Chem. Eur. J.* **2023**, *29*, e202300608.
19. H. M. Tay, A. Docker, A. Taylor, P. D. Beer, *Chem. Eur. J.* **2024**.
20. W. Chen, C. Guo, Q. He, X. Chi, V. M. Lynch, Z. Zhang, J. Su, H. Tian, J. L. Sessler, *J. Am. Chem. Soc.* **2019**, *141*, 14798-14806.
21. S. C. Patrick, R. Hein, P. D. Beer, J. J. Davis, *J. Am. Chem. Soc.* **2021**.
22. D. Lichosyt, P. Dydio, J. Jurczak, *Chem. Eur. J.* **2016**, *22*, 17673-17680.
23. M. H. Lee, J. S. Kim, J. L. Sessler, *Chem. Soc. Rev.* **2015**, *44*, 4185-4191.
24. M. R. Sambrook, S. Notman, *Chem. Soc. Rev.* **2013**, *42*, 9251.
25. Y. Gao, L. Zhang, Z. Wang, L. Lu, *ChemPlusChem* **2023**, *88*.
26. C. J. Walter, H. L. Anderson, J. K. M. Sanders, *J. Chem. Soc., Chem. Commun.* **1993**, 458-460.
27. R. L. Sutar, S. M. Huber, *ACS Catal.* **2019**, *9*, 9622-9639.
28. S. M. Walter, F. Kniep, E. Herdtweck, S. M. Huber, *Angew. Chem. Int. Ed.* **2011**, *50*, 7187-7191.
29. L. E. Bickerton, A. J. Sterling, P. D. Beer, F. Duarte, M. J. Langton, *Chem. Sci.* **2020**, *11*, 4722-4729.
30. A. P. Davis, D. N. Sheppard, B. D. Smith, *Chem. Soc. Rev.* **2007**, *36*, 348-357.
31. A. V. Koulov, J. M. Mahoney, B. D. Smith, *Org. Biomol. Chem.* **2003**, *1*, 27-29.
32. D. J. Sam, H. E. Simmons, *J. Am. Chem. Soc.* **1972**, *94*, 4024-4025.
33. A. Docker, J. G. Stevens, P. D. Beer, *Chem. Eur. J.* **2021**, *27*, 14600-14604.
34. B. Hua, L. Shao, Z. Zhang, J. Liu, F. Huang, *J. Am. Chem. Soc.* **2019**, *141*, 15008-15012.
35. Z.-H. Sun, F.-F. Pan, Triyanti, M. Albrecht, G. Raabe, *Eur. J. Org. Chem.* **2013**, *2013*, 7922-7932.
36. Nobel Prize Outreach AB, *The Nobel Prize in Chemistry 1987*, https://www.nobelprize.org/prizes/chemistry/1987/press-release, (accessed 15th August 2024).
37. C. J. Pedersen, *J. Am. Chem. Soc.* **1967**, *89*, 7017-7036.
38. D. J. Cram, T. Kaneda, R. C. Helgeson, S. B. Brown, C. B. Knobler, E. Maverick, K. N. Trueblood, *J. Am. Chem. Soc.* **1985**, *107*, 3645-3657.
39. D. J. Cram, G. M. Lein, *J. Am. Chem. Soc.* **1985**, *107*, 3657-3668.
40. J. M. Lehn, *Acc. Chem. Res.* **1978**, *11*, 49-57.
41. J. M. Lehn, J. P. Sauvage, *J. Am. Chem. Soc.* **1975**, *97*, 6700-6707.

42. J. M. Lehn, J. Simon, J. Wagner, *Angew. Chem. Int. Ed.* **1973**, *12*, 579-580.
43. G. T. Morgan, H. D. K. Drew, *J. Chem. Soc., Trans.* **1920**, *117*, 1456-1465.
44. D. K. Cabbiness, D. W. Margerum, *J. Am. Chem. Soc.* **1969**, *91*, 6540-6541.
45. R. D. Hancock, A. E. Martell, *Comments Inorg. Chem.* **1988**, *6*, 237-284.
46. B. Dietrich, D. L. Fyles, T. M. Fyles, J.-M. Lehn, *Helv. Chim. Acta* **1979**, *62*, 2763-2787.
47. C. Jia, Q.-Q. Wang, R. A. Begum, V. W. Day, K. Bowman-James, *Org. Biomol. Chem.* **2015**, *13*, 6953-6957.
48. D. J. Cram, *Angew. Chem. Int. Ed. Engl.* **1986**, *25*, 1039-1057.
49. A. E. Martell, R. D. Hancock, R. J. Motekaitis, *Coord. Chem. Rev.* **1994**, *133*, 39-65.
50. S. P. Artz, D. J. Cram, *J. Am. Chem. Soc.* **1984**, *106*, 2160-2171.
51. M. H. H. Voelkel, P. Wonner, S. M. Huber, *ChemistryOpen* **2020**, *9*, 214-224.
52. M. Ahmad, T. G. Johnson, M. Flerin, F. Duarte, M. J. Langton, *Angew. Chem. Int. Ed.* **2024**, *63*.
53. D. A. Kraut, P. A. Sigala, B. Pybus, C. W. Liu, D. Ringe, G. A. Petsko, D. Herschlag, *PLoS Biol.* **2006**, *4*, e99.
54. A. R. Fersht, *Proc. R. Soc. London, Ser. B* **1974**, *187*, 397-407.
55. E. Fischer, *Dtsch. Chem. Ges* **1894**, *27*, 2984-2993.
56. J. H. Arevalo, M. J. Taussig, I. A. Wilson, *Nature* **1993**, *365*, 859-863.
57. C. B. Saper, *J. Histochem. Cytochem.* **2009**, *57*, 1-5.
58. A. Bencini, C. Coluccini, A. Garau, C. Giorgi, V. Lippolis, L. Messori, D. Pasini, S. Puccioni, *Chem. Commun.* **2012**, *48*, 10428-10430.
59. S. C. Patrick, P. D. Beer, J. J. Davis, *Nat. Rev. Chem.* **2024**, *8*, 256-276.
60. F. Biedermann, V. D. Uzunova, O. A. Scherman, W. M. Nau, A. De Simone, *J. Am. Chem. Soc.* **2012**, *134*, 15318-15323.
61. T. P. Silverstein, *J. Chem. Educ.* **1998**, *75*, 116.
62. B. Gómez-González, L. García-Río, N. Basílio, J. C. Mejuto, J. Simal-Gandara, *Pharmaceutics* **2021**, *14*.
63. F. Sommer, Y. Marcus, S. Kubik, *ACS Omega* **2017**, *2*, 3669-3680.
64. N. N. Andersen, K. Eriksen, M. Lisbjerg, M. E. Ottesen, B. O. Milhøj, S. P. A. Sauer, M. Pittelkow, *J. Org. Chem.* **2019**, *84*, 2577-2584.
65. T. Fiala, K. Sleziakova, K. Marsalek, K. Salvadori, V. Sindelar, *J. Org. Chem.* **2018**, *83*, 1903-1912.
66. F. P. Schmidtchen, *Angew. Chem. Int. Ed. Engl.* **1977**, *16*, 720-721.
67. E. Graf, J. M. Lehn, *J. Am. Chem. Soc.* **1976**, *98*, 6403-6405.
68. A. M. Agafontsev, A. Ravi, T. A. Shumilova, A. S. Oshchepkov, E. A. Kataev, *Chem. Eur. J.* **2019**, *25*, 2684-2694.
69. J. M. Lowenstein, *Citric Acid Cycle*, Elsevier Science, **1969**.
70. M. P. Anderson, R. J. Gregory, S. Thompson, D. W. Souza, S. Paul, R. C. Mulligan, A. E. Smith, M. J. Welsh, *Science* **1991**, *253*, 202-205.
71. F. Delange, *Thyroid* **1994**, *4*, 107-128.
72. N. D. Carter, S. J. Dodgson, G. Gros, R. E. Tashian, *The Carbonic Anhydrases: Cellular Physiology and Molecular Genetics*, Springer US, **2013**.
73. *World Food and Agriculture – Statistical Yearbook 2023*, Food and Agriculture Organisation, United Nations, **2023**.
74. V. H. Smith, G. D. Tilman, J. C. Nekola, *Environ. Pollut.* **1999**, *100*, 179-196.
75. J. Murray, *About 90kg of dead fish removed from Walsall canal after sodium cyanide leak*, The Guardian, **19th August 2024**.
76. D. Banerjee, D. Kim, M. J. Schweiger, A. A. Kruger, P. K. Thallapally, *Chem. Soc. Rev.* **2016**, *45*, 2724-2739.
77. Nobel Prize Outreach AB, *The Nobel Prize in Physiology or Medicine 1998*, https://www.nobelprize.org/prizes/medicine/1998/summary/, (accessed 20th August 2024).
78. J. M. Fukuto, S. J. Carrington, D. J. Tantillo, J. G. Harrison, L. J. Ignarro, B. A. Freeman, A. Chen, D. A. Wink, *Chem. Res. Toxicol.* **2012**, *25*, 769-793.
79. R. U. Halden, *Annu. Rev. Public Health* **2010**, *31*, 179-194.
80. K. Jaga, C. Dharmani, *Int. J. Occup. Environ. Health* **2003**, *16*, 7-20.

81. D. W. Connell, P. Lam, B. Richardson, R. Wu, *Introduction to Ecotoxicology*, Wiley, **1999**.
82. D. K. Deshmukh, M. K. Deb, P. K. Hopke, Y. I. Tsai, *Aerosol Air Qual. Res.* **2012**, *12*, 683-696.
83. C. H. Gunderson, C. R. Lehmann, F. R. Sidell, B. Jabbari, *Neurology* **1992**, *42*, 946-946.
84. D. Lichosyt, S. Wasiłek, P. Dydio, J. Jurczak, *Chem. Eur. J.* **2018**, *24*, 11683-11692.
85. R. J. Fitzmaurice, G. M. Kyne, D. Douheret, J. D. Kilburn, *J. Chem. Soc., Perkin Trans. 1* **2002**, 841-864.
86. H. Bagha, R. Hein, J. Y. C. Lim, C. B. Durr, M. R. Sambrook, P. D. Beer, *Chem. Eur. J.* **2024**, *30*.
87. K. N. Han, *Minerals* **2020**, *10*, 178.
88. S. Boudon, A. Decian, J. Fischer, W. Hosseini, J.-M. Lehn, G. Wipff, *J. Coord. Chem.* **1991**, *23*, 113-135.
89. K. D. Collins, *Biophys. J.* **1997**, *72*, 65-76.
90. J. W. Steed, J. L. Atwood, *Supramolecular Chemistry*, 3rd ed., Wiley, **2022**.
91. R. Shannon, *Acta Crystallogr. A .* **1976**, *32*, 751-767.
92. L. H. Ahrens, *Geochim. Cosmochim. Acta* **1952**, *2*, 155-169.
93. C. L. Gibb, B. C. Gibb, *J. Am. Chem. Soc.* **2011**, *133*, 7344-7347.
94. R. Zangi, *J. Phys. Chem. B* **2010**, *114*, 643-650.
95. F. Hofmeister, *Pathol. Pharmakol* **1888**, *24*, 247-260.
96. J. L. Atwood, J. W. Steed, *Supramolecular chemistry*, John Wiley & Sons, **2009**.
97. A. P. Davis, *Chem. Soc. Rev.* **2020**, *49*, 2531-2545.
98. M. M. Rodrigo, M. A. Esteso, M. F. Barros, L. M. P. Verissimo, C. M. Romero, A. F. Suarez, M. L. Ramos, A. J. M. Valente, H. D. Burrows, A. C. F. Ribeiro, *J. Chem. Thermodyn.* **2017**, *104*, 110-117.
99. C. H. Park, H. E. Simmons, *J. Am. Chem. Soc.* **1968**, *90*, 2431-2432.
100. F. P. Schmidtchen, G. Müller, *J. Chem. Soc., Chem. Commun.* **1984**, 1115-1116.
101. R. L. Frost, D. W. James, *J. Chem. Soc., Faraday Trans. 1* **1982**, *78*, 3263-3279.
102. K. Worm, F. P. Schmidtchen, A. Schier, A. Schäfer, M. Hesse, *Angew. Chem. Int. Ed. Engl.* **1994**, *33*, 327-329.
103. J. Zhang, Y. He, K. Zhang, X. Liang, R. Bance-Soualhi, Y. Zhu, X. Ge, M. A. Shehzad, W. Yu, Z. Ge, *AlChE J.* **2021**, *67*, e17133.
104. P. D. Beer, T. A. Barendt, J. Y. C. Lim, *Supramolecular Chemistry: Fundamentals and Applications*, Oxford University Press, **2022**.
105. T. K. Ghanty, V. N. Staroverov, P. R. Koren, E. R. Davidson, *J. Am. Chem. Soc.* **2000**, *122*, 1210-1214.
106. E. D. Isaacs, A. Shukla, P. M. Platzman, D. R. Hamann, B. Barbiellini, C. A. Tulk, *Phys. Rev. Lett.* **1999**, *82*, 600-603.
107. P. A. Wood, F. H. Allen, E. Pidcock, *CrystEngComm* **2009**, *11*, 1563.
108. S. J. Grabowski, *J. Phys. Org. Chem.* **2004**, *17*, 18-31.
109. M. D. Hartle, J. S. Prell, M. D. Pluth, *Dalton Trans.* **2016**, *45*, 4843-4853.
110. L. C. Gilday, N. G. White, P. D. Beer, *Dalton Trans.* **2012**, *41*, 7092.
111. M. D. Josten, L. Schaad, *Hydrogen Bonding*, M. Dekker, New York, **1974**.
112. K. Thorstensen, I. Romslo, *Biochem. J* **1990**, *271*, 1-9.
113. S. C. Zimmerman, T. J. Murray, A. J. Kirby, D. H. Williams, *Philos. Trans. R. Soc. London, Ser. A* **1993**, *345*, 49-56.
114. G. R. Desiraju, P. S. Ho, L. Kloo, A. C. Legon, R. Marquardt, P. Metrangolo, P. Politzer, G. Resnati, K. Rissanen, *Pure Appl. Chem.* **2013**, *85*, 1711-1713.
115. M. Novák, C. Foroutan-Nejad, R. Marek, *Phys. Chem. Chem. Phys.* **2015**, *17*, 6440-6450.
116. U. Adhikari, S. Scheiner, *Chem. Phys. Lett.* **2012**, *532*, 31-35.
117. O. Hassel, J. Hvoslef, *Acta Chem. Scand.* **1954**, *8*, 873-873.
118. R. S. Mulliken, *J. Phys. Chem.* **1952**, *56*, 801-822.
119. O. Hassel, *Science* **1970**, *170*, 497-502.
120. S. W. Robinson, C. L. Mustoe, N. G. White, A. Brown, A. L. Thompson, P. Kennepohl, P. D. Beer, *J. Am. Chem. Soc.* **2015**, *137*, 499-507.
121. M. Erdélyi, *Chem. Soc. Rev.* **2012**, *41*, 3547.
122. B. Schulze, U. S. Schubert, *Chem. Soc. Rev.* **2014**, *43*, 2522-2571.

123. M. J. Langton, S. W. Robinson, I. Marques, V. Félix, P. D. Beer, *Nat. Chem.* **2014**, *6*, 1039-1043.
124. S. C. Patrick, R. Hein, M. Sharafeldin, X. Li, P. D. Beer, J. J. Davis, *Chem. Eur. J.* **2021**, *27*, 17700-17706.
125. G. Akerlof, *J. Am. Chem. Soc.* **1932**, *54*, 4125-4139.
126. C. C. Robertson, R. N. Perutz, L. Brammer, C. A. Hunter, *Chem. Sci.* **2014**, *5*, 4179-4183.
127. Z. P. Shields, J. S. Murray, P. Politzer, *Int. J. Quantum Chem* **2010**, *110*, 2823-2832.
128. F. Zapata, A. Caballero, N. G. White, T. D. W. Claridge, P. J. Costa, V. t. Félix, P. D. Beer, *J. Am. Chem. Soc.* **2012**, *134*, 11533-11541.
129. S. Mondal, A. Rashid, P. Ghosh, *J. Organomet. Chem.* **2021**, *952*, 122027.
130. M. M. Watt, M. S. Collins, D. W. Johnson, *Acc. Chem. Res.* **2013**, *46*, 955-966.
131. A. S. Mahadevi, G. N. Sastry, *Chem. Rev.* **2013**, *113*, 2100-2138.
132. R. Shukla, S. V. Lindeman, R. Rathore, *Chem. Commun.* **2009**, 5600-5602.
133. A. Das, S. Ghosh, *Angew. Chem. Int. Ed.* **2014**, *53*, 2038-2054.
134. L. M. Klivansky, D. Hanifi, G. Koshkakaryan, D. R. Holycross, E. K. Gorski, Q. Wu, M. Chai, Y. Liu, *Chem. Sci.* **2012**, *3*, 2009-2014.
135. V. Amendola, G. Bergamaschi, M. Boiocchi, R. Alberto, H. Braband, *Chem. Sci.* **2014**, *5*, 1820-1826.
136. C. A. Fitch, G. Platzer, M. Okon, B. Garcia-Moreno E., L. P. McIntosh, *Protein Sci.* **2015**, *24*, 752-761.
137. A. Metzger, V. M. Lynch, E. V. Anslyn, *Angew. Chem. Int. Ed. Engl.* **1997**, *36*, 862-865.
138. A. Docker, C. H. Guthrie, H. Kuhn, P. D. Beer, *Angew. Chem. Int. Ed.* **2021**, *60*, 21973-21978.
139. A. M. S. Riel, D. A. Decato, J. Sun, C. J. Massena, M. J. Jessop, O. B. Berryman, *Chem. Sci.* **2018**, *9*, 5828-5836.
140. C. J. Massena, A. M. S. Riel, G. F. Neuhaus, D. A. Decato, O. B. Berryman, *Chem. Commun.* **2015**, *51*, 1417-1420.
141. D. A. Decato, J. Sun, M. R. Boller, O. B. Berryman, *Chem. Sci.* **2022**, *13*, 11156-11162.
142. R. A. Pascal, J. Spergel, D. Van Engen, *Tetrahedron Lett.* **1986**, *27*, 4099-4102.
143. M. Cametti, K. Rissanen, *Chem. Commun.* **2009**, 2809-2829.
144. J. Cai, J. L. Sessler, *Chem. Soc. Rev.* **2014**, *43*, 6198-6213.
145. W. B. Farnham, D. Roe, D. A. Dixon, J. C. Calabrese, R. L. Harlow, *J. Am. Chem. Soc.* **1990**, *112*, 7707-7718.
146. C. W. Tornøe, C. Christensen, M. Meldal, *J. Org. Chem.* **2002**, *67*, 3057-3064.
147. V. V. Rostovtsev, L. G. Green, V. V. Fokin, K. B. Sharpless, *Angew. Chem. Int. Ed.* **2002**, *41*, 2596-2599.
148. Y. Li, A. H. Flood, *Angew. Chem. Int. Ed.* **2008**, *47*, 2649-2652.
149. Y. Liu, W. Zhao, C.-H. Chen, A. H. Flood, *Science* **2019**, *365*, 159-161.
150. A. Mele, P. Metrangolo, H. Neukirch, T. Pilati, G. Resnati, *J. Am. Chem. Soc.* **2005**, *127*, 14972-14973.
151. M. G. Sarwar, B. Dragisić, E. Dimitrijević, M. S. Taylor, *Chem. Eur. J.* **2013**, *19*, 2050-2058.
152. M. G. Sarwar, B. Dragisic, L. J. Salsberg, C. Gouliaras, M. S. Taylor, *J. Am. Chem. Soc.* **2010**, *132*, 1646-1653.
153. M. G. Sarwar, B. Dragisic, S. Sagoo, M. S. Taylor, *Angew. Chem. Int. Ed.* **2010**, *49*, 1674-1677.
154. H. Min Tay, T. G. Johnson, A. Docker, M. J. Langton, P. D. Beer, *Angew. Chem. Int. Ed.* **2023**, *62*, e202312745.
155. Y.-M. Wu, J. Deng, Y. Li, Q.-Y. Chen, *Synthesis* **2005**, 1314-1318.
156. J. E. Hein, J. C. Tripp, L. B. Krasnova, K. B. Sharpless, V. V. Fokin, *Angew. Chem. Int. Ed.* **2009**, *48*, 8018-8021.
157. W. S. Brotherton, R. J. Clark, L. Zhu, *J. Org. Chem.* **2012**, *77*, 6443-6455.
158. C. Spiteri, J. E. Moses, *Angew. Chem. Int. Ed.* **2010**, *49*, 31-33.
159. R. Tepper, B. Schulze, H. Görls, P. Bellstedt, M. Jäger, U. S. Schubert, *Org. Lett.* **2015**, *17*, 5740-5743.
160. D. Mungalpara, S. Stegmüller, S. Kubik, *Chem. Commun.* **2017**, *53*, 5095-5098.
161. D. Mungalpara, H. Kelm, A. Valkonen, K. Rissanen, S. Keller, S. Kubik, *Org. Biomol. Chem.* **2017**, *15*, 102-113.

162. D. Van Eker, S. K. Samanta, A. P. Davis, *Chem. Commun.* **2020**, *56*, 9268-9271.
163. K. Kriis, *J. Org. Chem.* **2022**.
164. N. Kato, T. Nanjo, Y. Takemoto, *ACS Catal.* **2022**, 7843-7849.
165. A. M. S. Riel, D. A. Decato, J. Sun, O. Berryman, *Chem. Commun.* **2022**.
166. A. J. McConnell, P. D. Beer, *Angew. Chem. Int. Ed.* **2012**, *51*, 5052-5061.
167. Y. C. Tse, A. Docker, Z. Zhang, P. D. Beer, *Chem. Commun.* **2021**, *57*, 4950-4953.
168. A. J. McConnell, A. Docker, P. D. Beer, *ChemPlusChem* **2020**, *85*, 1824-1841.
169. A. Docker, I. Marques, H. Kuhn, Z. Zhang, V. Félix, P. D. Beer, *J. Am. Chem. Soc.* **2022**, *144*, 14778-14789.
170. J. Romanski, P. Piątek, *Chem. Commun.* **2012**, *48*, 11346-11348.
171. D. Whitford, John Wiley & Sons Ltd., Chichester, England, **2005**, pp. 66-74.
172. N. J. Heo, J. H. Oh, A. Li, K. Lee, Q. He, J. L. Sessler, S. K. Kim, *Chem. Sci.* **2024**, *15*, 13958-13965.
173. R. Tepper, B. Schulze, P. Bellstedt, J. Heidler, H. Görls, M. Jäger, U. S. Schubert, *Chem. Commun.* **2017**, *53*, 2260-2263.
174. T. Bunchuay, A. Docker, U. Eiamprasert, P. Surawatanawong, A. Brown, P. D. Beer, *Angew. Chem. Int. Ed.* **2020**, *59*, 12007-12012.
175. T. Tozawa, S. Tokita, Y. Kubo, *Tetrahedron Lett.* **2002**, *43*, 3455-3457.
176. R. Hein, P. D. Beer, *Chem. Sci.* **2022**, *13*, 7098-7125.
177. R. Hein, A. Docker, J. J. Davis, P. D. Beer, *J. Am. Chem. Soc.* **2022**, *144*, 8827-8836.
178. R. Hein, P. D. Beer, J. J. Davis, *Chem. Rev.* **2020**, *120*, 1888-1935.
179. J. Dong, A. P. Davis, *Angew. Chem.* **2021**, *133*, 8113-8126.
180. Novo Nordisk, *Novo Nordisk acquires Ziylo Ltd to accelerate its development of glucose responsive insulins*, https://www.novonordisk.com/content/nncorp/global/en/news-and-media/news-and-ir-materials/news-details.html?id=533, (accessed 26th August 2024).
181. E. A. Kataev, *Chem. Commun.* **2023**, *59*, 1717-1727.
182. R. Martínez-Máñez, F. Sancenón, *J. Fluoresc.* **2005**, *15*, 267-285.
183. B. Zou, H. Liu, J. Mack, S. Wang, J. Tian, H. Lu, Z. Li, Z. Shen, *RSC Adv.* **2014**, *4*, 53864-53869.
184. M. Bojtár, A. Paudics, D. Hessz, M. Kubinyi, I. Bitter, *RSC Adv.* **2016**, *6*, 86269-86275.
185. H. Miyaji, W. Sato, J. L. Sessler, *Angew Chem Int Ed Engl* **2000**, *39*, 1777-1780.
186. P. Thordarson, *Chem. Soc. Rev.* **2011**, *40*, 1305-1323.
187. J. Y. Lim, P. D. Beer, *New J. Chem.* **2018**, *42*, 10472-10475.
188. E. M. Boyle, S. Comby, J. K. Molloy, T. Gunnlaugsson, *J. Org. Chem.* **2013**, *78*, 8312-8319.
189. F. Würthner, C. Thalacker, A. Sautter, *Adv. Mater.* **1999**, *11*, 754-758.
190. J. C. Pickup, F. Hussain, N. D. Evans, O. J. Rolinski, D. J. S. Birch, *Biosens. Bioelectron.* **2005**, *20*, 2555-2565.
191. Y. C. Tse, R. Hein, E. J. Mitchell, Z. Y. Zhang, P. D. Beer, *Chem. Eur. J.* **2021**, *27*, 14550-14559.
192. T. Gunnlaugsson, H. D. P. Ali, M. Glynn, P. E. Kruger, G. M. Hussey, F. M. Pfeffer, C. M. G. Dos Santos, J. Tierney, *J. Fluoresc.* **2005**, *15*, 287-299.
193. H. Niu, J. Liu, H. M. O'Connor, T. Gunnlaugsson, T. D. James, H. Zhang, *Chem. Soc. Rev.* **2023**, *52*, 2322-2357.
194. J. K. G. Karlsson, A. Harriman, *J. Phys. Chem. A* **2016**, *120*, 2537-2546.
195. G.-J. Zhao, K.-L. Han, *Acc. Chem. Res.* **2012**, *45*, 404-413.
196. H. M. Tay, P. Beer, *Org. Biomol. Chem.* **2021**, *19*, 4652-4677.
197. A. Docker, X. Shang, D. Yuan, H. Kuhn, Z. Zhang, J. J. Davis, P. D. Beer, M. J. Langton, *Angew. Chem. Int. Ed.* **2021**, *60*, 19442-19450.
198. P. A. Gale, C. Caltagirone, *Coord. Chem. Rev.* **2018**, *354*, 2-27.
199. P. Sabater, F. Zapata, A. Bastida, A. Caballero, *Org. Biomol. Chem.* **2020**, *18*, 3858-3866.
200. T. Gunnlaugsson, P. E. Kruger, T. C. Lee, R. Parkesh, F. M. Pfeffer, G. M. Hussey, *Tetrahedron Lett.* **2003**, *44*, 6575-6578.
201. B. Chowdhury, S. Sinha, P. Ghosh, *Chem. Eur. J.* **2016**, *22*, 18051-18059.
202. P. Sabater, F. Zapata, A. Caballero, N. de la Visitación, I. Alkorta, J. Elguero, P. Molina, *J. Org. Chem.* **2016**, *81*, 7448-7458.
203. M. Más-Montoya, D. Curiel, C. Ramírez de Arellano, A. Tárraga, P. Molina, *Eur. J. Org. Chem.* **2016**, *2016*, 3878-3883.

204. L. Healy, M. O'Shea, J. McNulty, G. King, E. Twomey, E. Treacy, E. Crushell, J. Hughes, I. Knerr, A. A. Monavari, *JIMD Rep* **2022**, *63*, 379-387.
205. P. Sabater, F. Zapata, B. López, I. Fernández, A. Caballero, P. Molina, *Dalton Trans.* **2018**, *47*, 15941-15947.
206. C. Guo, A. C. Sedgwick, T. Hirao, J. L. Sessler, *Coord. Chem. Rev.* **2021**, *427*, 213560.
207. A. A. Ahangar, I. Ahmad, A. A. Dar, *New J. Chem.* **2023**, *47*, 4775-4783.
208. T. B. Brill, K. J. James, *Chem. Rev.* **1993**, *93*, 2667-2692.
209. Y. Hong, J. W. Y. Lam, B. Z. Tang, *Chem. Soc. Rev.* **2011**, *40*, 5361-5388.
210. B. T. Nguyen, E. V. Anslyn, *Coord. Chem. Rev.* **2006**, *250*, 3118-3127.
211. A. F. Sierra, D. Hernández-Alonso, M. A. Romero, J. A. González-Delgado, U. Pischel, P. Ballester, *J. Am. Chem. Soc.* **2020**, *142*, 4276-4284.
212. R. M. Clegg, in *FRET and FLIM Techniques, Vol. 33*, Elsevier, **2009**, pp. 1-57.

Chapter 2

Halogen Bonding BODIPY Hosts for Redox-Modulated Fluorescence Anion Sensing

2 Halogen Bonding BODIPY Hosts for Redox-Modulated Fluorescence Anion Sensing

2.1 Introduction

2.1.1 Mechanisms of Fluorescence Modulation in Anion Sensors

The direction (either an increase or decrease in intensity) and magnitude of the fluorescence response to anion binding are important variables to control in the design of effective supramolecular emission-based optical anion sensors. As explained in Chapter One, Sections 1.3.2 & 1.3.3, large magnitude responses are desirable as they increase the signal-to-noise ratio of the sensor,[1-2] which in turn decreases the sensor's limit of detection (LoD), which is the lowest concentration of an analyte which can be reliably detected.[3-6]

Control over the direction of fluorescence response is also crucial – some applications of fluorescent probes require an emission enhancement (turn-on) response, whereas others prioritise a large magnitude response, indifferent to its direction, and therefore use sensors with a large quenching (turn-off) response. For example, for applications in cellular bioimaging, a turn-on response is more useful, because it gives a bright signal against a dark background, maximising spatial resolution.[7] In other settings, sensors with strong quenching responses have found application in O_2 sensing,[8] for example for *in vivo* monitoring of trees.[9]

Designing anion sensors with control over these important parameters requires an understanding of the mechanisms of fluorescence response at play.[10] Arguably the most common mechanism exploited to elicit a turn-on response is rigidification,[11-12] which is clearly illustrated by the boronic acid saccharide sensor reported by Shinkai and co-workers (Fig. 2.1a),[13] in which the stilbene fluorescence was turned-on by a factor of four

by melibiose binding (Fig. 2.1b), due to restriction of rotation about the stilbene double bond caused by the binding of the sugar. Restriction of rotation in this way reduces the rate of non-radiative internal conversion back to the ground electronic state without the emission of a photon, and thus increases the fluorescence quantum yield.[14-15] In the context of anion sensing, such guest binding-induced rigidification effects were invoked to explain the 50-fold turn-on sensing response of the naphthalene-based anion sensor reported by Hennrich upon the addition of CO_3^{2-} in methanol (Fig. 2.1c).[16]

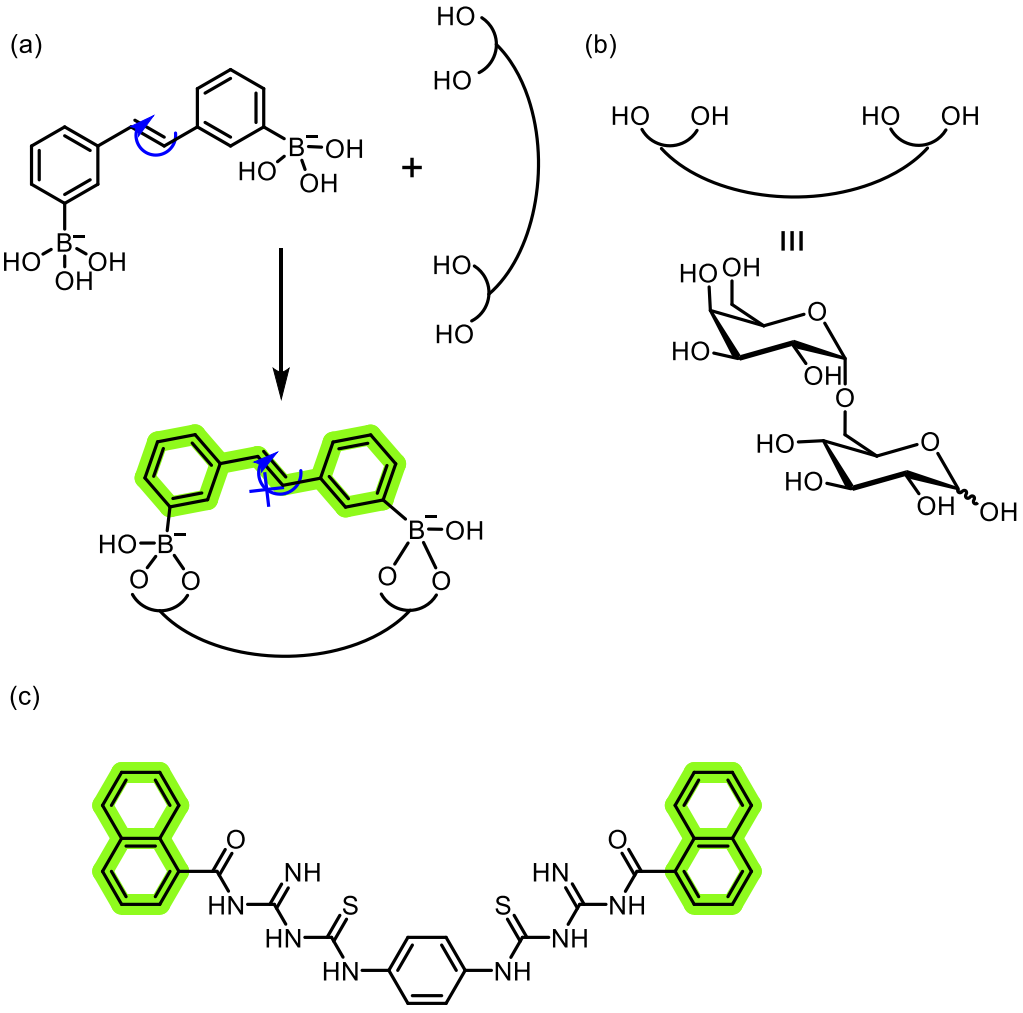


Fig. 2.1. (a) Shinkai's stilbene-based saccharide sensor exhibiting a turn-on response due to restricted rotation (shown by the blue arrow) caused by the binding of (b) melibiose. (c) Anthracene-based carbonate sensor reported by Hennrich.

Photo-induced electron transfer (PET) is a phenomenon often responsible for quenching responses of anion sensors.[11] PET refers to a process in which the absorption of a photon causes electronic excitation in the fluorophore, enabling it to donate or accept an electron and thus generate a charge separated state. This charge separated state can subsequently relax to the ground state non-radiatively, thus quenching the emission of a fluorophore.[17] Commonly, PET operates *via* transfer of an electron from an electron donor to the vacant orbital on the excited fluorophore (Fig. 2.2).

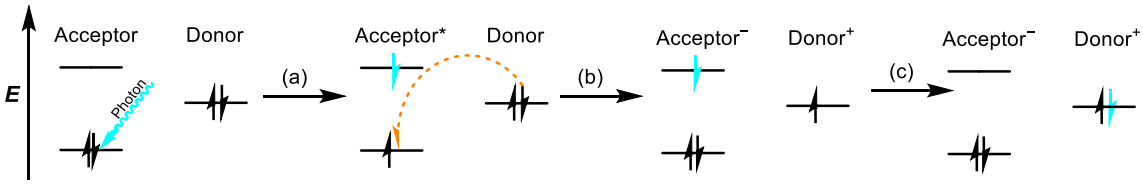


Fig. 2.2. Illustrative cartoon showing the orbital occupations during stages of the PET process: (a) Absorption of a photon, resulting in the excited state of the acceptor and (b) electron transfer from the donor to the vacant orbital in the acceptor, resulting in a charge separated state, which relaxes back to the ground state non-radiatively (c).

PET was the mechanism of fluorescence modulation in action in the pyrene-amide-appended calix[4]arene bromide sensor reported by Sutariya and co-workers in 2018 (Fig. 2.3).[18] The formation of hydrogen bonds between bromide and the amide moieties in acetonitrile enhanced the partial negative charge on the nitrogen atom adjacent to the fluorophore, activating PET quenching of the pyrene emission and thus resulting in a switch-off fluorescence response.

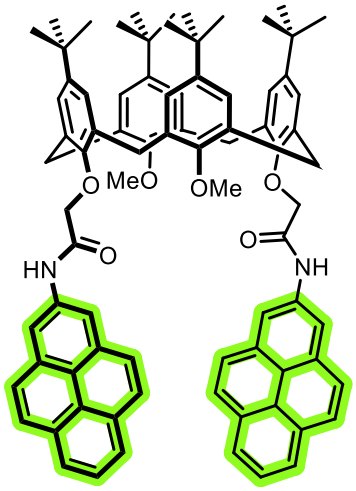


Fig. 2.3. Sutariya's bromide anion sensor, operating with a PET mechanism in acetonitrile.

2.1.2 Photo-Induced Electron Transfer in Ferrocene-BODIPY Dyads

4,4-Difluoro-4-bora-3a,4a-diaza-*s*-indacene (BODIPY) dyes are strongly absorbing molecules which emit sharp fluorescence peaks with high quantum yields at wavelengths of approximately 500-650 nm (Fig. 2.4).[19,*] In addition to these desirable optical properties, BODIPY dyes have the further advantages of being readily synthetically modified and derivatised, allowing tuning of their optical properties. They are also stable to physiological conditions and across a wide range of pH values.[19-22] This has led BODIPY to be deployed as a fluorescent reporter group in a variety of sensors for pH,[23] anions,[24] cations[25] and even viscosity.[26]

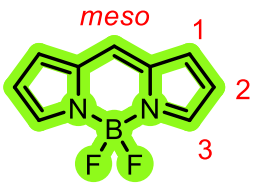


Fig. 2.4. Structure of the BODIPY fluorophore, with labels indicating the possible functionalisation positions.

[*] This combination of optical properties (strong absorption and high fluorescence quantum yields) leads to BODIPYs often being referred to as 'bright'.

Ferrocene-BODIPY dyad systems have been an area of interest to photochemists since a pair of reports in 2009,[27-28] which demonstrated their interesting electrochromic and spectroelectrochemical properties. Following these reports, Ravikanth and co-workers showed that the fluorescence properties of a ferrocene-BODIPY dyad were strongly affected by PET from the ferrocene moiety to the BODIPY fluorophore and that the emission of the BODIPY unit could be reversibly modulated by oxidation of the ferrocene group (Fig. 2.5a).[29] Specifically, the dyad shown in Fig. 2.5a exhibited negligible emission, due to highly effective PET quenching from the pendant ferrocene groups, but upon oxidation of the ferrocene moieties with $Fe(ClO_4)_3$ in toluene, the strong emission typical of BODIPY compounds was recovered, as the energy of the donor orbital situated on the ferrocene groups dropped in energy, thus switching off the PET quenching mechanism. The importance of the distance between the ferrocene and BODIPY motifs was highlighted in a 2016 report by Wu *et al.*,[30] in which the dyad with the short ethynylbenzene linker (Fig. 2.5b) showed stronger PET fluorescence quenching than the related dyad with a longer triazole linker (Fig. 2.5c).

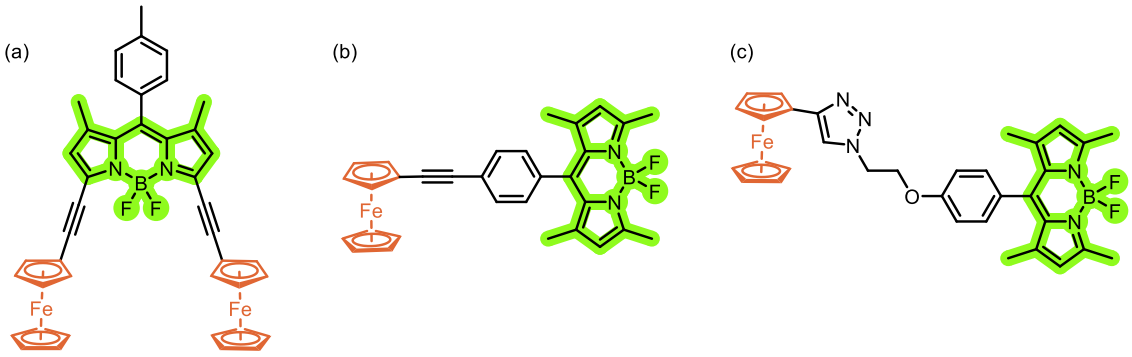


Fig. 2.5 (a) Ferrocene-BODIPY dyad reported by Ravikanth and co-workers and the dyads reported by Wu *et al.* containing (b) an ethynylbenzene linker and (c) a longer triazole linker.

2.1.3 Electrochemical Anion Sensing with Ferrocene Derivatives

The redox activity of the ferrocene motif can also be exploited for supramolecular electrochemical anion sensing, a sensing technique wherein electrochemical parameters are monitored to relay the presence of an anion. Typically, the shift in the ferrocene unit's ferrocene/ferrocenium (Fc/Fc^+) redox couple half-wave potential ($E_{1/2}$) is monitored. A key advantage of electrochemical sensors is that anion binding is enhanced by the oxidation of the sensor, which generates a cationic state, improving the sensitivity of the sensor. An archetypal ferrocene-based electrochemical anion sensor was reported by Veciana, Molina and co-workers in 2009,[31] which consisted of a thiourea anion binding site appended to a ferrocene group (Fig. 2.6a). Upon anion binding *via* HB interactions with the thiourea groups, a cathodic shift of up to –200 mV for $HP_2O_7^{3-}$ in the Fc/Fc^+ oxidation potential was observed in DMSO, meaning that the potential required to oxidise the ferrocene motif to ferrocenium was decreased, which is typical of electrochemical anion sensors. The reason for this frequently observed cathodic shift is the stabilisation of the cationic ferrocenium oxidation state by the nearby co-bound anion. Halogen bonding has shown advantages within this context, with XB ferrocene-based electrochemical sensors frequently displaying a relatively larger magnitude cathodic shift in the presence of an anion than their HB analogues – which is usually attributed to the greater covalency of the XB interaction.[32] For example, in 2015, Beer and co-workers reported the electrochemical anion sensors displayed in Fig. 2.6b. The XB analogue displayed a cathodic shift of –30 mV in the presence of 10 equivalents of chloride in acetonitrile, whereas the HB congener displayed a much smaller cathodic shift of –6 mV.

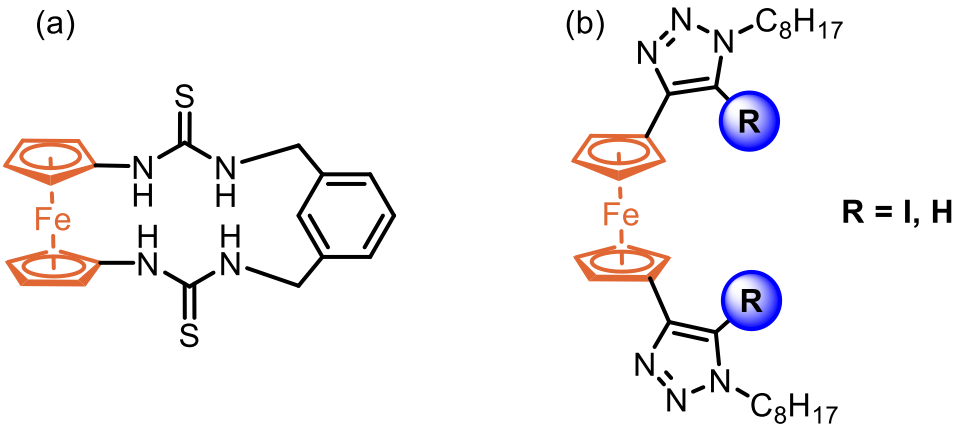


Fig. 2.6. (a) Veciana and Molina's ferrocene-based electrochemical anion sensor. (b) Beer's XB and HB electrochemical anion sensors.

2.1.4 Spectroelectrochemical Anion Sensing

Fluorescent and electrochemical anion sensors offer different advantages: fluorescent sensors benefit from the extremely high sensitivity of the technique, which allows very low quantities of the sensor to be used, and electrochemical sensors display oxidation-induced anion binding enhancement. Dual output sensors have been developed, such as the system reported by Tárraga and Molina containing both pyrene fluorescent and ferrocene electrochemical reporter groups,[33] which could sense pyrophosphate *independently and separately* through each modality (Fig. 2.7). However, a sensor which offers a *true combination* of the advantages of each technique, *i.e.*, electrochemical sensing with the sensitivity of a fluorescence technique (spectroelectrochemical anion sensing) remains hitherto undeveloped.

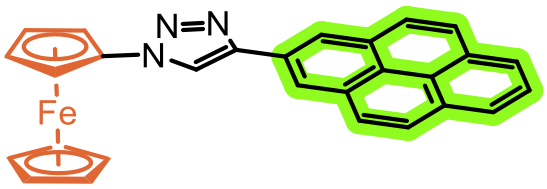


Fig. 2.7. Tárraga and Molina's dual output pyrophosphate sensor, with independent electrochemical and optical sensing modalities.

2.1.5 Chapter Aims

The fluorescence response to anion binding, particularly for XB sensors, is often complicated,[34] which has hampered efforts to investigate how anion binding influences fluorescence emission. Gaining a fundamental understanding of these mechanisms is crucial for designing anion sensors where the on or off direction of fluorescence changes induced by anion binding can be strategically controlled. The work described in this chapter seeks to address this challenge through the synthesis and study of a family of novel XB and HB BODIPY-based anion sensors (Fig. 2.8). The anion binding behaviour of these probes will be investigated and thermodynamic and kinetic studies will reveal the mechanisms of anion binding-induced fluorescence modulation at play in each of the sensors, which include PET.

Additionally, the presence of the redox-active ferrocene group in two of the compounds potentially allows these hosts to act as electrochemical anion sensors and this behaviour will also be studied. Finally, investigations into the possibility of spectroelectrochemical anion sensing will be conducted, with the objective of enabling electrochemical anion sensing at nanomolar host concentrations.

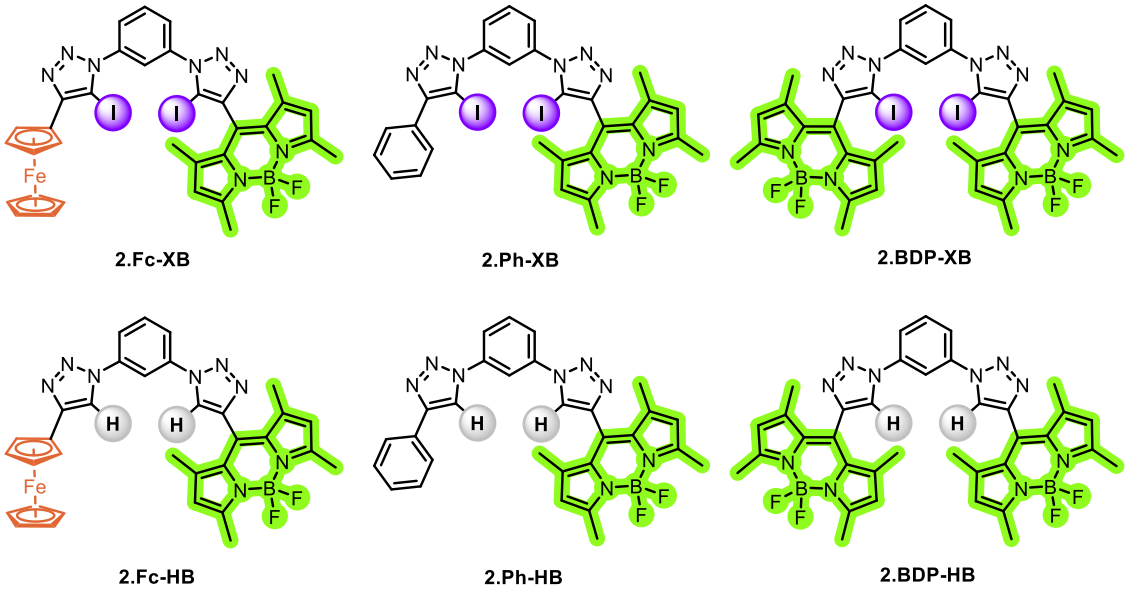


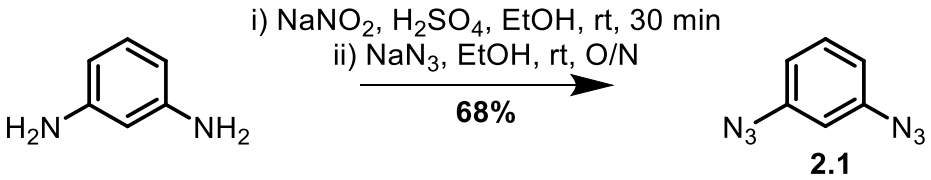
Fig. 2.8. The family of XB and HB BODIPY-based fluorescent anion sensors studied in this chapter.

2.2 Synthesis and Optical Characterisation of Target Anion Sensors

2.2.1 Synthesis of Target Anion Sensors

The target anion receptors incorporate the well-established 1,3-bis-(iodo)triazole benzene scaffold, known for its XB and HB mediated anion recognition.[35-37] This scaffold facilitates the straightforward modular synthesis, *via* CuAAC 'click' chemistry, of six novel fluorescent XB and HB anion sensors: **2.Fc-XB/HB**, **2.Ph-XB/HB**, and **2.BDP-XB/HB** (Fig. 2.8). In each case, the BODIPY fluorophore is linked to the (iodo)triazole *via* the BODIPY-*meso* position. The inclusion of the redox-active ferrocene in **2.Fc-XB/HB** was expected to cause PET quenching of BODIPY emission,[30, 38] with the extent of quenching potentially modifiable by anion binding due to changes in the receptor's electronic environment and conformation. **2.Ph-XB/HB**, and **2.BDP-XB/HB** were used as control compounds, enabling comparisons with receptors lacking this fluorescence modulation mechanism.

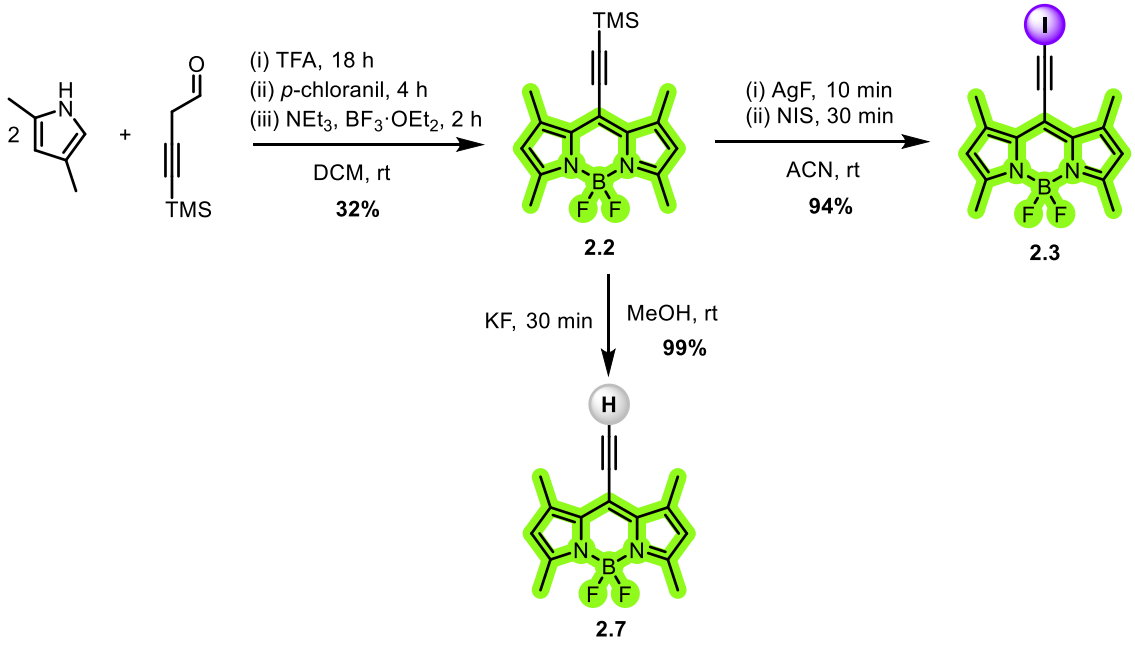
Synthesis began from 1,3-diaminobenzene, which was converted to 1,3-diazidobenzene (**2.1**) *via* diazotisation with $NaNO_2$ in the presence of H_2SO_4, followed by treatment with NaN_3, giving the bis-azide **2.1** in 68% yield following chromatographic purification (Scheme 2.1).



Scheme 2.1. Synthesis of compound **2.1**.[†]

[†] Compound **2.1** may be explosive, and therefore was only prepared on small scales.

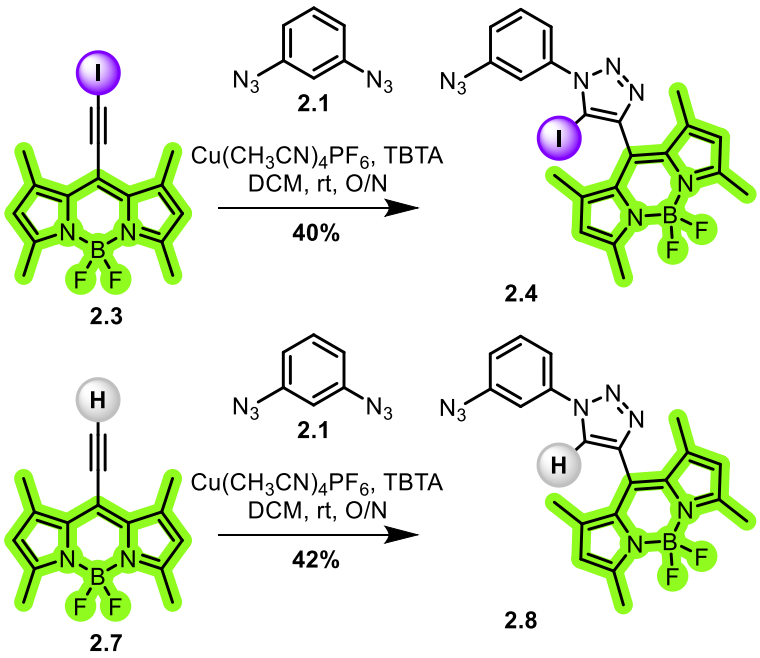
The requisite BODIPY (iodo)alkyne CuAAC coupling partners were prepared by first synthesising the TMS-protected BODIPY alkyne, **2.2**.[39] A mixture of 2,4-dimethylpyrrole and 3-trimethylsilylpropynal was stirred with catalytic trifluoracetic acid, followed by addition of the oxidising agent *p*-chloranil and finally triethylamine and boron trifluoride diethyl etherate to chelate the BF_2 unit.[39] The crude reaction mixture was purified by column chromatography to give the product, **2.2**, in 32% yield. The corresponding iodoalkyne, **2.3**, was prepared by reaction of **2.2** with AgF and NIS. Purification by column chromatography gave **2.3** as a red powder in 94% yield. Treatment of the TMS protected alkyne with KF gave the corresponding protoalkyne **2.7** in quantitative yield as a pink solid (Scheme 2.2).



Scheme 2.2 Synthesis of BODIPY alkynes **2.2**, **2.3** and **2.7**.

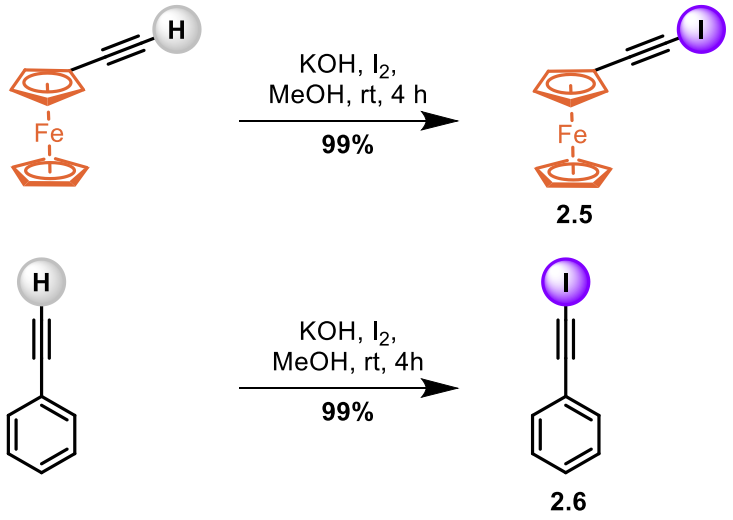
A CuAAC methodology was used to generate the useful monotriazole azide synthon **2.4**: the bis-azide **2.1** was statistically reacted with one equivalent of **2.3** in the presence of a Cu(I) catalyst and the rate accelerating ligand TBTA, producing synthon **2.4** in 40% yield following purification by column chromatography. The HB analogue of this

synthon was prepared in an equivalent manner, giving compound **2.8** in 42% yield (Scheme 2.3).



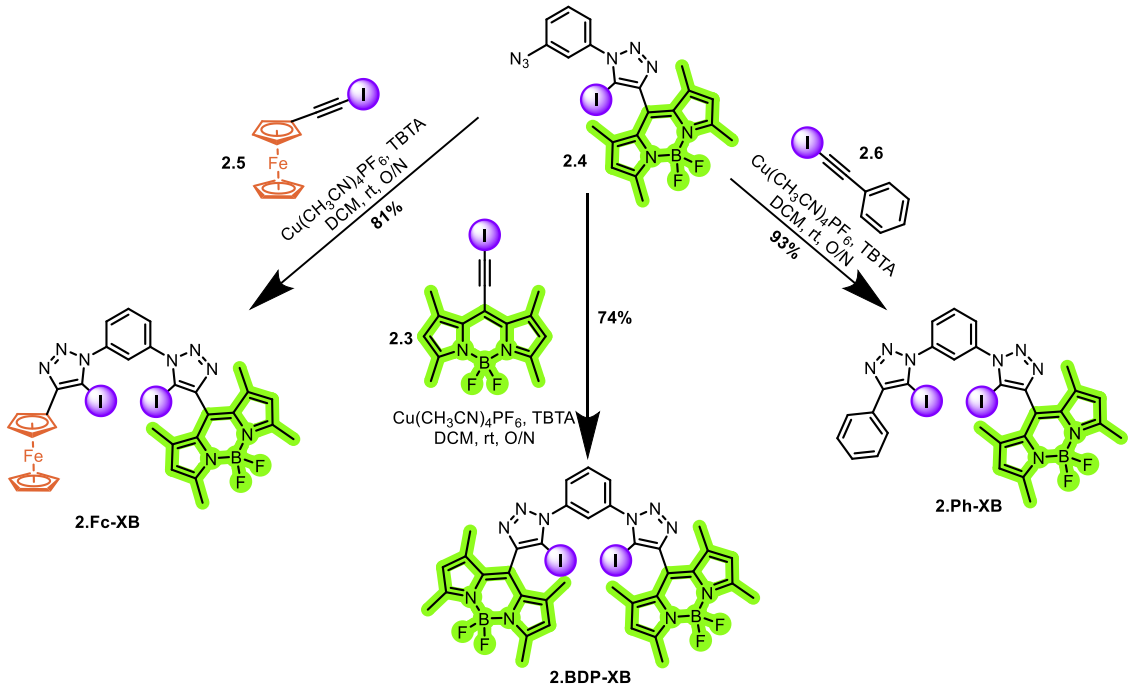
Scheme 2.3. Synthesis of azide synthons **2.4** and **2.8**.

With the azide synthons in hand, the requisite iodoalkynes for the next CuAAC reaction were generated by treatment of the commercially available parent protoalkynes with KOH and I_2, giving both iodoethynylferrocene **2.5** and iodoethynylbenzene **2.6** in quantitative yields (Scheme 2.4).



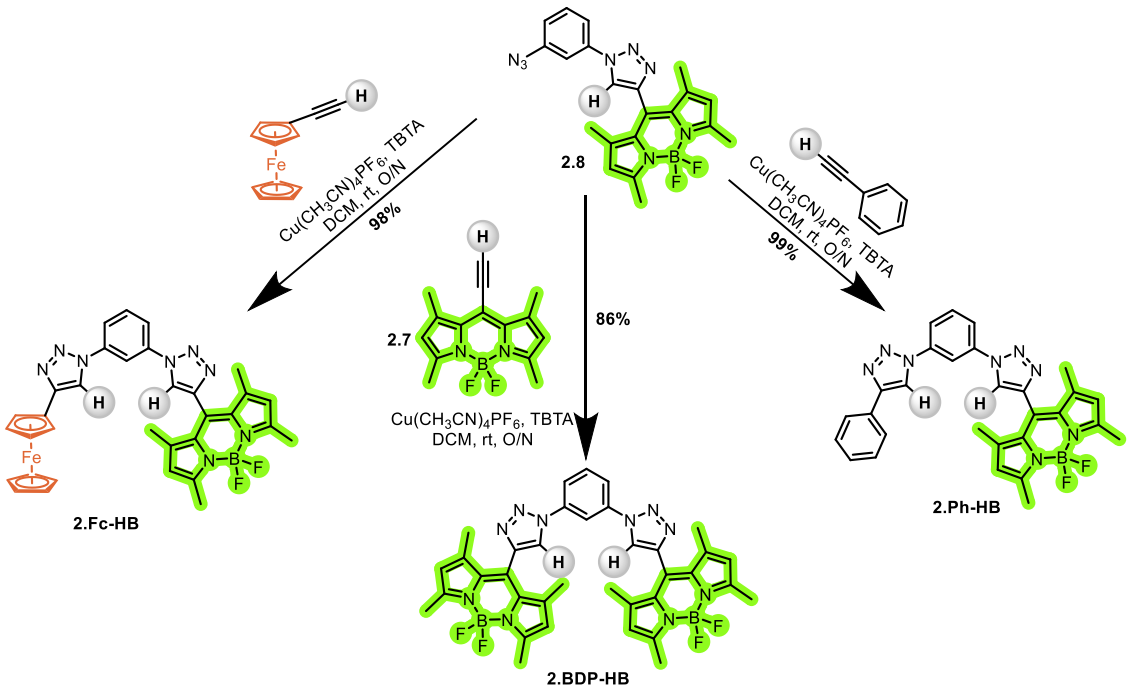
Scheme 2.4. Synthesis of iodoalkynes **2.5** and **2.6**.

The target XB receptors, **2.Fc-XB**, **2.Ph-XB**, and **2.BDP-XB**, were synthesised by re-subjecting synthon **2.4** to CuAAC conditions in the presence of iodoalkynes **2.5**, **2.6** or **2.3** respectively, giving the target XB anion sensors in 81%, 93% and 74% yields respectively, following chromatographic purification (Scheme 2.5).



Scheme 2.5. Synthesis of the target XB anion sensors **2.Fc-XB**, **2.Ph-XB**, and **2.BDP-XB**.

The HB sensors were obtained in an analogous manner, with HB azide synthon **2.8** being reacted with protoalkynes ethynylferrocene, ethynylbenzene and **2.7** to give **2.Fc-HB**, **2.Ph-HB**, and **2.BDP-HB** in 98%, 99% and 86% yields respectively, following purification by column chromatography (Scheme 2.6).



Scheme 2.6. Synthesis of the target HB anion sensors **2.Fc-HB**, **2.Ph-HB**, and **2.BDP-HB**.

The receptors were all characterised by ^{1}H NMR, ^{19}F NMR, ^{13}C NMR, HRMS, UV-vis absorbance and emission spectroscopy. The ^{1}H NMR spectra of **2.Fc-XB** and **2.BDP-HB** are shown as representative examples (Figs. 2.9 & 2.10).

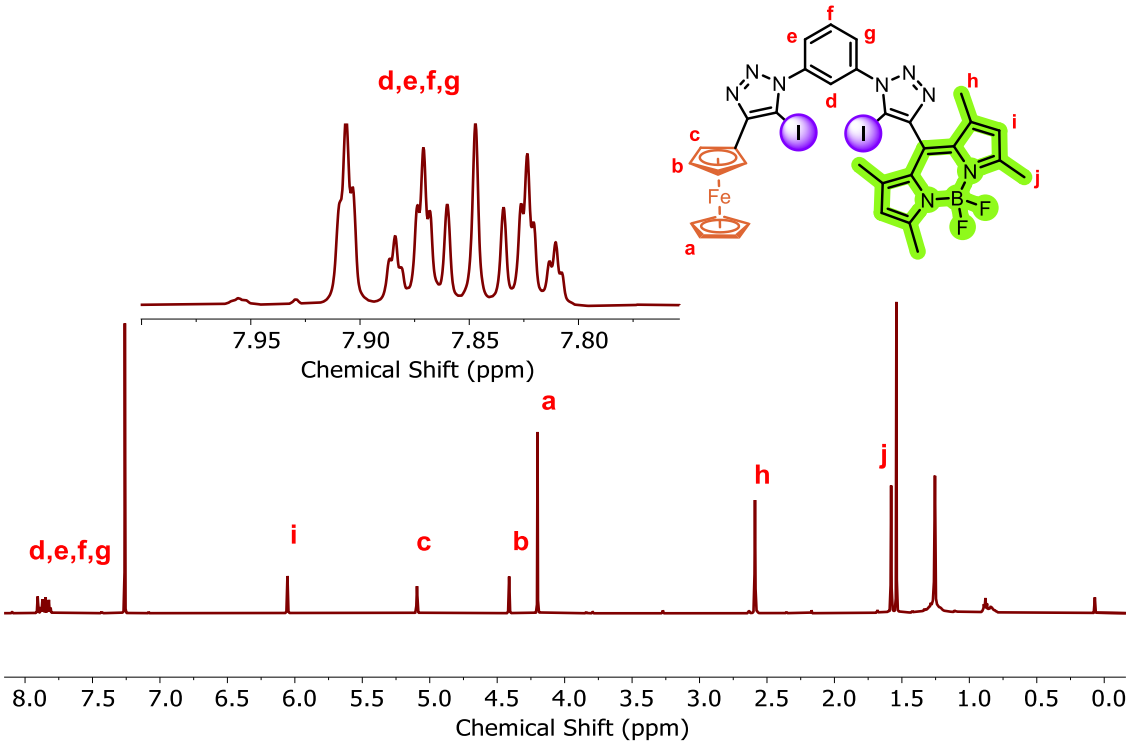


Figure 2.9 ^{1}H NMR spectrum of **2.Fc-XB**. ($CDCl_3$, 298 K)

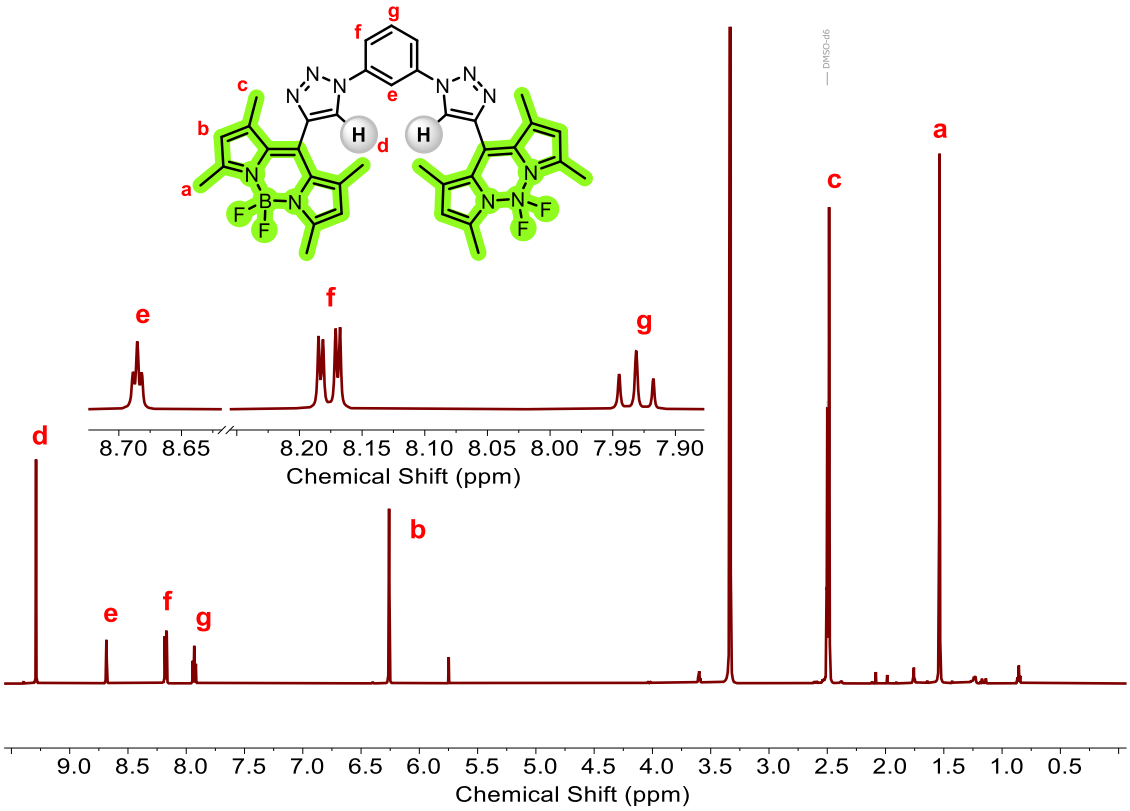


Fig. 2.10. ^{1}H NMR spectrum of **2.BDP-HB**. (DMSO-d_6, 298 K)

2.2.2 Optical Characterisation of Target Anion Sensors

The UV-vis absorbance and fluorescence spectral properties of the receptors were investigated in acetone to probe the differences in photophysical behaviour conferred by the differing (iodo)triazole substituents.‡

Table 2.1. Photophysical properties of the sensors in acetone (10 μM).

	2.Ph		**2.BDP**		**2.Fc**	
	XB	**HB**	**XB**	**HB**	**XB**	**HB**
$\lambda_{max,\ abs}$ (nm)	512	509	512	509	512	510
ε (M^{-1} cm^{-1})	74700	89500	140500	192000	76900	92600
$\lambda_{max,\ em}$ (nm)	521	519	521	520	521	519
Φ (%)[a]	17	4	14	4	6	3

[a] – measured against fluorescein as standard in 0.1 M NaOH.

As summarised in Table 2.1, all six receptors demonstrated the typical optical characteristics associated with BODIPY fluorophores.[19] Specifically, both the absorption and emission spectra featured sharp maxima, with absorption peaks centred around 510 nm and emission peaks around 520 nm – the resulting small Stokes shift suggesting fast decay of the excited state. These maxima were consistent across the sets of XB and HB receptors, which confirms that the Fc, Ph, and BODIPY substituents do not have a substantial impact on the wavelengths of the receptors' absorption and emission features, which is expected as they are distal to the BODIPY unit. However, the HB receptors exhibited slight hypsochromic shifts of approximately 2 nm compared to their XB

‡ Photophysical studies presented in this chapter were carried out in collaboration with Dr. Robert Hein.

analogues. This slight shift suggests minor differences in the electronic environment between the HB and XB hosts, which is expected due to the iodotriazole motif being relatively more electron-withdrawing than the prototriazole.[40] The molar absorption coefficient ε is also a little larger for all HB congeners (≈ 90000 M^{-1} cm^{-1} per BODIPY) than for the XB receptors (≈ 75000 M^{-1} cm^{-1} per BODIPY).

In addition to these basic spectral parameters, the fluorescence quantum yields Φ were determined for all six receptors by comparison to a fluorescein standard (Table 2.1).[41] These measurements revealed important differences, suggesting differing fluorescence quenching mechanisms in action in each of the sensors. For example, whilst Φ was identical within error for the XB sensors **2.Ph-XB** (Φ = 0.17) and **2.BDP-XB** (Φ = 0.14), indicative of minimal interaction between the two BODIPY units in **2.BDP-XB**, there were very large differences between this set of XB sensors and their HB congeners, **2.Ph-HB** and **2.BDP-HB**, which both exhibited a diminished fluorescence quantum yield of Φ = 0.04. This dramatic reduction in fluorescence quantum yield upon exchanging the iodotriazole groups for prototriazoles was initially unexpected, because the incorporation of heavy atoms, such as iodine, into the structures of BODIPY containing molecules is normally associated with a decrease in Φ,[42] due to an increase in the rate of intersystem crossing caused by the presence of the heavy atom, which allows the excited state of the BODIPY fluorophore to relax non-radiatively.[19, 43]

However, BODIPY derivatives functionalised in the *meso* position are known to non-radiatively relax through rotation about the BODIPY-*meso* bond.[19] Therefore, it seemed plausible that the bulkier iodotriazole substituent may significantly impede rotation about this bond, relative to the less bulky prototriazole, reducing the rate of non-radiative decay and hence boosting fluorescence quantum yield enough to overcome any

heavy atom quenching effect. To investigate this further, the emission spectrum of **2.Ph-HB** was measured in glycerol/MeOH mixtures of varying viscosity (Fig. 2.11). As the volume fraction of glycerol and hence the viscosity of the solution was increased, the emission intensity of **2.Ph-HB** was dramatically enhanced, due to the rotational decay pathway being inhibited. This indicated that the rotational pathway is a significant mode of decay for these hosts and thus supported the explanation posited above.[44]

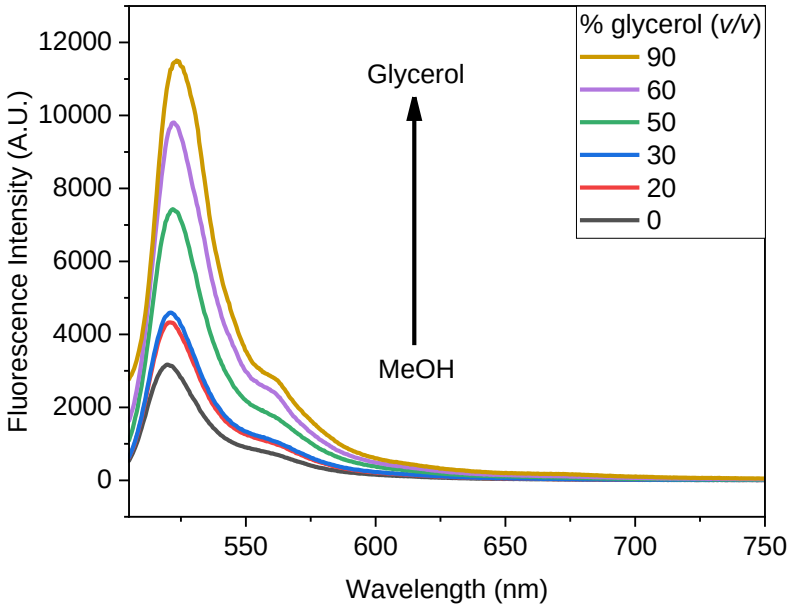


Fig. 2.11. Fluorescence spectra of **2.Ph-HB** in MeOH : glycerol mixtures. (1 μM, 298 K)

The ferrocene-containing hosts, **2.Fc-XB/HB**, exhibited dramatically different emission properties compared to the other sensors, with **2.Fc-XB** in particular showing a significantly reduced fluorescence quantum yield (Φ = 0.06), relative to the other XB hosts (Fig. 2.12). This significant fluorescence quenching is consistent with PET from the redox-active ferrocene motif to the BODIPY unit, as has been noted in previous studies.[30, 45-48] The nature of this PET quenching is the subject of further investigation later in the chapter (Sections 2.3.2 & 2.3.3).

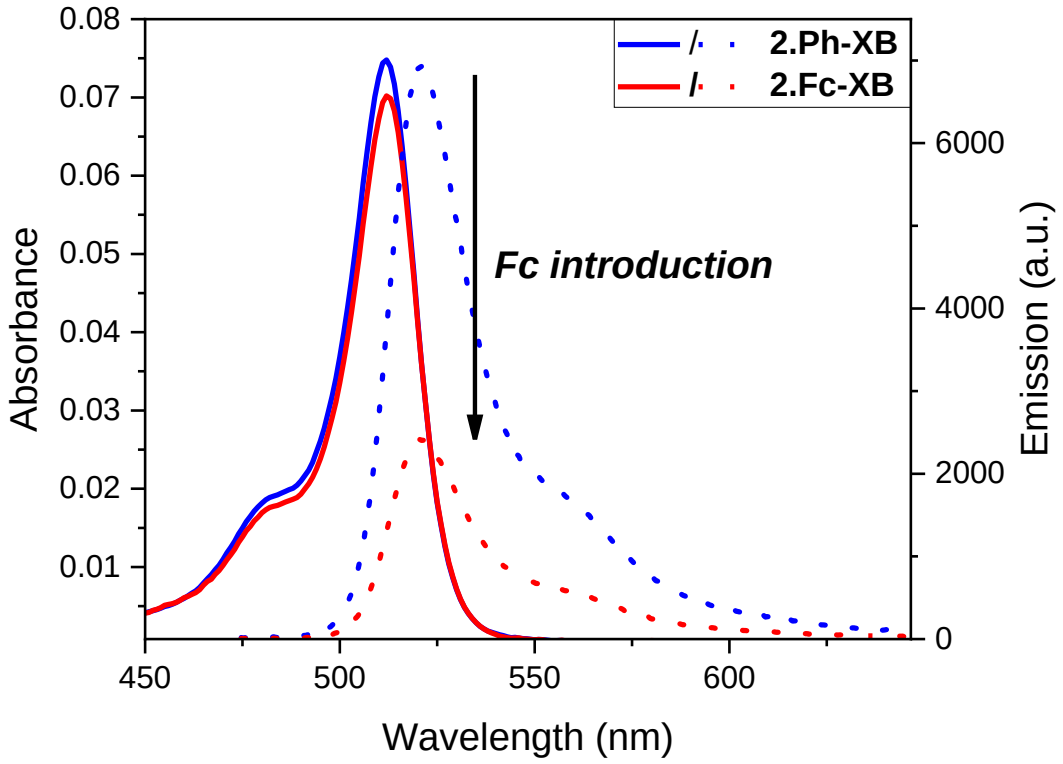


Figure 2.12. Absorbance (solid lines) and fluorescence emission intensity (dashed lines) of 1 μM **2.Ph-XB** (blue) and **2.Fc-XB** (red) in acetone.

2.3 Anion Binding Studies

2.3.1 Fluorescence Titration Studies

Initially, the anion binding properties of the XB receptors were probed by fluorescence titrations in acetone. Aliquots of TBAX (X = Cl, Br, I) were added to 1 μM solutions of the sensors and the emission spectra recorded after each addition. Addition of chloride and bromide anions elicited large increases in emission intensity of up to 100% from **2.Ph-XB** and **2.BDP-XB**, which was ascribed to anion binding-induced restriction of rotation about the BODIPY-*meso* bond (*vide infra*) (Fig. 2.13a). Iodide also caused turn-on fluorescence responses, albeit of a lower magnitude (27% for **2.BDP-XB** and 7% for **2.Ph-XB**) (Fig. 2.14).

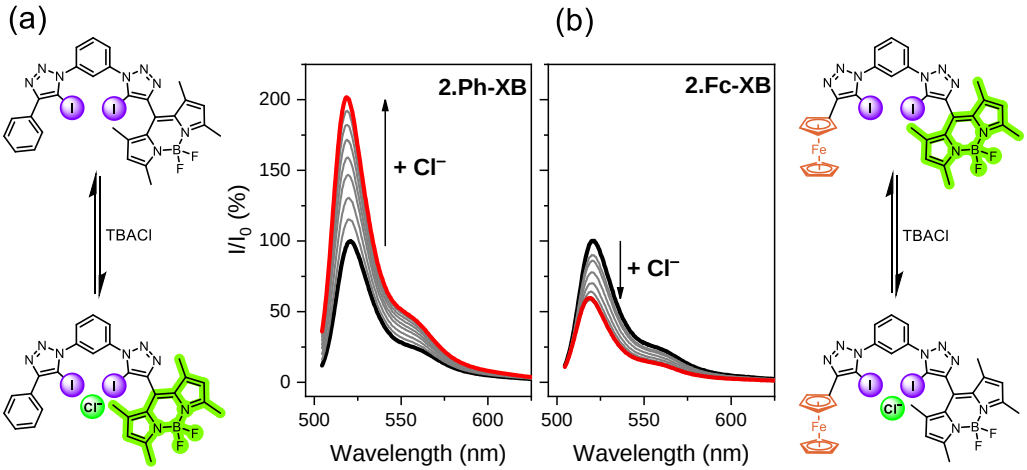


Fig. 2.13. Normalised fluorescence emission response of 1 μM (a) **2.Ph-XB** and (b) **2.Fc-XB** upon addition of increasing concentrations of Cl^- (up to ≈ 2.8 mM) in acetone.

2.Fc-XB showed dramatically different sensing behaviour, with a turn-off response of approximately 45% observed upon the addition of all three halide anions (Fig. 2.13b). This demonstrates that the alteration of the iodotriazole substituent to ferrocenyl induces a complete reversal in the halide anion sensing response from turn-on to turn-off. The fluorescence isotherms resulting from these titrations (Fig. 2.14) were

globally fitted to a 1:1 stoichiometric host-guest binding model, using Origin software,[49] to produce the association constants shown in Table 2.2.

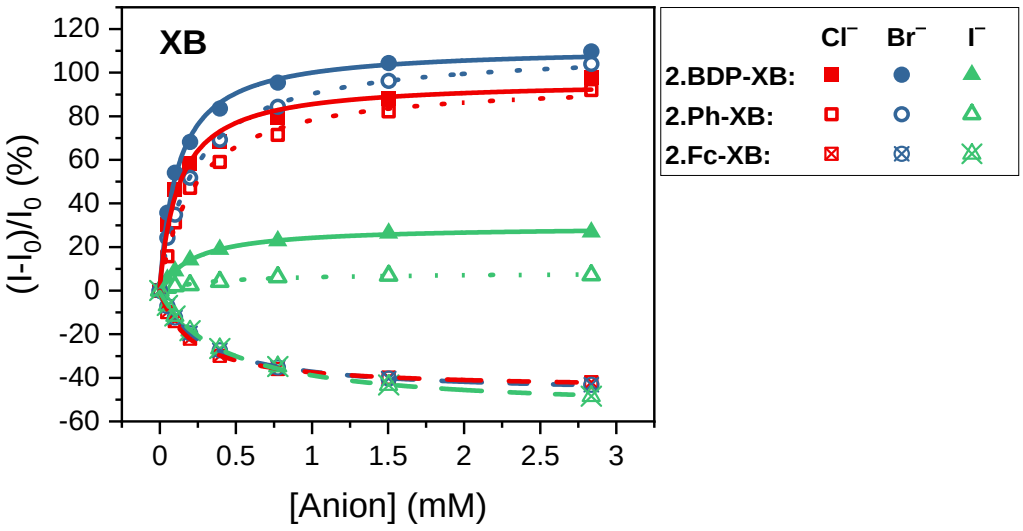


Fig. 2.14. Relative fluorescence response of 1 μM **2.BDP-XB** (filled symbols), **2.Ph-XB** (empty symbols) and **2.Fc-XB** (empty, crossed symbols) receptors in acetone upon addition of halide anions, with lines indicating fits to a 1:1 stoichiometric binding model.

As expected, all XB sensors bound chloride, the most charge-dense anion tested, more strongly than iodide in acetone and the relative anion affinities decreased in the order **2.BDP-XB** > **2.Ph-XB** > **2.Fc-XB**, which reflects the electron-withdrawing ability of the iodotriazole substituents and consequent activation of the XB donor motif by increased polarisation of the iodine atom. Fitting of the isotherms obtained from analogous titration experiments with the HB sensors (where possible) gave consistently lower association constant values, highlighting the increased anion affinity offered by XB interactions, which is consistent with numerous previous reports (Table 2.2).[1, 36, 50]

Table 2.2. Halide association constants K_a (M^{-1})[a] of all receptors.

	2.Ph		**2.BDP**		**2.Fc**	
	XB	**HB**	**XB**	**HB**	**XB**	**HB**
Cl^-	4480	126	7860	70	4390	n.d.
Br^-	4030	78	8600	28	3770	152[b]
I^-	2340	n.d.	4550	n.d.	2040	n.d.

[a] – determined in acetone at 298 K by global fitting of fluorescence isotherms to a 1:1 stoichiometric binding model. [b] Determined by ^{1}H NMR titration in acetone-d_6 and fitted to a 1:1 binding model with Bindfit.[51] All errors <6%. n.d. – not determined due to small fluorescence perturbations. Anions added as their TBA salts.

In the case of **2.Fc-HB**, no association constants could be obtained from the fluorescence titrations, due to the very small perturbations observed. A ^{1}H NMR titration with TBABr in acetone-d_6 confirmed that this lack of fluorescence response did not arise from a lack of binding ($K_a(Br^-)$ = 152 M^{-1}) and that the association constants of **2.Fc-HB** are of a similar magnitude to **2.Ph-HB**, as is the case with their XB analogues (Fig. 2.15). Therefore, the overall lack of fluorescence response is likely due to the simultaneous action of opposing turn-on and turn-off fluorescence response mechanisms, discussed further below. The ^{1}H NMR titration also confirmed the binding mode of the hosts, with large downfield shifts observed in the signals arising from the triazole protons (*d* and *i*) and the internal benzene proton *e*, which are consistent with convergent anion binding in the bis-(iodo)triazole cleft.

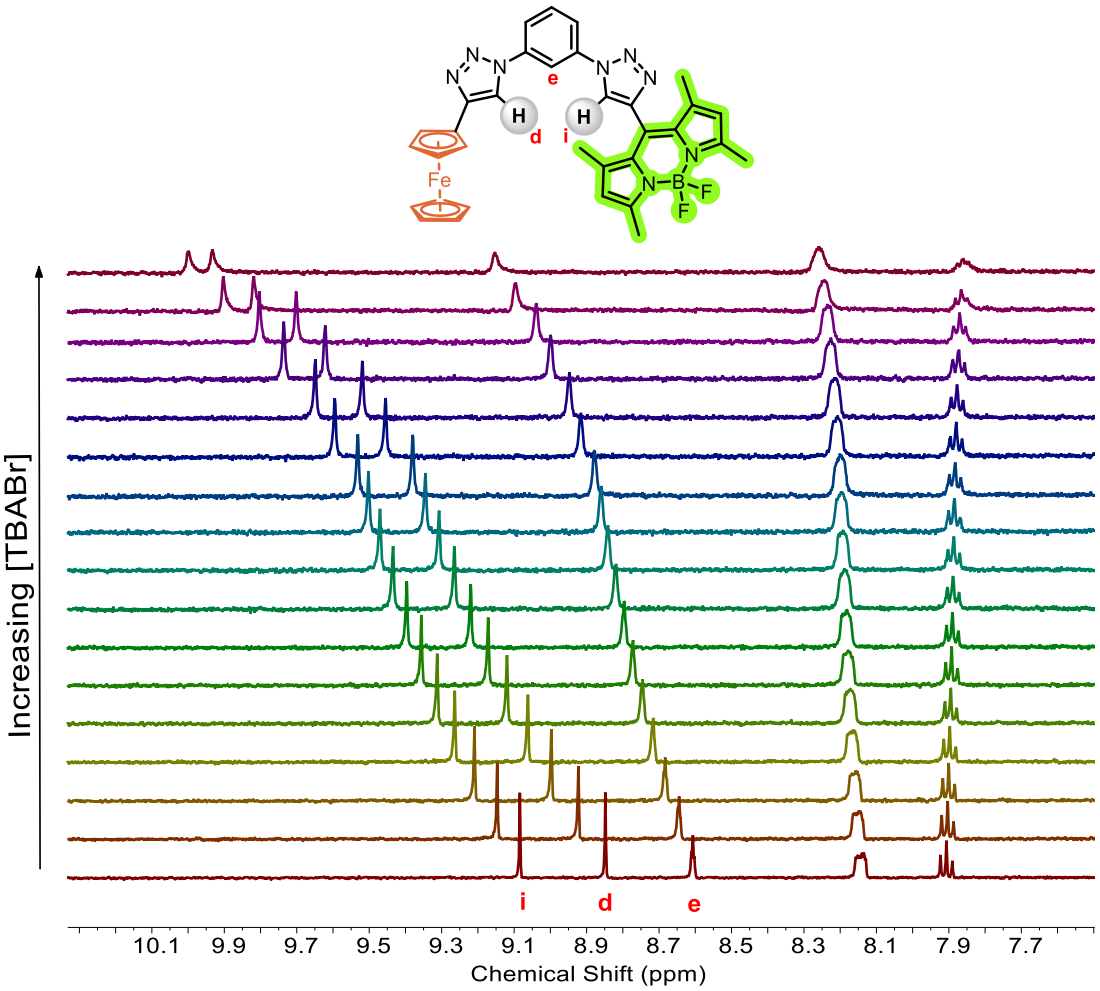


Fig. 2.15. Stacked, truncated ^{1}H NMR spectra of 1mM **2.Fc-HB** with up to 10 equivalents of TBABr. (Acetone-d_6, 298 K)

Indeed, the emission response to anion binding was markedly different for all the HB sensors in comparison to their XB congeners (Fig. 2.16). **2.Ph-HB** and **2.BDP-HB** exhibited very large turn-on responses of up to 250% upon addition of chloride and bromide, whereas iodide elicited modest quenching responses of approximately -25%. The degree of this iodide-induced quenching was approximately linearly related to the concentration of iodide and was therefore ascribed to non-specific heavy-atom quenching, rather than being a result of host-guest binding. Such an effect was not observed for the XB sensors due to their enhanced anion affinity, which meant that lower concentrations of iodide were used in the titrations.

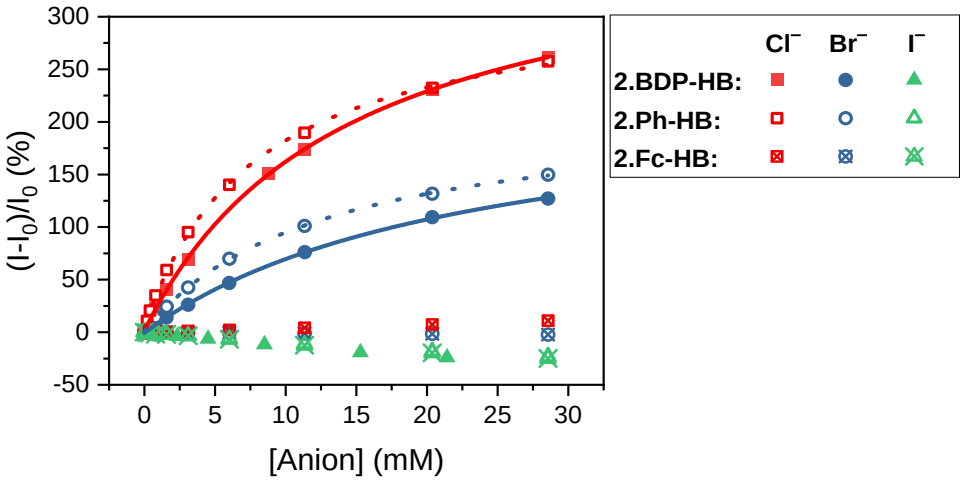


Fig. 2.16. Relative fluorescence response of 1 μM **2.BDP-HB** (filled symbols), **2.Ph-HB** (empty symbols) and **2.Fc-HB** (empty, crossed symbols) receptors in acetone upon addition of halide anions, with lines indicating fits to a 1:1 stoichiometric binding model where possible.

2.3.2 Fluorescence Lifetime Studies

Studies of the fluorescence lifetimes of the receptors were conducted in order to rationalise the contrasting anion binding-induced fluorescence responses of the sensors. In particular, the studies sought to explain the turn-off response observed for **2.Fc-XB** in the presence of anions, which was in stark contrast to the turn-on response displayed by **2.Ph-XB** and **2.BDP-XB**. To this end, the fluorescence lifetimes of each of the receptors in the presence and absence of bromide (used as a model anion) were measured (Table 2.3).

Table 2.3. Fluorescence lifetimes[a] (ns) of all receptors in the presence and absence of TBABr[b].

	2.Ph		**2.BDP**		**2.Fc**	
	XB	**HB**	**XB**	**HB**	**XB**	**HB**
Free Host	1.28	0.25	1.14	0.28	0.41	0.17
Host•Br^-	2.49	0.92	2.32	0.97	0.24	0.18

[a] Determined in acetone at 298 K. Errors < 5%. [b] 3 mM for XB and 30 mM for HB.

As expected, all of the lifetimes measured were mono-exponential and in the ps-ns range, which is typical for BODIPY systems.[19] It is important to highlight that for the XB receptors, the changes in fluorescence lifetime (τ_f) upon anion binding are strongly correlated with the extent of fluorescence intensity changes observed during anion titrations. For instance, **2.BDP-XB** shows a 109% increase in fluorescence intensity by the end of the titration, along with a 103% rise in fluorescence lifetime and, in contrast, **2.Fc-XB** exhibits 43% quenching in fluorescence intensity in the presence of excess bromide, accompanied by a 41% reduction in lifetime (Fig. 2.17).[§]

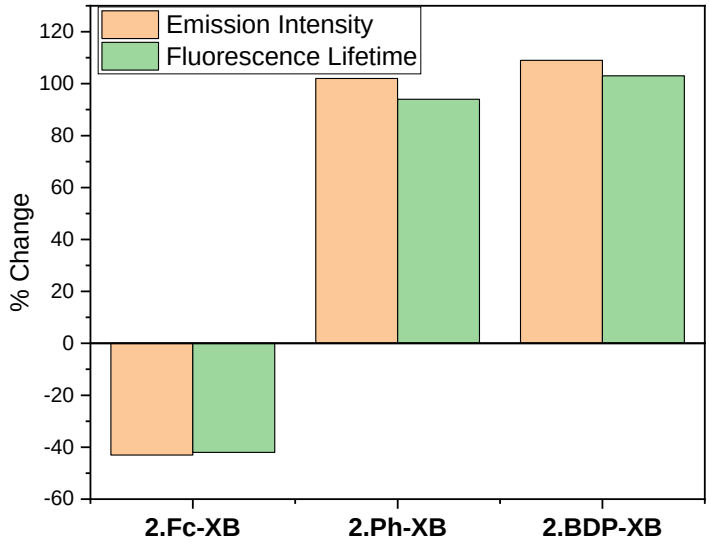


Fig. 2.17. Bar chart of the percentage change in emission intensity and fluorescence lifetime in the presence of 3 mM bromide anions for each of **2.Fc-XB**, **2.Ph-XB** and **2.BDP-XB**.

Therefore, for a given XB receptor, τ_f and Φ appear to be affected by the same factor A upon bromide binding, namely:

$$\phi_{f,0} = A\phi_{f,Br} \qquad \text{(Eqn. 2.1)}$$

[§] The lifetimes of the HB sensors show the same qualitative trends, but they are too low to be reliably analysed.

$$\tau_{f,0} = A\tau_{f,Br} \quad \text{(Eqn. 2.2)}$$

where the subscripts *0* and *Br* indicate the absence and presence of 3 mM bromide respectively. The fluorescence lifetime τ_f is given by:

$$\tau_f = \frac{1}{k_f + k'} \quad \text{(Eqn. 2.3)}$$

k_f is the rate of emission from the S_1 state and k' is the combined rate of all other, non-radiative decay processes from the S_1 state. The fluorescence quantum yield Φ (which is proportional to fluorescence intensity) is given by

$$\phi = k_f \tau_f = \frac{k_f}{k_f + k'} \quad \text{(Eqn. 2.4).}$$

Dividing Eqn. 2.1 by Eqn. 2.2:

$$\frac{\phi_{f,0}}{\tau_{f,0}} = \frac{\phi_{f,Br}}{\tau_{f,Br}} \quad \text{(Eqn. 2.5)}$$

and inserting the relation in Eqn. 2.4:

$$k_{f,0} = k_{f,Br} \quad \text{(Eqn. 2.6).}$$

The result shown in Eqn. 2.6 indicates that when both fluorescence intensity and fluorescence lifetime are modulated by the same factor, *A*, the changes must be attributed to variations in k', rather than k_f. This can be clearly illustrated by considering the counterfactual: if the anion binding-induced increase in fluorescence intensity for **2.BDP-XB** or **2.Ph-XB** was driven by an increase in k_f, a concomitant decrease in the fluorescence lifetime would be expected, but in fact an increase in lifetime is observed. Therefore, the differing fluorescence responses of the XB sensors must be due to the

differing effects anion binding has on the rate of non-radiative decay processes in each of the hosts. In the case of **2.BDP-XB** and **2.Ph-XB**, anion binding causes rigidification of the molecular structure, which reduces the rate of internal conversion, lowering k' and consequently increasing both τ_f and fluorescence intensity (Fig. 2.18). In a similar manner to earlier discussions on the influence of steric bulk adjacent to the BODIPY-*meso* bond, this can be explained by anion binding further "locking" rotation and hence enhancing quantum yields. This rigidification mechanism likely also explains the very large increase in emission intensity seen in **2.BDP-HB** and **2.Ph-HB**, both of which also exhibit an increase in fluorescence lifetime. As the HB free hosts are less rotationally restricted and hence have a lower fluorescence quantum yield in the unbound state, the impact of anion binding is greater for these receptors, leading to a larger emission turn-on response.

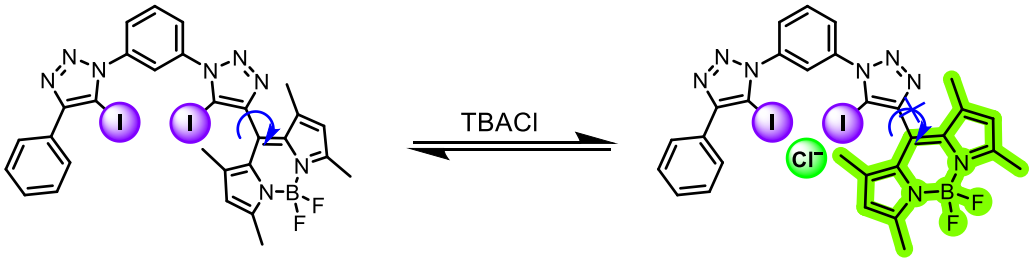


Fig. 2.18. Cartoon showing the restriction of rotation about the BODIPY-*meso* bond upon anion binding in **2.Ph-XB**.

In the cases of **2.Fc-XB/HB**, an additional, opposing influence overcomes this rigidification effect, to the extent that, for **2.Fc-XB**, k' is actually increased – causing a *decrease* in τ_f and Φ. To probe the origin of this increase in k' and given the precedent of PET in BODIPY-ferrocene dyads, the rate of electron transfer k_{ET} from the ferrocene motif to the BODIPY fluorophore was calculated in the presence and absence of bromide. k_{ET} can be calculated for **2.Fc-XB** from the fluorescence lifetimes by comparison with a "reference" compound which does not undergo PET, in this case **2.Ph-XB**:[52]

$$k_{\mathrm{ET,Fc-XB}} = \frac{1}{\tau_{\mathrm{Fc-XB}}} - \frac{1}{\tau_{\mathrm{Ph-XB}}} = 1.66 \times 10^{9}\ s^{-1} \quad \text{(Eqn. 2.7)}$$

For **2.Fc-HB** this rate is similar at 1.88 × 10^9 s^{-1}, however the errors associated with the lifetime measurements are larger for the HB sensor, which subsequently increases the error in k_{ET}. Nonetheless, both of these values are consistent with similar systems which have previously been reported.[53] Upon the addition of bromide, the rate of electron transfer expectedly increases approximately two-fold for **2.Fc-XB**, in line with a more efficient PET process:

$$k_{\mathrm{ET,Fc-XB,Br^-}} = \frac{1}{\tau_{\mathrm{Fc-XB,Br^-}}} - \frac{1}{\tau_{\mathrm{Ph-XB,Br^-}}} = 3.77 \times 10^{9}\ s^{-1}$$

For **2.Fc-HB**, k_{ET} in the presence of bromide also increases by a similar factor to 4.47 × 10^9 s^{-1} Additionally, the PET efficiency θ_{ET} for **2.Fc-XB** can be calculated *via*:

$$\theta_{\mathrm{ET,Fc-XB}} = 1 - \frac{\tau_{\mathrm{Fc-XB}}}{\tau_{\mathrm{Ph-XB}}} = 0.68 \quad \text{(Eqn. 2.8)}$$

θ_{ET} increases to 0.90 in the presence of bromide and a similar increase in θ_{ET} was noted for **2.Fc-HB** from 0.68 (free host) to 0.80 (in the presence of bromide).

These results indicate the PET is kinetically enhanced upon anion binding, which can be attributed, at least to some extent, to conformational changes in the host upon anion binding. In particular, it is conceivable that the ferrocene donor motif is held closer to the BODIPY acceptor unit in the binding conformation, which, as the rate of PET is generally accepted to decay exponentially with donor-acceptor separation,[54] would lead to an increase in the PET efficiency and therefore a decrease in fluorescence emission intensity (Fig. 2.19).

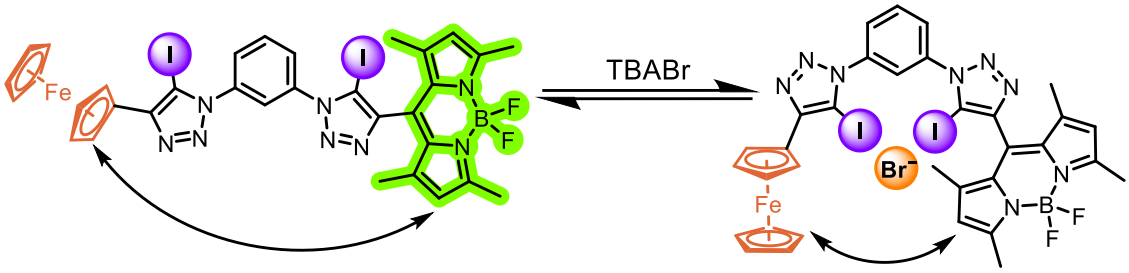


Fig. 2.19. Schematic cartoon showing the kinetic enhancement of PET in **2.Fc-XB** upon anion binding *via* conformational changes.

2.3.3 Electrochemical Studies

Having confirmed the kinetic enhancement to the PET process in **2.Fc-XB/HB** in the presence of a bound anion, the potential thermodynamic contributions to the enhancement of PET were also considered and investigated. This necessitated the acquisition of the electrochemical parameters displayed in Table 2.4.[**] The electrochemical measurements were undertaken in anhydrous, degassed acetonitrile in the presence of 100 mM $TBAPF_6$ as the supporting electrolyte. The change in solvent was required because acetone has an insufficient electrochemical potential solvent window to allow electrochemical characterisation of both the ferrocene and BODIPY motifs.

Table 2.4. Half-wave potentials ($E_{1/2}$) in V[a] *vs.* Fc/Fc^+ of electrochemical couples of **2.Fc-XB/HB** in anhydrous, degassed ACN obtained by SWV.

	2.Fc	
	XB	**HB**
BDP/BDP^-	-1.400	-1.402
Fc/Fc^+	0.097	0.073

[a] Estimated error ± 2 mV.

[**] DPhil student Sophie Patrick carried out these electrochemical measurements.

For both the XB and HB hosts, the ferrocene/ferrocenium and reductive BODIPY/BODIPY^{-} redox couples displayed good chemical reversibility (Fig. 2.30). The half-wave potential for the reductive BODIPY couple was identical within error for both sensors, whilst the Fc/Fc^{+} oxidation required a more oxidising potential in the XB system, which is indicative of the increased electron-withdrawing ability of the iodotriazole group and in concordance with previously reported related systems.[55-56] Having obtained these parameters, the Gibbs free energy of electron transfer ΔG_{ET} was calculated *via* the following equation:[30, 38, 52]

$$\Delta G_{ET} = e\left[E_{\mathrm{Ox,Don}} - E_{\mathrm{Red,Acc}}\right] - E_{00} - \Delta G_{\mathrm{S}} \qquad \text{(Eqn. 2.9)}$$

in which E_{Ox} and E_{Red} refer to the half-wave potentials of the donor (Fc) and acceptor (BODIPY) respectively, E_{00} the BODIPY photoexcitation energy (taken as the midpoint of the absorption and emission maxima),[57] and ΔG_{S} is the coulombic energy of the charge separated state generated by the PET process.[††] Reassuringly, ΔG_{ET} was found to be thermodynamically favourable for both the XB and HB hosts (Table 2.5).

Table 2.5. ΔG_{ET} and E_{00} of **2.Fc-XB/HB** in the presence and absence of excess TBABr.[a]

	2.Fc	
	XB	**HB**
ΔG_{ET} (eV)	-0.903	-0.935
ΔG_{ET} (eV) (in the presence of excess TBABr)	-0.933	n.d.
E_{00} (eV)	2.40	2.41

[a] In acetonitrile in the presence of 0 or up to 50 mM TBABr. n.d. – not determined

[††] The ΔG_{S} term is negligible in this case, see Chapter Six for further discussion.

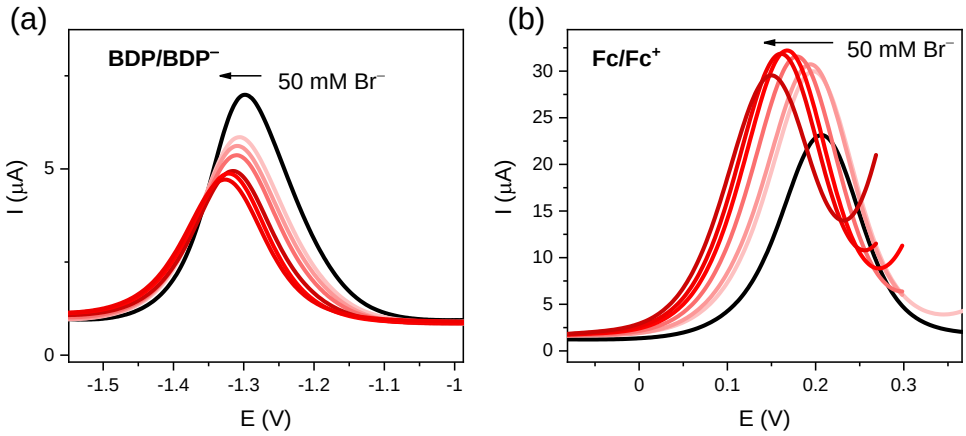


Fig. 2.20. SWVs of 0.5 mM **2.Fc-XB** in anhydrous, degassed ACN, 100 mM $TBAPF_6$, upon titration with Br^-. (a) Reductive BDP couple. (b) Oxidative Fc couple. The overall ionic strength was kept constant at 100 mM throughout.

To assess the change in the thermodynamic favourability of PET upon anion binding, values of E_{Ox} and E_{Red} in the presence of 50 mM TBABr were acquired by electrochemical voltammetric anion binding titrations in acetonitrile. Upon addition of bromide anions, notable cathodic shifts in both the ferrocene/ferrocenium and reductive BODIPY/BODIPY$^-$ redox couples were observed, which reflects the anion binding-induced stabilisation of the ferrocenium and destabilisation of the reduced BODIPY$^-$ state respectively, caused by the increase in local electron density (Fig. 2.20). Despite the polar solvent, the Fc/Fc$^+$ redox couple shifted significantly by up to 60 mV, reflecting the high sensitivity of the directly conjugated ferrocene unit to anion binding.[58] Importantly, the cathodic shift in the Fc/Fc$^+$ redox couple was 30 mV larger than the shift in the BODIPY/BODIPY$^-$ couple and therefore the absolute value of [$E_{Ox} - E_{Red}$] overall becomes less positive, leading to a more favourable ΔG_{ET} of –0.933 eV for **2.Fc-XB** in the presence of bromide (Table 2.5).[⌗] Together with the results obtained from the fluorescence lifetimes,

[⌗] It is important to note that in acetone, the solvent for the anion titration experiments, the influence of anion binding on ΔG_{ET} will be greater, due to the larger voltammetric shifts typically observed in this solvent, leading to a greater PET enhancement.

this suggests that anion binding enhances PET quenching of BODIPY emission in **2.Fc-XB/HB** both kinetically and thermodynamically, through conformational changes and through stabilisation of the ferrocenium cation (Fig. 2.21).

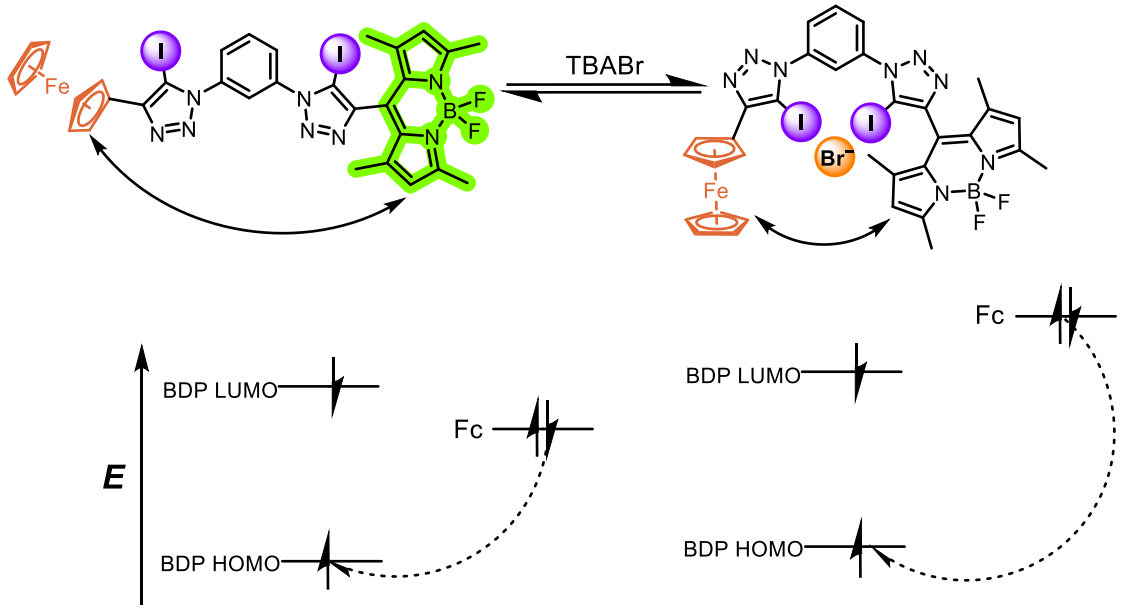


Fig. 2.21. Schematic cartoon showing both the kinetic and thermodynamic enhancement of PET in **2.Fc-XB** upon anion binding, *via* receptor conformational changes and an increase in the electron density at the ferrocene donor, respectively.

The electrochemical response of the ferrocene motif to anion binding allowed **2.Fc-XB/HB** to also act as electrochemical anion sensors and was used to calculate anion association constants for **2.Fc-XB/HB** in a variety of solvent media using a model derived from the Nernst equation (Eqn. 2.10).[59] The use of such a model allows simultaneous determination of the anion association constant with both the reduced form of the host, K_{Red}, and the oxidised form of the host, K_{Ox}. K_{Ox} is typically significantly larger than K_{Red}, due to the additional electrostatic attraction between the cationic receptor and the anion, alongside increased polarisation of the XB/HB donor motif.[40] Fitting of the cathodic voltammetric shifts obtained from titration experiments (Fig. 2.22) to a 1:1 Nernst binding model yielded the association constants shown in Table 2.6.

$$\Delta E = -\frac{RT}{nF}\ln\left(\frac{1+K_{\mathrm{Ox}}[A^-]}{1+K_{\mathrm{Red}}[A^-]}\right) \qquad \text{Eqn. 2.10}$$

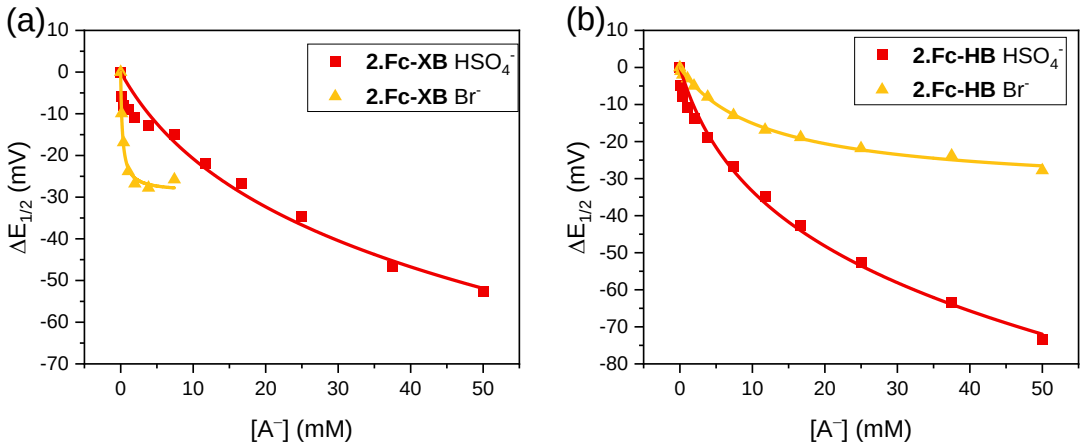


Fig. 2.22. Cathodic voltammetric shifts of 0.1 mM (a) **2.Fc-XB** and (b) **2.Fc-HB** in acetone, 100 mM $TBAClO_4$ upon titration with various anions. The overall ionic strength was kept constant at 100 mM throughout. Solid lines represent fits to a 1:1 host-guest Nernst model (Eqn. 2.10).

The redox-sensing properties of **2.Fc-XB/HB** were first probed in acetone, wherein significant cathodic voltammetric perturbations of the Fc/Fc^+ redox couple were observed in the presence of Br^- or HSO_4^- (Fig. 2.22),[§§] which is in good agreement with numerous reports on related systems.[40, 60-63] Reassuringly, the measured anion association constants with the neutral form of the receptors, K_{Red} (Table 2.6), were of the same order of magnitude as those measured by fluorescence and ^{1}H NMR experiments (Table 2.2), with the superior halide anion affinity offered by XB interactions again evident ($K_{\mathrm{Red}}^{\mathrm{XB}}(Br^-)$ = 2290 M^{-1}, $K_{\mathrm{Red}}^{\mathrm{HB}}(Br^-)$ = 43 M^{-1}). The small differences in association constants measured by each method can be rationalised by considering the large range of sensor concentrations spanned by each of these measurement techniques: fluorescence – 1 μM, voltammetry – 100 μM, ^{1}H NMR – 1000 μM. This in turn affects the concentration of the anion titrant

[§§] Cl^- binding data could not be determined in acetone/$TBAClO_4$ due to the instability of the ferrocenium species in the presence of the halide. I^- cannot be studied due to its low oxidation potential.

solution used for each method and therefore, through differences in ion-pairing amongst other effects, affects the true activity of the anion.[64] Additionally, the electrochemical studies require the use of a 100 mM supporting electrolyte ($TBAClO_4$ or $TBAPF_6$), which although non-coordinating, affects the ionic strength of the solution.

Table 2.6. Maximum cathodic voltammetric shift (ΔE_{Max}, mV), K_{Ox} and K_{Red} (M^{-1}) of hosts **2.Fc-XB/HB** in response to 50 mM of various anions.[a]

	Solvent	**Anion**	ΔE_{Max} **(mV)**	K_{Ox} **(M^{-1})**	K_{Red} **(M^{-1})**
2.Fc-XB	Acetone	Br^-	-28[b]	7040	2290
	Acetone	HSO_4^-	-53	122	n.b.
	ACN : H_2O 99:1 (*v/v*)	Cl^-	-21	98	34
	ACN : H_2O 99:1 (*v/v*)	Br^-	-26	180	57
	ACN : H_2O 99:1 (*v/v*)	HSO_4^-	-2	n.b.	n.b.
2.Fc-HB	Acetone	Br^-	-28	160	43
	Acetone	HSO_4^-	-73	260	n.b.
	ACN : H_2O 99:1 (*v/v*)	Br^-	-23	159	60
	ACN : H_2O 99:1 (*v/v*)	HSO_4^-	-37	89	n.b.

[a] added as their TBA salts. [b] ΔE_{Max} observed at 3.9 mM. n.b. – no binding. All errors < 20%.

As expected, K_{Ox} was consistently of a larger magnitude than K_{Red} for all anions tested and in some cases oxidation of the ferrocene moiety was required to observe any anion binding at all. This was the case for **2.Fc-XB** with HSO_4^- in acetone, wherein K_{Red} was negligible and K_{Ox} = 122 M^{-1}. In the more competitive aqueous-containing solvent system

ACN : H_2O 99:1 (+100 μM $HClO_4$),[***] association constants and the maximum cathodic shifts for all anions were expectedly attenuated (Fig. 2.23). The additional stability of the oxidised ferrocenium moiety in this solvent mixture permitted the determination of a Cl^- association constant for **2.Fc-XB**, the value of which was lower than for Br^-, reflecting the Hofmeister solvation bias introduced by the presence of 1% H_2O. In contrast, no anion binding nor a significant cathodic shift were observed for **2.Fc-XB** upon the addition of HSO_4^- in the more competitive solvent mixture system, whereas a significant cathodic shift and weak HSO_4^- anion binding was seen for **2.Fc-HB**, which underscores the frequently observed XB-halide/HB-oxoanion preference.[40, 60-61, 65-66]

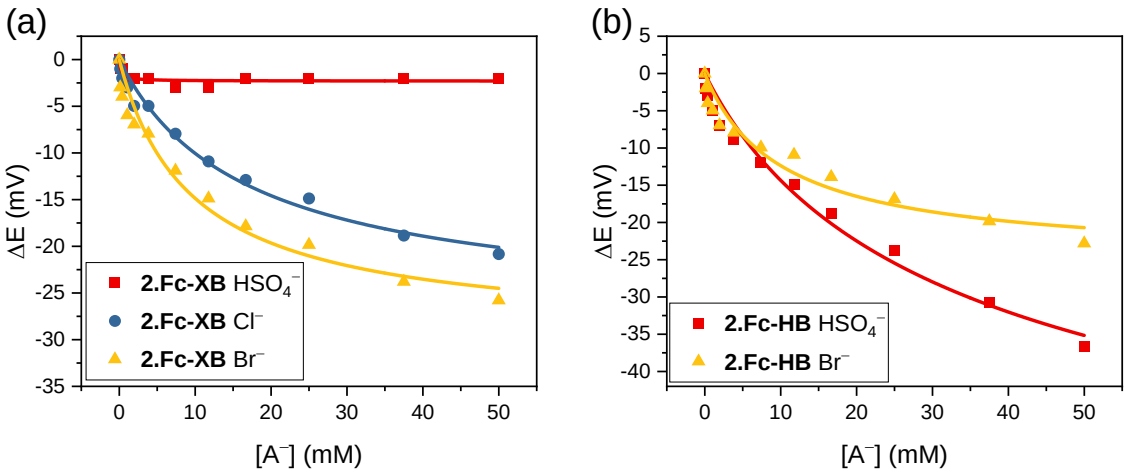


Fig. 2.23. Cathodic voltammetric shifts of 0.1 mM (a) **2.Fc-XB** and (b) **2.Fc-HB** in ACN : H_2O 99:1 (+100 μM $HClO_4$), 100 mM $TBAClO_4$ upon titration with various anions. The overall ionic strength was kept constant at 100 mM throughout. Solid lines represent fits to a 1:1 host-guest Nernst model (Eqn. 2.10).

[***] These electrolyte conditions were, as discussed in more detail below, chosen to further enhance the chemical stability of the ferrocenium redox-state.

2.4 Spectroelectrochemical Anion Sensing

Having studied the ability of this family of sensors to act as independent optical and electrochemical anion sensors, attention then turned to combining these methodologies to allow anion sensing with the advantages of both techniques: spectroelectrochemical anion sensing. Specifically, the hosts were designed so that information about the redox state of the ferrocene motif in **2.Fc-XB/HB** could be relayed optically through the BODIPY fluorophore, which could allow electrochemical anion sensing at low fluorescence concentrations. The fact that the ferrocene moiety in **2.Fc-XB/HB** has a significant effect on BODIPY emission in its native, neutral state, and that this influence is modulated by anion binding, was encouraging in this regard. Initial investigations therefore focused on establishing the effect of ferrocene oxidation on the BODIPY emission in **2.Fc-XB/HB**.

2.4.1 Influence of Ferrocene Oxidation State on BODIPY Fluorescence

In previous studies of ferrocene-BODIPY dyads, oxidation of the ferrocene moiety was typically associated with a recovery of fluorescence due to a turn-off of the PET pathway. For example, in 2015 Kovtun, Blank, Nemykin and co-workers reported a series of BODIPY derivatives functionalised *via* Knoevenagel condensation reactions with ferrocene units (Fig. 2.24).[46] Transient absorption spectroscopy measurements suggested a PET mechanism of fluorescence quenching, which was confirmed by oxidation of the ferrocene moieties, which led to a recovery of fluorescence emission of up to 100-fold. This is due to the oxidised Fe(III) metal centre in the ferrocenium being unable to transfer an electron to the excited BODIPY fluorophore in the same manner that the neutral, Fe(II)-containing ferrocene unit can.

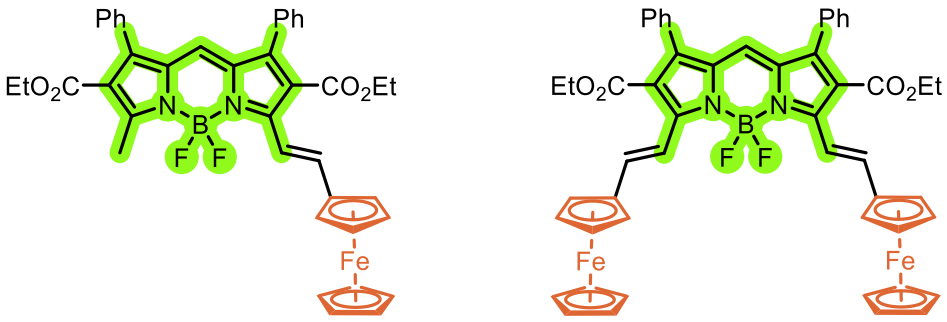


Fig. 2.24. Kovtun, Blank and Nemykin's ferrocene-BODIPY dyads.

However, such a recovery in emission intensity is not always observed upon ferrocene oxidation in dyad systems. For instance, in 2002 Tian and co-workers reported the ferrocene-naphthalimide dyad shown in Fig. 2.25a.[67] Relative to the control compound (Fig. 2.25b), the neutral dyad showed emission features of a 50-fold lower intensity, which was attributed to PET from the Fc moiety to the naphthalimide fluorophore. Upon oxidation to the ferrocenium cation, fluorescence emission was not recovered, as was expected, but instead remained 50-times lower than the control compound. This was attributed to an energy transfer *from* the excited naphthalimide unit *to* the oxidised ferrocenium, the reverse of the transfer observed in the neutral dyad. In a 1995 report,[68] an oxidative PET mechanism, wherein an electron is transferred from the excited state of a fluorophore to the cationic ferrocenium (Fig. 2.25c) was demonstrated to be responsible for the quenched emission of $Ru(phen)_3^{2+}$ in the presence of oxidised ferrocenium derivates (Fig. 2.25d).

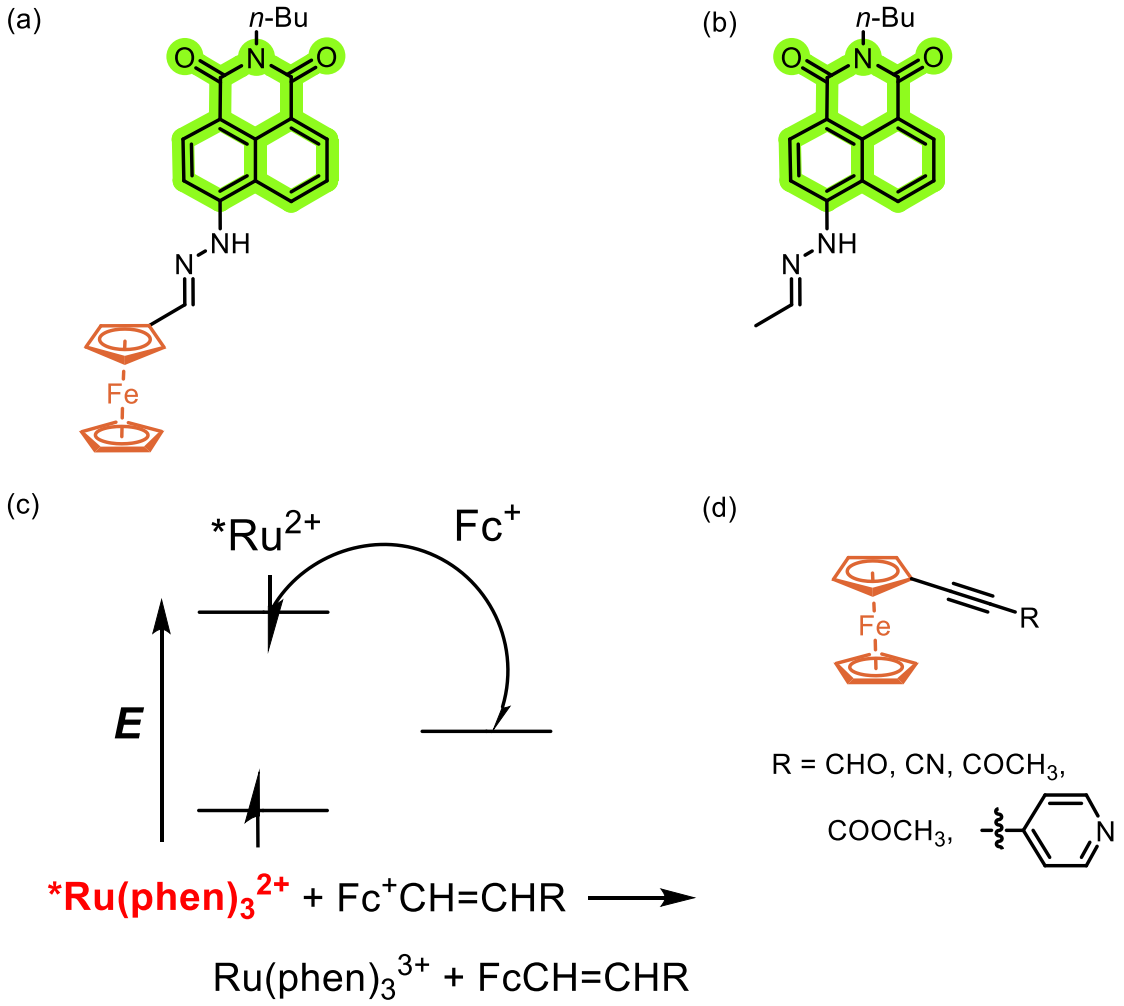


Fig. 2.25 (a) Tian's ferrocene-naphthalimide dyad and (b) control compound. (c) the oxidative PET mechanism active between $Ru(phen)_3^{2+}$ and the ferrocene derivatives shown in (d).

The influence of the ferrocene oxidation state on the BODIPY emission of **2.Fc-XB/HB** was initially probed by chemical oxidation of the Fc moiety using $Fe(ClO_4)_3$ as the oxidant in acetone (Fig. 2.26). The oxidation to the ferrocenium state (**2.Fc$^+$-XB/HB**) did not result in any noticeable alterations in either the BODIPY absorbance spectrum or the position of the fluorescence emission maximum. However, in contrast to most other ferrocene-BODIPY dyads, this oxidation caused a further reduction in fluorescence intensity of 20%-35%. Regardless of the direction of the emission changes, these experiments demonstrated that the redox state of the ferrocene moiety could be relayed

via the BODIPY emission intensity and therefore that spectroelectrochemical sensing may be possible.

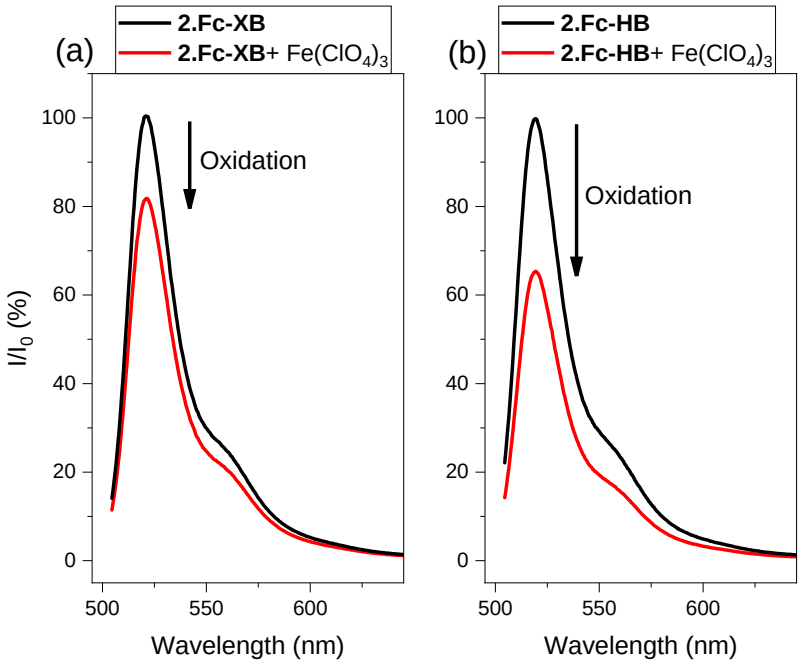


Fig. 2.26. Emission spectra of (a) **2.Fc-XB** and (b) **2.Fc-HB** before and after the addition of excess $Fe(ClO_4)_3$. (10 μM, acetone, 298 K)

Having established that fluorescence of **2.Fc-XB/HB** is highly sensitive not only to the presence of the neutral ferrocene moiety but also to its oxidation state, focus shifted to electrochemically modulating the oxidation state of the ferrocene unit in a reliable and reversible way, whilst monitoring the emission of **2.Fc-XB/HB**, with the aim of measuring electrochemical parameters at very low concentrations *via* fluorescence spectroscopy. In order to simultaneously monitor the emission of **2.Fc-XB/HB** and also apply an electrochemical potential to the solution, a spectroelectrochemical cell was constructed. This consisted of a standard quartz fluorescence cuvette (1 × 1 × 3 cm), to which was fitted a 3D printed cap, which held a three-electrode electrochemistry setup (Pt grid working electrode, non-aqueous Ag|$AgNO_3$ reference electrode and a Pt wire counter electrode) in the solution but above the light path (Fig. 2.27). The solvent was stirred rapidly throughout

measurements, using a stirrer bar below the light path, to ensure that complete bulk electrolysis was achieved.

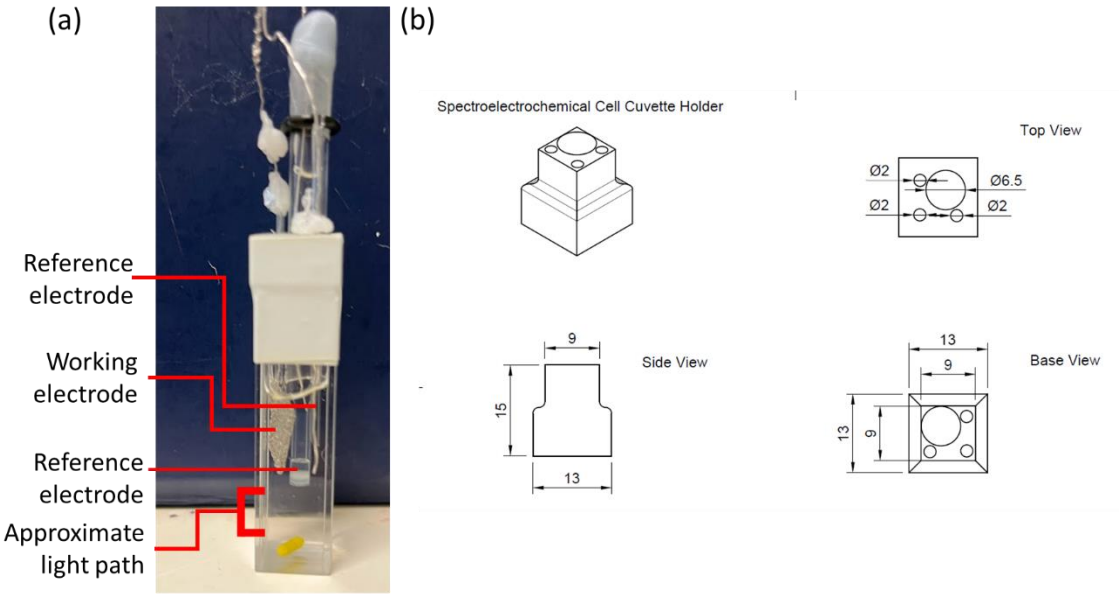


Fig. 2.27. (a) The cuvette used for spectroelectrochemical experiments with electrodes labelled and (b) the schematic of the 3D-printed cap used to hold the electrodes in place.

In order to improve the chemical stability of the oxidized ferrocenium receptor during repeated cycles of bulk electrolysis, while minimizing the formation of undesirable electrolysis by-products, ACN : H_2O 99:1 (*v*/*v*) and 100 μM $HClO_4$ was used as the solvent with 100 mM $TBAClO_4$ as the supporting electrolyte. In a typical experiment, the emission intensity at λ_{max} was monitored whilst alternating oxidative and reductive potentials were applied. As illustrated in Fig. 2.28, repeated bulk electrolysis of a rapidly stirred solution of 100 nM **2.Fc-XB** resulted in well-defined, highly reversible fluorescence switching. The high sensitivity of the fluorescence technique allows for the use of very low probe concentrations, facilitating rapid bulk electrolysis. These results again demonstrated the clear redox-dependent modulation of fluorescence emission, with a two-fold change in

emission intensity, but also demonstrated that this switching could be achieved electrochemically and reversibly.

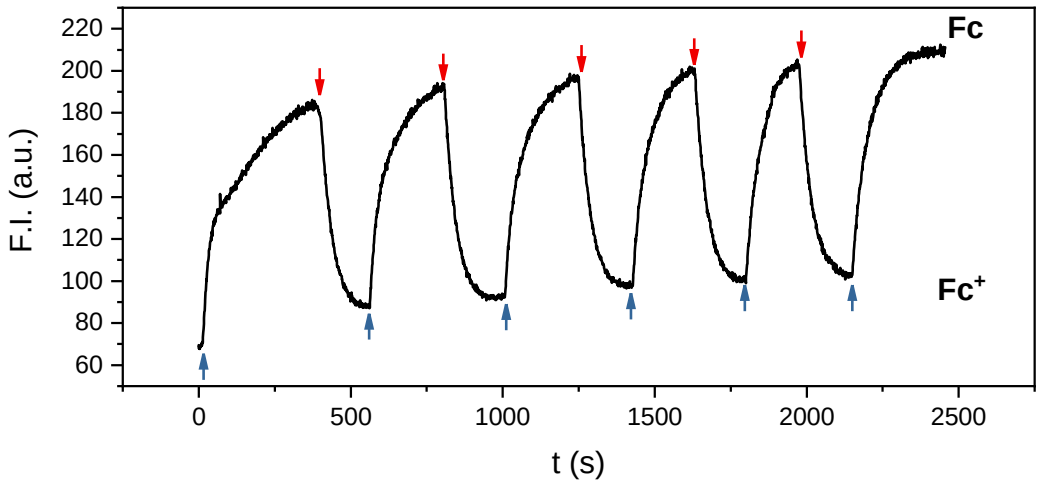


Fig. 2.28. Fluorescence of 100 nM **2.Fc-XB** in ACN : H_2O 99:1 (*v/v*), 100 mM $TBAClO_4$, 100 µM $HClO_4$ under alternating reductive (blue arrows) and oxidative potentials (red arrows). Note under these conditions the receptor is initially present in its oxidised state.

Having determined the methods and conditions required to reliably electrochemically address a solution of **2.Fc-XB/HB** whilst monitoring its emission output, attention turned to using this technique to measure the redox properties of **2.Fc-XB/HB**. By gradually and cyclically varying the potential applied to the electrochemical cell while monitoring the emission from a 500 nM solution of **2.Fc-XB/HB**, a "fluorescence cyclic voltammogram" (CV) could be generated (Fig. 2.29).

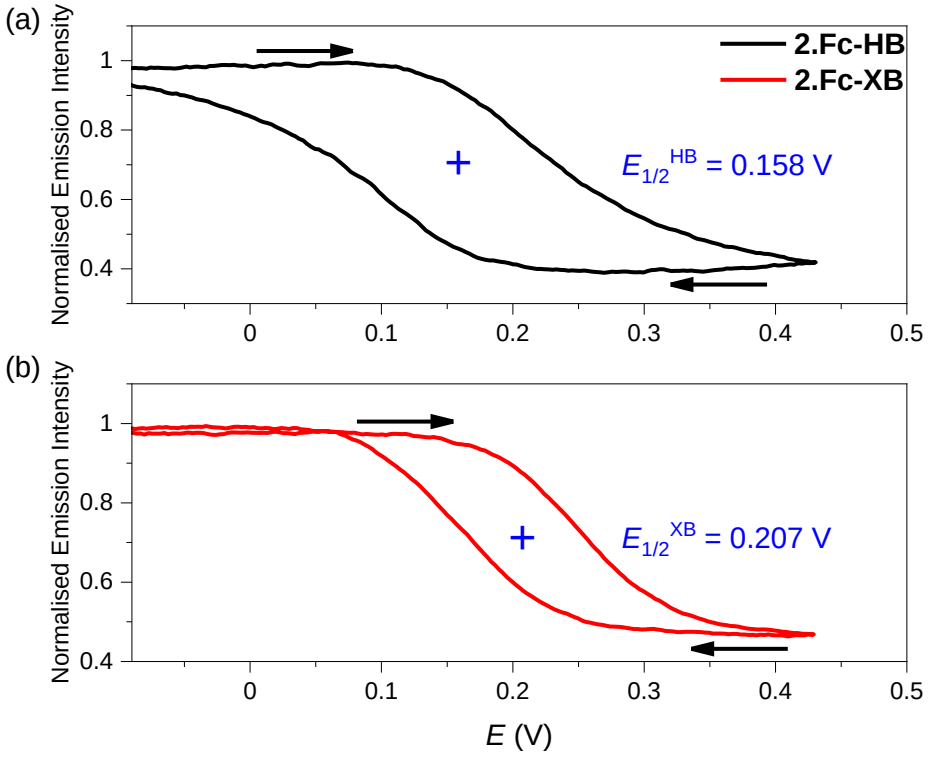


Fig. 2.29. Normalised and smoothed fluorescence emission of 500 nM (a) **2.Fc-HB** and (b) **2.Fc-XB** in ACN, 100 mM $TBAClO_4$, 200 μM $HClO_4$ during one CV scan between –0.1 and 0.45 V at 0.75 mV/s. Black arrows indicate the scan direction. Blue crosses indicate the mid-point of the half-wave potentials of the forward and backward scans.

This 'fluorescence CV' serves as a direct optical readout of the Nernstian redox distribution imposed on the bulk solution in the cell by the applied potential. Due to a kinetic delay between the application of the potential and equilibrium being established in the cell, likely caused by slow mass transport in the densely packed cuvette, the forward and backward scans do not overlap. Despite this, the receptor's half-wave potential ($E_{1/2}$) can still be determined by taking the arithmetic mean of the forward and backward potentials, resulting in a value for **2.Fc-HB** of $E_{1/2}^{HB}$ = 0.158 V (*vs.* Ag|$AgNO_3$). This value is identical within error to the $E_{1/2}^{HB}$ of 0.16 V measured through traditional electrochemical methods under nearly identical conditions (Fig. 2.30). By the same fluorescence method, $E_{1/2}^{XB}$ for **2.Fc-XB** was determined to be 0.207 V, which is still reassuringly close to the value

of 0.197 V measured electrochemically. Notably, this spectroelectrochemical technique provides a highly sensitive measure of the electrochemical parameters of the sensors at *much lower concentrations* (in this case, 500-fold) compared to conventional voltammetric techniques, which typically require concentrations exceeding 100 µM.

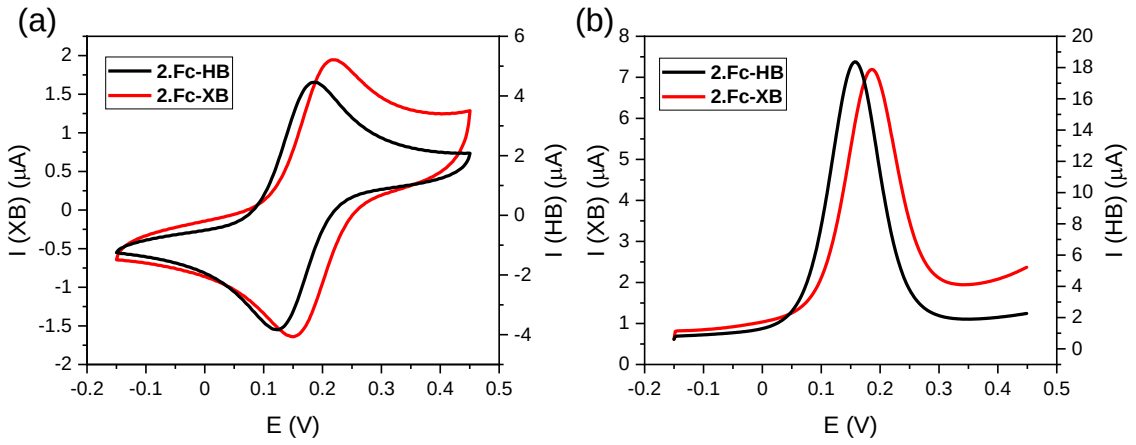


Fig. 2.30. Measurement of electrochemical parameters of **2.Fc-XB/HB** by traditional electrochemical means in ACN : H_2O 99:1 (*v/v*) and 100 µM $HClO_4$ with 100 mM $TBAClO_4$ as the supporting electrolyte. (a) Cyclic voltammogram of 0.25 mM **2.Fc-XB/HB** (red/black lines, respectively) at a scan rate of 100 mV s^{-1}. (b) Square wave voltammogram of 0.1 mM **2.Fc-XB/HB** (red/black lines, respectively). Potentials wrt. $Ag|AgNO_3$.

2.4.2 Spectroelectrochemical Anion Sensing

Following these promising results, attempts were made to use this spectroelectrochemical methodology for anion sensing by measuring a cathodic shift in the 'fluorescence CV' upon addition of anions. Initial attempts focused on sensing chloride with **2.Fc-XB** in ACN with 100 mM $TBAClO_4$ and 200 µM $HClO_4$, the anhydrous conditions and charge-dense anion being selected to maximise the cathodic shift and therefore maximise the probability that anion binding could be observed with this technique. However, whilst the oxidised ferrocenium state was stable in isolation under these conditions, addition of 20 mM chloride caused decomposition of the oxidised sensor, indicated by a large and irreversible increase in fluorescence intensity upon oxidation of the sensor in the

presence of chloride, likely due to the decomposition of the Fc PET donor motif caused by the nucleophilic anion (Fig. 2.31).

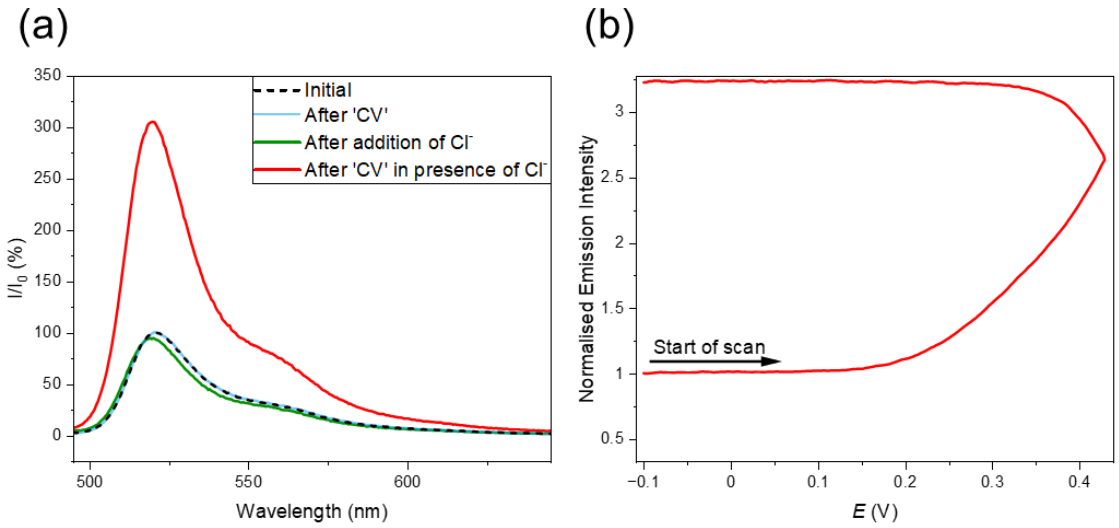


Fig. 2.31. (a) Emission spectra of **2.XB-Fc** showing the decomposition of the ferrocenium state in the presence of chloride anions. No changes in the emission spectrum were observed after recording the 'fluorescence CV' in the absence of chloride (black and blue lines nearly perfectly overlap) and a small shift was observed upon the addition of chloride to the neutral receptor (green line). However, upon recording the fluorescence CV in the presence of chloride, a large and irreversible increase in fluorescence intensity was observed (red line). (b) Attempted 'fluorescence CV' of **2.Fc-XB** in the presence of chloride, showing the irreversible changes to emission intensity. (500 nM, ACN, 100 mM $TBAClO_4$, 200 µM $HClO_4$, 298 K)

This result indicated that the Fc^+ state is not stable under bulk electrolysis conditions in the presence of the chloride anion. Therefore, attention turned to sensing the less nucleophilic HSO_4^- anion. Earlier conventional electrochemical sensing experiments had shown that the HB redox-active sensor **2.Fc-HB** had displayed a much larger cathodic shift in response to this anion, compared to **2.Fc-XB** (Table 2.6). Therefore, **2.Fc-HB** was used for subsequent spectroelectrochemical sensing studies.

Satisfyingly, increasing the concentration of HSO_4^- in a solution of **2.Fc-HB** resulted in significant cathodic shifts measured by successive 'fluorescence CV' scans (Fig. 2.32).

Specifically, shifts of –11 mV and –19 mV were observed in the presence of 20 mM and 40 mM HSO_4^-, respectively. Although these shifts are smaller than those measured under similar experimental conditions using conventional voltammetry (Table 2.6), importantly, in a proof-of-principle, these findings nonetheless demonstrate the possibility of spectroelectrochemical anion sensing. This novel method not only permits measurement of the anion binding-induced cathodic shift at very low concentrations (500 nM), but also allows the fluorescence response to anion binding of the *oxidised* state of the receptor to be measured. In this case, as evident from inspection of the anodic vertices of the 'fluorescence CV' scans shown in Fig. 2.32a, the oxidised receptor, **2.Fc$^+$-HB**, showed an increase in emission intensity of up to 27% upon anion binding (ΔI_+), likely due to rigidification of the receptor in analogy to earlier findings.

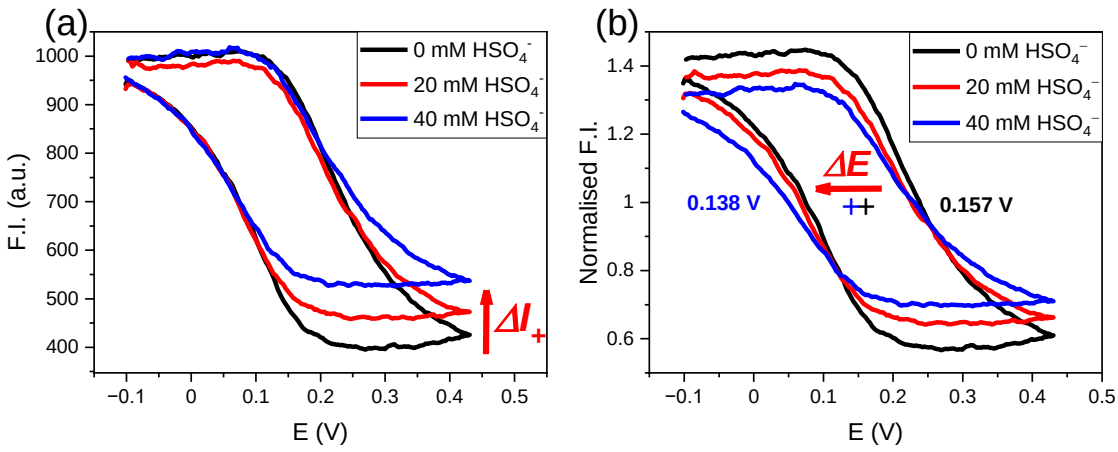


Fig. 2.32. 'Fluorescence CVs' of **2.Fc-HB** in the presence of varying concentrations of $TBAHSO_4$. The emission was monitored at λ_{max} in all cases. All potentials are wrt. $Ag|AgNO_3$. (a) Absolute fluorescence intensity. The red arrow labelled ΔI_+ indicates the change in fluorescence emission in the oxidized receptor state. (b) Normalized fluorescence intensity. Each set of data is normalized by the fluorescence intensity at $E_{1/2}$ to highlight the cathodic potential shift (pluses and red arrow). (500 nM, ACN, 100 mM $TBAClO_4$, 200 µM $HClO_4$, 298 K)

The change in emission intensity at the anodic vertex obscures the cathodic shift caused by anion binding. By normalising the fluorescence intensity of each of the scans

such that the intensity at $E_{1/2}$ is equal to 1, the cathodic shift becomes visibly apparent (Fig. 2.32b). It is important to note that the observed changes upon anion addition cannot arise from signal decay, as the initial fluorescence intensity is regained at the cathodic vertex in each run when the absolute intensity is plotted (Fig. 2.32a).

No change in emission intensity is observed at the cathodic vertex, because the neutral form of **2.Fc-HB** is not expected to bind HSO_4^- in this competitive solvent, as indicated by the electrochemical titrations (Table 2.6). This was further confirmed by fluorescence titrations of **2.Ph-HB**, which has very similar anion affinity to **2.Fc-HB** but is optically responsive, which indicated no appreciable binding of HSO_4^- in ACN and only very weak binding in the less competitive solvent acetone ($K_a(HSO_4^-)$ = 43 M^{-1}) (Fig. 2.33). This highlights a crucial advantage of the spectroelectrochemical technique, namely that sensing of HSO_4^- in ACN with **2.Fc-HB** would not be possible by conventional optical techniques, because the neutral HB receptor has no significant affinity for HSO_4^-. However, due to the anion binding enhancement associated with electrochemical oxidation and *in situ* generation of the cationic ferrocenium state, the oxidised form of **2.Fc-HB** can bind and sense HSO_4^- in this competitive solvent medium.

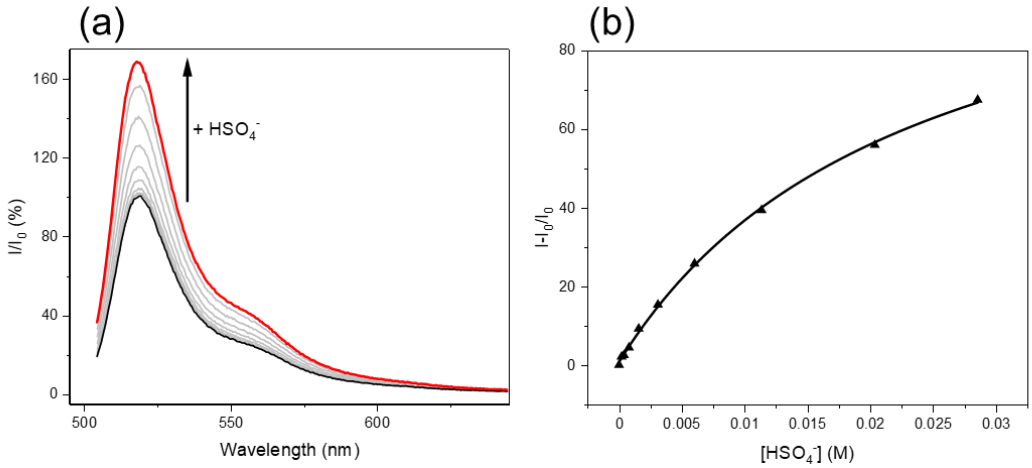


Fig. 2.33. (a) Normalised fluorescence emission response of 1 μM **2.Ph-HB** upon addition of increasing concentrations of HSO_4^- (up to ≈ 28 mM) in acetone and (b) relative fluorescence response of 1 μM **2.Ph-HB** in acetone upon addition of increasing concentrations of HSO_4^-, with the line indicating a fit to a 1:1 stoichiometric binding model.

Further advantages of this spectroelectrochemical sensing modality include the ability to simultaneously measure three separate sensing parameters: the cathodic shift, the change in emission intensity of the neutral sensor and the change in emission intensity of the oxidised sensor upon anion binding ($\Delta E_{1/2}$, ΔI_{Red} and ΔI_{Ox} respectively), which can otherwise only be obtained through separate experiments or are difficult to access at all (ΔI_{Ox}). All of these parameters can be measured at very low concentrations due to the sensitivity of the fluorescence technique, which compares very favourably to conventional voltammetry which requires concentrations approximately 500-fold higher.

2.5 Chapter Conclusions and Future Work

A family of six novel XB and HB, redox-active, fluorescent anion sensors were synthesised by a convenient CuAAC methodology and optically characterised, which revealed a suppressed fluorescence quantum yield in the Fc-containing hosts **2.Fc-XB/HB**. Electrochemical experiments and calculations with respect to reference compounds determined that PET from the Fc unit to the BODIPY fluorophore is thermodynamically feasible for both of these compounds, explaining their quenched emission.

Detailed fluorescence and electrochemical anion binding studies were conducted on this family of receptors, which demonstrated that, in the non-redox active hosts **2.Ph-XB/HB** and **2.BDP-XB/HB**, anion binding is associated with a large increase in emission intensity, which was attributed to restriction of rotation about the BODIPY-*meso* bond. In a complete reversal, the redox active XB sensor **2.Fc-XB** exhibited a turn-off response to anion binding, which was demonstrated, through electrochemical and fluorescence lifetime measurements, to be due to both kinetic and thermodynamic enhancements to the PET quenching mechanism. Therefore, the series of anion sensors described in this chapter offers control of the direction of fluorescence response to anion binding through simple substitution of the iodotriazole substituent. Importantly, only the XB series of hosts offered this level of control, as **2.Fc-HB** was optically unresponsive to anion binding in its neutral state. Additionally, the XB sensors also offered significantly higher anion affinity relative to their HB analogues.

The ferrocene electrochemical reporter group present in **2.Fc-XB/HB** also facilitated electrochemical anion sensing, rendering **2.Fc-XB/HB** dual-channel anion sensors. Measured anion association constants with the neutral forms of the receptors

(K_{Red}) accorded well with the affinities measured by other techniques (fluorescence and ^{1}H NMR) and were also significantly lower than the association constants with the cationic, ferrocenium form of the sensor (K_{Ox}) which is generated *in situ* in the course of the electrochemical titration experiments.

Through experiments using $Fe(ClO_4)_3$ as a chemical oxidant, it was demonstrated that the redox state of the Fc moiety in **2.Fc-XB/HB** could be relayed *via* the intensity of the BODIPY fluorescence emission. The development of a spectroelectrochemistry setup allowed a solution of **2.Fc-XB/HB** to be electrochemically addressed whilst its emission spectrum was simultaneously measured. This enabled electrochemical measurements to be undertaken at exceedingly low concentrations relative to conventional techniques.

Finally and most importantly, both sensing modalities offered by **2.Fc-HB** were united in a novel spectroelectrochemical sensing technique which combined the advantages of fluorescence and electrochemical sensing to allow the redox-modulation of anion binding through *in situ* generation of a charged receptor state at nanomolar concentrations. This technique facilitated the proof-of-principle spectroelectrochemical sensing of bisulfate in acetonitrile, which was not possible with conventional optical methods due to the low affinity of **2.Fc-HB** for HSO_4^- in this competitive solvent. The unprecedented combined 'fluorescence CV' experiment simultaneously allowed the measurement of both the optical response of the sensor in two different oxidation states and the voltammetric response of the redox probe.

The directional control of fluorescence response to anion binding could facilitate future work in the development of more advanced optical ion sensors. For example, this principle could be extended to cation or ion-pair sensing, by incorporation of a ferrocene

PET quencher and a BODIPY PET acceptor into a conformationally dynamic ion-pair host scaffold (Fig. 2.34). Conceivably, such a design would allow the selective sensing of potassium salts over sodium salts, due to the known propensity of K^+ to form 2:1 stoichiometric 'sandwich' complexes with benzo-15-crown-5,[36] which would bring the Fc and BODIPY moieties close together, enhancing PET. Such a response would not be observed for sodium cations, which form 1:1 complexes with benzo-15-crown-5.

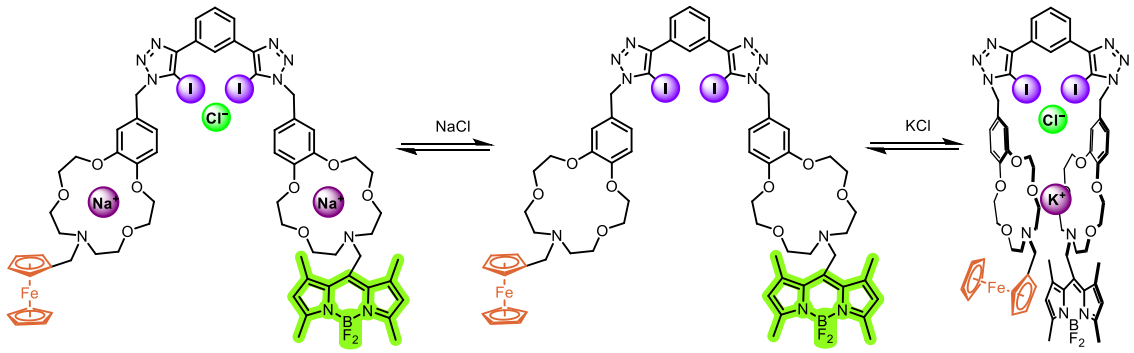


Fig. 2.34. Possible structure of a conformationally dynamic ion-pair sensor, designed to be selective for potassium salts.

Further development of the spectroelectrochemical sensing modality could include the design of quantitative spectroelectrochemical sensors. One drawback of the present design is that BODIPY emission is affected by *both* the redox state of the Fc unit *and* anion binding, which makes changes in the emission spectrum difficult to fit to a binding model. Future work could therefore focus on the synthesis of sensors in which the BODIPY optical reporter group is remote from the anion binding site and thus only responsive to the Fc redox state, which would simplify the optical response and allow quantitative data to be extracted (Fig. 2.35).

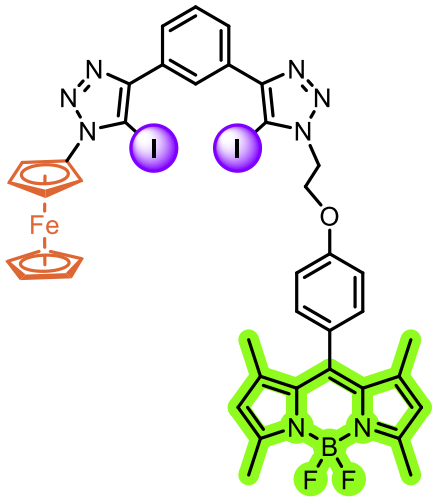


Fig. 2.35. Potential design of a second generation spectroelectrochemical anion sensor in which the BODIPY fluorophore is remote to the anion binding site and therefore only responsive to the redox state of the Fc moiety.

2.6 References for Chapter Two

1. R. Hein, P. D. Beer, *Chem. Sci.* **2022**, *13*, 7098-7125.
2. P. Thordarson, *Chem. Soc. Rev.* **2011**, *40*, 1305-1323.
3. M. Burnworth, S. J. Rowan, C. Weder, *Chem. Eur. J.* **2007**, *13*, 7828-7836.
4. W. Chen, C. Guo, Q. He, X. Chi, V. M. Lynch, Z. Zhang, J. Su, H. Tian, J. L. Sessler, *J. Am. Chem. Soc.* **2019**, *141*, 14798-14806.
5. E. J. Mitchell, A. J. Beecroft, J. Martin, S. Thompson, I. Marques, V. Félix, P. D. Beer, *Angew. Chem. Int. Ed.* **2021**, *60*, 24048-24053.
6. A. C. Olivieri, *Anal. Chim. Acta* **2015**, *868*, 10-22.
7. J. Chan, S. C. Dodani, C. J. Chang, *Nat. Chem.* **2012**, *4*, 973-984.
8. S. J. Payne, G. L. Fiore, C. L. Fraser, J. N. Demas, *Anal. Chem.* **2010**, *82*, 917-921.
9. A. M. del Hierro, W. Kronberger, P. Hietz, I. Offenthaler, H. Richter, *J. Exp. Bot.* **2002**, *53*, 559-563.
10. A. P. de Silva, H. Q. N. Gunaratne, T. Gunnlaugsson, A. J. M. Huxley, C. P. McCoy, J. T. Rademacher, T. E. Rice, *Chem. Rev.* **1997**, *97*, 1515-1566.
11. H. M. Tay, P. Beer, *Org. Biomol. Chem.* **2021**, *19*, 4652-4677.
12. R. Martínez-Máñez, F. Sancenón, *Chem. Rev.* **2003**, *103*, 4419-4476.
13. K. R. A. S. Sandanayake, K. Nakashima, S. Shinkai, *J. Chem. Soc., Chem. Commun.* **1994**, 1621-1622.
14. F. Szemes, D. Hesek, Z. Chen, S. W. Dent, M. G. B. Drew, A. J. Goulden, A. R. Graydon, A. Grieve, R. J. Mortimer, T. Wear, J. S. Weightman, P. D. Beer, *Inorg. Chem.* **1996**, *35*, 5868-5879.
15. D. Villarón, S. J. Wezenberg, *Angew. Chem.* **2020**, *132*, 13292-13302.
16. G. Hennrich, H. Sonnenschein, U. Resch-Genger, *Tetrahedron Lett.* **2001**, *42*, 2805-2808.
17. G. J. Kavarnos, *Fundamental concepts of photoinduced electron transfer*, Springer Berlin Heidelberg, Berlin, Heidelberg, **1990**.
18. P. G. Sutariya, H. Soni, S. A. Gandhi, A. Pandya, *New J. Chem.* **2019**, *43*, 737-747.
19. A. Loudet, K. Burgess, *Chem. Rev.* **2007**, *107*, 4891-4932.
20. F. J. Frank, P. G. Waddell, M. J. Hall, J. G. Knight, *Org. Lett.* **2021**, *23*, 8595-8599.
21. W. Li, Q. Gong, X. Guo, Q. Wu, F. Chang, H. Wang, F. Zhang, E. Hao, L. Jiao, *J. Org. Chem.* **2021**.
22. L. Jiao, C. Yu, J. Wang, E. A. Briggs, N. A. Besley, D. Robinson, M. J. Ruedas-Rama, A. Orte, L. Crovetto, E. M. Talavera, J. M. Alvarez-Pez, M. Van Der Auweraer, N. Boens, *RSC Adv.* **2015**, *5*, 89375-89388.
23. R. Arumugaperumal, P. Venkatesan, T. Shukla, P. Raghunath, R. Singh, S.-P. Wu, M.-C. Lin, H.-C. Lin, *Sens. Actuators B Chem.* **2018**, *270*, 382-395.
24. Y. Cheong Tse, R. Hein, E. J. Mitchell, Z. Zhang, P. D. Beer, *Chem. Eur. J.* **2021**, *27*, 14550-14559.
25. N. A. Bumagina, E. V. Antina, *Coord. Chem. Rev.* **2024**, *505*, 215688.
26. S. Toliautas, J. Dodonova, A. Žvirblis, I. Čiplys, A. Polita, A. Devižis, S. Tumkevičius, J. Šulskus, A. Vyšniauskas, *Chem. Eur. J.* **2019**, *25*, 10342-10349.
27. X. Yin, Y. Li, Y. Li, Y. Zhu, X. Tang, H. Zheng, D. Zhu, *Tetrahedron* **2009**, *65*, 8373-8377.
28. R. Ziessel, P. Retailleau, K. J. Elliott, A. Harriman, *Chem. Eur. J.* **2009**, *15*, 10369-10374.
29. M. R. Rao, K. V. P. Kumar, M. Ravikanth, *J. Organomet. Chem.* **2010**, *695*, 863-869.
30. X. Wu, W. Wu, X. Cui, J. Zhao, M. Wu, *J. Mater. Chem. C* **2016**, *4*, 2843-2853.
31. F. Otón, A. Espinosa, A. Tárraga, I. Ratera, K. Wurst, J. Veciana, P. Molina, *Inorg. Chem.* **2009**, *48*, 1566-1576.
32. S. C. Patrick, R. Hein, M. Sharafeldin, X. Li, P. D. Beer, J. J. Davis, *Chem. Eur. J.* **2021**, *27*, 17700-17706.
33. T. Romero, A. Caballero, A. Tárraga, P. Molina, *Org. Lett.* **2009**, *11*, 3466-3469.
34. R. Kampes, R. Tepper, H. Görls, P. Bellstedt, M. Jäger, U. S. Schubert, *Chem. Eur. J.* **2020**, *26*, 14679-14687.
35. A. Docker, C. H. Guthrie, H. Kuhn, P. D. Beer, *Angew. Chem. Int. Ed.* **2021**, *60*, 21973-21978.
36. A. J. Taylor, A. Docker, P. D. Beer, *Chem. Asian J.* **2023**, *18*, e202201170.

37. A. Docker, Y. C. Tse, H. M. Tay, A. J. Taylor, Z. Zhang, P. D. Beer, *Angew. Chem. Int. Ed.* **2022**, *61*, e202214523.
38. Y. V. Zatsikha, T. S. Blesener, A. J. King, A. T. Healy, P. C. Goff, N. O. Didukh, D. A. Blank, Y. P. Kovtun, V. N. Nemykin, *J. Phys. Chem. B* **2020**, *125*, 360-371.
39. M. Albrecht, A. Lippach, M. P. Exner, J. Jerbi, M. Springborg, N. Budisa, G. Wenz, *Org. Biomol. Chem.* **2015**, *13*, 6728-6736.
40. R. Hein, X. Li, P. D. Beer, J. J. Davis, *Chem. Sci.* **2021**, *12*, 2433-2440.
41. C. Würth, M. Grabolle, J. Pauli, M. Spieles, U. Resch-Genger, *Nat. Protoc.* **2013**, *8*, 1535-1550.
42. E. Bassan, Y. Dai, D. Fazzi, A. Gualandi, P. G. Cozzi, F. Negri, P. Ceroni, *Photochem. Photobiol. Sci.* **2022**.
43. K. Chen, Y. Dong, X. Zhao, M. Imran, G. Tang, J. Zhao, Q. Liu, *Frontiers in Chemistry* **2019**, *7*.
44. Y. V. Zatsikha, N. O. Didukh, R. K. Swedin, V. P. Yakubovskyi, T. S. Blesener, A. T. Healy, D. E. Herbert, D. A. Blank, V. N. Nemykin, Y. P. Kovtun, *Org. Lett.* **2019**, *21*, 5713-5718.
45. D. Brunel, G. Noirbent, F. Dumur, *Dyes Pigm.* **2019**, *170*, 107611.
46. Y. V. Zatsikha, E. Maligaspe, A. A. Purchel, N. O. Didukh, Y. Wang, Y. P. Kovtun, D. A. Blank, V. N. Nemykin, *Inorg. Chem.* **2015**, *54*, 7915-7928.
47. T. K. Khan, R. R. Pissurlenkar, M. S. Shaikh, M. Ravikanth, *J. Organomet. Chem.* **2012**, *697*, 65-73.
48. O. Galangau, I. Fabre-Francke, S. Munteanu, C. Dumas-Verdes, G. Clavier, R. Méallet-Renault, R. Pansu, F. Hartl, F. Miomandre, *Electrochim. Acta* **2013**, *87*, 809-815.
49. Origin Corporation, *OriginPro*, **2023**.
50. J. Y. Lim, P. D. Beer, *New J. Chem.* **2018**, *42*, 10472-10475.
51. *Bindfit v0.5*, http://app.supramolecular.org/bindfit/. (accessed periodically and repeatedly).
52. J. Ding, K. Feng, C.-H. Tung, L.-Z. Wu, *J. Phys. Chem. C* **2011**, *115*, 833-839.
53. X. Wu, W. Wu, X. Cui, J. Zhao, M. Wu, *J. Mater. Chem. C* **2016**, *4*, 2843-2853.
54. H. Chen, M. A. Ratner, G. C. Schatz, *J. Phys. Chem. C* **2011**, *115*, 18810-18821.
55. J. Y. C. Lim, P. D. Beer, *Eur. J. Inorg. Chem.* **2017**, *2017*, 220-224.
56. J. Y. C. Lim, M. J. Cunningham, J. J. Davis, P. D. Beer, *Chem. Commun.* **2015**, *51*, 14640-14643.
57. R. Marcus, *J. Phys. Chem.* **1989**, *93*, 3078-3086.
58. K. M. Bąk, S. C. Patrick, X. Li, P. D. Beer, J. J. Davis, *Angew. Chem. Int. Ed.* **2023**, *62*.
59. R. Oliveira, S. Groni, C. Fave, M. Branca, F. Mavré, D. Lorcy, M. Fourmigué, B. Schöllhorn, *Phys. Chem. Chem. Phys.* **2016**, *18*, 15867-15873.
60. R. Hein, P. D. Beer, J. J. Davis, *Chem. Rev.* **2020**, *120*, 1888-1935.
61. S. C. Patrick, R. Hein, A. Docker, P. D. Beer, J. J. Davis, *Chem. Eur. J.* **2021**, *27*, 10201-10209.
62. R. Oliveira, S. Groni, C. Fave, M. Branca, F. Mavre, D. Lorcy, M. Fourmigue, B. Schollhorn, *Phys. Chem. Chem. Phys.* **2016**, *18*, 15867-15873.
63. C. Fave, B. Schöllhorn, *Curr. Opin. Electrochem.* **2019**, *15*, 89-96.
64. B. Gómez-González, N. Basílio, B. Vaz, M. Pérez-Lorenzo, L. García-Río, *Angew. Chem.* **2024**.
65. J. Y. C. Lim, P. D. Beer, *Chem* **2018**, *4*, 731-783.
66. J. Pancholi, P. D. Beer, *Coord. Chem. Rev.* **2020**, *416*, 213281.
67. J. Gan, H. Tian, Z. Wang, K. Chen, J. Hill, P. A. Lane, M. D. Rahn, A. M. Fox, D. D. C. Bradley, *J. Organomet. Chem.* **2002**, *645*, 168-175.
68. X.-B. Xia, Z.-F. Ding, J.-Z. Liu, *J. Photochem. Photobiol. A* **1995**, *88*, 81-84.

Chapter 3

Aza-BODIPY Hosts for Ratiometric Anion Sensing and Tuneable Singlet Oxygen Generation

3 Aza-BODIPY Hosts for Ratiometric Anion Sensing and Tuneable Singlet Oxygen Generation

3.1 Introduction

3.1.1 Red-Shifted Fluorophores and the Near Infra-Red Window

One of the most important applications of fluorescent probes is in intracellular biological imaging.[1-2] This refers to the use of fluorescent probes to visualise the local properties of sub-cellular environments, such as pH,[3] viscosity,[4] and the concentration of ions,[5-6] oxygen,[7] and glucose.[8] Such imaging techniques are critical for understanding the mechanism of various diseases,[5, 9-10] elucidating cell signalling pathways and function,[11-12] and have been used in the study[13] and treatment of various cancers.[14]

Although some probes are in effect single-use chemidosimeters,[15] such as the intracellular H_2S probe reported by Wang and Zhao in 2023,[16] in which the chlorine-functionalised BODIPY fluorophore undergoes a nucleophilic substitution reaction to form a thiol, causing a dramatic increase in emission (Fig. 3.1a), a distinct advantage of fluorescence imaging is that it allows the study of living cells, which means that reversible and dynamic sensors are therefore preferred. An early such example is the halide sensor 6-methoxy-*N*-(3-sulfopropyl)quinolinium (SPQ), which simply functions *via* collisional quenching of its fluorescence (Fig. 3.1b).[17] However, as SPQ and other related dyes do not possess an anion binding domain, they are not specific to any particular anion and therefore their use for halide imaging suffers from interference from numerous other anion species such as nitrate, sulfite, sulfate and phosphate.[18]

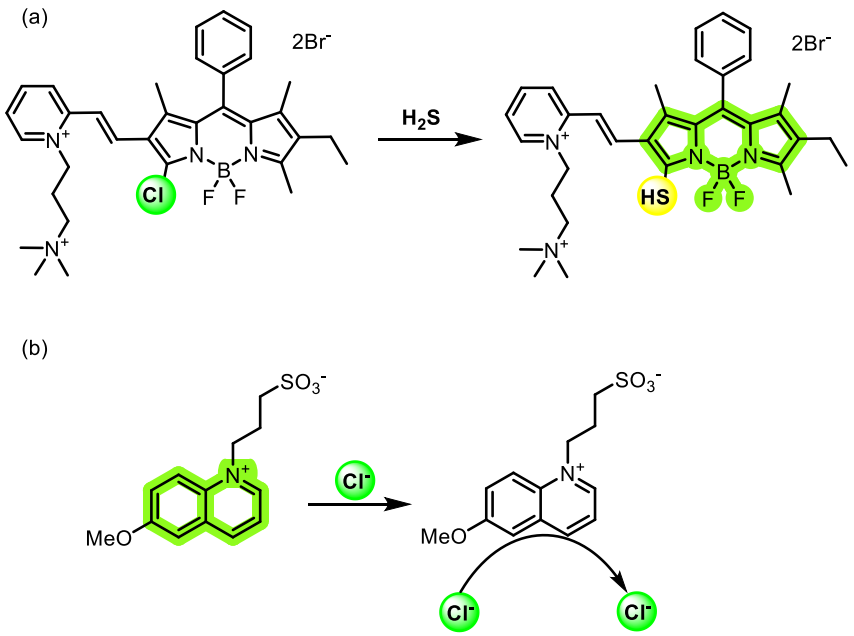


Fig. 3.1. (a) Wang and Zhao's chemidosimeter intracellular H_2S probe and (b) the halide probe SPQ, operating *via* a collisional quenching mechanism.

A further disadvantage of quinoline-based probes is their optical properties. In particular, SPQ has absorption and emission maxima of 348 nm and 442 nm respectively,[19] which means that imaging with these probes requires irradiating the biological sample with UV light. Dyes with short wavelength absorption and emission features (λ_{abs} or λ_{em}< 600 nm) have many disadvantages for biological imaging, which include:[20-21] (i) tissue and DNA damage caused by exposure to high-energy radiation;[22] (ii) poor tissue penetration, due to the strong absorption of short wavelengths by biological chromophores such as haemoglobin, preventing imaging of deeper-lying tissues; (iii) interference from emissive biological molecules, such as cytochromes and myoglobin, which emit in this region;[23] and (iv) poor photostability of fluorescent probes irradiated with high-energy light, causing photobleaching over time.

These disadvantages have led to intense interest in the development of probes which operate in the biologically-relevant near-infra-red 1 (NIR-1) window of 650-950 nm.

This wavelength window is of particular interest because biological tissue is particularly optically transparent in this region (Fig. 3.2).[24-25]

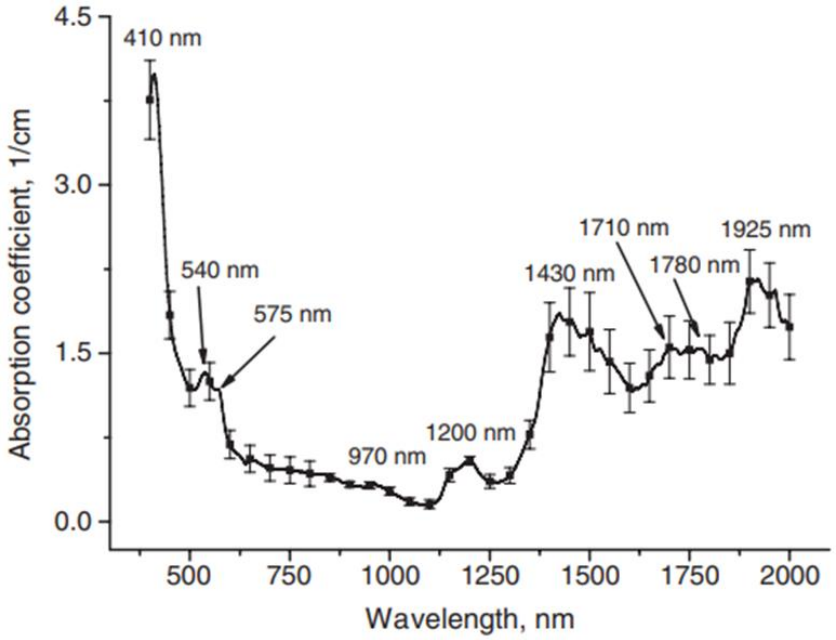


Fig. 3.2. The wavelength dependence of the absorption coefficient of human skin *in vitro*. Copyright IOPScience, 2005, reproduced with permission.[25]

Structural modification of fluorophores which ordinarily absorb and emit at shorter wavelengths can extend their optical features into the NIR-1 window. Common strategies include increasing the extent of the conjugated π-system and introducing electron-withdrawing groups to decrease the energy of the LUMO and thus decrease the energy gap to the HOMO (Fig. 3.3).[26]

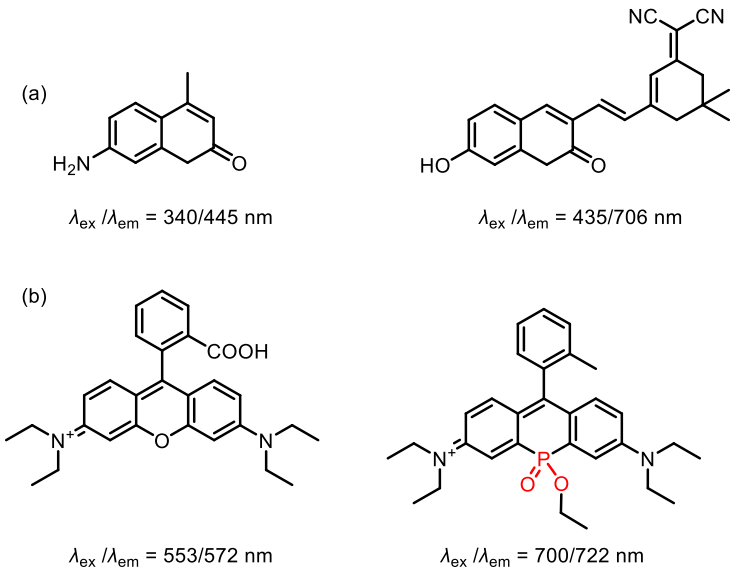


Fig. 3.3. Increasing the wavelength of absorption/emission features of fluorophores by (a) extending the π-system and incorporation of electron withdrawing groups[27] and (b) incorporation of electron-withdrawing chelating group.[28]

First reported in 2002,[29] aza-borondipyrromethene (aza-BODIPY) compounds retain many of the advantages of the related BODIPY class of fluorophore, but with the additional advantage of displaying dramatically red-shifted absorption and emission features, caused by their greater conjugation and incorporation of the electron-withdrawing aza-*N* atom.[30] The aza-BODIPY core can also be derivatised at a variety of positions to give many different geometries and conformations, including at the pyrrolic positions (Fig. 3.4a),[31] on the peripheral aromatics (Fig. 3.4b),[32] and at the boron centre (Fig. 3.4c).[33]

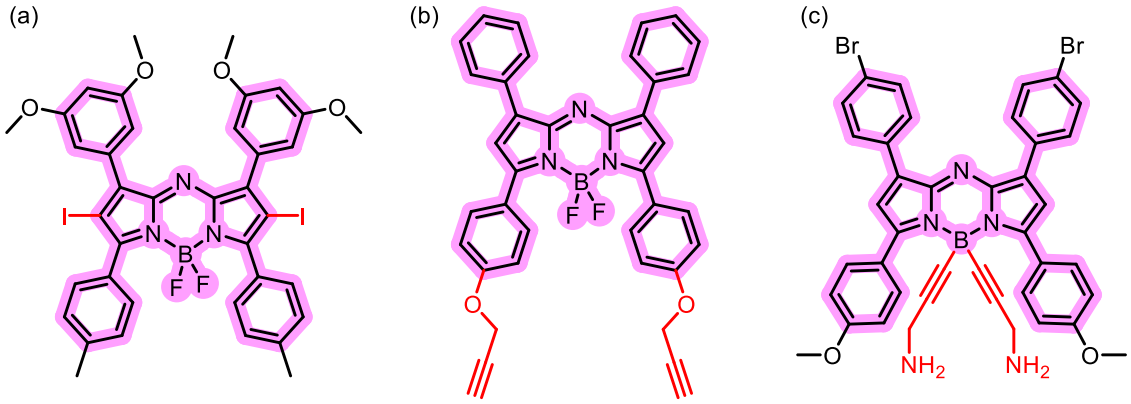


Fig. 3.4. Possible derivatisation (shown in red) of the aza-BODIPY core: (a) pyrrolic positions, (b) peripheral aromatics, and (c) at the boron centre.

The unique combination of these advantageous optical properties and the synthetic versatility of aza-BODIPY compounds makes them highly promising candidates for use in the development of supramolecular sensors. Indeed, they have been used as sensors for various cations, including alkali metals (Fig. 3.5a),[34] mercury,[35] and copper.[36] Aza-BODIPY compounds have also been employed as pH sensors (Fig. 3.5b).[37-39] In the field of anion sensing, aza-BODIPY-based chemidosimeters have been developed for NO_2^-,[40] F^- (Fig. 3.5c),[41] CN^-,[42] and ClO^-,[43] but notably these compounds are not reversible supramolecular anion sensors, which are not yet known for the aza-BODIPY fluorophore.

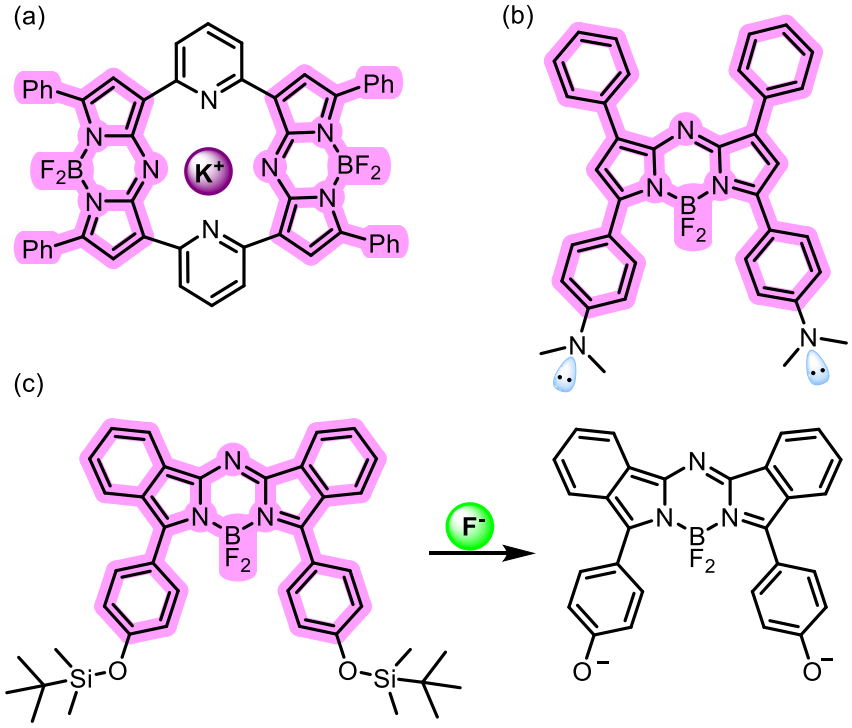


Fig. 3.5. Aza-BODIPY sensors: (a) Tang's Na^+/K^+ probe,[34] (b) O'Shea's pH probe,[37] and (c) Shen's chemidosimeter for fluoride.[41]

3.1.2 Oxygen Sensitisation and Photodynamic Therapy

Relative to the very bright BODIPY class of fluorophores, aza-BODIPYs often exhibit lower fluorescence quantum yields,[44] due in part to increased singlet-to-triplet intersystem crossing.[31] This increased intersystem crossing, whilst slightly detrimental to their fluorescence applications, means that aza-BODIPY compounds are capable of sensitising triplet oxygen to generate singlet oxygen ($^1O_2$), *via* their triplet state (Fig. 3.6).[45-46]

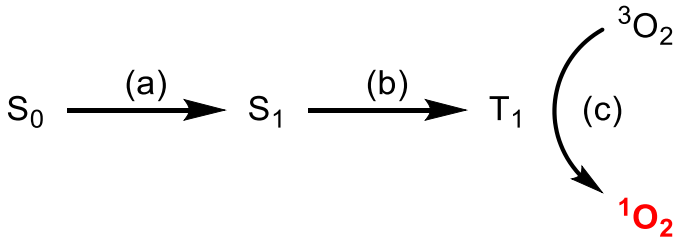


Fig. 3.6. Photophysical pathway for the generation of $^1O_2$. (a) Excitation, (b) intersystem crossing, (c) energy transfer.

$^1O_2$ is a highly reactive oxygen species (ROS) which, when generated in biological cells, can be used to disrupt metabolic processes and induce cell death. Therefore, photosensitising compounds, which generate $^1O_2$, can be used in the treatment of certain diseases. First, the photosensitiser is delivered to the relevant area and, second, the area is irradiated to excite the photosensitiser and generate ROS (Fig. 3.7). This treatment, known as photodynamic therapy (PDT), is used to treat age-related macular degeneration, acne and certain cancers, amongst other diseases.[47]

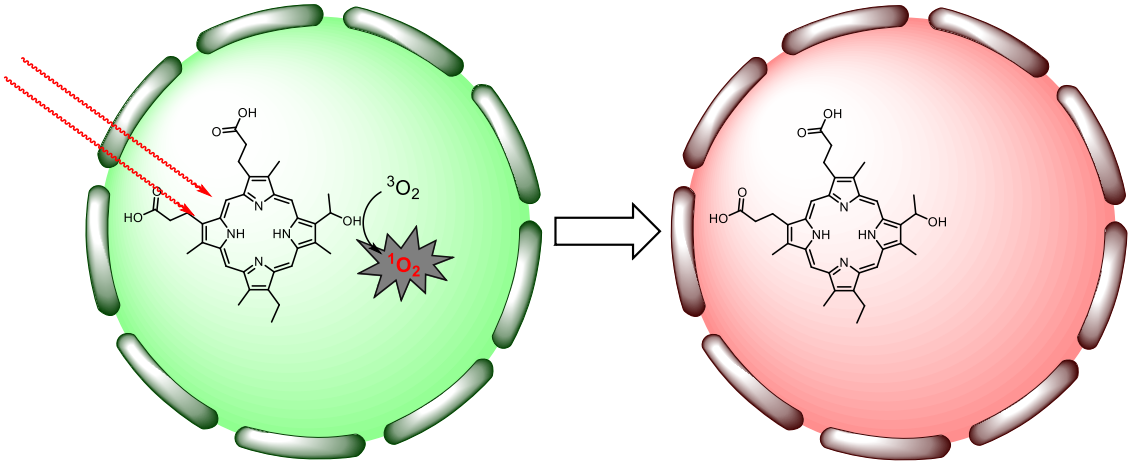


Fig. 3.7. Cartoon representing the PDT process leading to cell death. The photosensitiser shown is Photofrin, the first licensed PDT agent.[48]

The incorporation of heavy atoms into the structure of aza-BODIPY compounds increases the rate of intersystem crossing and therefore improves the $^1O_2$ generation ability of the photosensitiser, which was demonstrated in a report by Ramaiah and co-workers.[31] The highly halogenated compound (Fig. 3.8a) showed a triplet quantum yield and a $^1O_2$ quantum yield of 0.86 and 0.80 respectively, whereas the non-halogenated compound (Fig. 3.8b) exhibited triplet and $^1O_2$ quantum yields of 0.01 and 0.009 respectively.

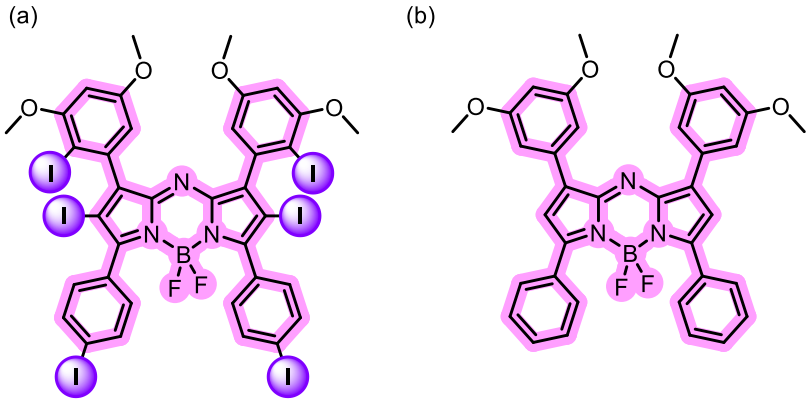


Fig. 3.8. Photosensitising aza-BODIPY compounds reported by Ramaiah.

One of the chief advantages of PDT over conventional treatments is the spatial selectivity offered by the irradiation step – ROS are only generated where the radiation is applied and therefore the treatment is localised. However, further improvements to the selectivity of PDT techniques are still highly desirable, due to the difficulty in selectively irradiating only unwanted cells. Therefore, considerable efforts have been made to develop switchable photosensitisers. For example, Yi and co-workers reported a series of silyl-protected methylene blue (MB) derivatives,[49] which, upon the addition of fluoride, were deprotected, switching on the photosensitising properties of the MB fluorophore (Fig. 3.9). The active MB subsequently demonstrated antimicrobial activity. Importantly, this activation was irreversible and whilst other anion-activated photosensitisers are known, they have all focused on irreversible approaches to date.[49-50]

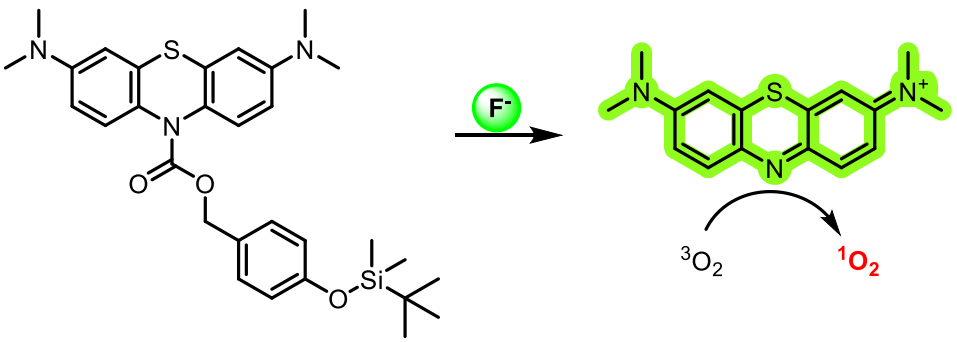


Fig. 3.9. Yi's fluoride-activated MB PDT agent.

3.1.3 Ratiometric Sensing

Ratiometric sensing is a highly useful analytical tool for biological sensing applications. This sensing method functions *via* measurement of the relative changes in multiple emission or excitation features to detect changes in analyte concentration, as opposed to simply monitoring one feature.[51] Ratiometric sensors have several advantages over simpler fluorescence sensors, most importantly: sensing *via* ratiometric compounds is not affected by probe loading and therefore is particularly well-suited to applications in which the exact concentration of the sensor is not known, such as in intracellular imaging. Furthermore, ratiometric compounds can be thought of as being 'internally referenced', such that sensing by ratiometric means is also unaffected by photobleaching, optical path length or illumination intensity, which are also challenging to control in biological settings, further strengthening the case for ratiometric sensors. For example, the most commonly used liposomal membrane assay used in trans-membrane transport studies employs a ratiometric pH probe, 8-hydroxypyrene-1,3,6-trisulfonic acid (HPTS, Fig. 3.10), which has also been used in intracellular studies.[52] The protonated form of the indicator absorbs strongly at 403 nm, whereas the deprotonated form absorbs strongly at the longer wavelength 460 nm. Both forms emit at 510 nm and therefore the ratio of the 510 nm emission intensity, when excited at either 403 or 460 nm, indicates the relative concentration of the protonated and deprotonated forms of the sensor and therefore the pH of the solution.

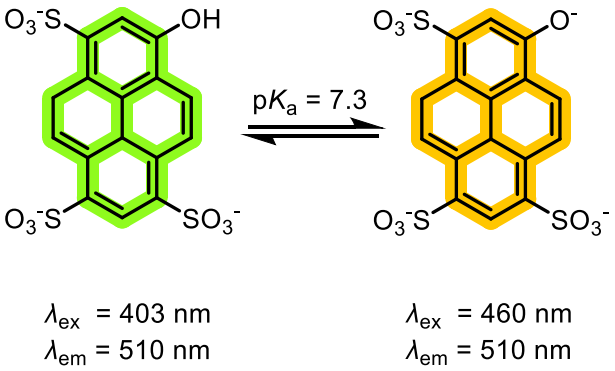


Fig. 3.10. HPTS, the ratiometric pH sensor used in trans-membrane transport assays.

A further advantage of ratiometric sensing is that it has been shown that the *identity* of an unknown analyte in solution can be ascertained through ratiometric methods, due to the unique effect that each analyte has on the fluorescence spectrum of a ratiometric system.[53] For example, in 2006 Coskun and Akkaya reported a ratiometric bis-BODIPY dyad, which could selectively sense Hg^{2+} cations through changes in the ratio of emission at 600 and 700 nm (Fig. 3.11). Upon binding of Hg^{2+}, the efficiency of energy transfer from the left (highlighted in green) to right (highlighted in yellow) BODIPY unit increased dramatically, which led to a large increase in emission at 600 nm from the rightmost BODIPY unit. This emission enhancement led to a dramatic increase in the ratio of emission at 600 nm relative to 700 nm (I_{600}/I_{700}), which was only observed for Hg^{2+}, allowing selective sensing over other cations such as Ag^+, Ba^{2+}, Cu^{2+} and K^+ in THF.

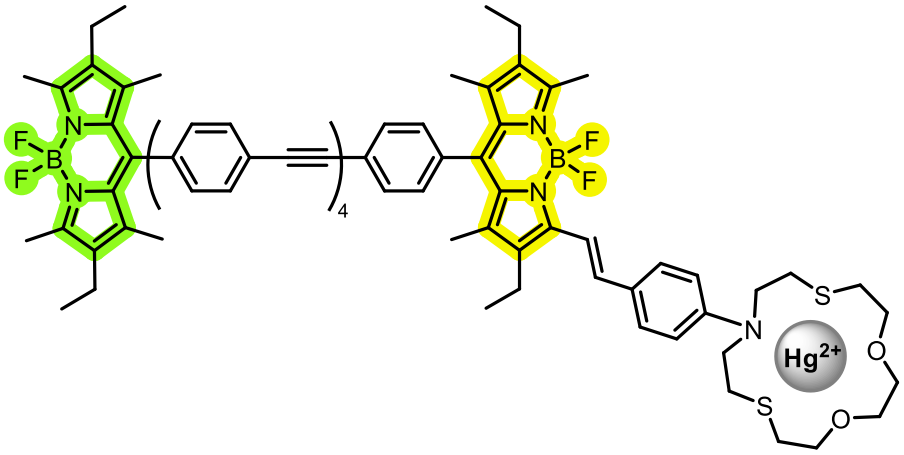


Fig. 3.11. Akkaya's ratiometric, Hg^{2+}-selective BODIPY dyad.

3.1.4 Chapter Aims

Given the advantages of XB in the context of fluorescent anion sensing, both in terms of anion affinity and magnitude of fluorescence response, it is of interest to extend the operating wavelength range of XB fluorescent anion sensors into the biologically-relevant NIR-1 window. Furthermore, supramolecular aza-BODIPY-based anions sensors are very rare and therefore little is known about the relationship between the structure, anion binding affinity and emission response of such systems. The work described in this chapter first seeks to address these points through the construction of two novel XB aza-BODIPY anion sensors, **3.14** and **3.15** (Fig. 3.12). Optical fluorescence anion binding titration studies with these sensors will enable the binding properties of these sensors to be ascertained and inform the design of future, long-wavelength XB anion sensors. Additionally, the ability of these sensors to bind ion-pairs *via* coordination to a cation through the aza-*N* atom will be studied.

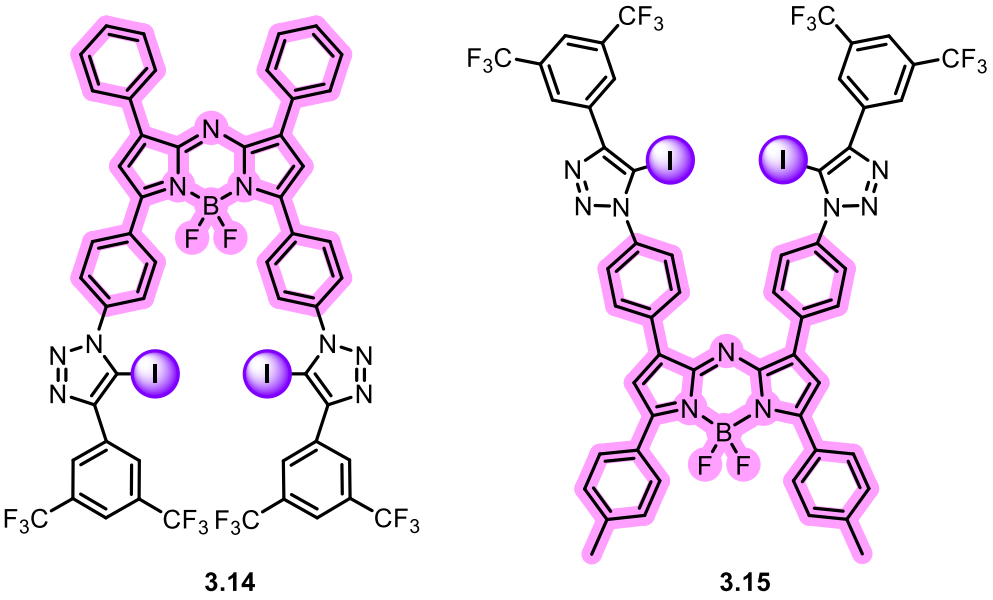
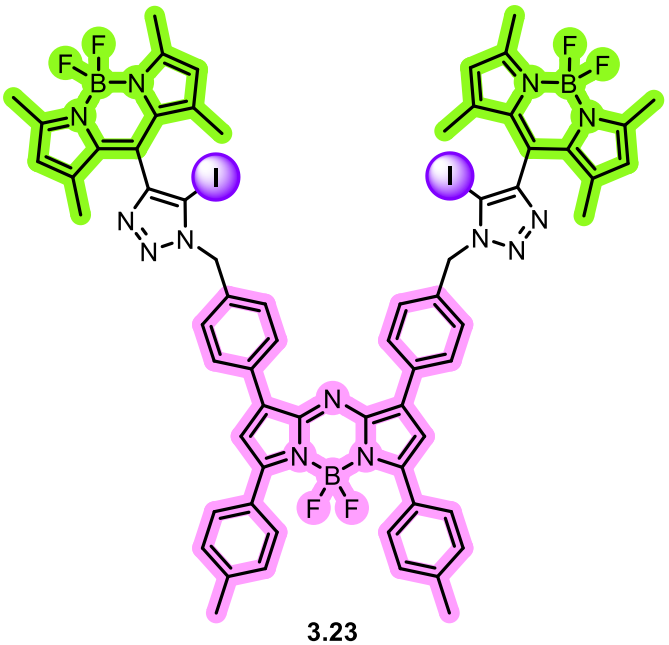


Fig. 3.12. The 1st generation XB aza-BODIPY anion sensors studied in this chapter.

These heavy atom-appended aza-BODIPY compounds are also potentially well-suited to act as photosensitisers for the generation of $^1O_2$, which will be investigated. The impact of anion binding on the $^1O_2$ production of **3.14** will be studied, because the ability to modulate $^1O_2$ generation in response to the surrounding local environment, therefore conferring selectivity to a photodynamic therapy agent, is of great interest.

By integrating the BODIPY fluorophore studied in Chapter Two into an aza-BODIPY core, a second generation XB ratiometric anion sensor **3.23** will be synthesised (Fig. 3.13). Anion binding studies on this sensor will also be undertaken and its ability to act as a useful ratiometric sensor will be assessed.



3.23

Fig. 3.13. Structure of ratiometric XB anion sensor **3.23**.

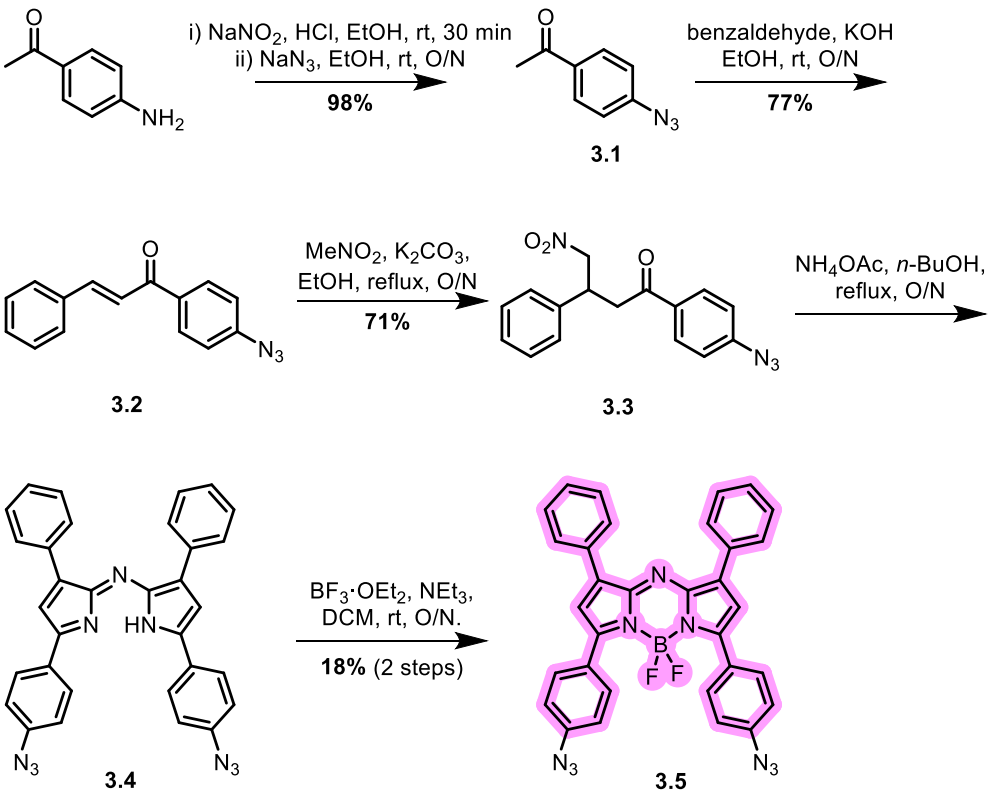
3.2 First Generation Aza-BODIPY Sensors

3.2.1 Synthesis and Characterisation

The target first generation aza-BODIPY anion sensors again incorporate a bis-iodotriazole anion binding site, but in contrast to the family of BODIPY sensors reported in Chapter Two, the fluorogenic aza-BODIPY unit forms the core of the sensor, rather than being appended to a known anion binding motif. Hence, the complementarity and potency of the anion binding site was not known, nor the direction and magnitude of the fluorescence response offered by this sensor design. Nevertheless, it was anticipated that convergent anion binding in close proximity to the aza-BODIPY core would induce changes to the fluorophore's emission spectrum and facilitate optical anion sensing. Therefore, two different sensors were initially targeted, each with differing connectivity to the aza-BODIPY core, in order to investigate the relationship between the structure and anion sensing function of this class of sensors. Electron-withdrawing aromatic motifs, bearing -CF_3 groups, were used to polarise the iodotriazole XB donors to improve anion binding affinity (Fig. 3.12).[54]

Despite the structural similarity to BODIPY, the preparation of aza-BODIPY compounds follows a very different synthetic route. Initially, the parent aza-BODIPY azide compound **3.5** was targeted, which could subsequently be coupled with an iodoalkyne *via* a CuAAC 'click' reaction to produce the required iodotriazole XB donor motifs. Synthesis of **3.5** began from the diazotisation of *p*-aminobenzophenone, accomplished by treatment with $NaNO_2$ in ethanol in the presence of HCl, followed by the slow addition of NaN_3, which converted the diazonium intermediate to *p*-azidobenzophenone **3.1** in 98% yield, following chromatographic purification (Scheme 3.1). An aldol reaction between **3.1** and benzaldehyde in the presence of KOH gave the chalcone **3.2** in 77% yield following

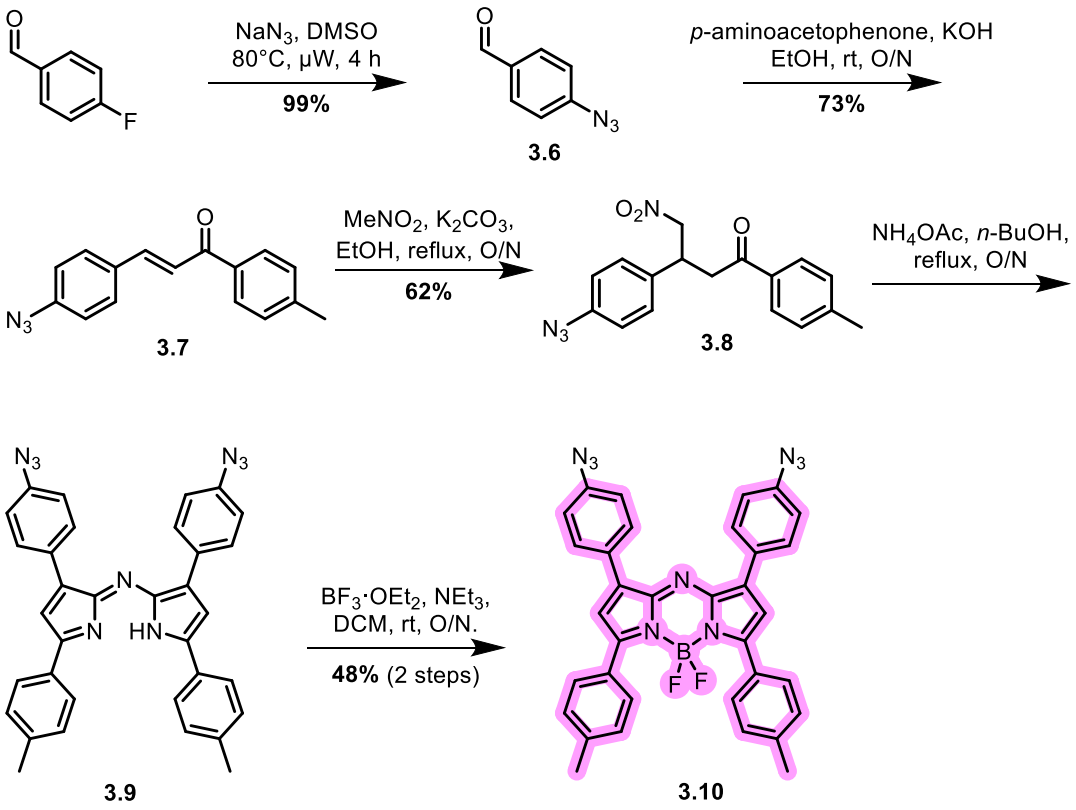
purification by recrystallisation from hot ethanol. Michael addition of nitromethane to **3.2** in the presence of K_2CO_3 gave the nitro-compound **3.3** as a thick yellow oil in 71% yield, following chromatographic purification. Compound **3.3** was refluxed in *n*-butanol with excess NH_4OAc for 24 h before the solution was cooled to 0°C and diluted with hexane. The solution was filtered, and the solid carefully washed with the minimum amount of cold ethanol to yield the intermediate **3.4** as a blue solid. Without further purification, chelation of the BF_2 unit was accomplished *via* treatment of **3.4** with $BF_3{\cdot}OEt_2$ and NEt_3, giving **3.5** as a green solid in 18% yield over two steps, following purification by flash column chromatography.



Scheme 3.1. Synthesis of aza-BODIPY azide **3.5**.

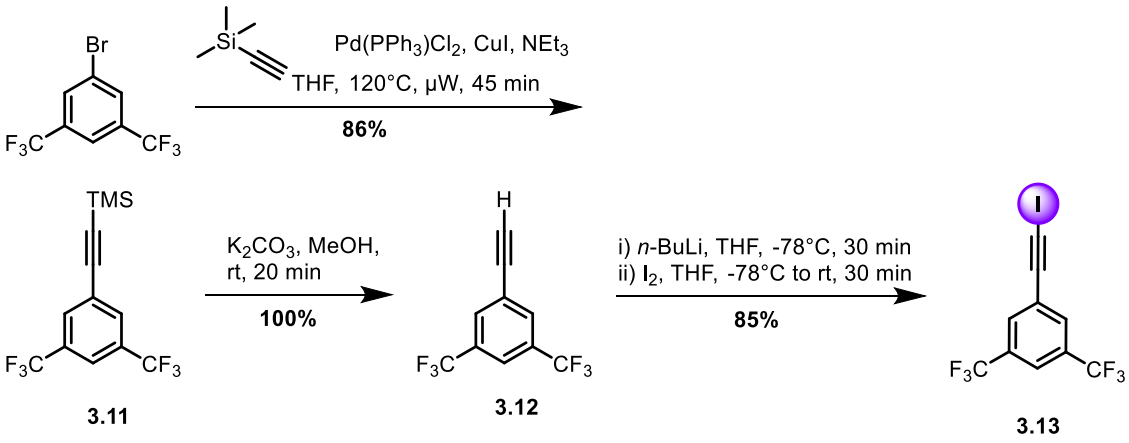
The second aza-BODIPY azide **3.10** was prepared in a similar manner, starting from *p*-fluorobenzaldehyde, which was heated in a microwave reactor with NaN_3 to form

p-azidobenzaldehyde **3.6** in quantitative yield with no need for additional purification (Scheme 3.2). An aldol coupling reaction of **3.6** with *p*-aminoacetophenone in the presence of KOH afforded chalcone **3.7** in 73% yield, following purification by recrystallisation from hot methanol. Treatment of **3.7** with nitromethane in the presence of K_2CO_3 base in ethanol under reflux gave the Michael addition product **3.8** in 62% yield following chromatographic purification. Compound **3.8** was condensed with NH_4OAc by refluxing in *n*-butanol overnight, to give the intermediate **3.9**, which was purified by precipitation from *n*-butanol by addition of hexane. Treatment of a DCM solution of **3.9** with $BF_3{\cdot}OEt_2$ and NEt_3 furnished azide **3.10** in 48% yield over two steps, following chromatographic purification.



Scheme 3.2. Synthesis of aza-BODIPY azide **3.10**.

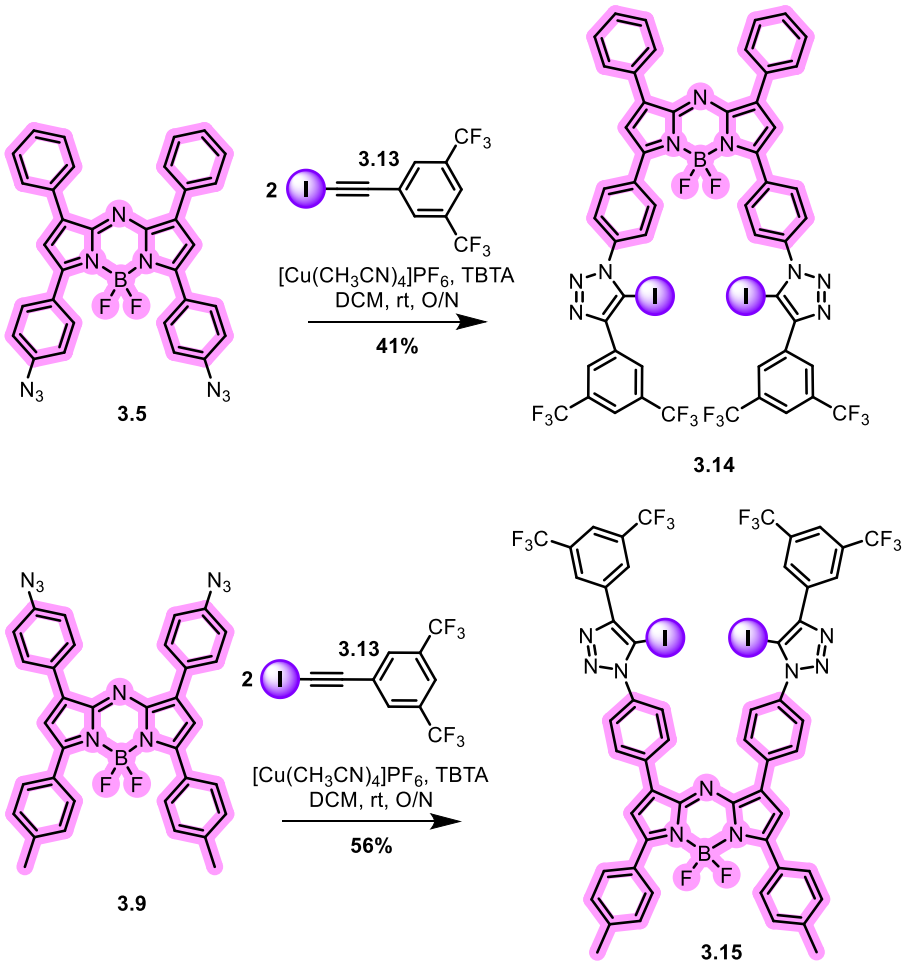
Synthesis of the electron-deficient iodoalkyne CuAAC coupling partner began from 1-bromo-3,5-bis(trifluoromethyl)benzene, which underwent a Sonogashira coupling reaction in a microwave reactor with trimethylsilylacetylene, to give the TMS-protected alkyne **3.11** in 86% yield, following chromatographic purification (Scheme 3.3). **3.11** was quantitatively deprotected by treatment with K_2CO_3 in methanol, affording protoalkyne **3.12**. The corresponding iodoalkyne, **3.13**, was prepared by treating an anhydrous THF solution of **3.12**, cooled to -78° C, with *n*-butyl lithium, generating the lithium acetylide. Addition of I_2 to a suspension of the acetylide formed the iodoalkyne **3.13** in 85% yield, following chromatographic purification (Scheme 3.3).



Scheme 3.3. Synthesis of iodoalkyne CuAAC coupling partner **3.13**.

The target XB aza-BODIPY anion receptors **3.14** and **3.15** were synthesised in 41% and 56% yield respectively, following purification by column and thin layer preparative chromatography. **3.14** and **3.15** were synthesised *via* a CuAAC methodology, combining **3.5** and **3.10** with two equivalents of **3.13** (Scheme 3.4). Synthesis of the HB analogues of **3.14** and **3.15** was attempted using an analogous CuAAC reaction protocol with two equivalents of **3.12**. However, the extremely low solubility of the HB products in all

common organic solvents precluded purification of the crude reaction mixtures, although the presence of the target compounds was observed by HRMS.



Scheme 3.4. Synthesis of the first generation aza-BODIPY anion sensors **3.14** and **3.15**.

Both XB aza-BODIPY anion receptors **3.14** and **3.15** were characterised by ^{1}H, ^{19}F and ^{11}B NMR and optical spectroscopy as well as HRMS, although the low solubility of the XB compounds in organic solvents prevented characterisation by ^{13}C NMR. The ^{1}H NMR, absorption and emission spectra of sensor **3.14** are shown below as representative examples (Figs. 3.14 & 3.15).

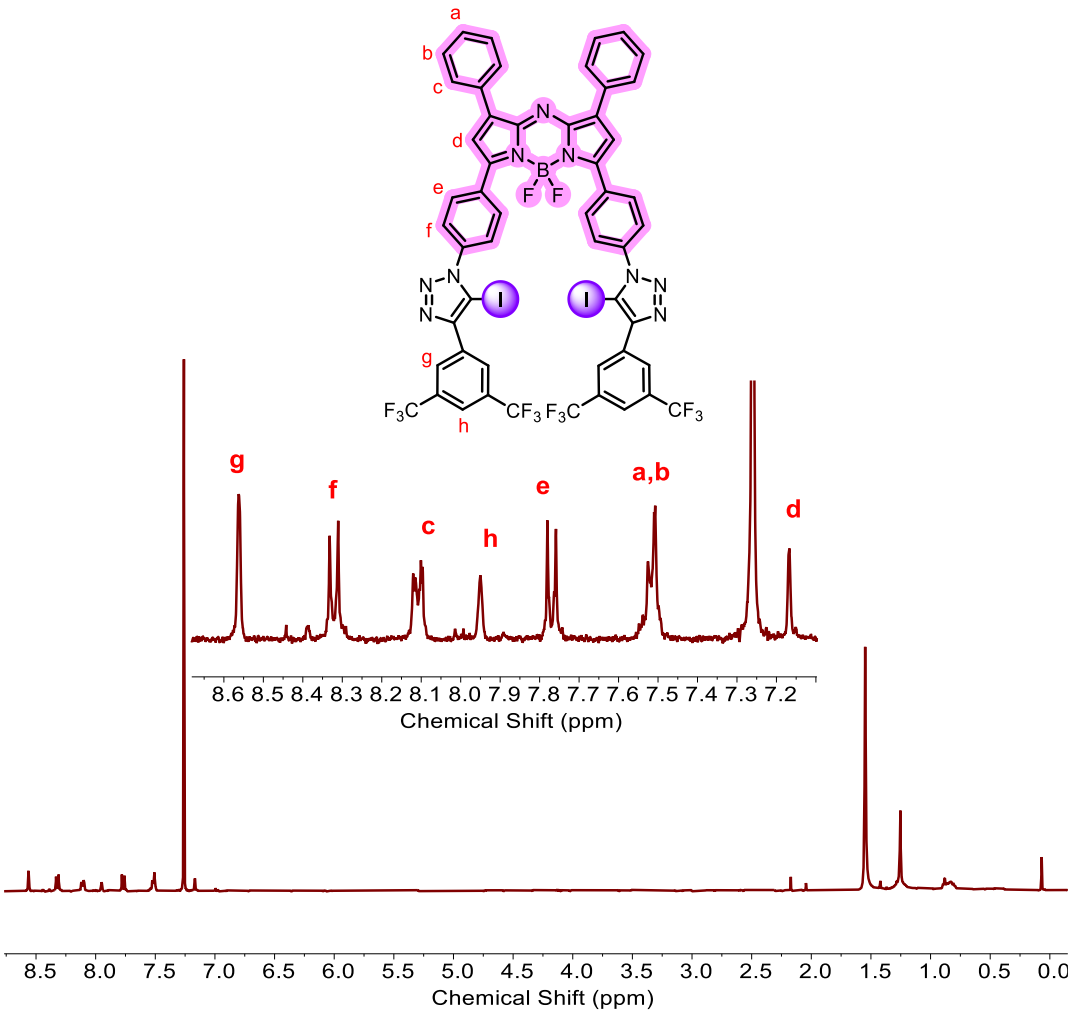


Fig. 3.14. ^{1}H NMR spectrum of sensor **3.14**. ($CDCl_3$, 298 K)

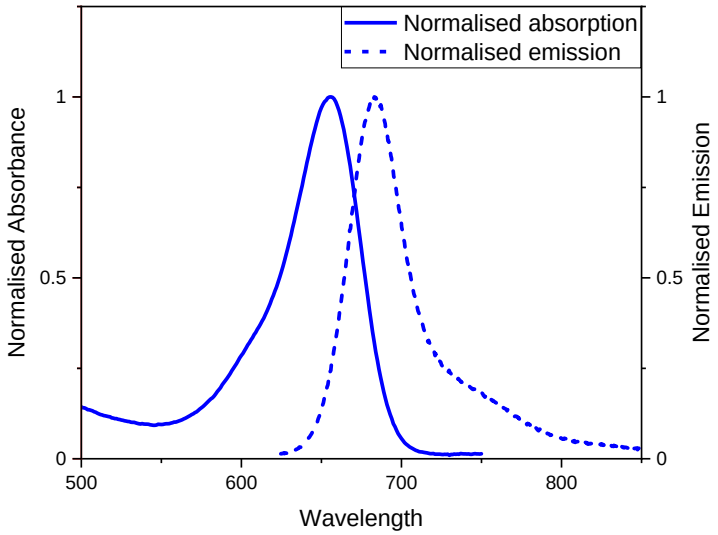


Fig. 3.15. Normalised absorption and emission spectra of sensor **3.14**. (Acetone, 10 μM, 298 K, 600 nm excitation wavelength)

Both receptors displayed characteristic aza-BODIPY optical properties,[31] with absorption and emission features in the biologically-relevant NIR-1 wavelength range and typical Stokes shifts of approximately 30 nm (Fig. 3.15 & Table 3.1).

Table 3.1. Photophysical properties of sensors **3.14** and **3.15**. (Acetone, 10 μM, 298 K)

	3.14	**3.15**
$\lambda_{max,\ abs}$ (nm)	656	670
ε (M^{-1} cm^{-1})	30,000	33,000
$\lambda_{max,\ em}$ (nm)	684	701
Stokes shift (nm)	28	31

3.2.2 Anion Sensing Studies

Initially, the fluorescence response of both receptors to anion binding was investigated in acetone, by addition of aliquots of a variety of tetrabutylammonium salts (TBAX, X = Cl, Br, I, HSO_4, OAc, H_2PO_4). Upon addition of halide anions, both receptors exhibited a significant turn-off quenching response with negligible changes in either absorbance or emission wavelength maxima, which enabled halide anion sensing (Fig. 3.16).

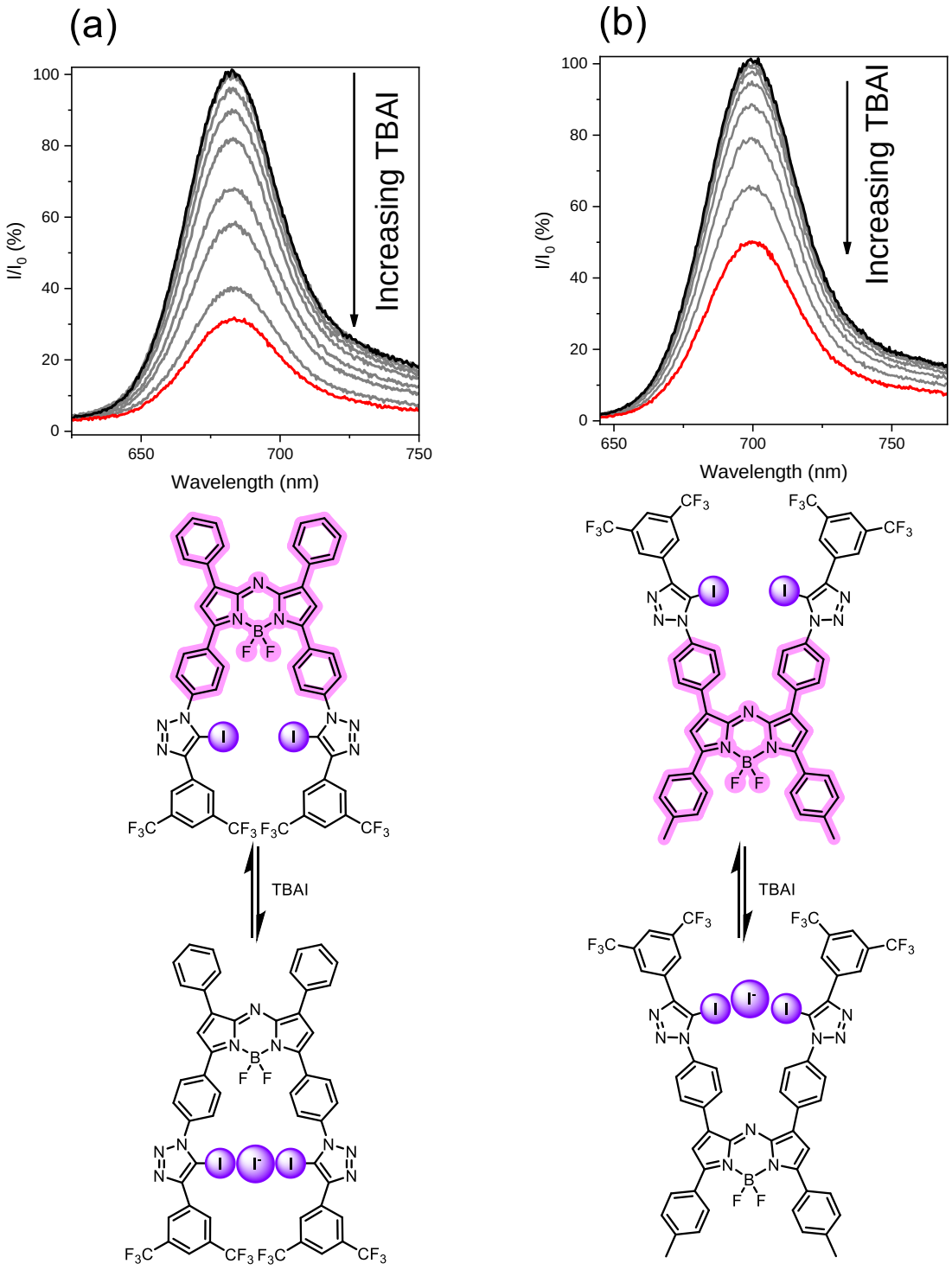


Fig. 3.16. (a) Normalised fluorescence emission response of sensor **3.14** and (b) sensor **3.15** upon addition of increasing concentrations of I^- (up to 2.8 mM). (Acetone, 1 μM, 298 K)

In contrast, no emission response was observed upon addition of $TBAHSO_4$ or $TBAH_2PO_4$, which is consistent with the frequently observed and previously mentioned

preference of XB sensors for halide anions (Fig. 3.17).[55] Addition of the relatively basic $^{-}$OAc anion resulted in decomposition of both sensors, as indicated by time-dependent emission changes, which ultimately resulted in total loss of all emission.

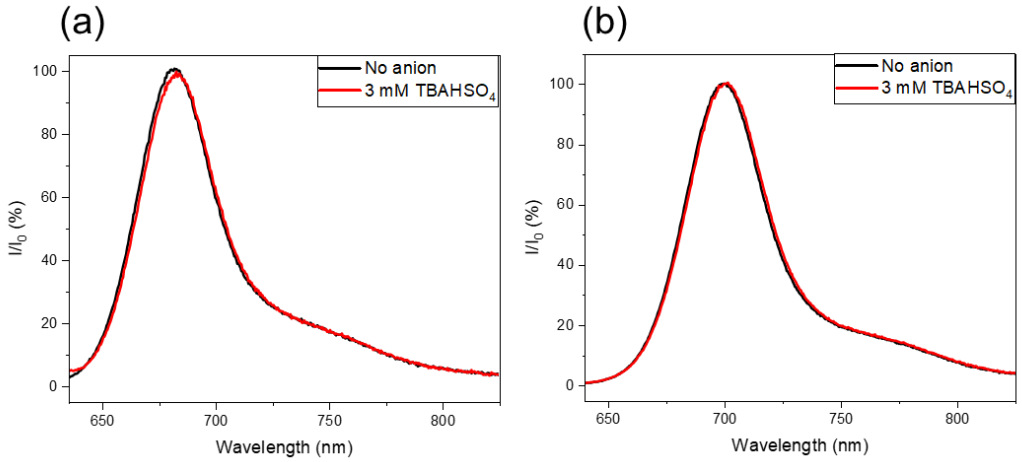


Fig. 3.17. (a) Normalised fluorescence emission spectra of sensor **3.14** and (b) sensor **3.15** upon addition of 3 mM HSO_4^-, indicating the lack of fluorescence response. (Acetone, 1 μM, 298 K)

The absorbance spectrum of both sensors was unaffected by the presence of anions, which suggests that a dynamic fluorescence quenching mechanism, whereby the excited state of the sensor is affected by anion binding, rather than the ground state, is at play. Aza-BODIPY compounds have been shown to exhibit non-radiative decay *via* high energy vibronic modes.[30, 56] It is therefore conceivable that a similar vibronic quenching mechanism could be responsible for quenching in these sensors through XB interactions with the bound anion.

Sensor **3.14** invariably displayed the greater turn-off response for each halide anion tested and iodide consistently induced the greatest degree of quenching, which was attributed to an additional heavy-atom effect increasing the rate of intersystem crossing and thus reducing fluorescence quantum yield. Indeed, receptor **3.14** displayed an

impressively large quenching response of 70% upon addition of iodide in acetone (Fig. 3.18).

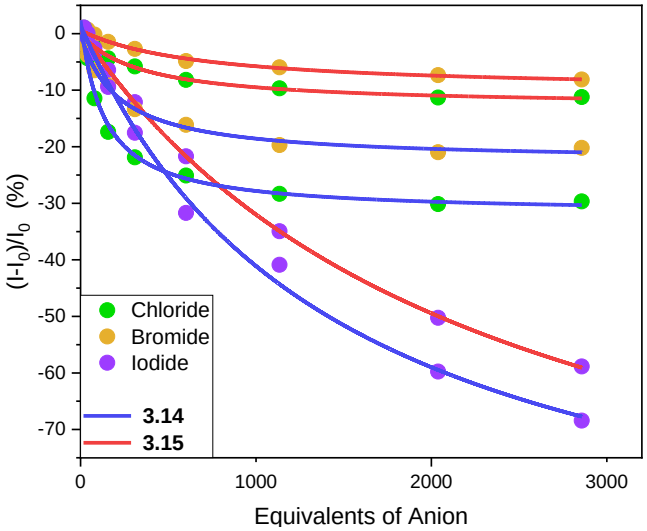


Fig. 3.18. Representative fluorescence isotherms for the titration of halide anions with sensors **3.14** (blue) and **3.15** (red). (Acetone, 1 μM, 298 K)

Global fitting of the halide titration data around the emission maximum to a 1:1 stoichiometric host-guest binding model determined the association constants shown in Table 3.2. The association constants for the halide anions follow the expected charge density trend for organic solvents,[57] with chloride being bound more strongly than bromide, which is bound more strongly than iodide. Notably, receptor **3.14** generally showed stronger halide binding, which may be due to the iodotriazole motifs of the convergent XB donor binding cavity being relatively closer to one another and therefore of a more complementary conformation compared to receptor **3.15**, which is suggested by a computational study of similar compounds.[30] Importantly, the observed enhanced halide anion binding affinity and larger magnitude of fluorescence response offered by the structural connectivity of receptor **3.14** should be considered in the design of future aza-BODIPY anion sensors.

Table 3.2. Halide association constants (M^{-1})[a] of sensors **3.14** and **3.15**. (Acetone, 1 μM, 298 K)

Anion	**3.14**	**3.15**
Cl^-	7100	2900
Br^-	4100	1200
I^-	730	440

[a] Determined in acetone by global fitting to a 1:1 binding model. All errors < 10%.

Biological probes used in intracellular imaging must be capable of operating in aqueous media. Although **3.14** and **3.15** are not fully water-soluble, they remain emissive in the presence of water and pleasingly retain their responsiveness to excess chloride in acetone : water 9:1 (*v*/*v*), with **3.15** showing a particularly marked response (Fig. 3.19). This is particularly encouraging given that chloride has the highest hydration enthalpy of the halide anions tested and reflects the resistance of the XB interactions employed by these sensors to increasing solvent polarity.

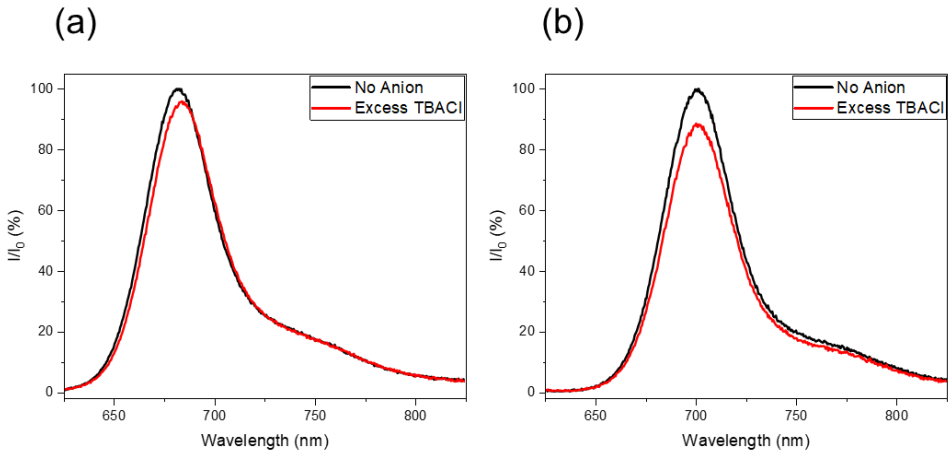


Fig. 3.18. Stacked emission spectra of (a) sensor **3.14** and (b) sensor **3.15** in the presence and absence of excess TBACl. (Acetone : water 9:1 (*v*/*v*), 1 μM, 298 K)

3.2.3 Ion-Pair Sensing Studies

Aza-BODIPY compounds have previously shown promise as fluorescent cation sensors.[58] In particular, receptors using the aza-*N* atom to coordinate to a metal ion have been reported. For example, in 2019 Gawale *et al.* reported a 3-ethoxy-*N*,*N*-diethylaniline substituted aza-BODIPY dye which was capable of selectively sensing Cu^{2+} cations in DCM.[59] Through a combination of UV-vis absorption, fluorescence emission and infra-red studies, the authors demonstrated the sequential formation of the 1:3 stoichiometric host-guest complex shown in Fig. 3.19. The peripheral diethyl amino groups are the primary cation binding motifs and only once these sites have been saturated does the third Cu^{2+} cation bind, complexed by the core aza-*N* atom and the *O* atoms of the two nearby ethoxy moieties. The coordination of the ethoxy groups restricts the rotation of the phenyl rings, rigidifying the structure and leading to a dramatic 50-fold increase in emission intensity at 700 nm.

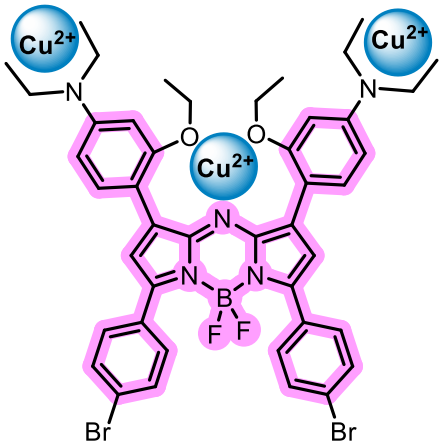


Fig. 3.19. Gawale *et al.*'s aza-BODIPY Cu^{2+} sensor, displaying a 1:3 host-guest stoichiometry.

Given their toxicity at high concentrations in water sources and increased use in batteries,[60-62] there is a pressing need to develop lithium salt sensors and the area of lithium salt recognition has seen an upsurge of interest in recent years, with nitrogen-

donor binding sites commonly employed for lithium cation recognition.[63-65] For example, in 2018, Kokan and Chmielewski reported a photo-switchable heteroditopic ion-pair receptor, consisting of a photo-isomerisable acylhydrazone motif, which also acted as the cation binding site, and an amide anion binding site (Fig. 3.20).[66] The active photo-isomer was capable of binding lithium halide ion-pairs in acetonitrile-d_3, *via* the binding mode indicated in Fig. 3.20, which was assessed by direct titration of the lithium halide salts.

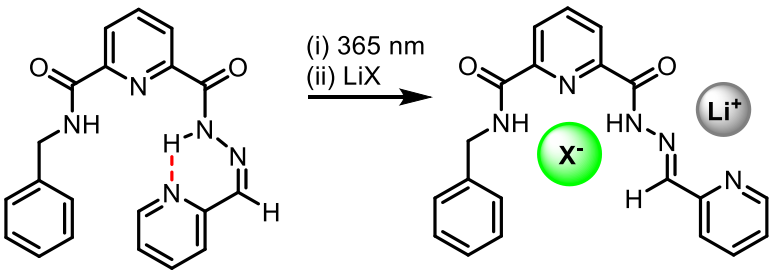


Fig. 3.20. Kokan and Chmielewski's photo-switchable ion-pair receptor.

Ion-pair fluorescence titration studies were conducted with both sensors **3.14** and **3.15**, initially in acetone. The unexpectedly high solubility of LiCl in this solvent and extremely low host concentrations allows the ion-pair salt to be directly titrated into a solution of the sensor, in a manner similar to that reported by Chmielewski above.[67] Upon addition of LiCl, **3.14** displayed a significant turn-off quenching fluorescence response of 15%, whereas **3.15** displayed no emission response (Fig. 3.21).

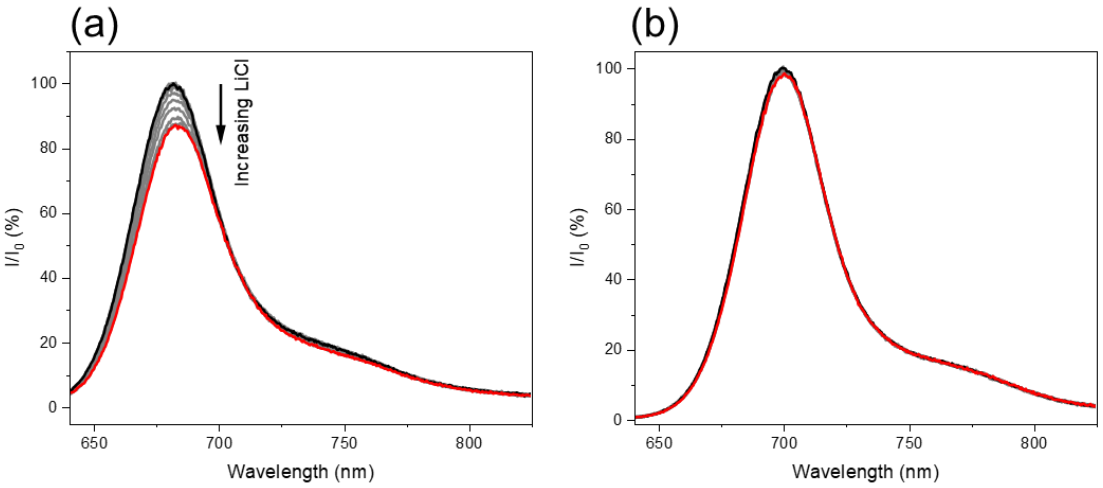


Fig. 3.21. Emission response of (a) **3.14** and (b) **3.15** upon addition of LiCl. (Acetone, 1 μM, 298 K)

Fitting of the **3.14** LiCl titration data to a 1:1 stoichiometric host-guest model produced the apparent chloride association constant shown in Table 3.3. The use of the apparent association constants in this case was justified by a control titration with lithium bis(trifluoromethanesulfonyl)imide (LiTFSI), a lithium salt with a non-coordinating anion. Addition of LiTFSI produced no significant emission response for either sensor (Fig. 3.22), confirming that the quenching effect observed in the LiCl titration experiment was due to solely chloride binding, which could therefore be fitted to a 1:1 binding model. Notably, $K_{App}(Cl^-)$ = 1400 M^{-1} was measured for LiCl, which is significantly less than $K_a(Cl^-)$ = 7100 M^{-1}, determined upon the addition of TBACl. This suggested that Li^+ is not significantly co-bound by the host and thus no positively cooperative effect on its Cl^- affinity is observed. Indeed, the diminished apparent association constant value is likely due to the high degree of solution LiCl ion-pairing outside of the receptor in the non-competitive acetone solvent.

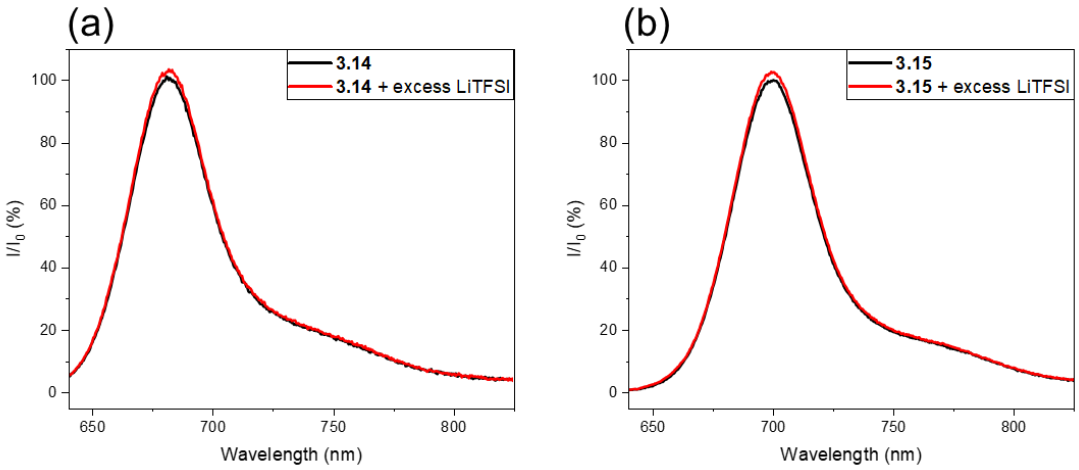


Fig. 3.22. Emission spectra of (a) **3.14** and (b) **3.15** in the presence and absence of excess LiTFSI, showing the lack of fluorescence response in each case. (Acetone, 1 μM, 298 K)

Analogous studies were conducted in acetonitrile, a more competitive solvent, to reduce the degree of LiCl ion-pairing in solution. Similarly, **3.14** displayed a quenching response upon addition of LiCl, which allowed calculation of an apparent Cl^- association constant of 770 M^{-1} (Fig. 3.23), and **3.15** proved unresponsive. However, $K_{App}(Cl^-)$ for **3.14** was within error of the Cl^- association constant measured upon addition of TBACl in the same acetonitrile solvent, indicating no cooperative behaviour and thus suggesting that the receptors do not bind Li^+ and therefore are unable to act as ion-pair sensors.

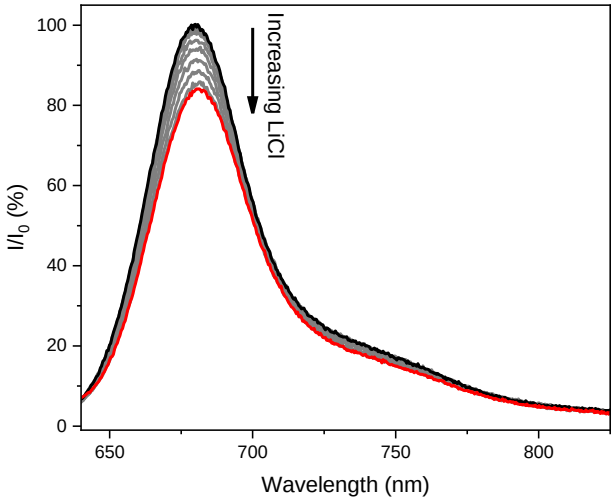


Fig. 3.23. Emission response of **3.14** upon addition of LiCl. (ACN, 1 μM, 298 K)

Table 3.3. Apparent halide association constants (M^{-1}) of sensors **3.14** and **3.15**. (1 μM, 298 K)

Solvent	Titrant	3.14	3.15
Acetone	LiCl	1400	n.r.
	TBACl	7100	2900
Acetonitrile	LiCl	770	n.r.
	TBACl	850	n.d.

Apparent association constants (M^{-1}) determined by global fitting to a 1:1 binding model. All errors < 10%. n.r. – no response. n.d. – not determined.

3.2.4 Singlet Oxygen Generation Studies

Having studied the anion sensing properties of both receptors, attention turned to investigating the photosensitising abilities of sensor **3.14**, which was the primary focus of this investigation because it had exhibited the largest magnitude of sensing response upon addition of halide ions. As outlined in the chapter introduction, the ability to modulate singlet oxygen generation in response to anion concentration would be of great interest in order to improve the selectivity of PDT agents. Therefore, studies of the $^1O_2$ generating ability of **3.14** were conducted in the absence and presence of anions.

The generation of singlet oxygen was monitored using a dye known to be a trap for singlet oxygen and other ROS: diphenylisobenzofuran (DPBF), which has a characteristic absorbance at 410 nm.[68-69] As DPBF reacts with $^1O_2$, it forms non-absorbing products and consequently the absorbance at 410 nm diminishes (Fig. 3.24). Therefore, the rate at which absorbance at 410 nm decreases is correlated to the singlet oxygen quantum yield of a given chromophore, all else being equal.[70]

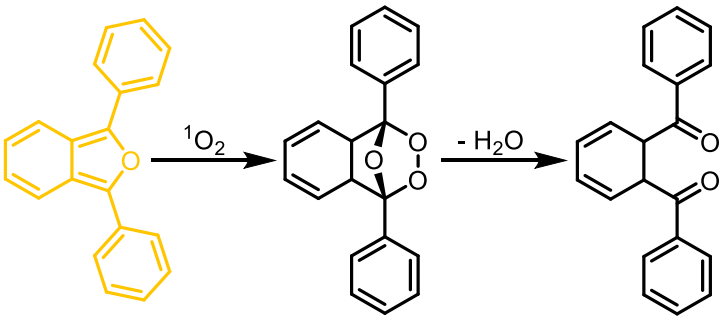


Fig. 3.24. DPBF and its reaction with $^1O_2$ to form non-absorbing products.[69]

In a typical experiment, an acetone solution of receptor **3.14** (20 μM) and DPBF (30 μM) was irradiated with an LED (625 nm) and the absorbance at 410 nm monitored. As displayed in Fig. 3.25, **3.14** proved capable of generating $^1O_2$, as shown by the diminishment of DPBF absorbance after 600 s of radiation. It is important to note that no changes in the aza-BODIPY absorbance at 656 nm were observed, indicating the photostability of sensor **3.14** under these conditions.

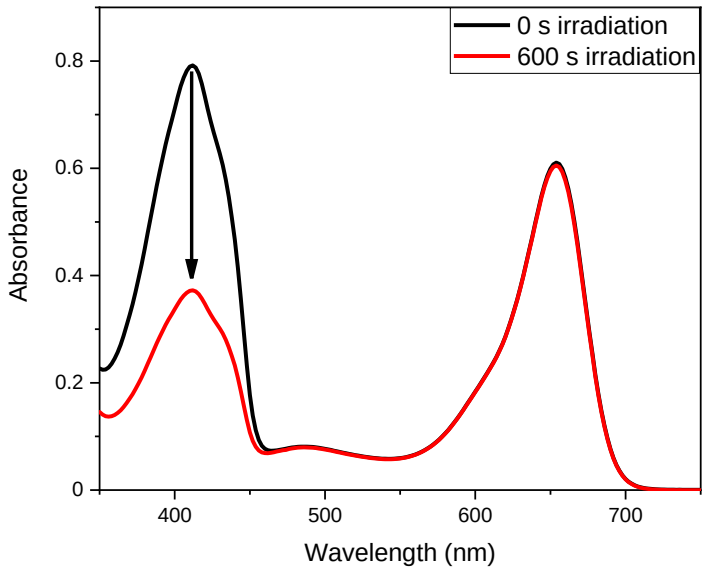


Fig. 3.25. Absorbance of a solution initially containing DPBF (30 μM) and sensor **3.14** (20 μM), before and after 600 s irradiation at 625 nm. (Acetone, 298 K)

Subsequently, an analogous experiment was conducted in the presence of 2 mM TBACl, in order to determine whether anion binding could modulate the production of

$^1O_2$. Chloride was selected as the anion for these studies because it had caused a large magnitude emission response from sensor **3.14** in anion binding studies. Despite the large magnitude sensing response induced by iodide, it could not be used in these studies due to its known propensity to react with $^1O_2$,[71] which would confound the results. Pleasingly, the rate of $^1O_2$ generation was diminished by 37% in the presence of chloride, indicating that reversible anion binding could indeed significantly modulate singlet oxygen production in a proof-of-principle (Fig. 3.26).

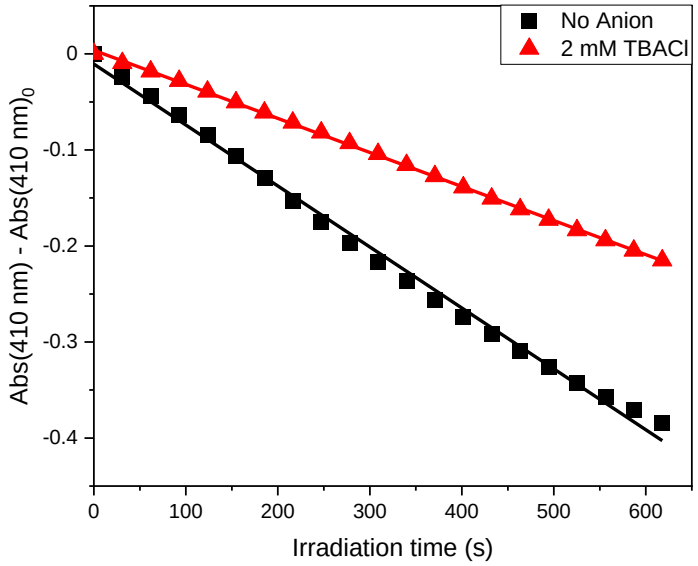


Fig. 3.26. Plot of DPBF absorbance against irradiation time, in the presence and absence of 2 mM TBACl. (Sensor **3.14**, acetone, 298 K)

In order to confirm that this observation was caused by anion binding to receptor **3.14** and to rule out any non-specific effects, control studies were conducted. First, the rate of $^1O_2$ generation of sensor **3.14** was measured in the presence of 2 mM PF_6^-, a non-coordinating anion which is not expected to bind to the receptor. No significant difference (< 5%) in the rate of DPBF consumption was observed, indicating that the presence of PF_6^- does not significantly affect the rate of $^1O_2$ production by receptor **3.14** (Fig. 3.27).

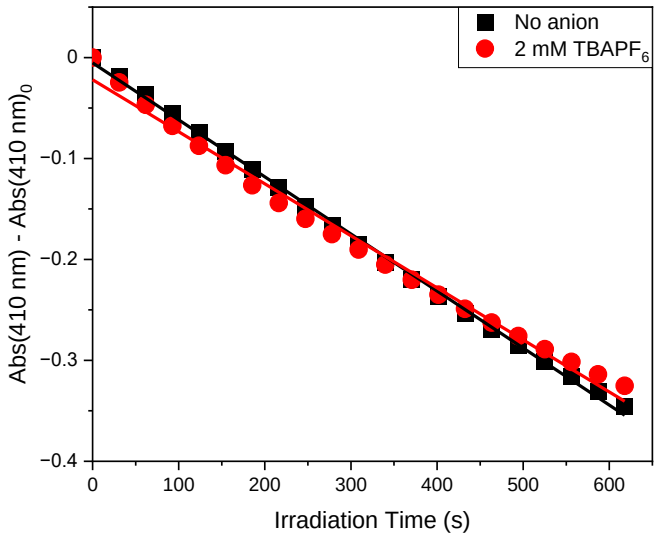


Fig. 3.27. Plot of DPBF absorbance against irradiation time, in the presence and absence of 2 mM $TBAPF_6$. (Sensor **3.14**, acetone, 298 K)

Further confirmation was provided by a study of the rate of $^1O_2$ generation by the azide precursor **3.5**, which showed that the presence of chloride had no appreciable impact on the rate of $^1O_2$ production of this compound, which lacks an anion binding site (Fig. 3.28).* This observation, taken together with the $TBAPF_6$ experiment, strongly support the finding that reversible anion binding modulates $^1O_2$ production in sensor **3.14**, which importantly opens new avenues for the development of selective PDT agents.

* Deviations from linearity are due to the high concentrations of compound **3.5** and DPBF required to observe significant DPBF quenching, because the $^1O_2$ generation efficiency of compound **3.5** is significantly diminished relative to sensor **3.14** as it does not contain any heavy atoms, such as iodine.

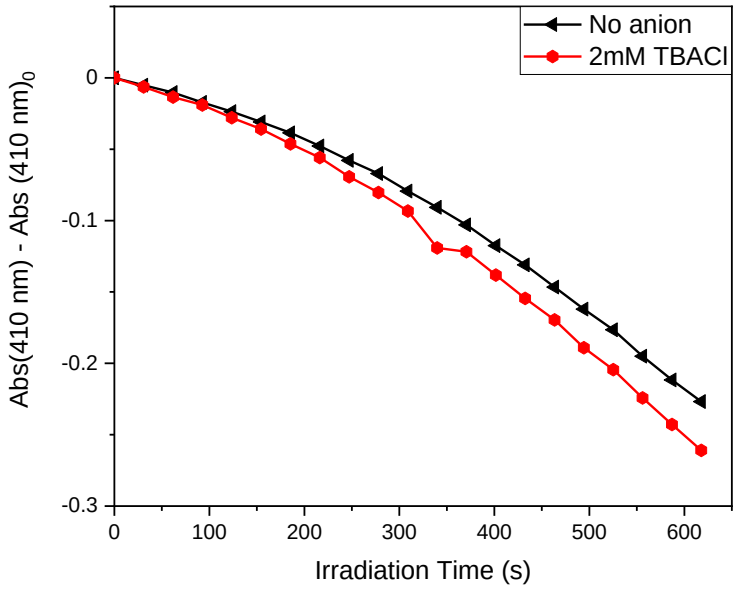


Fig. 3.28. Plot of DPBF (initially 60 μM) absorbance against irradiation time, in the presence and absence of 2 mM $TBAPF_6$. (40 μM compound **3.5**, acetone, 298 K)

In order to gain insight into the mechanism of host-guest anion binding-modulated $^1O_2$ generation, fluorescence lifetime measurements of sensor **3.14** were conducted in the presence and absence of 2 mM TBACl (Table 3.4).

Table 3.4. Fluorescence lifetimes (ns)[a] of sensor **3.14** in the presence and absence of 2 mM TBACl

Anion	τ_F
No anion	1.13
Cl^-	1.07

[a] Determined in acetone at 298 K. 1 μM sensor concentration. Errors < 5%

The fluorescence lifetime of sensor **3.14** was not significantly affected by anion binding, in contrast to the sensors reported in Chapter Two. However, this result is consistent with an increase in the rate of non-radiative decay pathways upon chloride binding.

As the emission intensity of receptor **3.14** is diminished upon Cl^- binding, the fluorescence quantum yield in the presence of 2 mM TBACl, Φ_f, is less than the fluorescence quantum yield in the absence TBACl:†

$$\phi_{f,\ Cl} < \phi_{f,\ 0} \qquad \text{(Eqn. 3.1)}$$

Therefore, using the relations in Eqns 2.3 & 2.4, the following inequality can be obtained, in which k_f is the rate of emission from the S_1 state and τ_f is the fluorescence lifetime of the S_1 state:

$$k_{f,\ Cl} \times \tau_{f,\ Cl} < k_{f,\ 0} \times \tau_{f,\ 0} \qquad \text{(Eqn. 3.2)}$$

The lifetime measurements indicated that there is no significant change in fluorescence lifetime upon Cl^- binding: $\tau_{f,\,0} = \tau_{f,\,Cl}$. Therefore:

$$k_{f,\ Cl} < k_{f,\ 0} \qquad \text{(Eqn. 3.3)}$$

Using the relation in Eqn. 2.3 again, the following can be determined, where k' is the combined rate of all other, non-radiative decay processes from the S_1 state:

$$k'_{Cl} > k'_0 \text{ (Eqn. 3.4)}$$

Eqn. 3.4 shows that the rate of non-radiative decay processes in sensor **3.14** is increased by anion binding. It is conceivable that these non-radiative decay processes increasingly compete with intersystem crossing, reducing the triplet quantum yield and

† The subscripts *0* and *Cl* denote the absence and presence of 2 mM chloride respectively.

therefore diminishing the $^1O_2$ quantum yield, which have been shown to be highly correlated.[31]

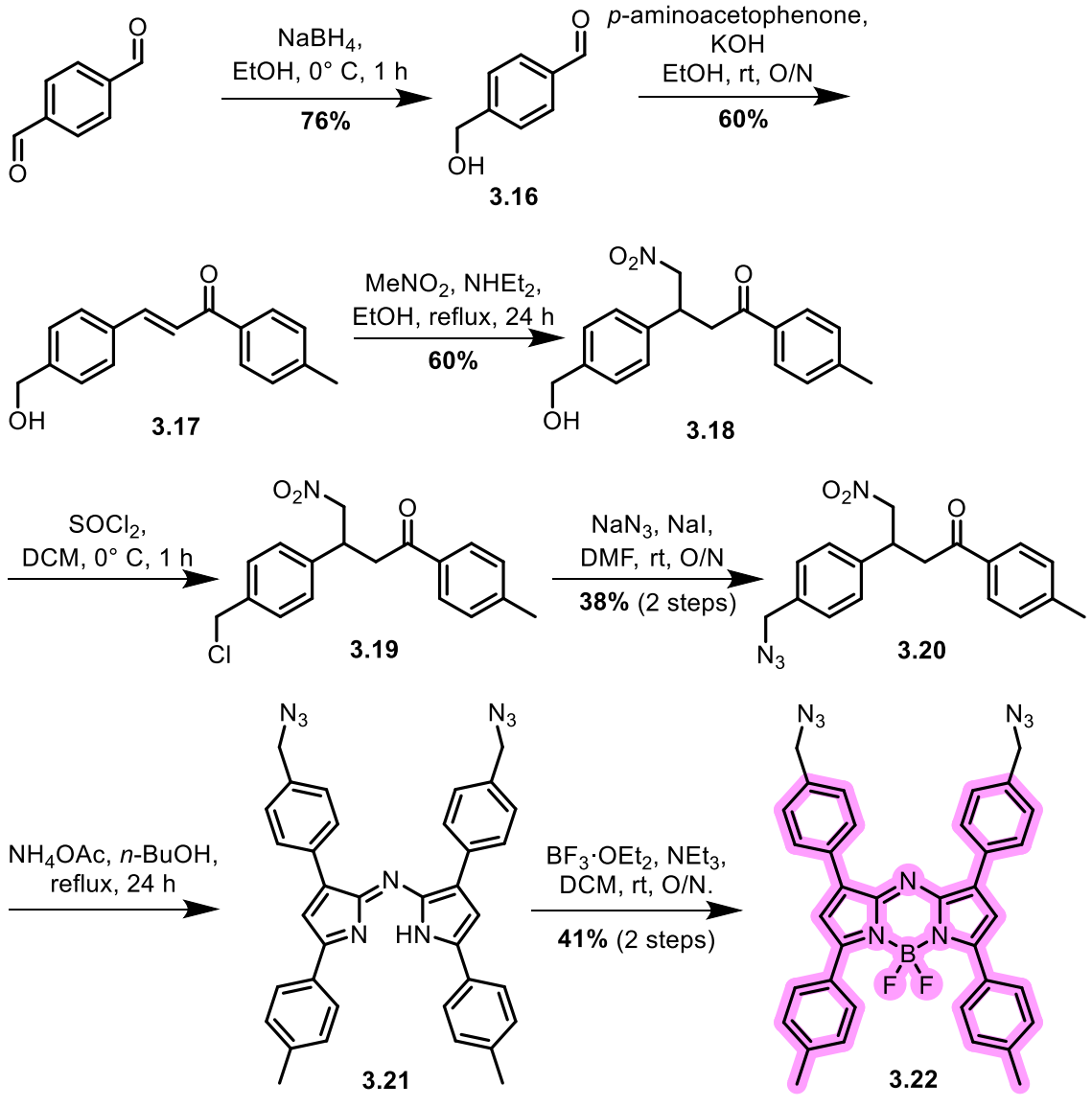
3.3 Second Generation Ratiometric (Aza)-BODIPY Anion Sensor

Having demonstrated the responsiveness of the aza-BODIPY core to proximal anion binding, the possibility of combining this long-wavelength fluorophore with the shorter wavelength BODIPY motif studied in Chapter Two, producing a ratiometric sensor with well-separated emission features, became apparent. To this end, compound **3.23** was targeted (Fig. 3.13), which features an additional methylene unit to add more flexibility between the aza-BODIPY core and the anion binding iodotriazole units, to improve the solubility of the sensor, which had been an issue with the first generation sensors.

3.3.1 Synthesis and Characterisation

A CuAAC methodology was again used to generate the iodotriazole XB donors in the final step of the synthesis, and therefore the parent azide **3.22** was the initial synthetic target. Synthesis began from terephthaldehyde, which was statistically reduced with $NaBH_4$ to give 4-(hydroxymethyl)benzaldehyde, **3.16**, in 76% yield following chromatographic purification (Scheme 3.5). Compound **3.16** underwent an aldol condensation in the presence of KOH with *p*-aminoacetophenone, affording the chalcone **3.17** in 60% yield, following recrystallisation from hot methanol. Michael addition of nitromethane in the presence of diethylamine base gave compound **3.18** in 60% yield, following purification by flash column chromatography. The alcohol **3.18** was converted to the benzylic chloride compound **3.19** by treatment with $SOCl_2$ at 0° C. However, it was not possible to purify **3.19** from the resulting crude mixture, which also included oligomers formed by reaction between the reactive benzylic chloride product and alcohol starting material. Therefore, the crude reaction mixture was exposed to NaN_3 under Finkelstein substitution conditions, which formed the azide compound **3.20**. This compound could be isolated

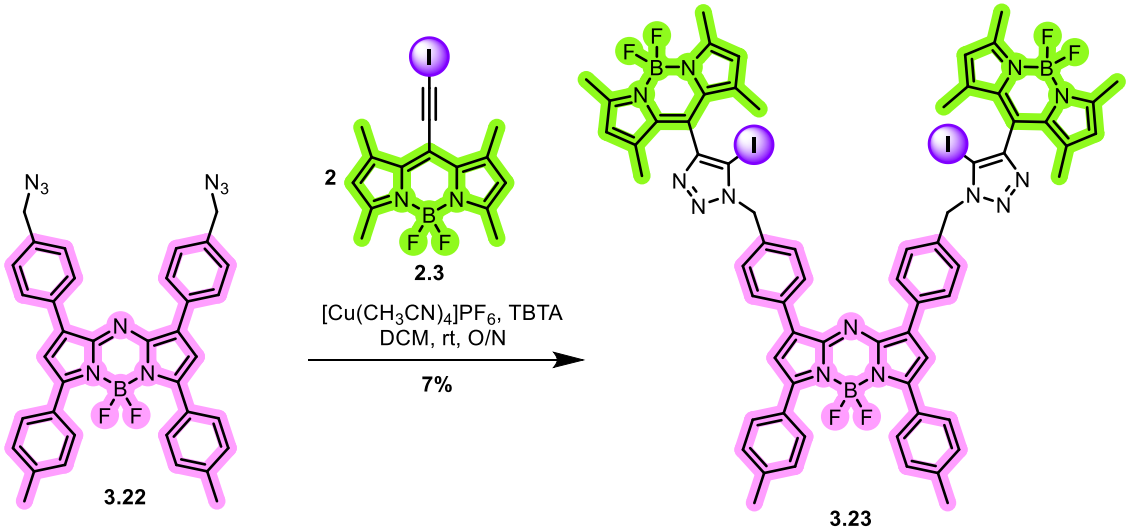
chromatographically from the reaction mixture in 38% yield over two steps. Finally, **3.20** was condensed with NH_4OAc in *n*-butanol, forming the intermediate **3.21**, which was subsequently exposed to $BF_3{\cdot}OEt_2$ in the presence of triethylamine, affording aza-BODIPY azide compound **3.22** in 41% yield over two steps, following purification by flash column chromatography (Scheme 3.5).



Scheme 3.5. Synthesis of aza-BODIPY azide **3.22**.

Aza-BODIPY azide compound **3.22** was then reacted with two equivalents of the BODIPY iodoalkyne **2.3**, under CuAAC conditions (Scheme 3.6). The product, **3.23**,

exhibited extremely limited solubility in common organic solvents, despite its increased flexibility, which severely hindered attempts to purify the crude reaction mixture. However, a small amount was purified by preparative thin layer chromatography, furnishing sensor **3.23** in modest 7% yield, which was sufficient for characterisation and optical anion binding studies.



Scheme 3.6. Synthesis of the second generation aza-BODIPY anion sensor **3.23**.

Sensor **3.23** was characterised by ^{1}H and ^{19}F NMR spectroscopy, UV-vis and emission spectroscopy, and HRMS (Figs. 3.29 & 3.30). The extremely low solubility of **3.23** in organic solvents precluded characterisation by ^{13}C NMR.

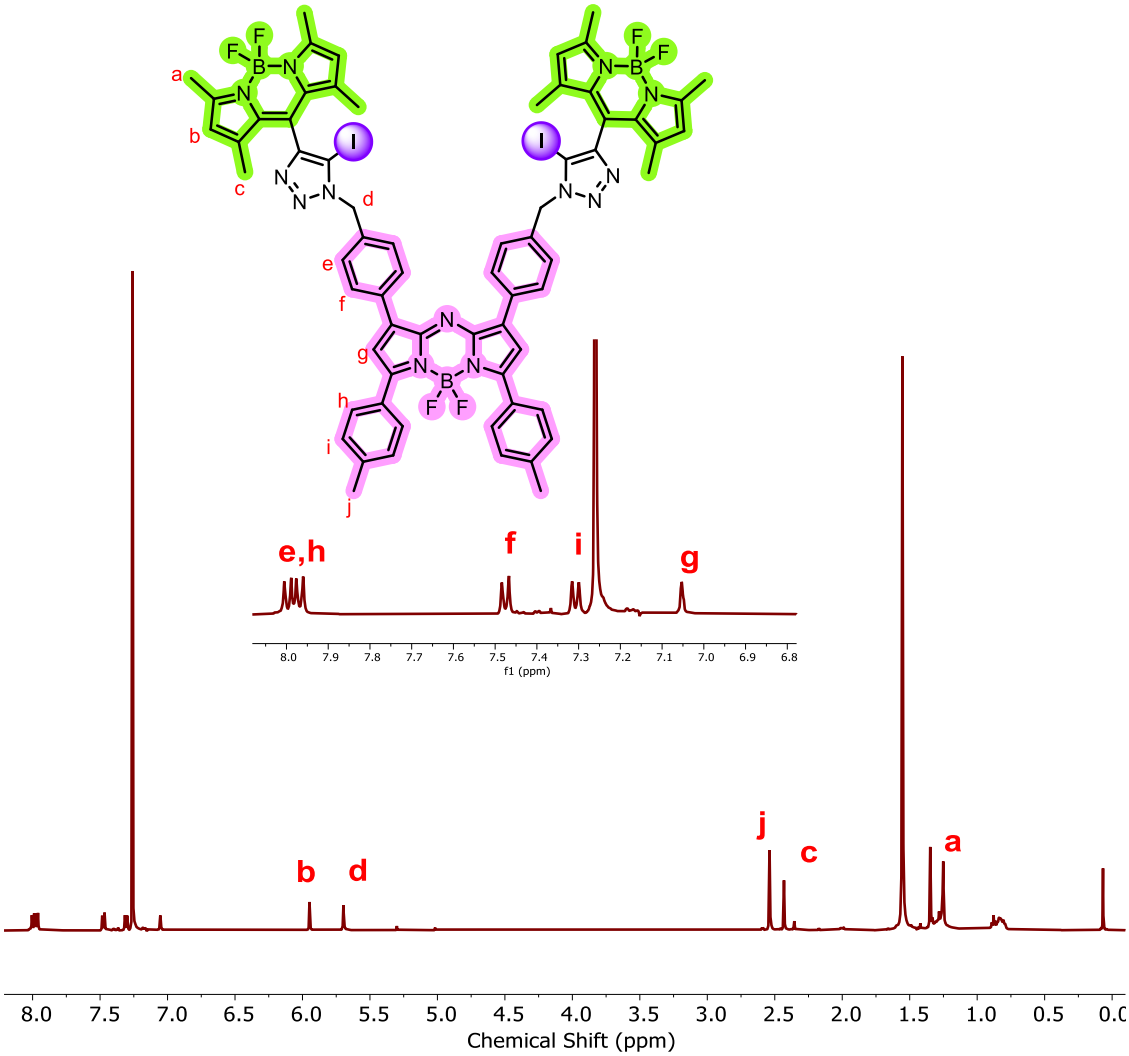


Fig. 3.29. ^{1}H NMR spectrum of sensor **3.23**. ($CDCl_3$, 298 K)

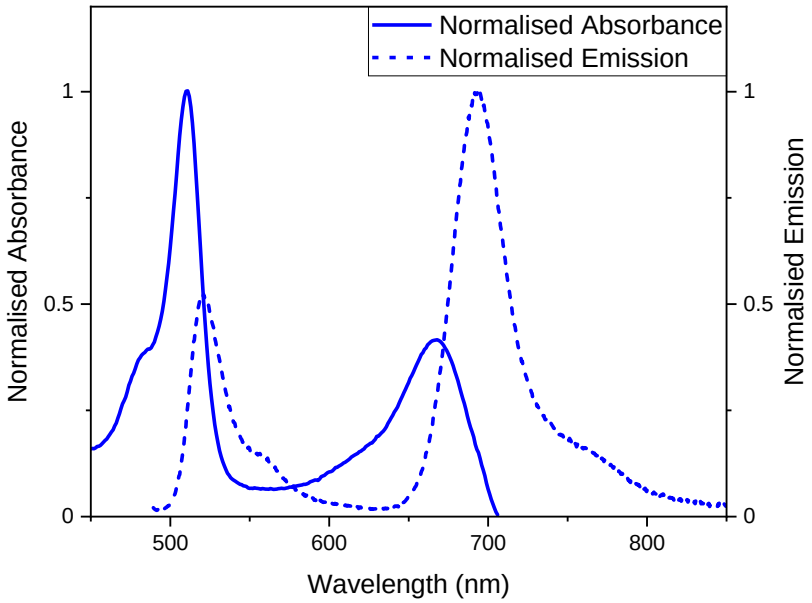


Fig. 3.30. Normalised absorption and emission spectra of sensor **3.23**. (Acetone, 1 μM, 298 K, 480 nm excitation wavelength)

Sensor **3.23** exhibits two absorption features, one with a maximum at 511 nm, corresponding to the two BODIPY units and another centred at 668 nm, corresponding to the aza-BODIPY core (Fig. 3.30). These features remain well separated and resolved,[72] which indicates that the ground state electronic properties of the fluorophores do not significantly affect each other, which is expected given that they are not conjugated to one another.

Interestingly, when compound **3.23** was excited at 480 nm, emission was observed from both the BODIPY and aza-BODIPY fluorophores. This observation indicates that the BODIPY units, which absorb at a higher energy, act as energy donors to the aza-BODIPY fluorophore, partially quenching the BODIPY emission and leading to emission from the aza-BODIPY core, which does not absorb at the excitation wavelength. The ratio of emission intensity from the aza-BODIPY and BODIPY features was invariant across sensor

concentrations from 1 – 5 μM, suggesting that the energy transfer is primarily intramolecular in this concentration range.[73]

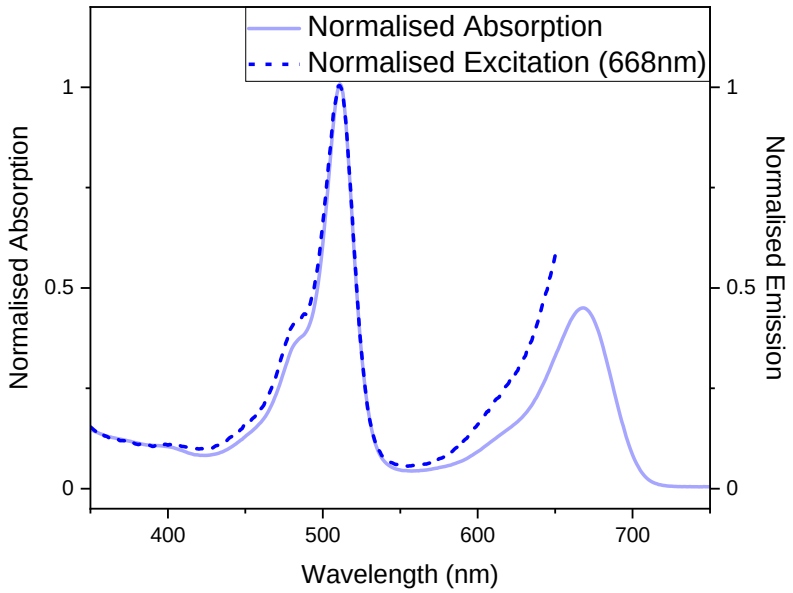


Fig. 3.31. Absorbance and excitation (668 nm) spectra of receptor **3.23**. (Acetone, 5 μM 298 K)

Further evidence for this energy transfer was provided by the excitation spectrum of receptor **3.23**, monitoring emission from the aza-BODIPY fluorophore (668 nm). The features of the excitation spectrum follow the absorbance spectrum, suggesting that photons absorbed by the peripheral BODIPY units cause emission from the aza-BODIPY core (Fig. 3.31) This finding opened the exciting possibility of studying anion binding *via* monitoring emission from two distinct fluorophores with one excitation wavelength.

3.3.2 Anion Binding Studies

The halide anion binding properties of sensor **3.23** were probed by titration experiments in acetone. In each case, two emission spectra were recorded: one with an excitation wavelength of 615 nm, which caused emission solely from the aza-BODIPY core; and one with an excitation wavelength of 490 nm, leading to emission from both the peripheral BODIPY fluorophores and the aza-BODIPY core (Fig. 3.32).

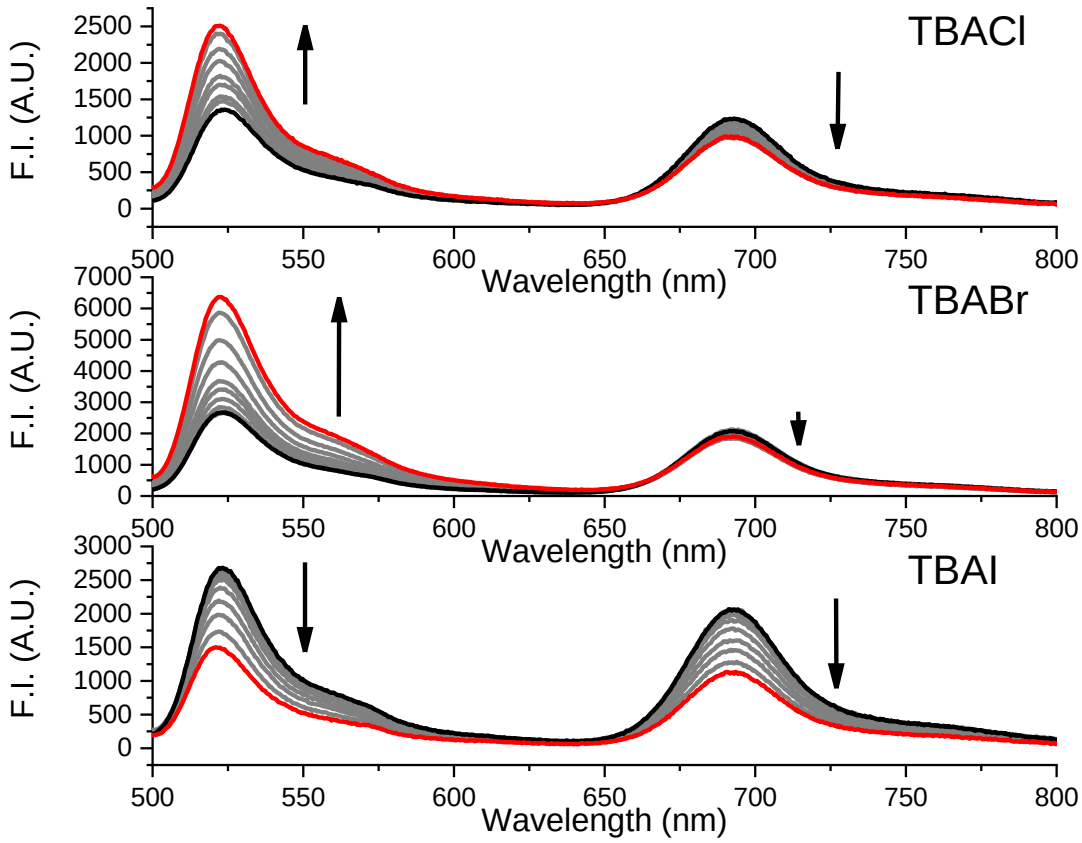


Fig. 3.32. Fluorescence emission response of sensor **3.23** upon addition of increasing concentrations of TBAX (X = Cl, Br, I) salts. (Acetone, 1 μM, 298 K, 490 nm excitation wavelength).

Upon addition of different TBAX (X =Cl, Br I) salts, qualitatively different emission responses were observed, characteristic of each halide anion (Figs. 3.32 & 3.33). Iodide caused quenching of both the aza-BODIPY and BODIPY emission features, ascribed to a heavy atom effect, whereas chloride and bromide both caused enhancement of the BODIPY emission. Chloride could be distinguished from bromide by considering the changes in the aza-BODIPY emission, which were minimal upon the addition of bromide, whereas significant quenching was observed in the case of chloride. Therefore, through these qualitatively different emission responses, discrimination between different halide anions could be achieved. It is noteworthy that the directions of these emission responses are consistent with both the first generation aza-BODIPY sensors reported above and the

BODIPY sensors described in Chapter Two, indicating that increasingly complex sensors with predictable sensing responses can be constructed from simpler building blocks.

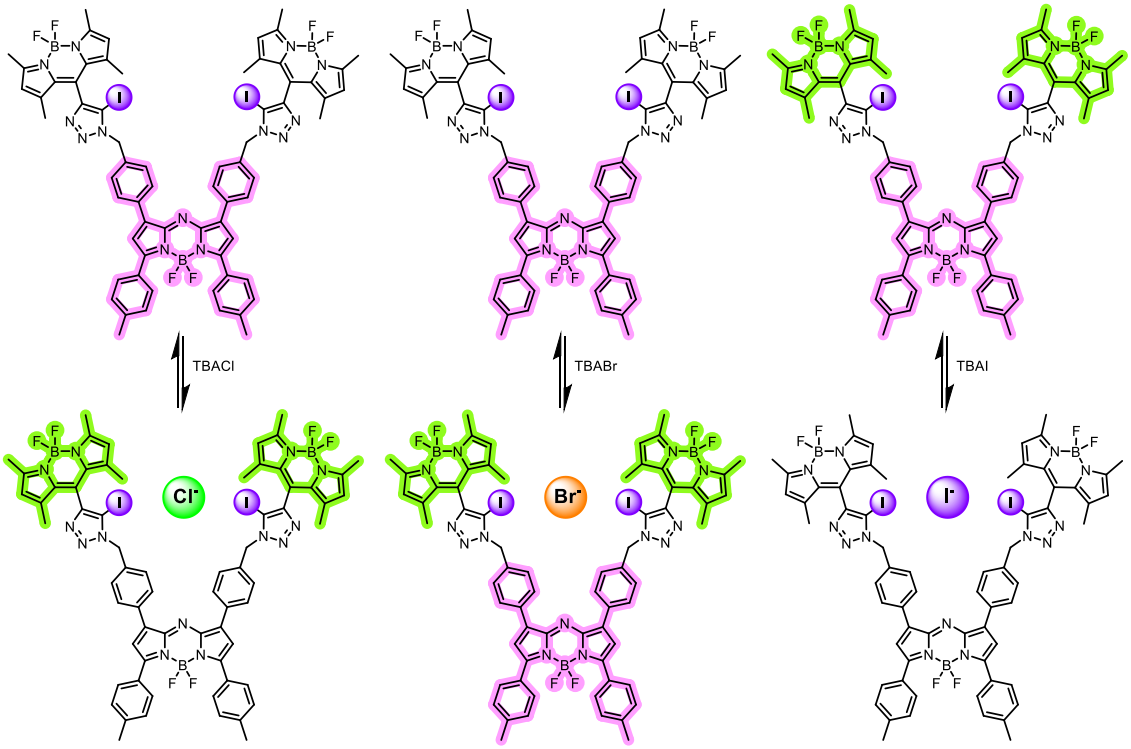


Fig. 3.33. Cartoon showing the qualitatively different emission responses exhibited by sensor **3.23** upon halide anion binding.

The emission response of the BODIPY emission fluorophore was fitted to a 1:1 stoichiometric host-guest binding model to determine the association constants shown in Table 3.5. The BODIPY emission was used for fitting because the aza-BODIPY emission exhibited very small changes upon the addition of TBABr. The halide association constant values are consistently lower for sensor **3.23**, compared to first generation sensors **3.14** and **3.15**, which is likely due to the increased conformational flexibility of **3.23**, due to the introduction of the additional methylene unit. Therefore, receptor **3.23** is relatively less pre-organised for anion binding, decreasing its halide anion affinity. The observed halide

selectivity trend again reflects their charge density, as seen for the other receptors in organic solvents.

Table 3.5. Halide association constants (M^{-1})[a] of sensor **3.23**. (Acetone, 1 μM, 298 K)

Anion	K_a
Cl^-	860
Br^-	210
I^-	190

[a] Determined in acetone by global fitting to a 1:1 binding model. All errors <10%.

Ratiometric anion sensors containing two fluorophores commonly use the emission from one fluorophore, which is invariant to anion concentration, as an internal reference for emission from the other fluorophore, which responds to anion binding.[74] However, in this case, the aza-BODIPY core also responds to anion binding (Fig. 3.32), so cannot simply act as an internal reference. In order to use compound **3.23** as a host concentration-independent ratiometric sensor, calibration curves must be constructed which relate the ratio of aza-BODIPY and BODIPY emission intensity to anion concentration, which were constructed for chloride and bromide (Fig. 3.34). This was not possible for iodide, as both emission features are quenched by approximately the same degree, such that their intensity ratio does not change upon varying the iodide concentration. Therefore, future work in this area of ratiometric sensor design should focus on preparing sensors which contain one fluorophore sufficiently remote from the anion binding site such that it is unresponsive to anion binding and can act as an internal reference.

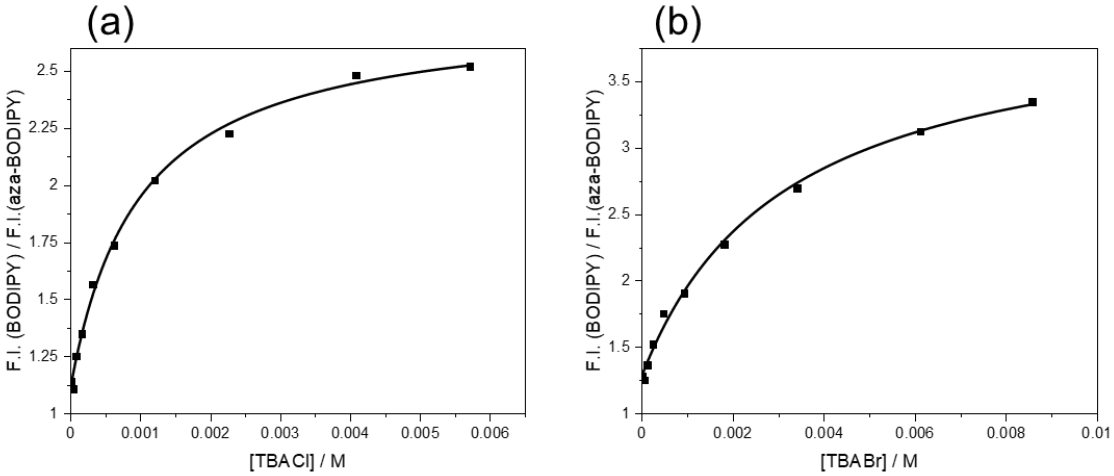


Fig. 3.34. Calibration curves relating the concentration of (a) chloride and (b) bromide to the ratio of emission intensity from the BODIPY and aza-BODIPY emission features of sensor **3.23**. (Acetone, 1 μM, 298 K)

3.4 Chapter Conclusions and Future Work

Initially, two novel, XB, first generation aza-BODIPY based anion sensors were synthesised *via* a CuAAC methodology. The sensors showed desirable optical properties, with strong emission in the biologically relevant NIR-1 window in both cases.

Anion binding titration studies revealed the selectivity of both sensors for the halide anions. They proved unresponsive to the addition of $TBAHSO_4$ and $TBAH_2PO_4$, whereas addition of halide anions elicited strong emission quenching responses of up to 70%. This work therefore extends the optical range of XB halide anion sensors into the biologically relevant NIR-1 window for the first time. Importantly, **3.14** displayed both larger magnitude sensing responses and greater anion affinity than **3.15**, which should inform the future development of sensor design utilising the aza-BODIPY motif. Lithium halide ion-pair sensing studies were attempted, but no evidence of lithium cation binding through the aza-*N* atom was found and no positive cooperativity was observed.

Having established the halide anion sensing properties of the first generation sensors, the ability of iodinated aza-BODIPY compounds to efficiently generate singlet oxygen was harnessed in the first demonstration of anion binding-modulated $^1O_2$ production. Receptor **3.14** proved capable of acting as a photosensitiser, efficiently generating $^1O_2$ and importantly, by combining this ability with its anion sensing capability, unprecedented supramolecular host-guest anion binding-modulated $^1O_2$ generation was demonstrated, which opens a new avenue for improving the selectivity of PDT agents. Control studies with both non-coordinating anions and the precursor azide **3.5** provided strong evidence that this observation can confidently be attributed to anion binding. Fluorescence lifetime investigations with receptor **3.14** in the absence and presence of

anions suggested that this host-anion $^1O_2$ generation modulation was due to an increase in the rate of non-radiative decay processes, which compete with intersystem crossing, reducing the triplet quantum yield and hence the rate of $^1O_2$ production.

A mixed BODIPY/aza-BODIPY dyad compound, **3.23**, was also prepared *via* a CuAAC methodology, in order to facilitate ratiometric anion sensing. Interestingly, energy transfer from the peripheral BODIPY units to the central aza-BODIPY core was observed, which allowed the emission response of both fluorophores to anion binding to be monitored simultaneously with one excitation wavelength. Unique and identifiable fluorescence responses were observed upon the addition of different halide anions, allowing the identity of an unknown halide anion to be determined. Halide anion association constants were determined for sensor **3.23** and, in the cases of chloride and bromide, calibration curves relating the anion concentration to the ratio of BODIPY to aza-BODIPY emission intensity were constructed, allowing **3.23** to act as a ratiometric sensor.

All three receptors exhibited turn-off quenching fluorescence responses in the NIR-1 window, but, as highlighted in the introduction to this chapter, turn-on responses are valued for biological imaging applications. Additionally, whilst the demonstration of anion-binding modulated $^1O_2$ production was promising, chloride binding to **3.14** led to a decrease in the rate of $^1O_2$ generation, when a switch-on in singlet oxygen production would perhaps be more desirable. These properties are related to each other, that is an aza-BODIPY anion sensor which displayed a turn-on sensing response to anion binding would also exhibit an *increase* in $^1O_2$ production upon anion binding. Therefore, future work could target such a turn-on sensor by exploring different connectivity of the anion binding site to the aza-BODIPY fluorophore (Fig. 3.35).

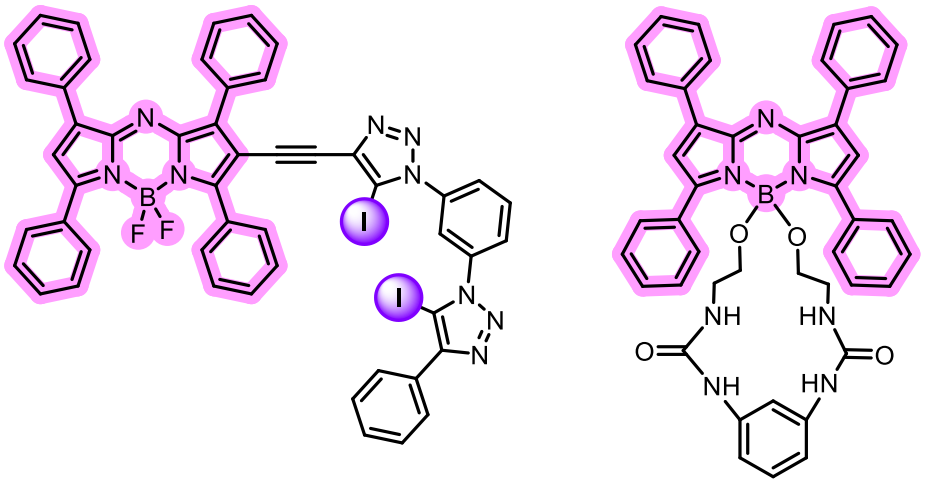


Fig. 3.35. Potential alternative aza-BODIPY connectivities to be explored in the pursuit of an anion binding-induced turn-on emission response.

A turn-on emission response and ion-pair sensing could also be achieved by a mechanically-bonded, interlocked host. For example, the sodium cation templated method for the synthesis of interlocked molecules, pioneered by Chiu and recently adopted for heteroditopic [2]catenane formation,[55, 75] could be used to prepare an aza-BODIPY integrated [2]catenane containing poly-ethylene glycol chains (Fig. 3.36). Indeed, preliminary attempts to synthesise this host were undertaken: the aza-BODIPY containing macrocycle was prepared and the interlocked catenane observed by HRMS, although not isolated. It is conceivable that ion-pair binding would rigidify the dynamic interlocked structure sufficiently to achieve a turn-on emission sensing response.

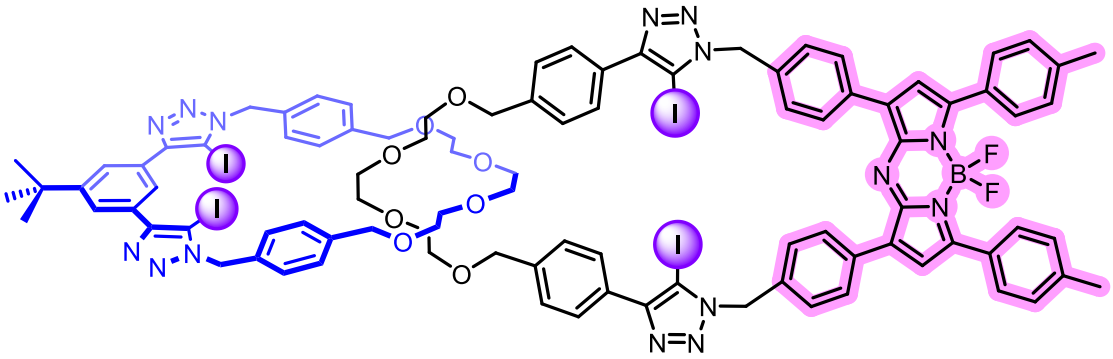


Fig. 3.36. An aza-BODIPY containing [2]catenane for ion-pair sensing.

3.5 References for Chapter Three

1. T. Terai, T. Nagano, *Curr. Opin. Chem. Biol.* **2008**, *12*, 515-521.
2. K. M. Dean, A. E. Palmer, *Nat. Chem. Biol.* **2014**, *10*, 512-523.
3. J. Han, K. Burgess, *Chem. Rev.* **2010**, *110*, 2709-2728.
4. H. Xiao, P. Li, B. Tang, *Chem. Eur. J.* **2021**, *27*, 6880-6898.
5. D. Arosio, G. M. Ratto, *Front. Cell. Neurosci.* **2014**, *8*.
6. R. A. de Melo Reis, H. R. Freitas, F. G. de Mello, *Front. Neurosci.* **2020**, *14*, 569361.
7. R. I. Dmitriev, D. B. Papkovsky, *Methods Appl. Fluoresc.* **2015**, *3*, 034001.
8. M.-S. Steiner, A. Duerkop, O. S. Wolfbeis, *Chem. Soc. Rev.* **2011**, *40*, 4805-4839.
9. C. A. Siciliano, K. M. Tye, *Alcohol* **2019**, *74*, 47-63.
10. J. Zhao, L. Jiang, A. Matlock, Y. Xu, J. Zhu, H. Zhu, L. Tian, B. Wolozin, J.-X. Cheng, *Light Sci. Appl.* **2023**, *12*, 147.
11. D. Kentner, V. Sourjik, *Annu. Rev. Microbiol.* **2010**, *64*, 373-390.
12. D. B. Zorov, E. Kobrinsky, M. Juhaszova, S. J. Sollott, *Circ. Res.* **2004**, *95*, 239-252.
13. Y. Woo, S. Chaurasiya, M. O'Leary, E. Han, Y. Fong, *Mol. Ther. Oncolytics* **2021**, *23*, 231-238.
14. Y. Kravchenko, K. Sikora, A. A. Wireko, M. Lyndin, *Heliyon* **2024**, *10*, e24390.
15. Y. Yang, Q. Zhao, W. Feng, F. Li, *Chem. Rev.* **2013**, *113*, 192-270.
16. J. Fang, X. Dong, L. Sun, J. Sun, C. Dong, R. Wang, C. Zhao, *Bioorg. Med. Chem. Lett.* **2023**, *96*, 129495.
17. O. S. Wolfbeis, E. Urbano, *J. Heterocycl. Chem.* **1982**, *19*, 841-843.
18. C. D. Geddes, K. Apperson, J. Karolin, D. J. S. Birch, *Anal. Biochem.* **2001**, *293*, 60-66.
19. C. D. Geddes, *Sens. Actuators B Chem.* **2001**, *72*, 188-195.
20. L. Yuan, W. Lin, K. Zheng, L. He, W. Huang, *Chem. Soc. Rev.* **2013**, *42*, 622-661.
21. Kenry, Y. Duan, B. Liu, *Adv. Mater.* **2018**, *30*, 1802394.
22. M. Zhivagui, A. Hoda, N. Valenzuela, Y.-Y. Yeh, J. Dai, Y. He, S. P. Nandi, B. Otlu, B. Van Houten, L. B. Alexandrov, *Nat. Comm.* **2023**, *14*, 276.
23. C. Ding, T. Ren, *Coord. Chem. Rev.* **2023**, *482*, 215080.
24. J. Cao, B. Zhu, K. Zheng, S. He, L. Meng, J. Song, H. Yang, *Front. Bioeng. Biotechnol.* **2020**, *7*.
25. A. N. Bashkatov, E. A. Genina, V. I. Kochubey, V. V. Tuchin, *J. Phys. D: Appl. Phys.* **2005**, *38*, 2543.
26. F. Bureš, *RSC Adv.* **2014**, *4*, 58826-58851.
27. Y. Fan, Y. Wu, J. Hou, P. Wang, X. Peng, G. Ge, *Coord. Chem. Rev.* **2023**, *480*, 215020.
28. X. Zhou, R. Lai, J. R. Beck, H. Li, C. I. Stains, *Chem. Commun.* **2016**, *52*, 12290-12293.
29. J. Killoran, L. Allen, J. F. Gallagher, W. M. Gallagher, D. F. O'Shea, *Chem. Commun.* **2002**, 1862-1863.
30. J. K. G. Karlsson, A. Harriman, *J. Phys. Chem. A* **2016**, *120*, 2537-2546.
31. N. Adarsh, M. Shanmugasundaram, R. R. Avirah, D. Ramaiah, *Chem. Eur. J.* **2012**, *18*, 12655-12662.
32. J. Murtagh, D. O. Frimannsson, D. F. O'Shea, *Org. Lett.* **2009**, *11*, 5386-5389.
33. O. Florès, J. Pliquett, L. Abad Galan, R. Lescure, F. Denat, O. Maury, A. Pallier, P.-S. Bellaye, B. Collin, S. Même, C. S. Bonnet, E. Bodio, C. Goze, *Inorg. Chem.* **2020**, *59*, 1306-1314.
34. L. Li, P. Li, J. Fang, Q. Li, H. Xiao, H. Zhou, B. Tang, *Anal. Chem.* **2015**, *87*, 6057-6063.
35. X.-D. Jiang, J. Zhao, Q. Li, C.-L. Sun, J. Guan, G.-T. Sun, L.-J. Xiao, *Dyes Pigm.* **2016**, *125*, 136-141.
36. J. Zuo, H. Pan, Y. Zhang, Y. Chen, H. Wang, X.-K. Ren, Z. Chen, *Dyes Pigm.* **2020**, *183*, 108714.
37. S. O. McDonnell, D. F. O'Shea, *Org. Lett.* **2006**, *8*, 3493-3496.
38. C. Staudinger, J. Breininger, I. Klimant, S. M. Borisov, *Analyst* **2019**, *144*, 2393-2402.
39. M. M. Salim, E. A. Owens, T. Gao, J. H. Lee, H. Hyun, H. S. Choi, M. Henary, *Analyst* **2014**, *139*, 4862-4873.
40. N. Adarsh, M. Shanmugasundaram, D. Ramaiah, *Anal. Chem.* **2013**, *85*, 10008-10012.
41. B. Zou, H. Liu, J. Mack, S. Wang, J. Tian, H. Lu, Z. Li, Z. Shen, *RSC Adv.* **2014**, *4*, 53864-53869.
42. F. Wu, H. Liu, C. Zhong, L. Zhu, *Tetrahedron Lett.* **2016**, *57*, 5120-5123.

43. Y. Gao, Y. Pan, Y. He, H. Chen, V. N. Nemykin, *Sens. Actuators B Chem.* **2018**, *269*, 151-157.
44. Y. Ge, D. F. O'Shea, *Chem. Soc. Rev.* **2016**, *45*, 3846-3864.
45. A. Li, X. Peng, M. Jiang, T. Wu, K. Chen, Z. Yang, S. Chen, X. Zhou, X. Zheng, Z.-X. Jiang, *Org. Biomol. Chem.* **2022**.
46. N. Adarsh, R. R. Avirah, D. Ramaiah, *Org. Lett.* **2010**, *12*, 5720-5723.
47. L. B. Josefsen, R. W. Boyle, *Met.-Based Drugs* **2008**, *2008*, 276109.
48. J. Usuda, H. Kato, T. Okunaka, K. Furukawa, H. Tsutsui, K. Yamada, Y. Suga, H. Honda, Y. Nagatsuka, T. Ohira, M. Tsuboi, T. Hirano, *J. Thorac. Oncol.* **2006**, *1*, 489-493.
49. P. Wei, F. Xue, Y. Shi, R. Strand, H. Chen, T. Yi, *Chem. Commun.* **2018**, *54*, 13115-13118.
50. T. Huang, H. Ji, S. Yan, Y. Zuo, J. Li, J. W. Y. Lam, C. Han, B. Z. Tang, *Biomater.* **2023**, *297*, 122108.
51. M. H. Lee, J. S. Kim, J. L. Sessler, *Chem. Soc. Rev.* **2015**, *44*, 4185-4191.
52. A. M. Gilchrist, P. Wang, I. Carreira-Barral, D. Alonso-Carrillo, X. Wu, R. Quesada, P. A. Gale, *Supramol. Chem.* **2021**, *33*, 325-344.
53. X.-M. Liu, Q. Zhao, W.-C. Song, X.-H. Bu, *Chem. Eur. J.* **2012**, *18*, 2806-2811.
54. A. Docker, C. H. Guthrie, H. Kuhn, P. D. Beer, *Angew. Chem. Int. Ed.* **2021**, *60*, 21973-21978.
55. H. Min Tay, T. G. Johnson, A. Docker, M. J. Langton, P. D. Beer, *Angew. Chem. Int. Ed.* **2023**, *62*, e202312745.
56. G.-J. Zhao, K.-L. Han, *Acc. Chem. Res.* **2012**, *45*, 404-413.
57. S. C. Patrick, P. D. Beer, J. J. Davis, *Nat. Rev. Chem.* **2024**, *8*, 256-276.
58. Y. Tachapermpon, S. Thavornpradit, A. Charoenpanich, J. Sirirak, K. Burgess, N. Wanichacheva, *Dalton Trans.* **2017**, *46*, 16251-16256.
59. Y. Gawale, S. Mangalath, N. Adarsh, J. Joseph, D. Ramaiah, N. Sekar, *Dyes Pigm.* **2019**, *171*, 107684.
60. G. Martin, L. Rentsch, M. Höck, M. Bertau, *Energy Storage Mater.* **2017**, *6*, 171-179.
61. L. A. Kszos, A. J. Stewart, *Ecotoxicol.* **2003**, *12*, 439-447.
62. F. Harari, A. Åkesson, E. Casimiro, Y. Lu, M. Vahter, *Environ. Res.* **2016**, *147*, 1-7.
63. V. K. Munasinghe, H. M. Tay, D. Manawadu, J. Pancholi, Z. Zhang, P. D. Beer, *Dalton Trans.* **2024**.
64. Q. He, Z. Zhang, J. T. Brewster, V. M. Lynch, S. K. Kim, J. L. Sessler, *J. Am. Chem. Soc.* **2016**, *138*, 9779-9782.
65. Y. C. Tse, A. Docker, Z. Zhang, P. D. Beer, *Chem. Commun.* **2021**, *57*, 4950-4953.
66. Z. Kokan, M. J. Chmielewski, *J. Am. Chem. Soc.* **2018**, *140*, 16010-16014.
67. V. A. Rabinovich, Z. Y. Havin, *Brief Chemical Reference Book (Russian)*, **1978**.
68. F. Mitzel, S. Fitzgerald, A. Beeby, R. Faust, *Chem. Commun.* **2001**, 2596-2597.
69. P. Carloni, E. Damiani, L. Greci, P. Stipa, F. Tanfani, E. Tartaglini, M. Wozniak, *Res. Chem. Intermed.* **1993**, *19*, 395-405.
70. S. O. McDonnell, M. J. Hall, L. T. Allen, A. Byrne, W. M. Gallagher, D. F. O'Shea, *J. Am. Chem. Soc.* **2005**, *127*, 16360-16361.
71. F. C. Küpper, L. J. Carpenter, G. B. McFiggans, C. J. Palmer, T. J. Waite, E.-M. Boneberg, S. Woitsch, M. Weiller, R. Abela, D. Grolimund, P. Potin, A. Butler, G. W. Luther, P. M. H. Kroneck, W. Meyer-Klaucke, M. C. Feiters, *Proc. Natl. Acad. Sci. U S A* **2008**, *105*, 6954-6958.
72. S. Kumar, K. G. Thorat, M. Ravikanth, *J. Org. Chem.* **2017**, *82*, 6568-6577.
73. R. K. Castellano, S. L. Craig, C. Nuckolls, J. Rebek, *J. Am. Chem. Soc.* **2000**, *122*, 7876-7882.
74. S. E. Plush, T. Gunnlaugsson, *Dalton Trans.* **2008**, 3801-3804.
75. S.-T. Tung, C.-C. Lai, Y.-H. Liu, S.-M. Peng, S.-H. Chiu, *Angew. Chem. Int. Ed.* **2013**, *52*, 13269-13272.

Chapter 4

Halogen Bonding, BODIPY-Functionalised Pillararene and Aza-Crown Ether Host Systems for Fluorescence Sensing of Anions, Neutral Species and Ion-Pairs

4 Halogen Bonding, BODIPY-Functionalised Pillararene and Aza-Crown Ether Host Systems for Fluorescence Sensing of Anions, Neutral Species and Ion-Pairs

4.1 Introduction

4.1.1 The Pillararene Macrocycle

As highlighted in Chapter One, due to their considerable advantages in guest binding affinity and selectivity, macrocyclic compounds have been developed by supramolecular chemists since the beginning of the field of host-guest chemistry, starting with the pioneering work of Pedersen, Cram and Lehn.[1-4] This has led to the advent of macrocyclic 'cavitands',[5] which are container shaped molecules, frequently formed from cyclic monomers, including cucurbiturils,[6] calixarenes,[7] calixpyrroles,[8] and cyclodextrins,[9] which have been used to bind a variety of charged and neutral species (Fig. 4.1).

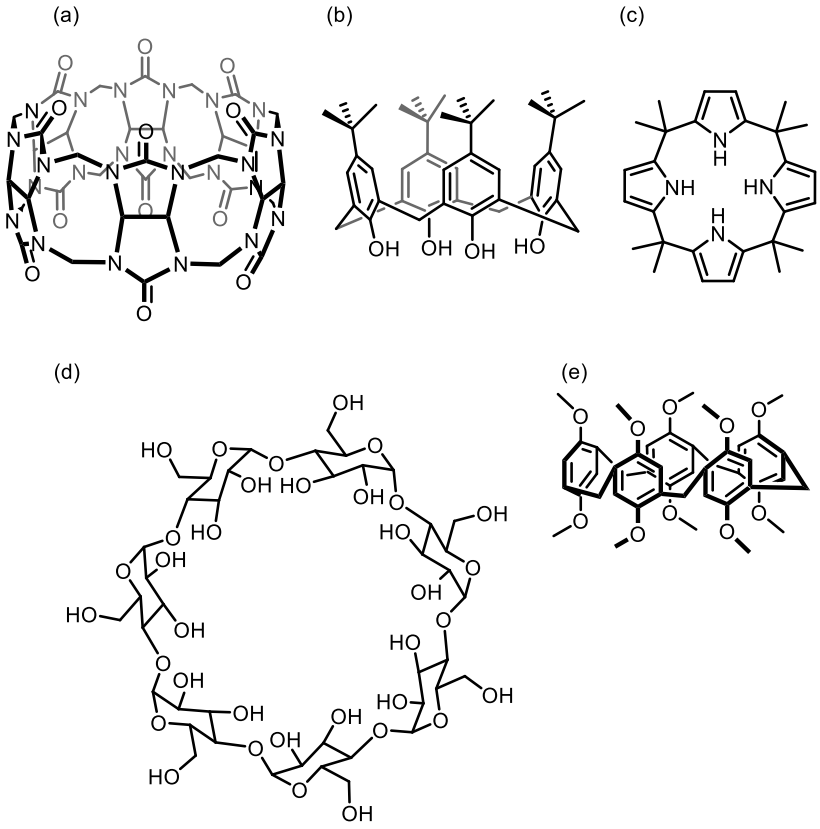
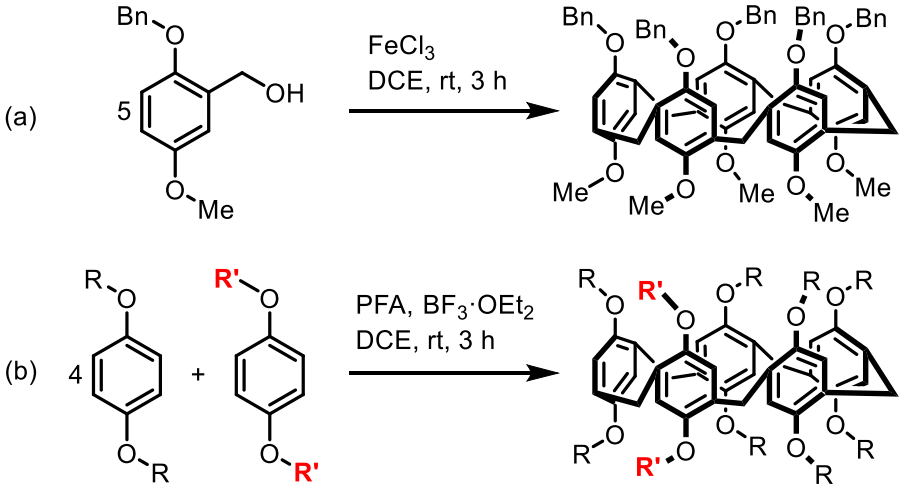


Fig. 4.1. Archetypal examples of macrocyclic cavitand host motifs: (a) cucurbit[6]uril, (b) calix[4]arene, (c) calix[4]pyrrole, (d) *β*-cyclodextrin, (e) pillar[5]arene.

A further addition to this class of compounds, pillar[*n*]arenes, was reported by Ogoshi and co-workers in 2008 (Fig. 4.1e).[10] Pillar[*n*]arenes are highly symmetrical, cylindrical macrocycles formed by the Lewis acid-catalysed condensation of *n* units of a 1,4-dialkoxybenzene monomer and paraformaldehyde (PFA), in a solvent templated synthesis. Variation of the solvent templates the formation of pillararenes with differing number of repeat units: use of 1,2-dichloroethane forms pillar[5]arenes (P5As),[11] whereas use of chlorocyclohexane gives P6As as the major product.[12] Pillararene synthesis has been further developed since their initial report to allow the formation of asymmetrically functionalised derivatives, in which either one 'rim' (Scheme 4.1a),[13-14] or one 'panel' (Scheme 4.1b) of the macrocycle is functionalised.[15]



Scheme 4.1. Synthesis of (a) rim-differentiated and (b) panel-differentiated P5As.

In addition to their ease of derivatisation, pillararenes have attracted interest from supramolecular chemists due to their propensity to form inclusion complexes, primarily with hydrophobic and/or electron-deficient guests.[16] The formation of inclusion complexes with electron-deficient viologen compounds was first demonstrated in Ogoshi's initial report of *per*-methoxy P5A,[10] and since then P5A inclusion complexes with imidazolium compounds,[17] triazoles[18] and ammonium compounds[19] have been reported in organic solvents, all leveraging interactions between the electron-rich P5A cavity and the electron-deficient guests (Fig. 4.2).[19]

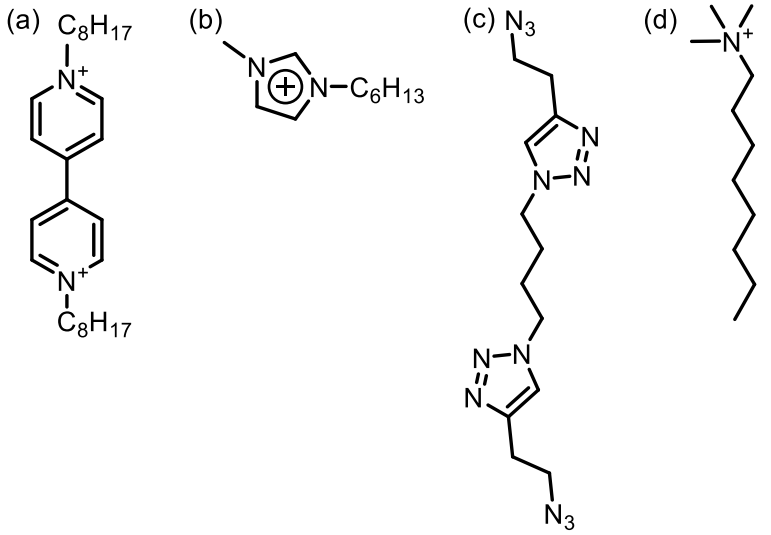


Fig. 4.2. Electron-deficient guests included by P5A derivatives: (a) viologens, (b) imidazolium compounds, (c) triazoles and (d) ammonium compounds.

Pillararene hosts have also displayed very strong binding of hydrophobic guests in aqueous-containing media,[20] normally attributed to hydrophobic effects,[21] as the internal pillararene cavity is very poorly hydrated. For example, in 2011, Stoddart and co-workers reported a P5A monofunctionalised with a pyrene fluorescent reporter group which was able to sense alkanediamines in ACN : H_2O 1:1 (*v/v*) (Fig. 4.3).[22] As demonstrated by ^{1}H NMR titration experiments, the hydrophobic alkylamine guests threaded through the P5A cavity, and the pyrene emission was quenched by PET from the amine lone pairs. Impressive association constant values of K_a = 21,200 M^{-1} and K_a = 36,000 M^{-1} were determined for 1,5-diaminopentane and 1,8-diaminooctane respectively, highlighting the remarkable strength of association possible between two neutral species driven by hydrophobic effects.

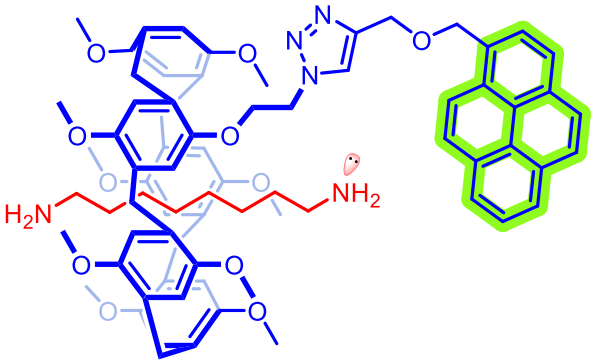


Fig. 4.3. Stoddart's pyrene-appended P5A for sensing of alkyldiamines.

4.1.2 Sensing of Dicarboxylates

Dicarboxylates (DCBs) and dicarboxylic acids play crucial roles as intermediates in numerous biosynthetic pathways,[23] including most notably the Krebs' cycle. Therefore, they are linked to several chronic diseases, such as kidney and liver disease.[24] Furthermore, DCBs and dicarboxylic acids are of increasing industrial importance, as plastic additives and as linkers in the production of metal-organic frameworks (MOFs),[25-26] which has raised concerns about their potential impact on ecosystems and human health.[25]

Given the dual relevance of dicarboxylates and dicarboxylic acids in both health and industry, and their potential environmental impact, effective methods to detect and monitor these compounds has become a critical area of research.[27-30] Due to their hydrophobic, central alkyl chain, dicarboxylates have been shown to be complementary guests for P5As. For example, in 2012, Wang and co-workers reported a bis-urea-appended P5A, which was able to bind dicarboxylates such as dodecanedioate (K_a = 69 M^{-1}) in DMSO-d_6, through the formation of an interpenetrated pseudo[2]rotaxane assembly, assisted by urea HB donor – carboxylate anion interactions (Fig. 4.4).[31]

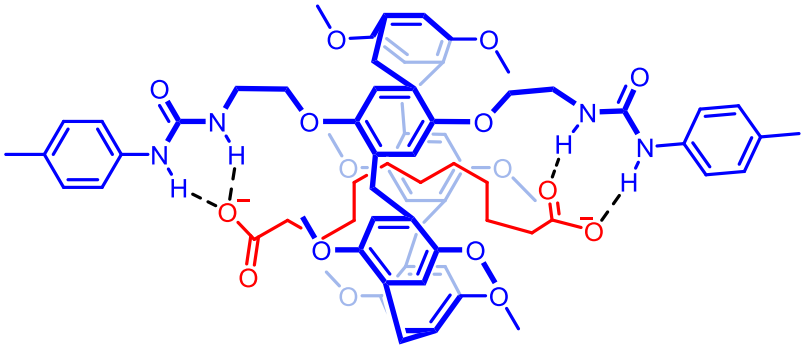


Fig. 4.4. Wang's P5A dicarboxylate receptor.

4.1.3 Sensing of Sulfur Mustard

Since its first deployment during World War I, sulfur mustard (Fig. 4.4a) has become notorious, having been used in numerous conflicts as a chemical warfare agent (CWA). Upon exposure, sulfur mustard induces severe blistering of the skin and mucous membranes within a short period, alongside posing grave, longer-term risks to the respiratory system, which can result in fatal outcomes.[32] Furthermore, sulfur mustard has been identified as having significant carcinogenic and mutagenic properties, adding to its persistent dangerous profile, after its acute effects.[32] Given the profound health hazards posed by sulfur mustard and other CWAs, the development of reliable detection methods for these agents is of paramount importance. Due to its toxicity, a simulant of sulfur mustard, 2-chloroethyl ethyl sulfide (CEES), is commonly used in its place in investigative sensing experiments (Fig. 4.4b).[33]

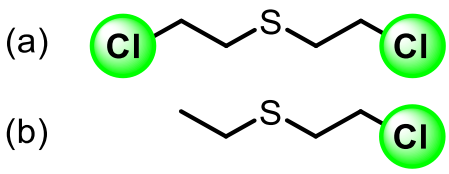


Fig. 4.4. The structures of: (a) sulfur mustard and (b) CEES.

Due to its relative lack of functionality and charge neutrality, sulfur mustard has remained an elusive target for supramolecular chemists.[34] Previous reports of sulfur

mustard hosts have exploited the nucleophilicity of the central sulfur atom, which has been shown to coordinate to Ag(I) centres in acetone, DMF and DMSO.[35] Similar metal coordination interactions have since been used to effect sulfur mustard sensing. In 2003, Brinkley *et al.* reported colourimetric sensing of CEES and other sulfides through the appearance of LMCT bands from the sulfide species to a Cu(II) acetate centre, embedded in a sol-gel matrix.[36] Also exploiting the reactivity of the sulfur centre, in 2013, Beer and co-workers reported gold nanoparticles, decorated with dansyl fluorophores, which acted as a turn-on sensor for sulfur mustard (Fig. 4.5).[37] The emission of the dansyl moiety was quenched by tethering to the gold nanoparticles, but, upon addition of sulfur mustard (or a simulant), the dansyl fluorophores were displaced from the gold nanoparticle surface, to allow the formation of strong Au–S interactions, leading to an irreversible increase in dansyl emission intensity.

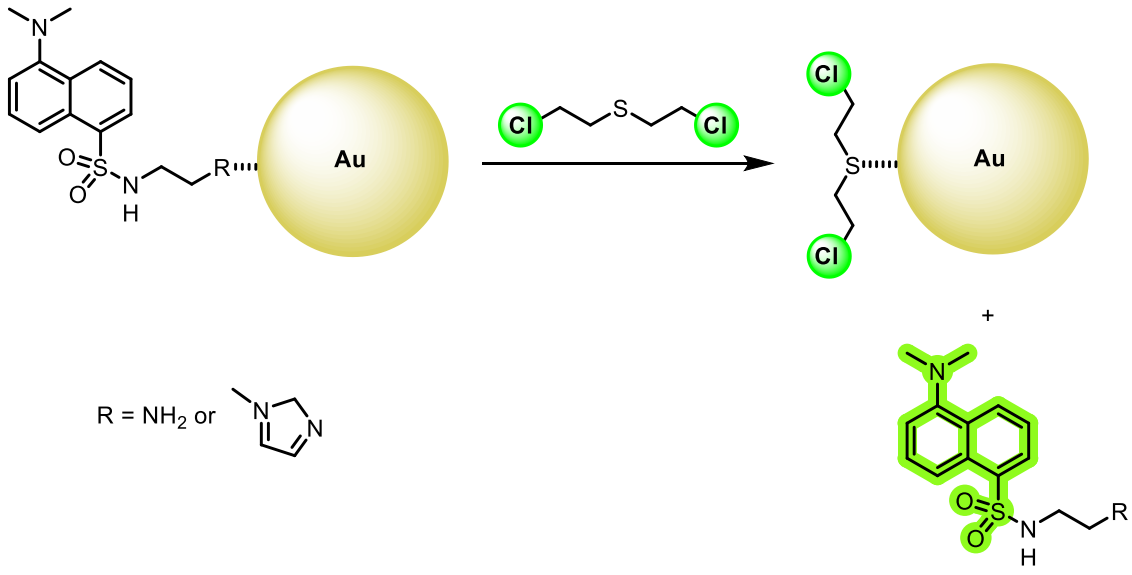


Fig. 4.5. Beer's sulfur mustard-sensing, dansyl-appended gold nanoparticles.

In addition to the nucleophilic sulfur atom, sulfur mustard also features two terminal electron-withdrawing chlorine atoms and a hydrophobic core. In this respect, sulfur mustard represents a similar sensing target to dicarboxylates, with their

hydrophobic central alkyl chain and negatively charged carboxylate groups, although a sulfur mustard sensor based on this approach has not yet been developed.

4.1.4 Aza-Crown Ether Macrocycles

Closely related to the crown ethers reported by Pedersen,[1] aza-crown ethers exhibit similar cation recognition properties to their all-oxygen analogues,[38] but are of particular interest to supramolecular chemists due to the reactive nitrogen atom(s) functionality in the ring, facilitating their incorporation into larger molecular architectures. For example, the appended pyridine 'arms' on the diaza-18-crown-6-based ligand reported by Tsukube and co-workers allowed the ligand to efficiently transport sodium cations through an organic membrane (Fig. 4.6a),[39] which the parent diaza-18-crown-6 macrocycle was incapable of doing. Aza-crown ether-containing compounds have also been used as cation sensors, an elegant example of which was reported by Bhosale and co-workers in 2017,[40] which consisted of an NDI core decorated with two aza-crown ether cation binding units (Fig. 4.6b). The sensor offered a selective, naked-eye detectable colourimetric response to Ca^{2+} over a variety of other metal cations in acetonitrile.

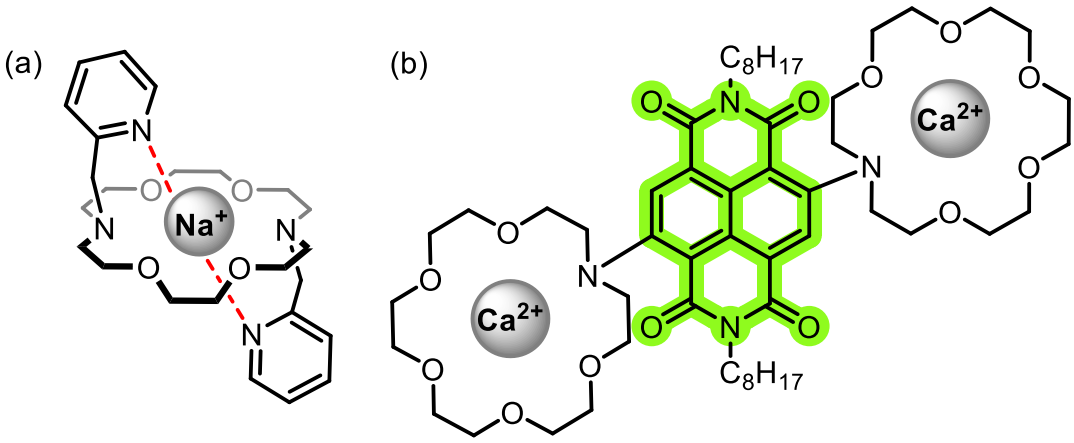


Fig 4.6. Aza-crown ethers incorporated into (a) Tsukube's cation transporting ligand and (b) Bhosale's Ca^{2+}-selective cation sensor.

In addition to their ability to recognise metal cations, (aza-)crown ethers are able to effectively bind ammonium compounds, which has given rise to a variety of supramolecular assemblies based on this behaviour.[41-43] For instance, in 2024, Kim and co-workers reported an aza-crown ether-based catalyst for hydroxyl functionalisation (Fig. 4.7).[44] The catalyst functioned *via* binding of the positively charged ammonium group to the aza-crown ether, allowing the pendant imidazole group to activate the hydroxyl moiety, enhancing its nucleophilicity.

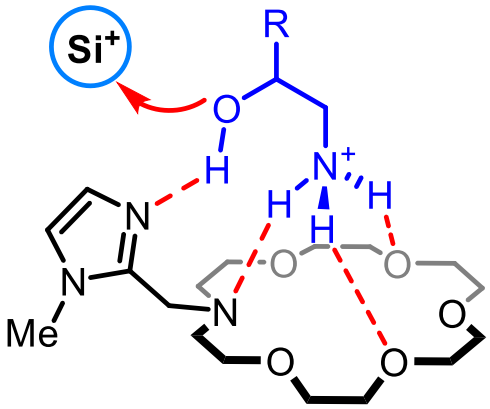


Fig. 4.7. Kim's aza-crown ether-based hydroxyl activation catalyst.

4.1.5 Ion-Pair Sensors

Aza-crown ethers have been used as the cation binding motif in a variety of optical ion-pair sensors.[40, 45-47] For example, in 2024, Romański and co-workers reported an ion-pair sensor consisting of a pyrene fluorescent reporter group appended to a squaramide anion binding site and an aza-crown ether cation recognition motif (Fig. 4.8).[48] The fluorescence emission of the pyrene unit was enhanced upon the addition of halide anions, enabling anion sensing. The presence of one equivalent of sodium cations was additionally shown to enhance the anion affinity of the receptor by a factor of up to 1.84 for iodide in

acetonitrile (K_a(NaI) = 3500 M^{-1}, K_a(TBAI) = 1900 M^{-1}), although direct sensing of sodium cation binding *via* the pyrene emission was not possible. Other ion-pair sensors include the tetraphenyl ethylene-based sensor reported by Caballero and Molina,[49] shown in Chapter One.

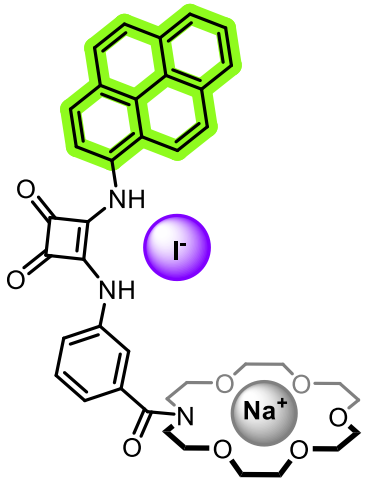


Fig. 4.8. Romański's aza-crown ether-based ion-pair sensor.

4.1.6 Chapter Aims

Due to their shared hydrophobic character, halogen bonding is a complementary interaction to deploy alongside a pillararene motif for the purpose of guest recognition. The combination of a pillararene macrocycle and XB donor groups is anticipated to exhibit strong binding of hydrophobic species, particularly in aqueous-containing media. Given their biological and environmental relevance, both dicarboxylates and sulfur mustard are important sensing targets, and, due to their similar molecular characteristics (hydrophobic core and electron-rich terminal groups) it is anticipated that a single receptor could prove capable of sensing both pollutants.

By deploying the responsive XB BODIPY sensing motif developed in Chapter Two, the initial work described in this chapter seeks to achieve the goal of dicarboxylate and

sulfur mustard sensing, through synthesis of pillar[5]arene-based compounds **4.2-XB** and **4.2-HB**, which are expected form interpenetrated assemblies in which the guest is threaded through the P5A cavity and interacts with the pendant (iodo-)triazole groups (Fig. 4.9). The use of XB interactions is anticipated to lead to improved performance in aqueous-containing media, relative to the previously reported urea HB donor-functionalised pillararene receptors described by Wang and co-workers (Fig. 4.4).[31]

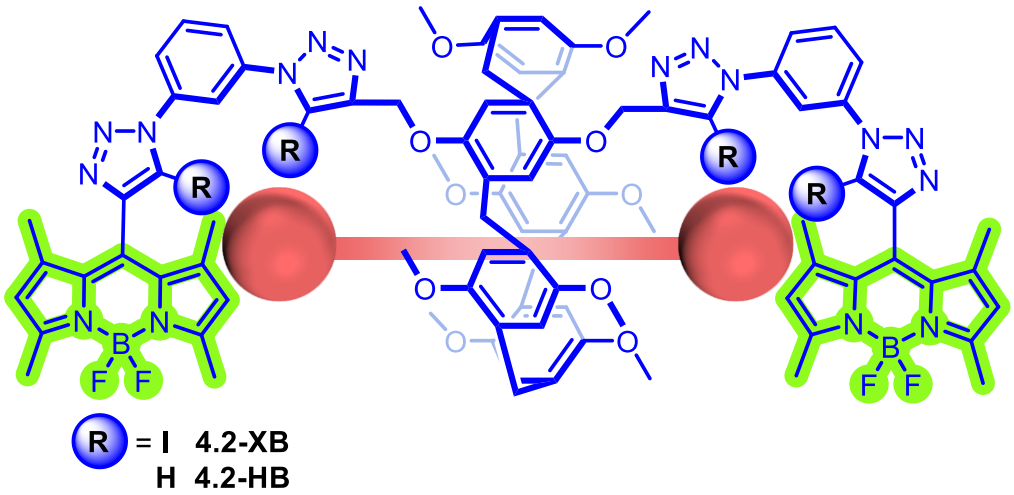


Fig. 4.9. Cartoon showing the structure of **4.2-XB/HB** and their expected guest binding mode.

The second aspect of the work described in this chapter has the aim of extending the use of XB interactions to fluorescent ion-pair sensing, by synthesis of the heteroditopic diaza-crown ether-containing receptor **4.7** (Fig. 4.10). Initially, the ability of **4.7**, which also contains the powerful XB BODIPY sensing fragment developed in Chapter Two, to bind and sense inorganic alkali metal halide salts will be investigated. Subsequently, by leveraging the ability of diaza-crown ethers to also recognise ammonium compounds, sensing of the hydrochloride salt of the neuromodulator molecule dopamine will also be studied.

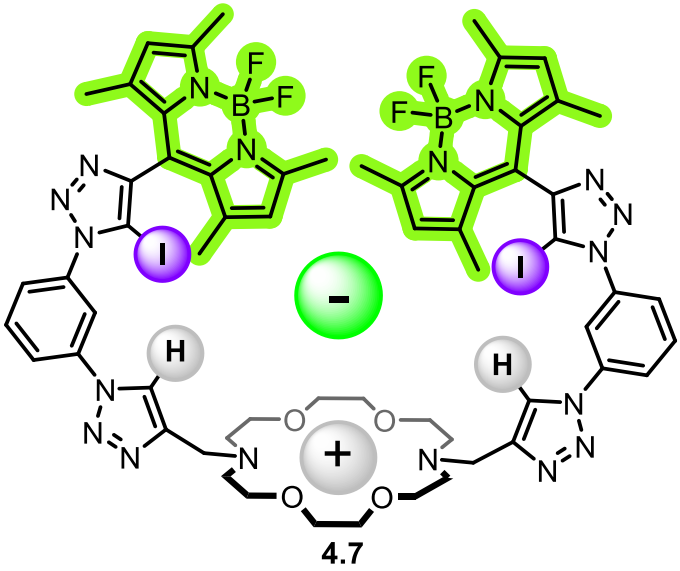


Fig. 4.10. Cartoon showing the structure of **4.7** and its expected ion-pair binding mode.

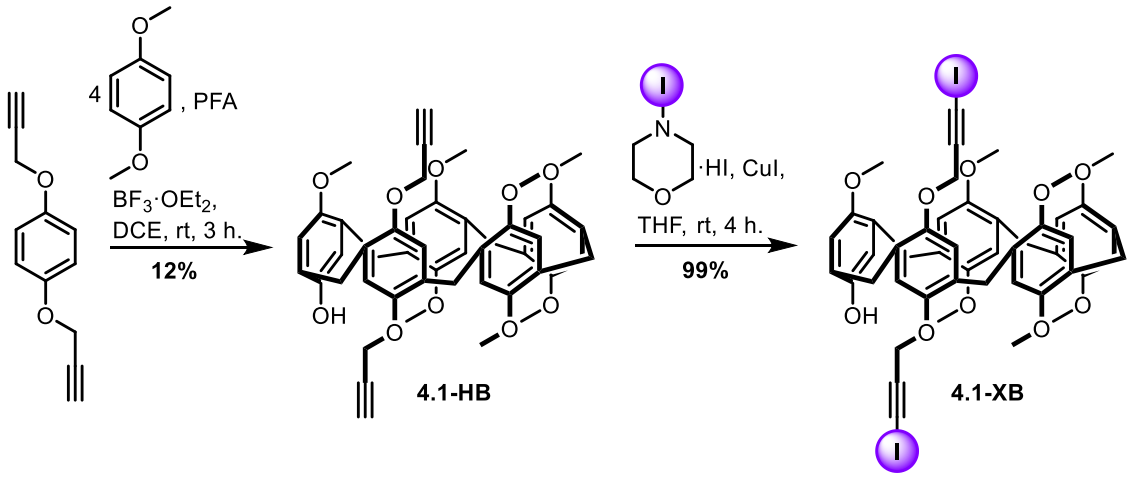
4.2 Sensing of Dicarboxylates and a Sulfur Mustard Simulant using a Halogen Bonding BODIPY-Appended P5A*

4.2.1 Synthesis and Characterisation

The preparation of the target XB BODIPY functionalised pillar[5]arene receptors **4.2-XB/HB** was achieved *via* CuAAC synthetic methodology, employing the bright and anion binding-responsive BODIPY fragments **2.4** and **2.8**. Therefore, to allow the attachment of one such fragment to each rim of the central P5A macrocycle, a pair of asymmetrical P5As, each with one aromatic panel functionalised with terminal (iodo)alkyne groups (**4.1-XB/HB**) were initially targeted.

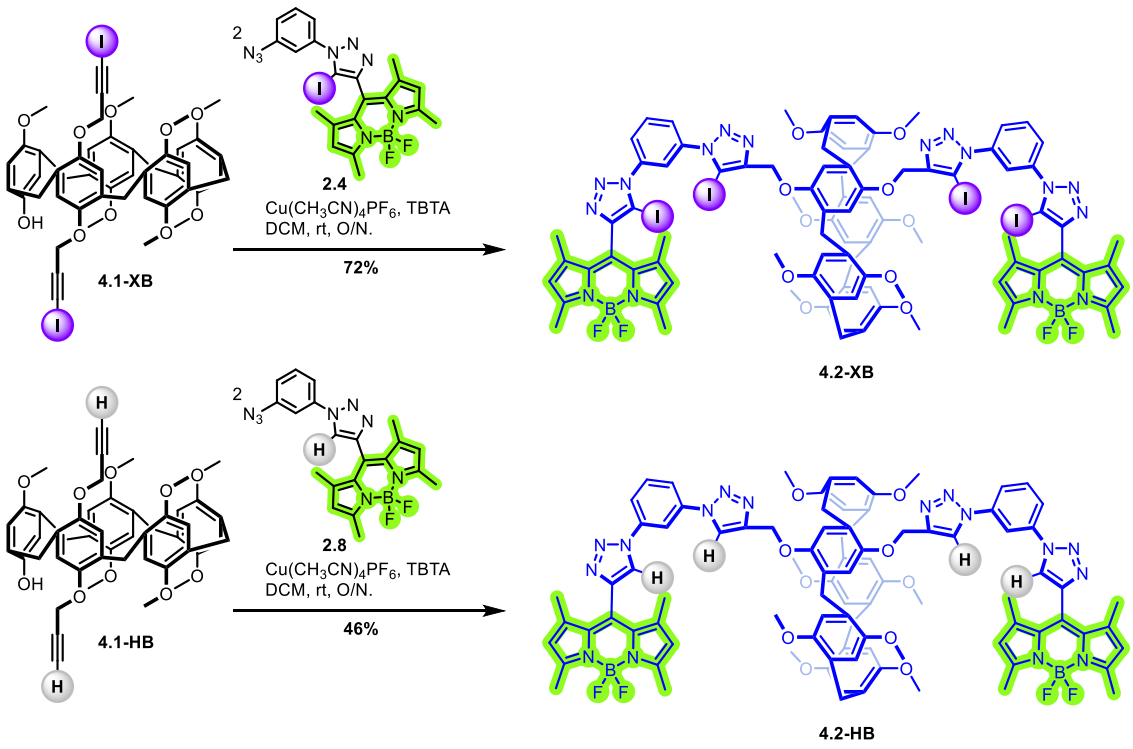
The protoalkyne, **4.1-HB**, was prepared *via* the statistical incorporation of 1,4-bis(prop-2-yn-1-yloxy)benzene into a P5A macrocycle, using a solvent templated method (Scheme 4.2).[12] This bis-alkyne precursor, 1,4-dimethoxybenzene and paraformaldehyde were condensed in DCE in the presence of BF_3,[50] to give **4.1-HB** in a modest 12% yield, following chromatographic purification to remove the polymeric, *per*-methoxy P5A and *tetra*-alkynyl side products. Iodination of **4.1-HB** was achieved by treatment with *N*-iodomorpholine hydroiodide, in the presence of a CuI catalyst, affording **4.1-XB** in quantitative yield (Scheme 4.2)

* This work was carried out in collaboration with Jamie T. Wilmore.



Scheme 4.2. Synthesis of alkyne precursors **4.1-XB/HB.**

The hosts, **4.2-XB/HB**, were prepared *via* a CuAAC reaction with two equivalents of the BODIPY-containing fragments **2.4** or **2.8** (Scheme 4.3). Purification by column chromatography afforded **4.2-XB/HB** in 72% and 46% yields respectively.



Scheme 4.3. Synthesis of P5A receptors **4.2-XB/HB**.

Both P5A receptors were characterised by ^{1}H and ^{13}C NMR, UV-vis absorption spectroscopy and HRMS. The ^{1}H NMR, absorption and emission spectra of **4.2-XB** are shown below as representative examples (Figs. 4.11 & 4.12).

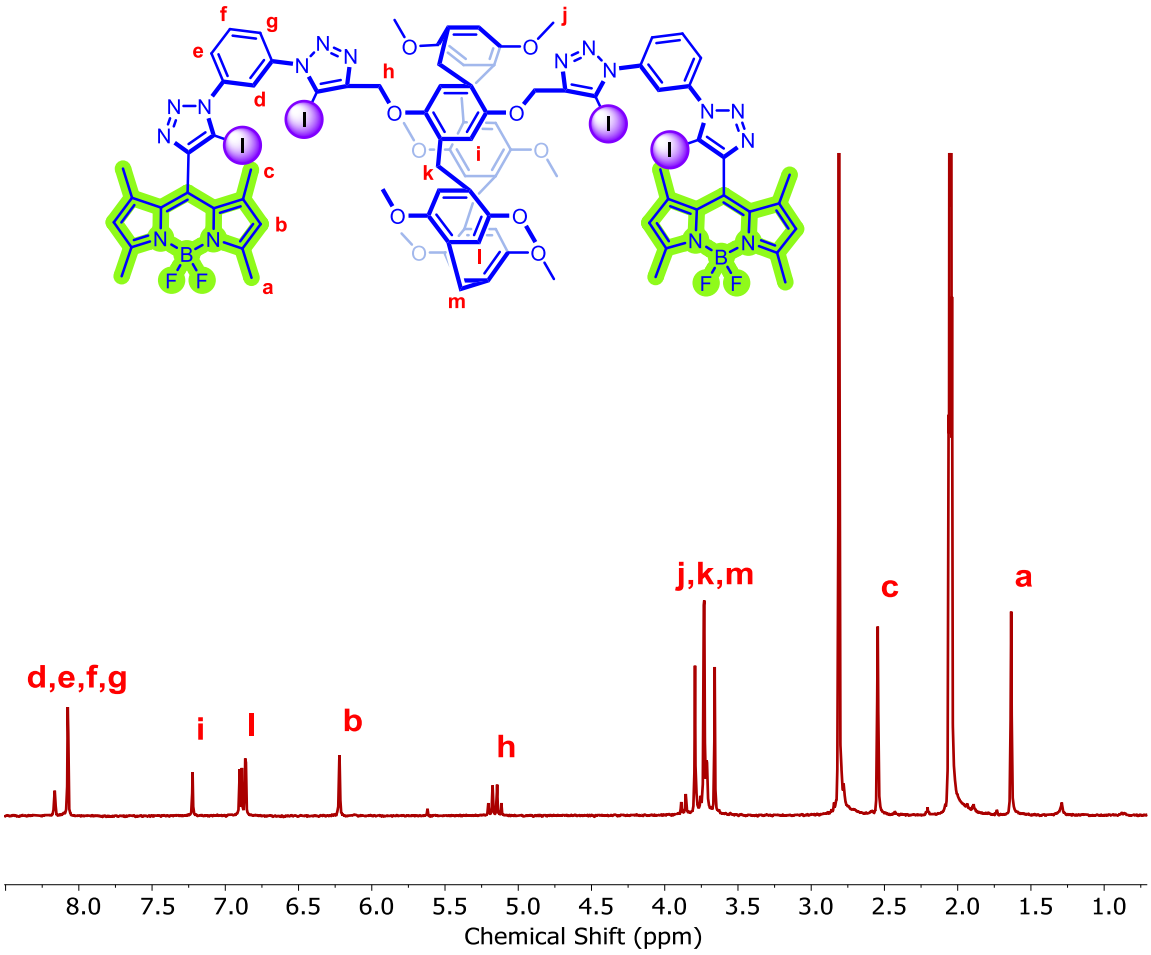


Fig. 4.11. ^{1}H NMR spectrum of **4.2-XB**. (Acetone-d_6, 298 K)

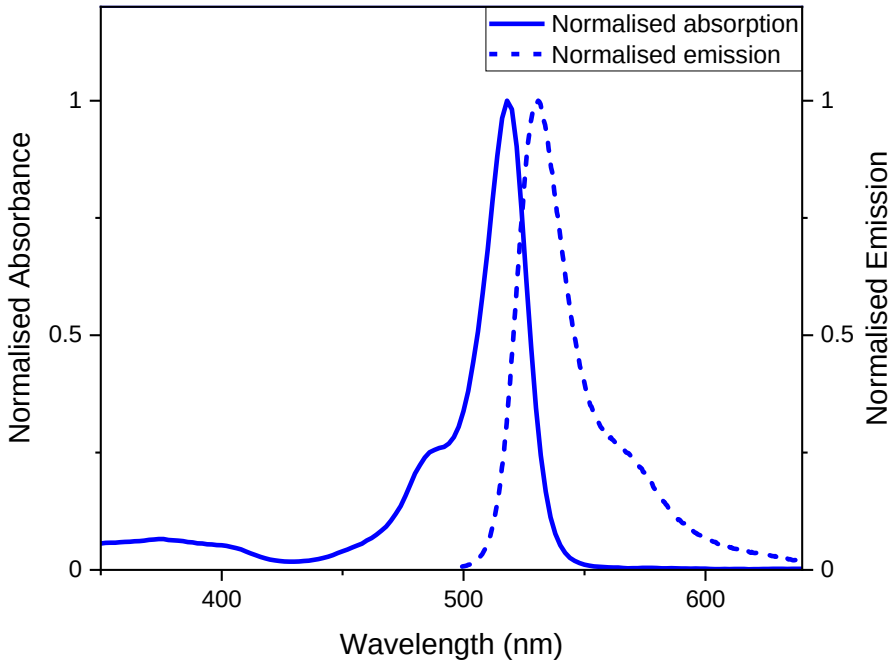


Fig. 4.12. Normalised absorption and emission spectra of **4.12-XB**. ($CHCl_3$, 10 μM, 490 nm excitation wavelength)

Both **4.2-XB/HB** receptors displayed typical BODIPY absorption and emission features in $CHCl_3$, with absorption maxima of 518 nm and 516 nm for **4.2-XB** and **4.2-HB** respectively, and corresponding emission maxima of 531 nm and 532 nm, all of which are consistent with the family of sensors reported in Chapter Two.

4.2.2 Fluorescence Sensing Studies in Organic Media

Initially, fluorescence sensing studies were conducted in $CHCl_3$, which was selected over acetone in this case due to acetone's known propensity to thread through the P5A cavity.[51] First, the fluorescence response towards simple anions, such as chloride, bromide, nitrate and acetate in $CHCl_3$ was assessed. Upon addition of aliquots of the TBA salts of these anions, **4.2-XB** displayed marked turn-on responses of up to 150% upon anion binding (Fig. 4.13), whereas **4.2-HB** remained unresponsive in all cases, highlighting the frequently observed superior signal transduction characteristics of XB interactions.[52] In a similar

manner to the sensors reported in previous chapters, the absorbance spectrum of **4.2-XB** remained unperturbed by anion binding, indicating a dynamic quenching mechanism.

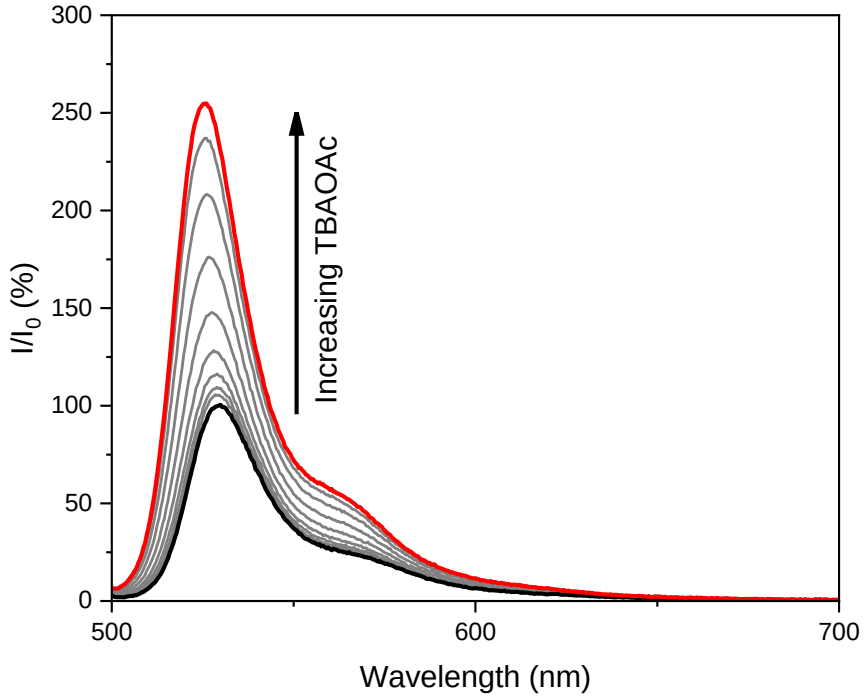


Fig. 4.13. Normalised fluorescence emission response of **4.2-XB** upon addition of increasing concentrations of $^{-}$OAc (up to 2.8 mM). ($CHCl_3$, 1 μM, 298 K)

Having established that **4.2-XB** is responsive to anion binding, attention then turned to ascertaining its ability to bind dicarboxylate (DCB) salts in organic media. The TBA salts of a variety of alkyl dicarboxylates ($^{-}OOC(CH_2)_nCOO^{-}$), with a differing number of carbon atoms in their backbone (n = 6, 8, 10, 12, 14), were added to solutions of **4.2-XB/HB** in $CHCl_3$. Again, **4.2-HB** proved to be unresponsive to dicarboxylate anion binding in this solvent medium (Fig. 4.14b), whereas **4.2-XB** exhibited strong emission enhancement turn-on responses of up to 160% (Fig. 4.14a). The turn-on response exhibited by **4.2-XB** upon addition of both simple monovalent anions and DCBs likely arises due to restriction of rotation about the BODIPY-*meso* bond caused by anion binding, as was observed for the related sensors reported in Chapter Two.

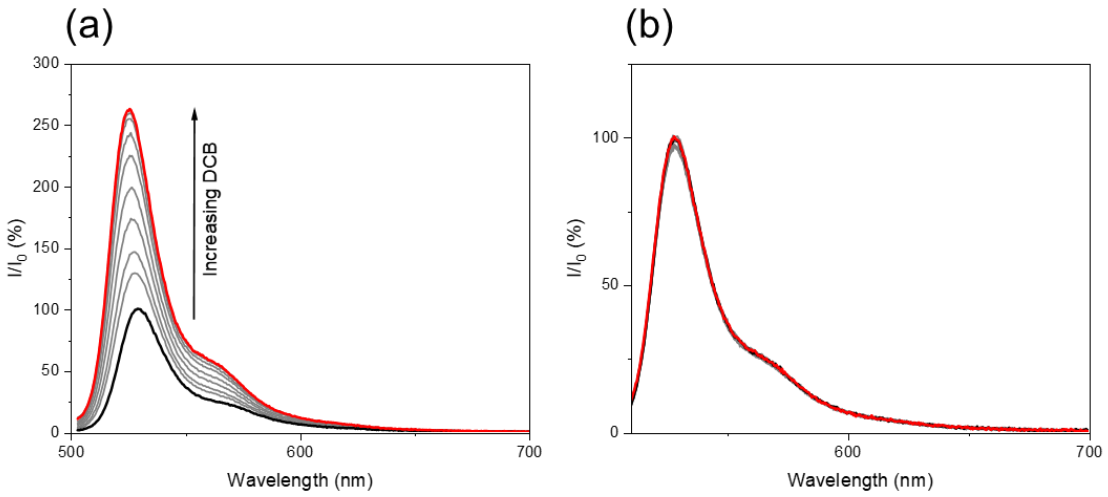


Fig. 4.14. Fluorescence emission response of (a) **4.2-XB** and (b) **4.2-HB** upon addition of increasing ($^{-}OOC(CH_2)_{10}COO^{-}$ (up to 142 μM). ($CHCl_3$, 1 μM, 298 K)

Global fitting of the **4.2-XB** anion titration data around the emission maximum determined the association constants shown in Table 4.1. The simple monovalent anion data were fitted to a 1:2 host-guest stoichiometric binding model with independent anion binding sites, whereas the dicarboxylate data were fitted to a 1:1 host-guest binding model, due to the anticipated interpenetrated binding mode.

Table 4.1. Association constants (M^{-1}) of sensor **4.2-XB** with DCBs ($^{-}OOC(CH_2)_nCOO^{-}$) and simple monovalent anions. ($CHCl_3$, 1 μM, 298 K)

Guest	K_{11}
$^{-}OOC(CH_2)_6COO^{-}$ [a]	6800
$^{-}OOC(CH_2)_8COO^{-}$ [a]	8400
$^{-}OOC(CH_2)_{10}COO^{-}$ [a]	9900
$^{-}OOC(CH_2)_{12}COO^{-}$ [b]	8600
$^{-}OOC(CH_2)_{14}COO^{-}$ [a]	6700
^{-}OAc [c]	240

Cl^{-} [c]	1300
Br^{-} [c]	4700
NO_3^{-} [c]	55

[a] Determined by global fitting of fluorescence isotherms to a 1:1 binding model and errors <5% unless otherwise noted. [b] Error < 7%. [c] Fitted to 1:2 host-guest binding model, K_{11} reported. Error < 10%.

The measured association constants for the dicarboxylates showed that the strength of DCB binding is strongly dependent on the length of the alkyl backbone, with the strongest binding observed when n = 10, which likely arises due to complementarity between the length of the DCB guest and the distance between the XB donor anion binding sites in **4.2-XB**. It is also important to note that all the DCB association constants are at least an order of magnitude greater than the acetate association constant, which is likely due to the additional stabilisation of the host-guest complex afforded by the DCB–P5A threading interaction. A qualitative ^{1}H NMR binding study of **4.2-XB** in $CDCl_3$ was conducted to confirm the DCB binding mode, using the TBA salt of $^{-}OOC(CH_2)_{10}COO^{-}$, as it had exhibited the strongest association in fluorescence binding studies (Fig. 4.15). Upon addition of the DCB salt, P5A phenyl proton resonance H_i underwent a marked upfield shift, which is consistent with threading of the DCB through the P5A cavity.[53] Additional upfield shifts in the methylene protons of the DCB guest were also observed, again consistent with the formation of an interpenetrated assembly.

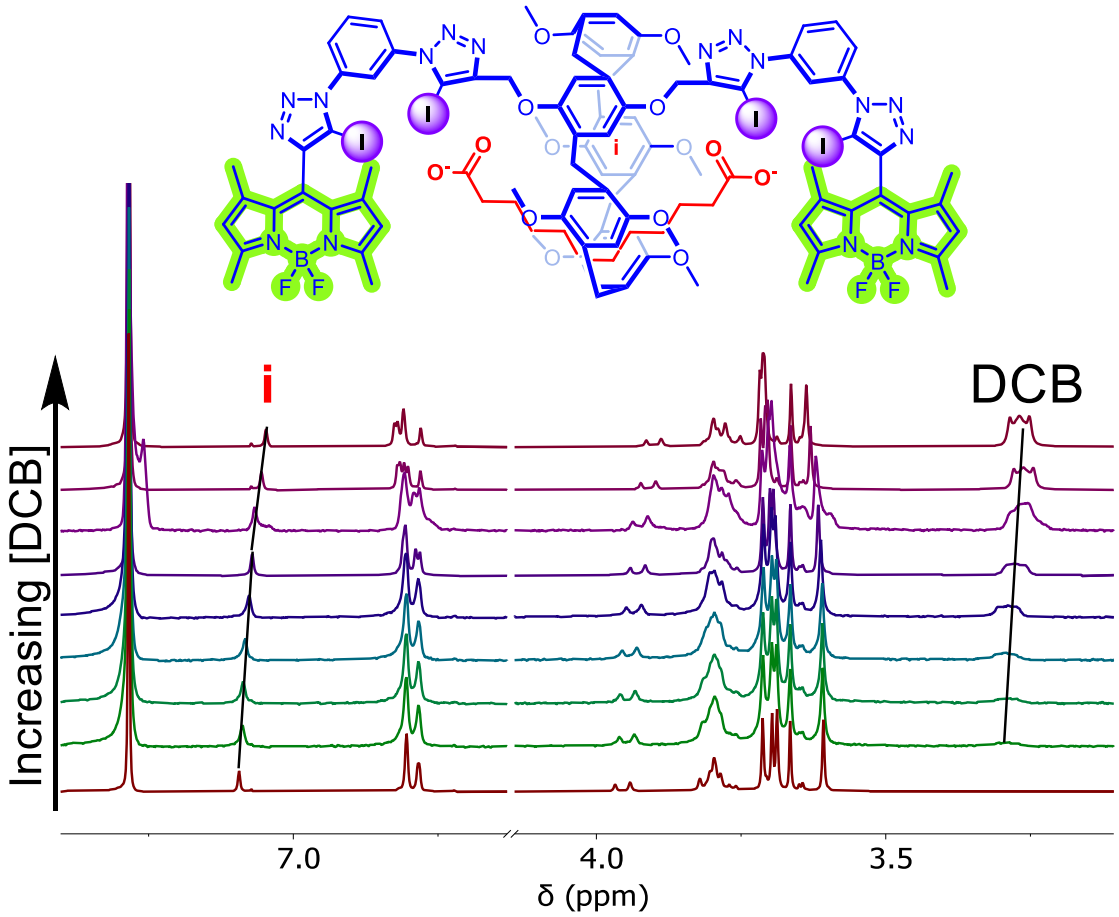


Fig. 4.15. Stacked, truncated ^{1}H NMR spectra of **4.2-XB** upon addition of increasing concentrations of $^{-}OOC(CH_2)_{10}COO^{-}$. ($CDCl_3$, 1 mM, 298 K)

A similar qualitative ^{1}H NMR study was conducted with **4.2-HB**, which again indicated threading of the DCB anion through the P5A cavity and also HB interactions between the terminal carboxylate groups and the triazole HB donors, indicated by a significant downfield shift in resonance H_d (Fig. 4.16). This study therefore confirms that **4.2-HB** binds DCB anions, however the binding event is not transduced into a fluorescence response and thus only **4.2-XB** functions as a DCB sensor in organic media.

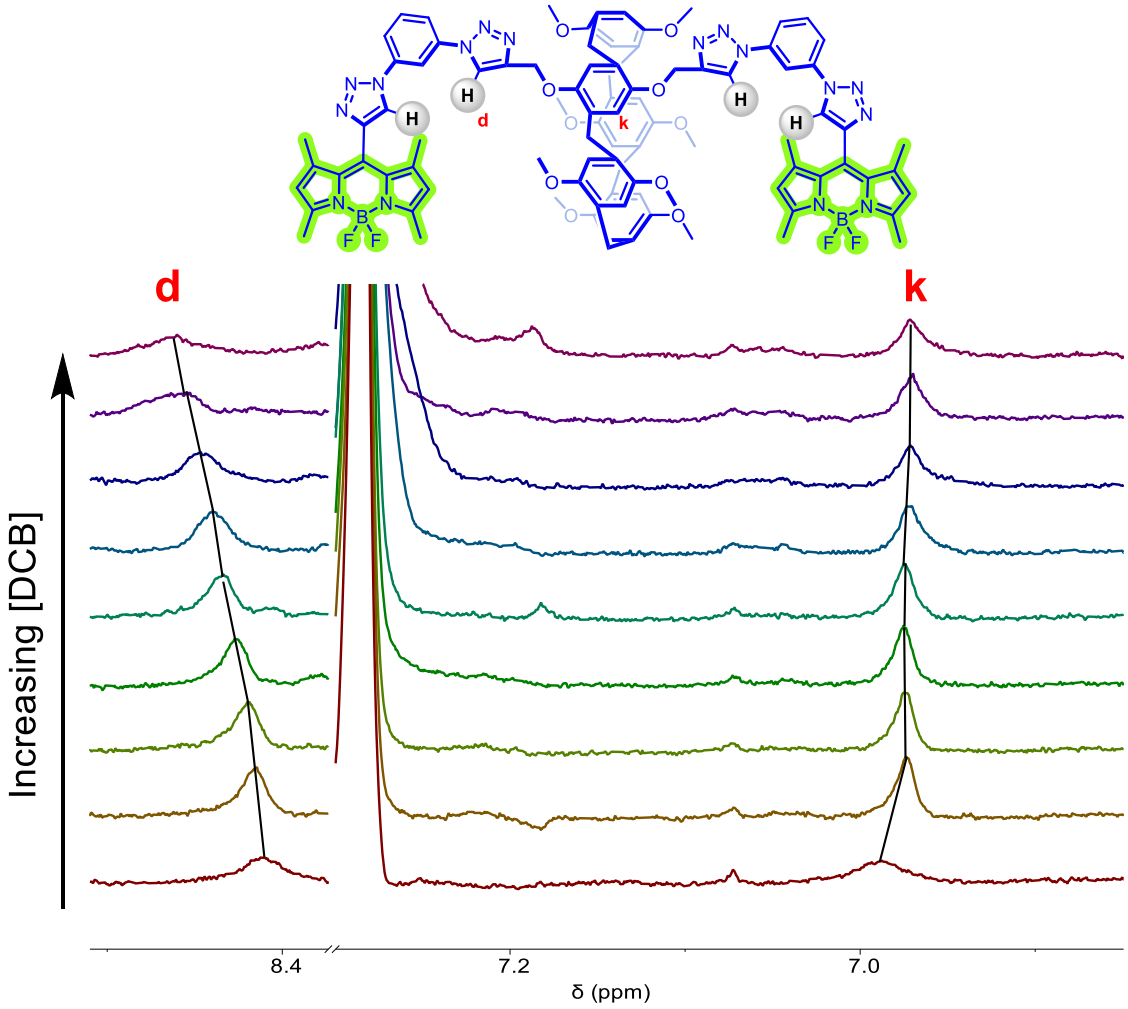


Fig. 4.16. Stacked, truncated ^{1}H NMR spectra of **4.2-HB** upon addition of increasing concentrations of $^{-}OOC(CH_2)_{10}COO^{-}$. ($CDCl_3$, 1 mM, 298 K)

4.2.3 Fluorescence Sensing Studies in Aqueous-Containing Media

Having observed the threading of DCB guests through the P5A macrocycle of **4.2-XB/HB** to form interpenetrated assemblies in organic media and noting the hydrophobicity of the P5A cavity,[20] it was anticipated that the strength of guest binding would be significantly increased in the presence of water, by exploitation of hydrophobic effects. Therefore, further DCB sensing studies were conducted in ACN : H_2O 1:1 (*v*/*v*) (buffered to pH = 8.0 with 50 mM HEPES), using the TBA salt of $^{-}OOC(CH_2)_{10}COO^{-}$, as it had exhibited the strongest association with the XB sensor in organic media (Fig. 4.17).

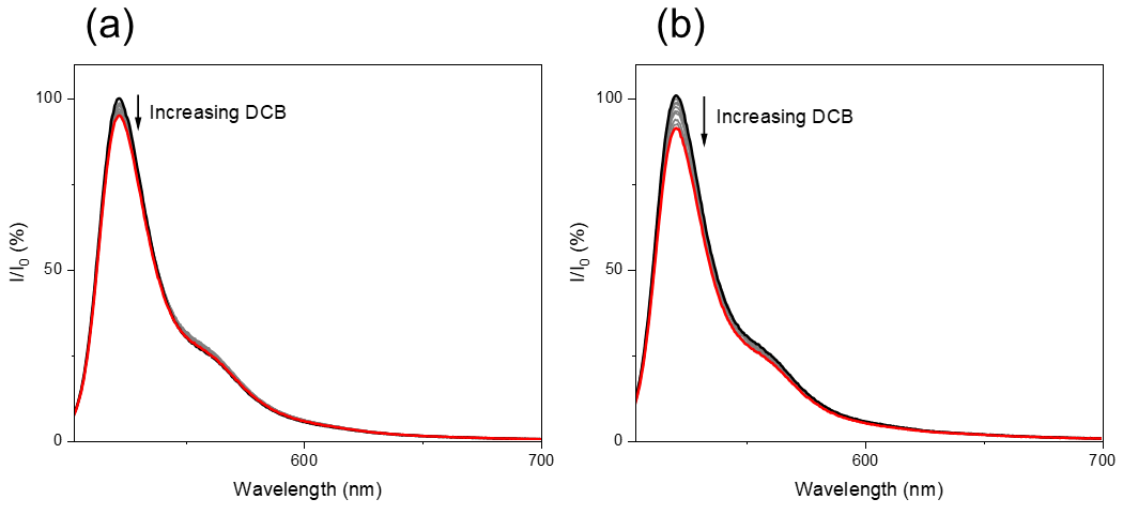


Fig. 4.17. Fluorescence emission response of (a) **4.2-XB** and (b) **4.2-HB** upon addition of increasing concentrations of $^{-}OOC(CH_2)_{10}COO^{-}$ (up to 142 μM). (ACN : H_2O 1:1 (*v/v*) (buffered to pH = 8.0 with 50 mM HEPES), 1 μM, 298 K)

Notably in this aqueous-containing solvent mixture, **4.2-XB** exhibited a *quenching* fluorescence emission response upon addition of the DCB salt, highlighting the influence of solvent on the behaviour of fluorescent sensors. Additionally, in contrast to the behaviour observed in organic solvent, **4.2-HB** proved to be responsive in this medium, also displaying a quenching response of *c.* 10%. Fitting of the changes in emission to a 1:1 host-guest binding model determined impressively high DCB association constants of 104,000 M^{-1} and 28,500 M^{-1} for **4.2-XB** and **4.2-HB** respectively (Table 4.2), with the 4-fold higher association constant value for the XB host reflecting the hydrophobicity of the XB donor anion binding sites and their consequent resistance to changes in solvation.[54] Additionally, the DCB association constant value for the XB sensor was enhanced over 10-fold relative to the same equilibrium in $CHCl_3$, highlighting how in certain cases, use of more competitive solvents can boost the affinity of receptors by exploiting hydrophobic effects.

As mentioned in the introduction to this chapter, sulfur mustard is also a pollutant and CWA of grave concern which represents a similar sensing target to dicarboxylates, due to its hydrophobic core and electron-rich terminal groups. It was therefore anticipated that sulfur mustard would be bound and sensed by **4.2-XB/HB**. As sulfur mustard is a restricted chemical, titration experiments were conducted with CEES, a commonly used simulant. Upon addition of CEES to a ACN : H_2O 1:1 (*v/v*) solution of the sensors, a modest quenching response of *c.* 10% was observed and impressive association constants of 528,000 M^{-1} and 145,000 M^{-1} were obtained for **4.2-XB** and **4.2-HB** respectively (Fig 4.18 & Table 4.2). The increased affinity of the sensors for CEES over the TBA salt of dodecanedioic acid was attributed to the increased hydrophobicity of the neutral CEES molecule, relative to the dianionic DCB. The importance of this hydrophobic contribution was highlighted by an analogous titration experiment with **4.2-XB** and CEES, conducted in $CHCl_3$, which revealed an association constant at least an order of magnitude lower.[†] The continued importance of the interaction between the guest and the (iodo-)triazole binding site was highlighted by the 4-fold increased CEES association constant for the XB sensor over its HB analogue.

[†] The relatively small changes in emission intensity (<3%) precluded the accurate determination of an association constant, but it is at least 10-fold lower than in the aqueous-containing solvent.

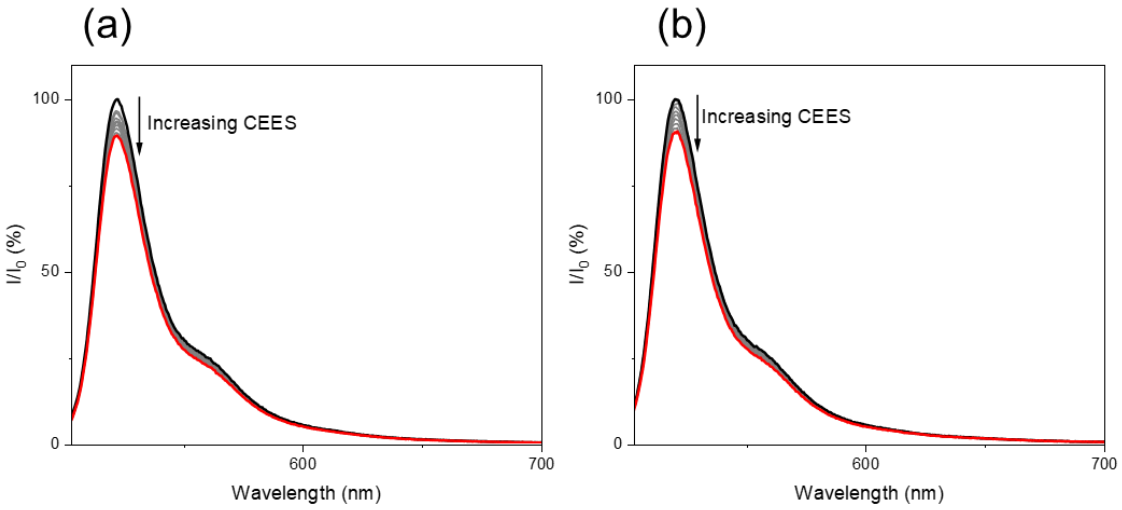


Fig. 4.18. Fluorescence emission response of (a) **4.2-XB** and (b) **4.2-HB** upon addition of increasing concentrations of CEES (up to 57 μM). (ACN : H_2O 1:1 (*v/v*), 1 μM, 298 K)

Table 4.2. Association constants (M^{-1})[a] of sensors **4.2-XB** and **4.2-HB** in aqueous-containing media. (1 μM, 298 K)

Guest	**4.2-XB**	**4.2-HB**
$^{-}OOC(CH_2)_{10}COO^{-}$ [b]	104,000	28,500
CEES[c]	528,000	145,000

[a] Determined by global fitting of fluorescence isotherms to a 1:1 binding model [b] Solvent: ACN : H_2O 1:1 (*v/v*) (buffered to pH = 8.0 with 50 mM HEPES), errors <15% [c] Solvent: ACN : H_2O 1:1 (*v/v*), errors <7%.

Having established that the sensors are capable of detecting CEES in aqueous-containing media, attention then turned to ascertaining the selectivity of the sensing response over other CWA simulants and non-toxic hydrolysis products of sulfur mustard; and also quantifying the limit of detection (LoD) of these sensors. In order to probe the selectivity of the sensors, tributyl phosphate, a simulant of organophosphorus nerve agent CWAs,[55-56] and thiodiglycol, the non-toxic hydrolysis product of sulfur mustard, were added to solutions of the sensors in ACN : H_2O 1:1 (*v/v*). Pleasingly, no significant emission

response to these compounds was exhibited by either sensor, highlighting the selectivity of these systems for sulfur mustard simulants and therefore likely the CWA itself (Fig. 4.19).

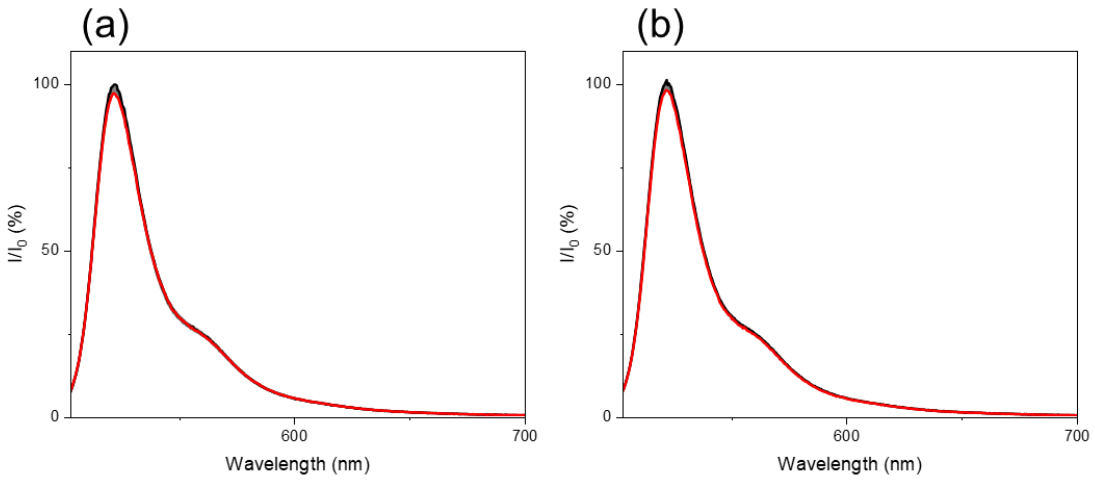


Fig. 4.19. Normalised fluorescence emission spectra of **4.2-XB** upon addition of (a) 57 μM tributyl phosphate and (b) 57 μM thiodiglycol, showing the lack of response in each case. (ACN : H_2O 1:1 (*v/v*), 1 μM, 298 K)

The LoD of CEES, which refers to the lowest concentration of CEES that can be detected with statistical confidence, was determined for both sensors using Equation 4.1, in which σ is the standard deviation in the emission intensity at the emission maximum and S is the initial slope of the emission response curve upon addition of CEES.[57]

$$LoD = {}^{3\sigma}/_{S} \quad \text{(Eqn. 4.1)}$$

The standard deviation σ was determined by repeated recordings of the emission spectra of each of the sensors prior to the addition of an analyte, and S was determined graphically (Fig. 4.20). The LoD for CEES was determined to be 0.13 μM and 0.40 μM for **4.2-XB** and **4.2-HB** respectively. These very low LoDs highlight the high sensitivity of the fluorescence technique, despite the modest emission response exhibited by each of the receptors. This

impressive sensing performance, taken together with the selectivity over organophosphorus CWA simulants and the non-toxic hydrolysis product of sulfur mustard, demonstrates the potency of combining the recognition properties of the hydrophobic P5A macrocycle and XB donors with the sensitivity of the fluorescence sensing technique.

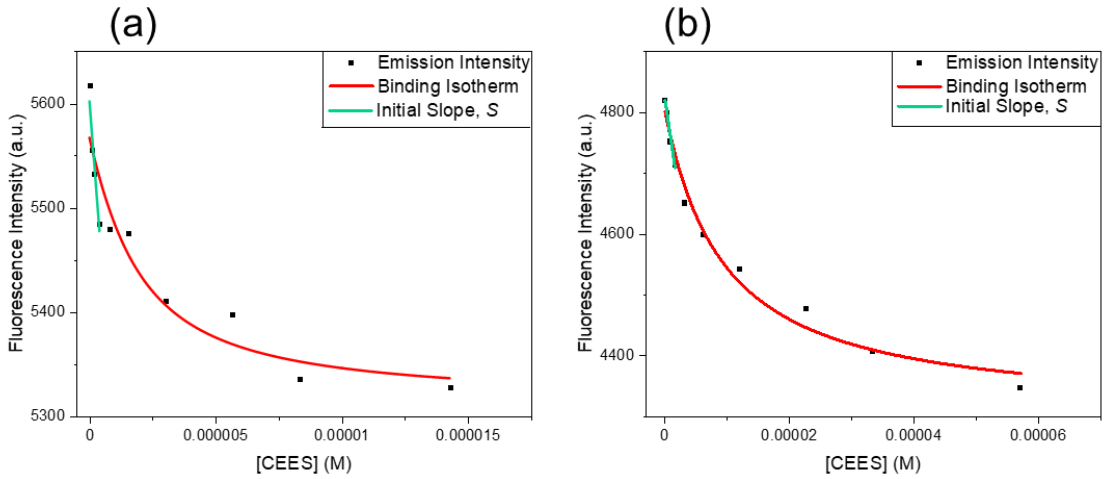


Fig. 4.20. Fluorescence response of (a) **4.2-XB** and (b) **4.2-HB** at the emission maximum upon addition of increasing concentrations of CEES, the corresponding binding isotherm and the linear fit used for the determination of the LoD. (ACN : H_2O 1:1 (*v/v*), 1 μM, 298 K)

4.3 Sensing of Ion-Pairs Using a Halogen Bonding BODIPY-Appended Aza-Crown Ether[‡]

Having demonstrated the general applicability of the XB BODIPY fragment developed in Chapter Two to sensing charged and neutral species *via* the formation of interpenetrated host-guest assemblies with an XB BODIPY-functionalised P5A, attention turned to deploying this motif for the sensing of ion-pairs. Therefore, the diaza-crown ether-based structure (**4.7**) shown in Fig. 4.10 and its *tetra*-XB analogue were targeted.

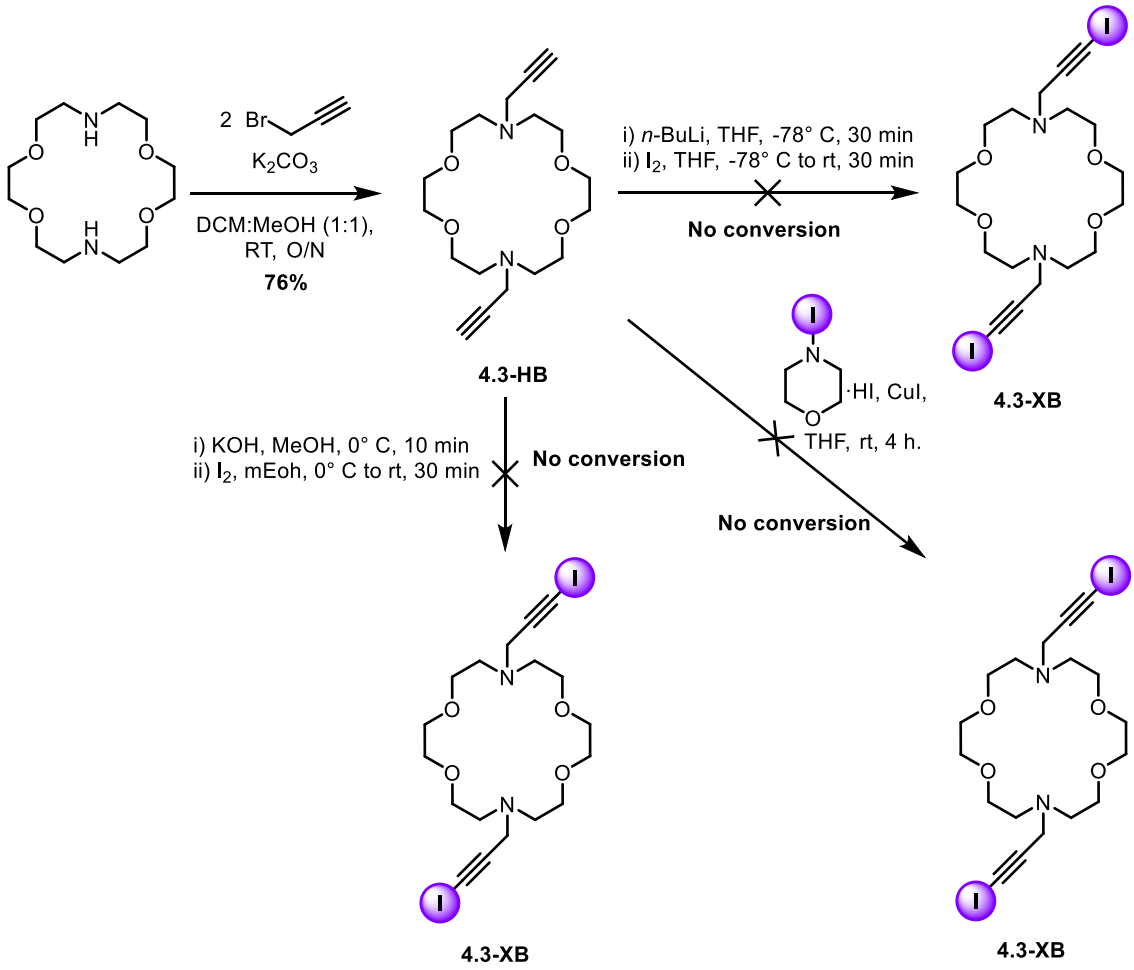
4.3.1 Synthesis and Characterisation

The target ion-pair sensors feature a diaza-18-crown-6 cation binding macrocycle, decorated with two bidentate 1,3-bis-(iodo-)triazole benzene anion binding sites, each respectively appended with a BODIPY fluorescent reporter group. It was anticipated that the combination of this motif with the diaza-crown ether cation binding unit would allow for positively cooperative ion-pair binding, due to the close proximity of the concomitantly bound components of the ion-pair and consequent electrostatic attraction between them.

Initially, the *tetra*-XB donor sensor was targeted, which required the synthesis of the corresponding bis-iodoalkyne diaza-crown ether **4.3-XB** (Scheme 4.4). The bis-protoalkyne diaza-crown ether **4.3-HB** was synthesised from diaza-18-crown-6 by reaction with two equivalents of propargyl bromide in the presence of K_2CO_3. Purification by alumina column chromatography gave the intermediate alkyne **4.3-HB** as a colourless wax in 76% yield. Various attempts were then made to convert this protoalkyne to its iodoalkyne analogue **4.3-XB**, including by treatment with KOH and I_2 in MeOH, treatment with *N*-iodomorpholine hydroiodide in the presence of a CuI catalyst, and also by trapping

[‡] This work was carried out in collaboration with Jamie T. Wilmore.

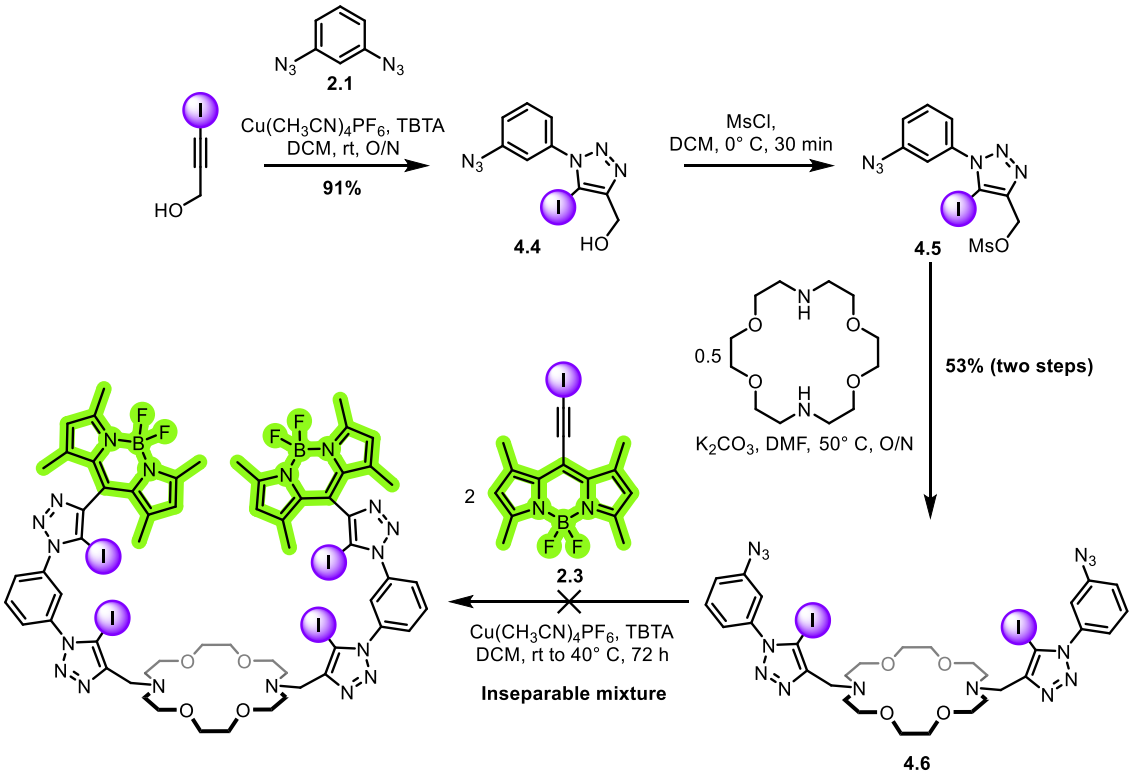
the lithium acetylide with I_2 in anhydrous THF at -78° C. However, all of these methods failed to appreciably convert the protoalkyne moiety to the iodoalkyne.



Scheme 4.4. Synthesis of alkyne **4.3-HB** and attempts to synthesise **4.3-XB**.

Therefore, an alternative synthetic route to the *tetra*-XB target was sought, in which the iodotriazole moiety was generated first, before being appended to the diaza-crown ether macrocycle (Scheme 4.5). Initially, a CuAAC reaction between **2.1** and 3-iodo-2-propyn-1-ol[58] gave XB synthon **4.4** in 91% yield following chromatographic purification. Synthon **4.4** was converted to the mesylate **4.5**, *via* treatment with methanesulfonyl chloride at 0° C, and two equivalents of the *in situ* generated reactive mesylate **4.5** was immediately heated with diaza-18-crown-6 in the presence of K_2CO_3 base in DMF, giving

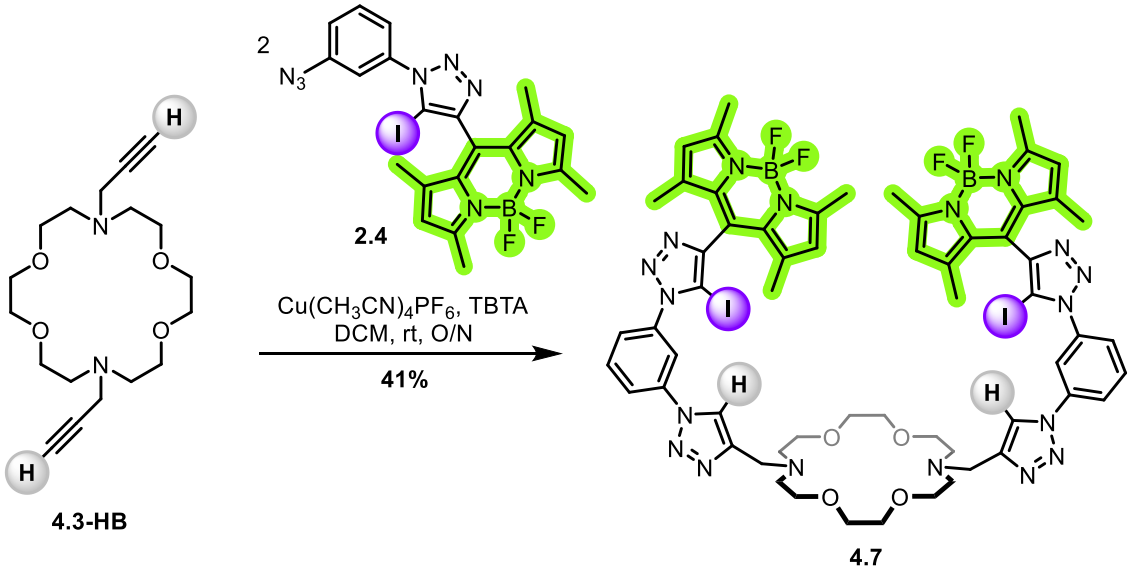
compound **4.6** in 53% yield over two steps, following purification by column chromatography. A CuAAC reaction between **4.6** and two equivalents of BODIPY iodoalkyne **2.3** was subsequently attempted, and formation of the *tetra*-XB product was observed *via* mass spectrometry, although the 'click' reaction proceeded very slowly. However, using silica and alumina column chromatography, it proved impossible to separate the desired product from the reaction mixture, which also contained unreacted **4.6**, the 'mono-click' intermediate, and various prototriazole containing products.



Scheme 4.5. Synthesis of aza-crown ether-containing synthon **4.6** and attempted CuAAC reaction to form the *tetra*-XB product.

Due to the difficulty in preparing the *tetra*-XB sensor, synthesis of the mixed XB/HB analogue **4.7** was attempted, which still retains the enhanced signal transduction offered by XB interactions between the anion binding site and the BODIPY fluorescent reporter group. Bis-protoalkyne diaza-crown ether **4.3-HB** was reacted with two equivalents of the

azide fragment **2.4** under CuAAC conditions to afford the target XB BODIPY diaza-crown ether heteroditopic receptor **4.7** in an isolated 41% yield following purification *via* alumina column chromatography (Scheme 4.6). Receptor **4.7** was characterised by ^{1}H and ^{13}C NMR, UV-vis spectroscopy and HRMS (Figs. 4.21 & 4.22), all of which were typical of BODIPY-containing compounds.



Scheme 4.6. Synthesis of ion-pair sensor **4.7**.

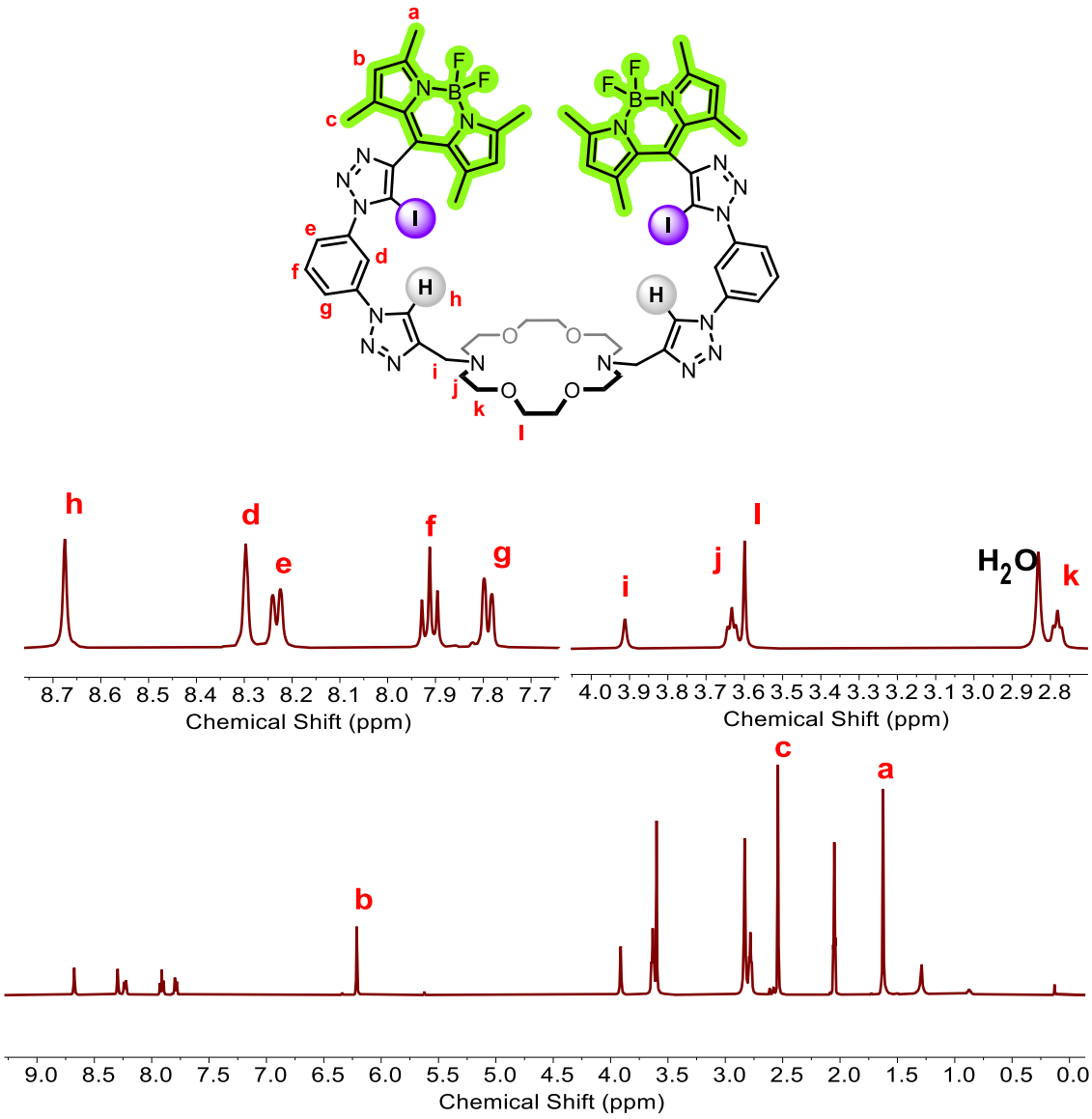


Fig. 4.21. ^{1}H NMR spectrum of **4.7**. (Acetone-d_6, 298 K)

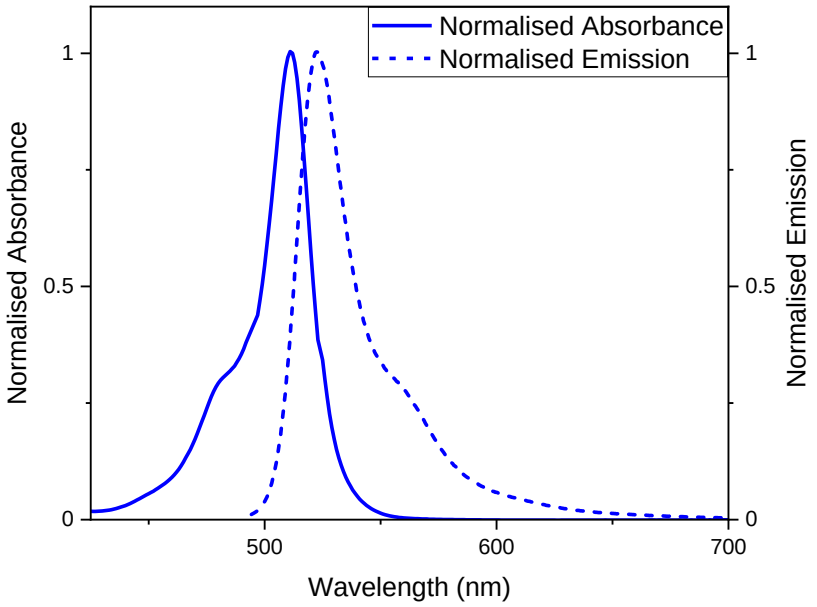


Fig. 4.22. Normalised absorption and emission spectra of **4.7**. (ACN, 10 μM, 485 nm excitation wavelength)

4.3.2 Alkali Metal and Ammonium Halide Ion-Pair Sensing Studies

Initially, the fluorescence sensing behaviour of **4.7** upon sodium and potassium cation binding was assessed through fluorescence titration experiments. In these experiments, aliquots of sodium and potassium cations as their non-coordinating $BAr^{F}_{4}{}^{-}$ salts were added to an ACN : MeOH 1:1 (*v/v*) solution of **4.7** and the emission spectrum monitored. A modest turn-on increase in BODIPY emission intensity of 8% was observed upon addition of $KBAr^{F}_{4}$ (Fig. 4.23). As expected, the association between the diaza-crown ether and the K^{+} cation was very strong, and an association constant of 31,300 M^{-1} was calculated by global fitting of the titration data to a 1:1 host-guest stoichiometric binding model.

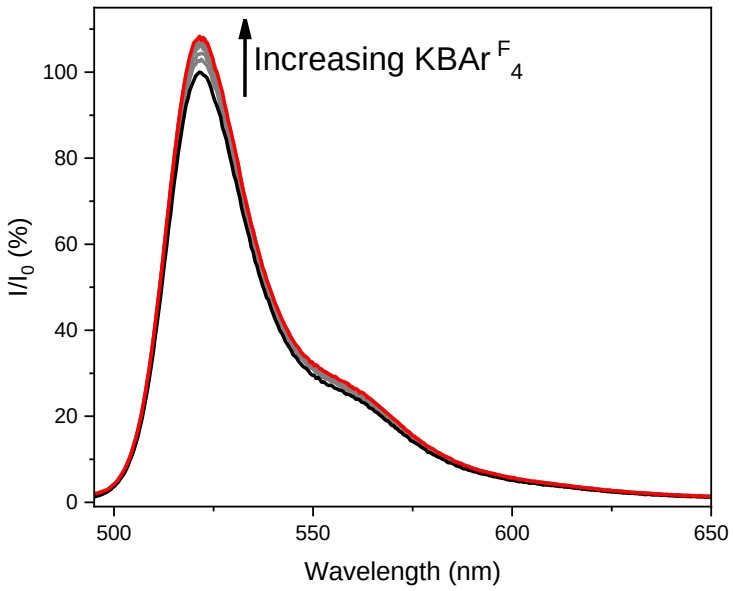


Fig. 4.23. Normalised fluorescence emission response of **4.7** upon addition of increasing concentrations of K^+ (up to 2.86 mM). (ACN : MeOH 1:1 (*v/v*), 1 μM, 298 K)

In contrast, addition of $NaBAr^{F}{}_4$ led to negligible (<3%) changes in the emission spectrum of **4.7** (Fig. 4.24), which was initially surprising, given the sensing behaviour of **4.7** in response to potassium cation binding and the known ability of the diaza-18-crown-6 macrocycle to bind sodium cations. Importantly however, this contrasting emission response behaviour means that sensor **4.7** exhibits the ability to discriminate between Na^+ and K^+ cations.

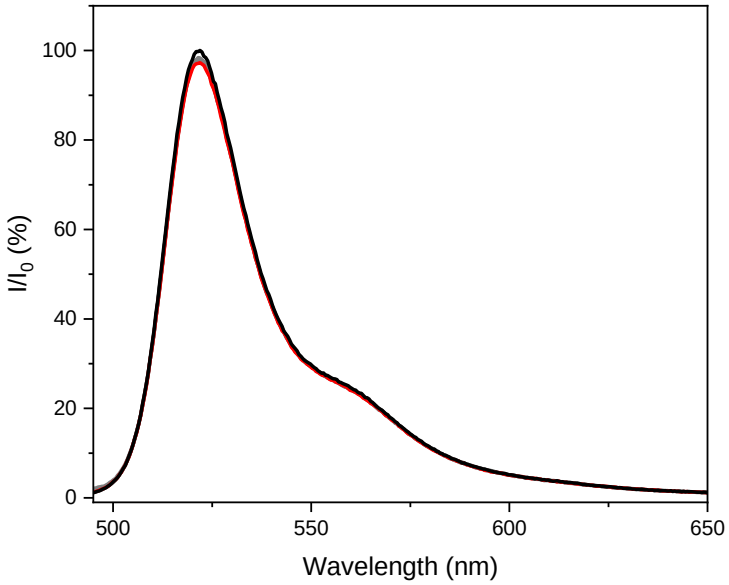


Fig. 4.24. Normalised fluorescence emission spectra of **4.7** upon addition of increasing concentrations of Na^+ (up to 2.86 mM), showing the lack of response. (ACN : MeOH 1:1 (*v*/*v*), 1 µM, 298 K)

In order to investigate the origin of the surprisingly contrasting fluorescence emission responses of **4.7** to K^+ and Na^+ binding, ^{1}H NMR titrations were conducted, again using the alkali metal $BAr^F{}_4^-$ salts. Due to the much higher concentrations required for ^{1}H NMR experiments, these titrations were conducted in acetone-d_6 for solubility reasons. Addition of both cations caused significant downfield shifts in the diaza-crown ether methylene proton resonances (such as H_j), which plateaued after the addition of one equivalent of $MBAr^F{}_4$ in both cases, consistent with the formation of a strong 1:1 host-guest stoichiometric complex (Fig. 4.25).

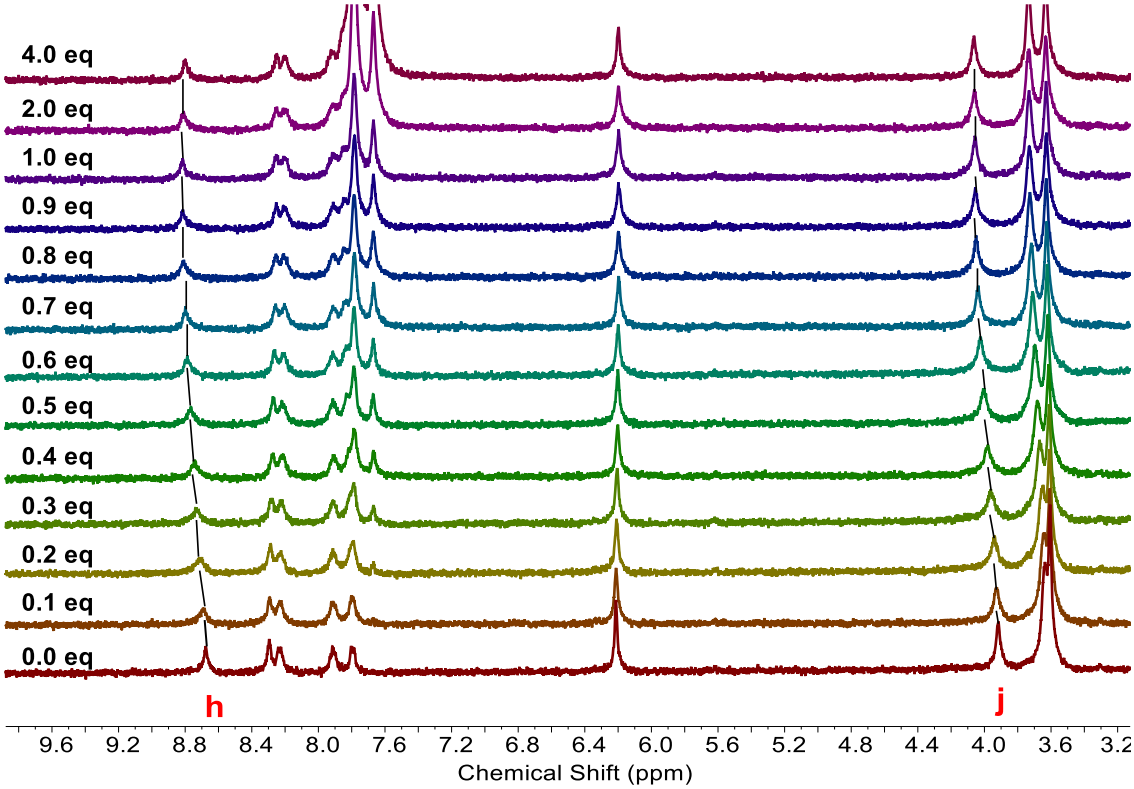


Fig. 4.25. Stacked ^{1}H NMR spectra of **4.7** with increasing concentrations of $KBAr^{F}_{4}$. (1 mM, acetone-d_6, 298 K)

Interestingly however, notably different changes to the triazole proton H_h chemical shift were observed upon the addition of sodium and potassium cations (Fig. 4.26). Upon potassium cation binding, the triazole H_h resonance shifted significantly downfield, indicating de-shielding, which can be attributed to the coordination of both triazole *N*-atoms to the larger potassium cation, in a bis-lariat fashion (Fig. 4.27).[59] In contrast, a far smaller shift was observed when sodium cations were added, suggesting that the triazole *N*-atom does not coordinate to this smaller cation.

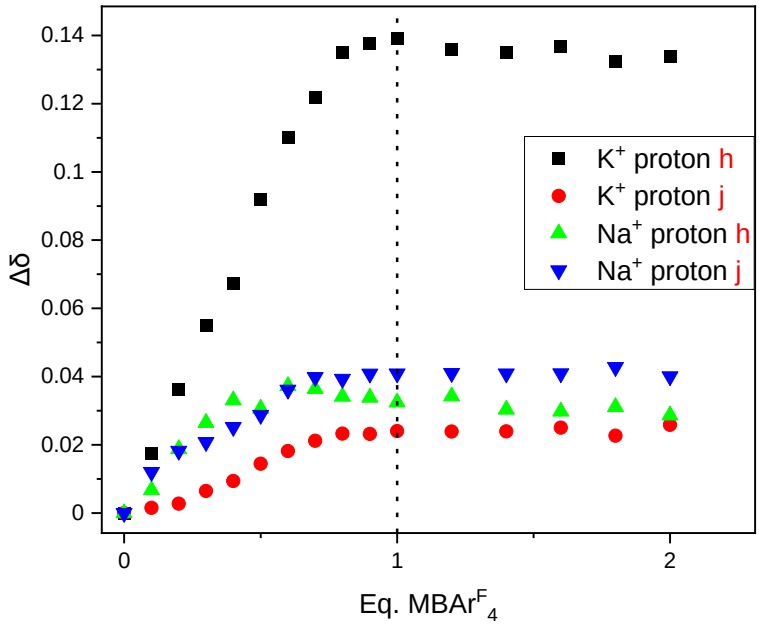


Fig. 4.26. Monitoring the shift of protons H_h and H_j in **4.7** as a function of alkali metal cation concentration.[§] (Acetone-d_6, 1 mM, 298 K)

This in turn offers a possible explanation for the differing fluorescence changes observed: the coordination of the triazole motifs to the bound potassium cation reduces the conformational flexibility of the receptor, increasing its rigidity and therefore reducing the rate of non-radiative decay processes, leading to an increase in fluorescence quantum yield and hence emission intensity, in a similar manner to the sensors reported in Chapter Two. In contrast, no such rigidification is induced by sodium cation binding, and hence the fluorescence response is significantly smaller. Thus, the selective potassium over sodium cation sensing capability of **4.7** is not primarily due to an appreciably increased affinity for potassium cations, but rather can be attributed to a different metal cation binding mode producing a relatively enhanced emission response, in a similar

[§] The change in chemical shifts appears to plateau slightly before the addition of one equivalent of cation, which may be due to inaccuracies in sample preparation.

manner to the chloride-selective [2]rotaxane sensor reported by Tay *et al.*,[60] shown in Chapter One.

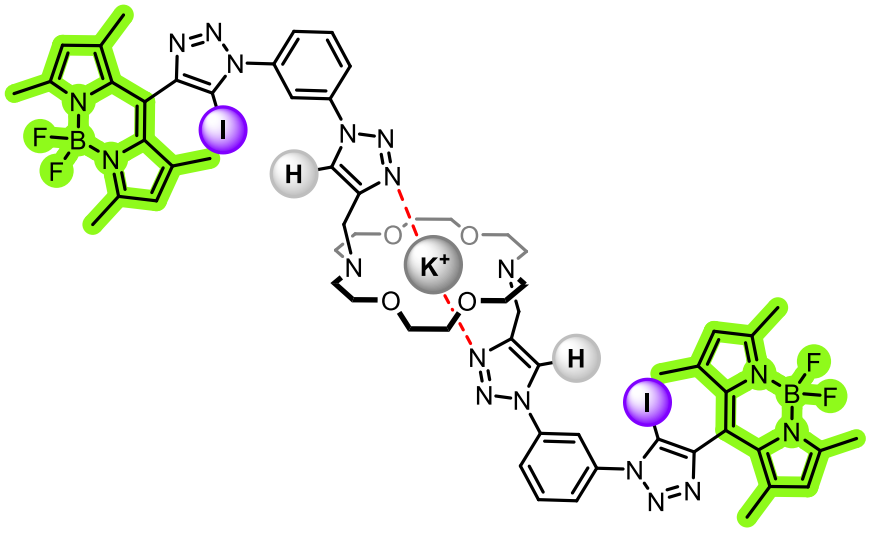


Fig. 4.27. Cartoon displaying a possible K^+ binding conformation of sensor **4.7**, showing the coordination of the triazole groups to the bound K^+ cation.

Following the cation sensing studies, attention then turned to probing the inorganic ion-pair sensing ability of **4.7**. The use of the competitive ACN : MeOH 1:1 (*v*/*v*) solvent mixture and the low host concentrations required for fluorescence studies allowed a direct ion-pair salt titration method to be used,[61] as the ion-pair salts were sufficiently soluble in this mixed organic solvent medium. Pleasingly, addition of KCl, KBr, RbCl, CsCl, NH_4Cl and NH_4Br to a solution of **4.7** in ACN : MeOH 1:1 (*v*/*v*) all caused increases in BODIPY emission intensity of up to 19%, attributed to rigidification of the heteroditopic host structure and the restriction of rotation about the BODIPY-*meso* bond upon ion-pair binding, again in a similar manner to the sensors reported in Chapter Two (Fig. 4.28).

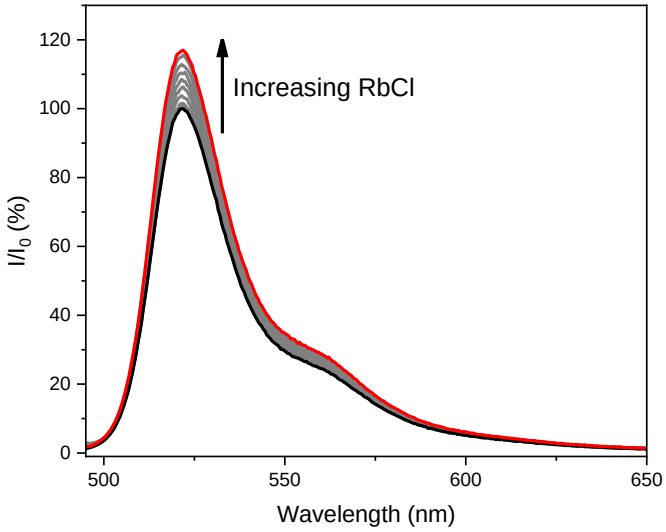


Fig. 4.28. Normalised fluorescence emission response of **4.7** upon addition of increasing concentrations of RbCl (up to 7.14 mM). (ACN : MeOH 1:1 (*v*/*v*), 1 μM, 298 K)

The titration data were fitted to a 1:1 host-guest stoichiometric binding model, to produce the apparent anion association constant (K_{App}) values shown in Table 4.3. This method of calculating apparent anion association constants assumes that cation binding is quantitative upon the first addition of an aliquot of the ion-pair, and that the anion then binds to the cationic [**4.7**-M]$^+$ complex over the course of the titration. This assumption is justified by the very large association constant value measured for K^+, the higher titrant concentration used for the ion-pair titrations, and the likely positive cooperativity between proximal cation and anion binding.

Table 4.3. Apparent anion association constants (K_{App}) (M^{-1})[a] of heteroditopic receptor **4.7** with various ion-pairs. (1 μM, 298 K)

Guest	K_{App}
KCl	3200
RbCl	970
CsCl	780
NH_4Cl	1020
KBr	2890
NH_4Br	550
TBACl	130
TBABr	110

[a] Determined in ACN : MeOH 1:1 (*v/v*) by global fitting of fluorescence isotherms to a 1:1 binding model; errors <15%.

Notably, the apparent halide anion affinities were significantly higher in the presence of a coordinating alkali metal or ammonium cation – with the Cl^- binding affinity increased by an impressive factor of 25 upon changing the counter-cation to K^+ from TBA^+. This was attributed to both an electrostatic mechanism of cooperativity and also the activation of the hydrogen-bonding triazole moiety for anion binding *via* coordination to the co-bound cation, as shown in the cartoon in Fig. 4.27. A similar magnitude of binding enhancement has been observed previously in other ion-pair receptors with electrostatic and through-bond polarisation mechanisms of cooperativity.[62] The trend of decreasing $K_{App}(Cl^-)$ upon descending the group 1 metal cations reflects their increasing radius, and thus decreasing charge density and consequently weaker electrostatic attraction to the co-bound anion. The affinity of the diaza-18-crown-6 cation binding motif for the group 1

metal/ammonium cations is related to the size complementarity between the host and guest and is greatest for potassium cations.[63] Therefore, the strength of cation association decreases as their radii increase down the group,[63-64] which is also reflected in the values of K_{App} determined for their chloride salts.

The increased apparent anion association constant for KCl over KBr can be rationalised by the increased charge density of the chloride anion, which enhances both the strength of interactions formed between the bound anion and the XB/HB donors and also the electrostatic attraction to the co-bound K^+ cation. A similar trend was also observed between NH_4Cl and NH_4Br, with the difference in apparent halide association constants particularly pronounced in this case due to possible NH_4^+–X^- HB interactions which are significantly stronger when formed to the charge dense chloride anion.

These results therefore confirmed the ability of **4.7** to sense cations, anions and ion-pair species in a competitive solvent medium, with the heteroditopic receptor displaying significant positive cooperativity in anion binding, improving its ion-pair sensing capability.

4.3.3 Hydrogen Bonding-Assisted Sensing of Biological Ammonium Compounds

Having established the ability of **4.7** to sense ammonium halide ion-pairs, attention turned to probing its ability to also bind organic ammonium species, such as the hydrochloride salts of the neurologically-relevant molecule dopamine and related phenethylamine compounds (Fig. 4.29). Fluorescence ion-pair titrations were conducted in the same ACN : MeOH 1:1 (*v/v*) solvent medium, with significant increases in BODIPY emission intensity of up to 18% being observed upon addition of the organic ammonium salts (Fig. 4.30). The titration data were fitted to a 1:1 host-guest stoichiometric binding model,

in an analogous manner to the inorganic ion-pair titration data, to produce the apparent chloride anion association constants shown in Table 4.4.

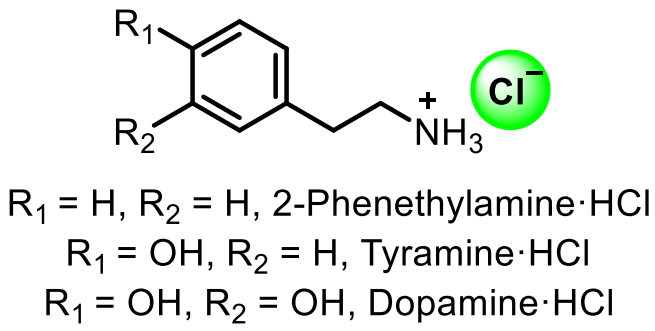


Fig. 4.29. The structures of the phenethylamine salt derivatives used in organic ammonium halide ion-pair binding studies.

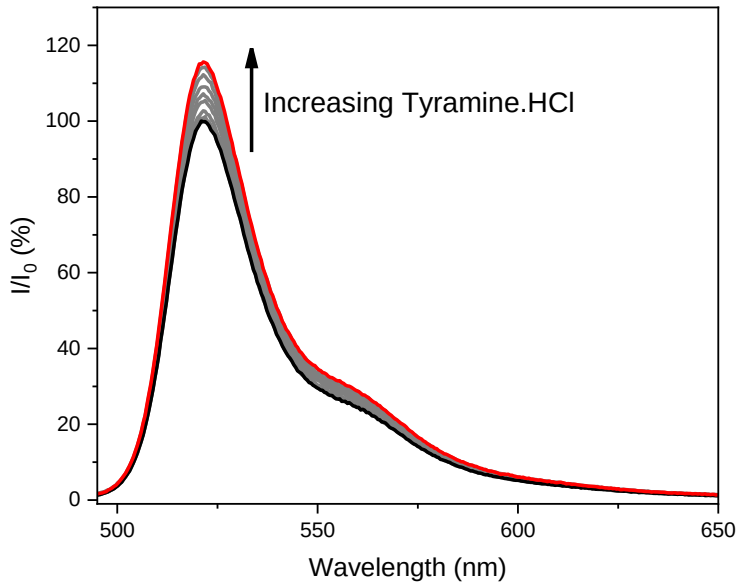


Fig. 4.30. Normalised fluorescence emission response of **4.7** upon addition of increasing concentrations of tyramine.HCl (up to 1.43 mM). (ACN : MeOH 1:1 (*v/v*), 1 μM, 298 K)

Table 4.4. Apparent anion association constants (K_{App}) (M^{-1})[a] of sensor **4.7** with various organic ammonium halide ion-pairs. (1 μM, 298 K)

Guest	K_{App}
Dopamine.HCl	1530
Tyramine.HCl	830
2-Phenethylamine.HCl	810

[a] Determined in ACN : MeOH 1:1 (*v/v*) by global fitting of fluorescence isotherms to a 1:1 binding model and errors <16%.

Pleasingly, sensor **4.7** demonstrated stronger binding and selectivity for the neurologically-relevant dopamine.HCl ion-pair over the other related phenethylamine-derivative ammonium hydrochloride salts. In 2006, Smith and co-workers reported that simple catechol derivatives are capable of binding chloride anions through chelating phenolic hydrogen bonding interactions in competitive, aqueous-containing solvent mixtures.[65] Therefore, the significantly increased affinity of the [**4.7**-dopamine.H]$^+$ complex for chloride could be attributed to the formation of hydrogen bonds between the catechol hydroxyl groups of the bound [dopamine.H]$^+$ cation and the chloride anion, which act as an additional stabilising interaction to the XB/HB interactions between chloride and **4.7**, as shown in the cartoon in Fig. 4.31.

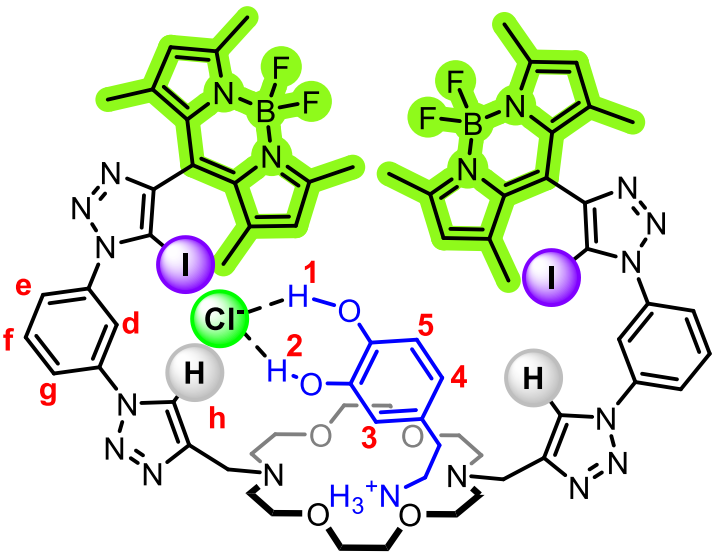


Fig. 4.31. Cartoon displaying a possible dopamine.HCl binding conformation of sensor **4.7**, showing the formation of hydrogen bonds between the catechol -OH groups of dopamine and the co-bound Cl^- anion.

In order to provide additional evidence for these putative hydrogen bonding interactions between the catechol hydroxyl groups of the bound $[dopamine.H]^+$ cation and the co-bound chloride anion, a ^1H NMR titration study in acetone-d_6 was undertaken. First, receptor **4.7** was complexed with one equivalent of dopamine.HPF_6, followed by addition of aliquots of TBACl. Upon the addition of dopamine.HPF_6, significant downfield shifts were observed in the aliphatic diaza-crown ether proton resonances, such as H_j, confirming binding of the alkyl ammonium cation within the crown ether cavity. Importantly, upon subsequent TBACl addition, marked downfield shifts in the signals arising from triazole H_h in **4.7** *and* the dopamine catechol hydroxyl protons H_1 and H_2 were observed, strongly supporting the proposed binding mode (Fig. 4.32). This binding mode creates a chloride binding pocket which is highly reminiscent of biotic anion host systems, where multiple different HB donors are highly pre-organised to bind a charged guest in a three-dimensional cavity.[66] Such additional stabilising catechol-based chelating HB donor interactions are absent in the tyramine.HCl and 2-phenethylamine.HCl ion-pairs, which

rationalises their diminished apparent anion association constant values and thus the impressive dopamine selectivity exhibited by **4.7**.

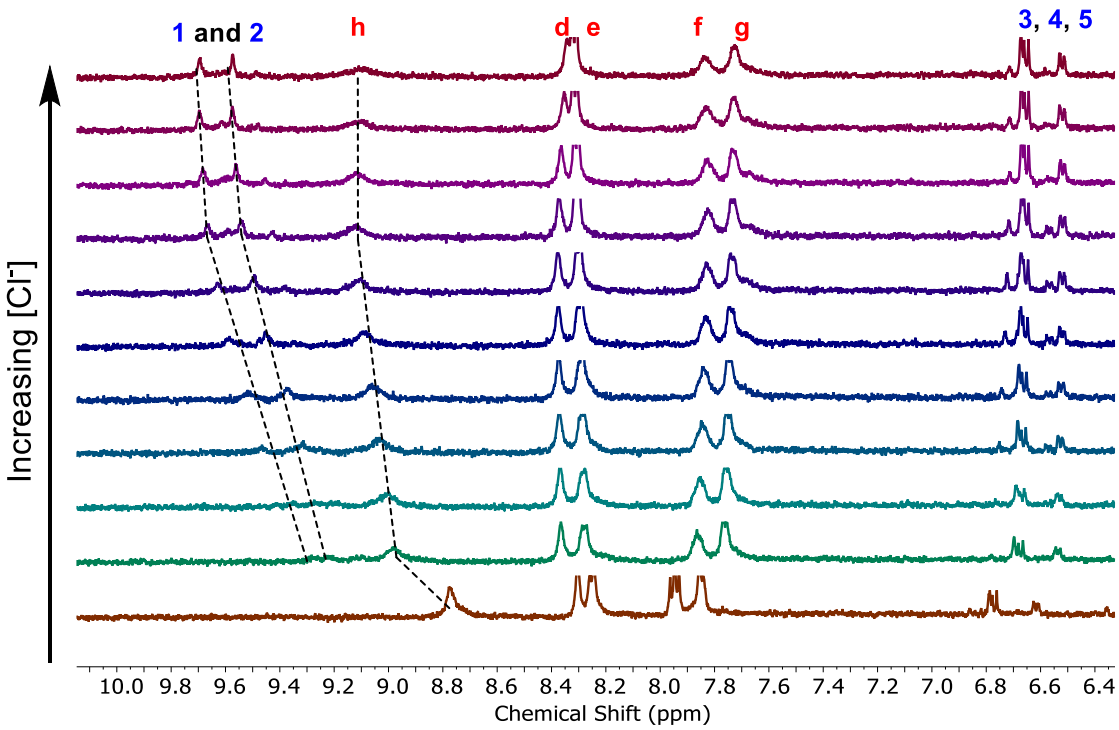


Fig. 4.32. Stacked ^{1}H NMR spectra of **4.7**-[dopamine.H]$^{+}$ complex showing the aromatic region upon increasing concentrations of Cl^{-}. (Acetone-d_6, 1 mM, 298 K)

4.4 Chapter Conclusions and Future Work

The initial work described in this chapter aimed to sense species of biological and environmental interest, namely dicarboxylate anions and a simulant of the CWA sulfur mustard, both of which contain hydrophobic cores, which make them suitable for recognition by a pillararene-based host. Two P5A-based receptors, **4.2-XB/HB**, appended with (iodo)triazole XB/HB guest binding sites, designed to interact with the electron-rich carboxylate and chloro terminal groups of DCBs and CEES respectively, and BODIPY fluorescent reporter groups, were prepared *via* a CuAAC synthetic methodology.

In organic $CHCl_3$ solvent, the superior signal transduction characteristics of XB donors in the context of fluorescence sensing were highlighted by the strong BODIPY emission response of **4.2-XB** to dicarboxylate anion binding, whereas its HB analogue, **4.2-HB** was unresponsive. ^{1}H NMR experiments demonstrated that both receptors form interpenetrated pseudo[2]rotaxane assemblies with DCB anions in $CDCl_3$, confirming that the lack of emission response of **4.2-HB** does not arise from the absence of guest binding, but instead is due to poor signal transduction. The importance of the formation of such interpenetrated assemblies to the strength of guest binding by **4.2-XB** was emphasised by its dramatically enhanced DCB affinity, relative to its affinity for acetate. Additionally, **4.2-XB** demonstrated a preference for $^-OOC(CH_2)_{10}COO^-$ over DCB anions of different lengths, which was ascribed to host-guest size complementarity.

Further binding studies were subsequently conducted in aqueous-containing solvent media, in which both **4.2-XB** and **4.2-HB** functioned as turn-off fluorescent sensors for DCBs in ACN : H_2O 1:1 (*v/v*) (buffered to pH = 8.0 with 50 mM HEPES), highlighting the important influence of the surrounding solvent on the direction of fluorescence response.

In this solvent mixture, the combination of the hydrophobic P5A guest binding macrocycle and the hydrophobic XB donors proved particularly potent. The presence of water enhanced the strength of DCB binding to **4.2-XB**, through the exploitation of hydrophobic effects, with $K_a(^-OOC(CH_2)_{10}COO^-)$ increased from 9900 M^{-1} in $CHCl_3$ to 104,000 M^{-1} in ACN : H_2O 1:1 (*v/v*) (buffered to pH = 8.0 with 50 mM HEPES), which was four-fold higher than the analogous association constant with **4.2-HB** in the organo-aqueous mixture.

Both **4.2-XB** and **4.2-HB** also proved capable of sensing CEES, a simulant of the CWA sulfur mustard, with remarkably high affinity, which was ascribed to the hydrophobic interactions between between the highly lipophilic guest and the hydrophobic regions of the host, which include the XB donors. Importantly, the sensors exhibited low LoDs and excellent selectivity over other CWA simulants and the non-toxic hydrolysis product of sulfur mustard. In summary, the combination of a bright BODIPY fluorescent reporter group, the hydrophobic P5A macrocycle and potent XB donors rendered **4.2-XB** a highly potent system for the sensing of both charged and neutral anthropogenic pollutants.

Future work related to these P5A systems includes the synthesis of fully water-soluble hosts in order to achieve sensing in pure water. This could be accomplished by appending either zwitterionic groups or PEG chains to the existing XB sensor molecular structure (Fig. 4.33). Sensing in pure water is not only more practically relevant, but would also increase the strength of the hydrophobic effect which drives the formation of the interpenetrated assemblies, thus boosting binding affinity even further.

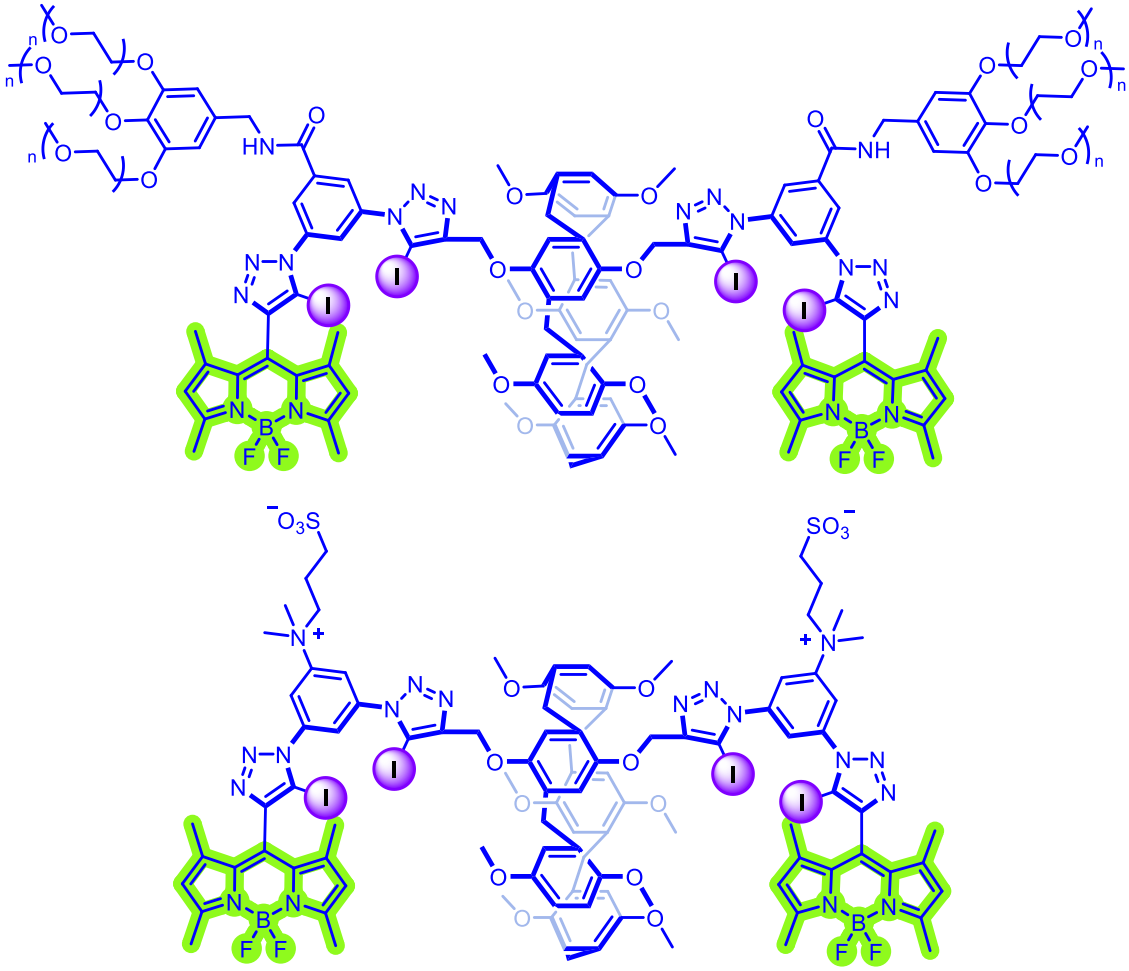


Fig. 4.33. Potential water-soluble P5A-based sensors.

A mixed XB/HB heteroditopic ion-pair sensor, **4.7**, utilising the same BODIPY fluorescent reporter group, but in this case appended to a central diaza-crown ether cation-binding macrocycle, was also developed. The heteroditopic receptor **4.7** proved capable of sensing cations, anions and ion-pairs in a competitive ACN : MeOH 1:1 (*v*/*v*) solvent medium. Importantly, **4.7** displayed a selective emission enhancement response towards potassium cations over sodium cations, with the smaller alkali metal cation inducing no significant emission response. Through ^{1}H NMR experiments, this K^{+}-selective emission response was attributed to the coordination of the proximal triazole motifs to the K^{+} cation, in a manner similar to lariat ether macrocycles. This binding mode did not occur upon binding of the smaller Na^{+} cation. Through this mechanism, receptor **4.7**

displayed a selective turn-on sensing response upon binding of K^+, despite both K^+ and Na^+ being bound by the diaza-crown motif with similarly high affinity.

Direct ion-pair titration experiments with a variety of alkali metal and ammonium halide salts revealed receptor **4.7** to exhibit strongly cooperative ion-pair binding and sensing, with a BODIPY emission enhancement of 18% observed upon addition of RbCl. For instance, the apparent chloride association constant value of receptor **4.7** was increased 25-fold in the presence of a co-bound K^+ cation, relative to the neutral receptor in the absence of a coordinating cation. This positive cooperativity was attributed to both electrostatic effects and also through-bond polarisation of the HB donor by coordination of the triazole motifs to the co-bound cation. Receptor **4.7** demonstrated the highest apparent chloride affinity when complexed with K^+ cations, with other, larger group 1 and ammonium cations eliciting smaller enhancements in apparent chloride association constant values, which was ascribed to their lower charge density.

The ability of the diaza-crown ether cation binding macrocycle in receptor **4.7** to recognise alkyl ammonium compounds allowed it to also bind and sense organic ammonium halide salts, exhibiting an 18% increase in emission intensity upon addition of the HCl salt of tyramine. Receptor **4.7** demonstrated a particular affinity for the HCl salt of the neuromodulator dopamine, showing an apparent chloride association constant in the presence of a co-bound dopamine-H^+ cation approximately a factor of two greater than in the cases of other related phenethylamine compounds. ^{1}H NMR titration experiments showed that this preferential binding arose from the formation of HB interactions between the co-bound components of the dopamine.HCl ion-pair, specifically the catechol hydroxyl groups on the dopamine-H^+ cation and the chloride anion, in a manner reminiscent of biological anion host systems.

Future work in this regard includes computational modelling studies to corroborate the proposed mechanism of K^+ *vs* Na^+ discrimination and dopamine.HCl binding preference exhibited by **4.7**, which could then inform the design of further, more selective ion-pair sensors, utilising a biologically-inspired approach. This computational modelling work is currently underway in a collaborator's laboratory.

Furthermore, an asymmetric derivative of the ion-pair sensor could be appended to an optically-transparent surface *via* a linking motif, to produce a sensing device to allow ion-pair sensing under continuous flow, which is of crucial importance for much needed real-world environmental sensing applications (Fig. 4.34).

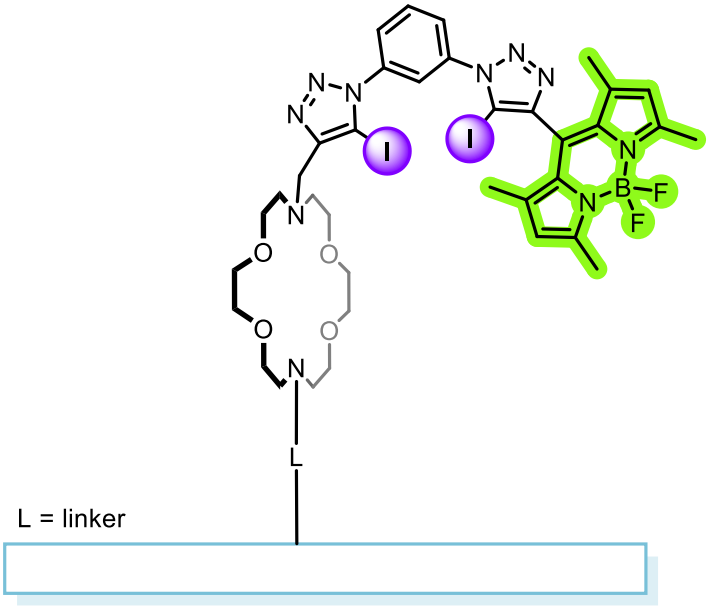


Fig. 4.34. Possible surface-tethered fluorescent anion sensor.

4.5 References for Chapter Four

1. C. J. Pedersen, *J. Am. Chem. Soc.* **1967**, *89*, 7017-7036.
2. D. J. Cram, T. Kaneda, R. C. Helgeson, S. B. Brown, C. B. Knobler, E. Maverick, K. N. Trueblood, *J. Am. Chem. Soc.* **1985**, *107*, 3645-3657.
3. J. M. Lehn, *Acc. Chem. Res.* **1978**, *11*, 49-57.
4. E. Graf, J. M. Lehn, *J. Am. Chem. Soc.* **1976**, *98*, 6403-6405.
5. D. J. Cram, *Science* **1983**, *219*, 1177-1183.
6. K. I. Assaf, W. M. Nau, *Chem. Soc. Rev.* **2015**, *44*, 394-418.
7. V. Böhmer, *Angew. Chem. Int. Ed. Engl.* **1995**, *34*, 713-745.
8. P. A. Gale, P. Anzenbacher Jr, J. L. Sessler, *Coord. Chem. Rev.* **2001**, *222*, 57-102.
9. G. Chen, M. Jiang, *Chem. Soc. Rev.* **2011**, *40*, 2254-2266.
10. T. Ogoshi, S. Kanai, S. Fujinami, T.-A. Yamagishi, Y. Nakamoto, *J. Am. Chem. Soc.* **2008**, *130*, 5022-5023.
11. T. Boinski, A. Szumna, *Tetrahedron* **2012**, *68*, 9419-9422.
12. T. Ogoshi, N. Ueshima, T. Akutsu, D. Yamafuji, T. Furuta, F. Sakakibara, T.-A. Yamagishi, *Chem. Commun.* **2014**, *50*, 5774-5777.
13. P. Demay-Drouhard, K. Du, K. Samanta, X. Wan, W. Yang, R. Srinivasan, A. C. H. Sue, H. Zuilhof, *Org. Lett.* **2019**, *21*, 3976-3980.
14. M. Guo, X. Wang, C. Zhan, P. Demay-Drouhard, W. Li, K. Du, M. A. Olson, H. Zuilhof, A. C.-H. Sue, *J. Am. Chem. Soc.* **2018**, *140*, 74-77.
15. Z. Zhang, B. Xia, C. Han, Y. Yu, F. Huang, *Org. Lett.* **2010**, *12*, 3285-3287.
16. M. Xue, Y. Yang, X. Chi, Z. Zhang, F. Huang, *Acc. Chem. Res.* **2012**, *45*, 1294-1308.
17. T. Ogoshi, S. Tanaka, T.-a. Yamagishi, Y. Nakamoto, *Chem. Lett.* **2011**, *40*, 96-98.
18. A. Mapp, J. T. Wilmore, P. D. Beer, J. M. Goicoechea, *Angew. Chem. Int. Ed.* **2023**, *62*, e202309211.
19. T. Ogoshi, *J. Incl. Phenom. Macrocycl. Chem.* **2012**, *72*, 247-262.
20. B. Gómez-González, L. García-Río, N. Basílio, J. C. Mejuto, J. Simal-Gandara, *Pharmaceutics* **2021**, *14*.
21. T. Ogoshi, M. Hashizume, T.-A. Yamagishi, Y. Nakamoto, *Chem. Commun.* **2010**, *46*, 3708.
22. N. L. Strutt, R. S. Forgan, J. M. Spruell, Y. Y. Botros, J. F. Stoddart, *J. Am. Chem. Soc.* **2011**, *133*, 5668-5671.
23. D. M. Greenberg, *Chemical pathways of metabolism*, Academic Press, **2014**.
24. B. Hoppe, *Nat. Rev. Nephrol.* **2012**, *8*, 467-475.
25. P. A. Przybylińska, M. Wyszkowski, *Ecol. Chem. Eng. S.* **2016**, *23*, 347-356.
26. S. Dang, Q.-L. Zhu, Q. Xu, *Nat. Rev. Mater.* **2017**, *3*, 17075.
27. S. M. Butler, K. A. Jolliffe, *Org. Biomol. Chem.* **2020**, *18*, 8236-8254.
28. D. Curiel, M. Más-Montoya, G. Sánchez, *Coord. Chem. Rev.* **2015**, *284*, 19-66.
29. R. J. Fitzmaurice, G. M. Kyne, D. Douheret, J. D. Kilburn, *J. Chem. Soc., Perkin Trans. 1* **2002**, 841-864.
30. W. Chen, C. Guo, Q. He, X. Chi, V. M. Lynch, Z. Zhang, J. Su, H. Tian, J. L. Sessler, *J. Am. Chem. Soc.* **2019**, *141*, 14798-14806.
31. Q. Duan, W. Xia, X. Hu, M. Ni, J. Jiang, C. Lin, Y. Pan, L. Wang, *Chem. Commun.* **2012**, *48*, 8532.
32. G. Institute of Medicine Committee on the Survey of the Health Effects of Mustard, Lewisite, in *Veterans at Risk: The Health Effects of Mustard Gas and Lewisite* (Eds.: C. M. Pechura, D. P. Rall), National Academies Press (US), Washington (DC), **1993**.
33. B. Picard, I. Chataigner, J. Maddaluno, J. Legros, *Org. Biomol. Chem.* **2019**, *17*, 6528-6537.
34. M. R. Sambrook, S. Notman, *Chem. Soc. Rev.* **2013**, *42*, 9251.
35. R. I. Tilley, *Aust. J. Chem.* **1990**, *43*, 1573-1576.
36. J. Brinkley, M. Kirkey, A. Marques, C. Lin, *Chem. Phys. Lett.* **2003**, *367*, 39-43.
37. R. C. Knighton, M. R. Sambrook, J. C. Vincent, S. A. Smith, C. J. Serpell, J. Cookson, M. S. Vickers, P. D. Beer, *Chem. Commun.* **2013**, *49*, 2293-2295.

38. K. E. Krakowiak, J. S. Bradshaw, D. J. Zamecka-Krakowiak, *Chem. Rev.* **1989**, *89*, 929-972.
39. H. Tsukube, K. Yamashita, T. Iwachido, M. Zenki, *J. Org. Chem.* **1991**, *56*, 268-272.
40. W. Hughes, A. Rananaware, D. D. La, L. A. Jones, S. Bhargava, S. V. Bhosale, *Sens. Actuators B Chem.* **2017**, *244*, 854-860.
41. G. Gholami, K. Zhu, G. Baggi, E. Schott, X. Zarate, S. J. Loeb, *Chem. Sci.* **2017**, *8*, 7718-7723.
42. H. V. Schröder, S. Sobottka, M. Nößler, H. Hupatz, M. Gaedke, B. Sarkar, C. A. Schalley, *Chem. Sci.* **2017**, *8*, 6300-6306.
43. P. R. Ashton, P. J. Campbell, P. T. Glink, D. Philp, N. Spencer, J. F. Stoddart, E. J. T. Chrystal, S. Menzer, D. J. Williams, P. A. Tasker, *Angew. Chem. Int. Ed. Engl.* **1995**, *34*, 1865-1869.
44. A. G. Seilkop, A. S. Odoh, N. J. Coradi, J. I. Wright, J. Barroso, B. Kim, *J. Org. Chem.* **2024**, *89*, 13338-13344.
45. J. Li, D. Yim, W.-D. Jang, J. Yoon, *Chem. Soc. Rev.* **2017**, *46*, 2437-2458.
46. T. Zhang, G. She, X. Qi, L. Mu, *Tetrahedron* **2013**, *69*, 7102-7106.
47. K. Rurack, M. Kollmannsberger, U. Resch-Genger, J. Daub, *J. Am. Chem. Soc.* **2000**, *122*, 968-969.
48. D. Jagleniec, Ł. Dobrzycki, J. Romański, *J. Mol. Liq.* **2024**, *399*, 124410.
49. P. Sabater, F. Zapata, B. López, I. Fernández, A. Caballero, P. Molina, *Dalton Trans.* **2018**, *47*, 15941-15947.
50. J. Bi, X. Zeng, D. Tian, H. Li, *Org. Lett.* **2016**, *18*, 1092-1095.
51. T. Ogoshi, T. Aoki, K. Kitajima, S. Fujinami, T.-a. Yamagishi, Y. Nakamoto, *J. Org. Chem.* **2011**, *76*, 328-331.
52. J. Y. Lim, P. D. Beer, *New J. Chem.* **2018**, *42*, 10472-10475.
53. T. Ogoshi, R. Iizuka, D. Kotera, T.-A. Yamagishi, *Org. Lett.* **2015**, *17*, 350-353.
54. C. C. Robertson, R. N. Perutz, L. Brammer, C. A. Hunter, *Chem. Sci.* **2014**, *5*, 4179-4183.
55. K. Kim, O. G. Tsay, D. A. Atwood, D. G. Churchill, *Chem. Rev.* **2011**, *111*, 5345-5403.
56. M. R. Sambrook, J. C. Vincent, J. A. Ede, I. A. Gass, P. J. Cragg, *RSC Adv.* **2017**, *7*, 38069-38076.
57. E. J. Mitchell, A. J. Beecroft, J. Martin, S. Thompson, I. Marques, V. Félix, P. D. Beer, *Angew. Chem. Int. Ed.* **2021**, *60*, 24048-24053.
58. E. Jahnke, J. Weiss, S. Neuhaus, T. N. Hoheisel, H. Frauenrath, *Chem. Eur. J.* **2009**, *15*, 388-404.
59. D. M. Goli, D. M. Dishong, C. J. Diamond, G. W. Gokel, *Tetrahedron Lett.* **1982**, *23*, 5243-5246.
60. H. M. Tay, A. Docker, A. Taylor, P. D. Beer, *Chem. Eur. J.* **2024**.
61. Z. Kokan, M. J. Chmielewski, *J. Am. Chem. Soc.* **2018**, *140*, 16010-16014.
62. A. J. Taylor, A. Docker, P. D. Beer, *Chem. Asian J.* **2023**, *18*, e202201170.
63. R. M. Izatt, J. S. Bradshaw, S. A. Nielsen, J. D. Lamb, J. J. Christensen, D. Sen, *Chem. Rev.* **1985**, *85*, 271-339.
64. S. Kulstad, L. Å. Malmsten, *J. Inorg. Nucl. Chem.* **1980**, *42*, 573-578.
65. K. J. Winstanley, A. M. Sayer, D. K. Smith, *Org. Biomol. Chem.* **2006**, *4*, 1760-1767.
66. R. K. Skitchenko, D. Usoltsev, M. Uspenskaya, A. V. Kajava, A. Guskov, *Bioinformatics* **2020**, *36*, 3064-3071.

Chapter 5

Conclusions

5 Conclusions

5.1 Conclusions

The work described in this thesis had the overarching goal of developing novel, fluorescent, halogen bonding sensors for the detection of anions, ion-pairs and neutral species. In particular, it sought to address three challenges outlined in Chapter One, namely: to understand the mechanisms of fluorescence modulation induced by guest binding; to extend the wavelength range of XB fluorescent sensors into the biologically-relevant wavelength window and to bring the benefits of XB interactions to the sensing of neutral guests.

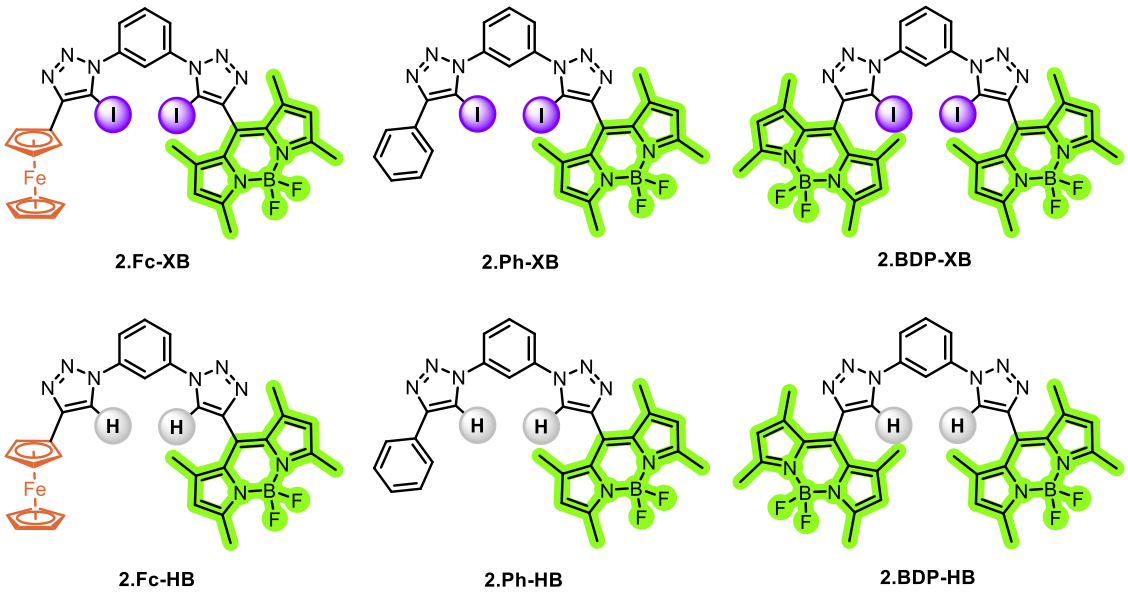


Fig. 5.1. The family of XB and HB BODIPY-based fluorescent anion sensors studied in Chapter Two.

Chapter Two described a family of six redox-active ferrocene-appended XB and HB BODIPY fluorescent anion sensors, synthesised by a CuAAC methodology (Fig. 5.1). By varying the triazole substituent from Ph/BODIPY to Fc, control over the either a turn-on enhancement or a turn-off quenching anion binding-induced fluorescence response could be achieved in the XB family of sensors. The combination of electrochemical experiments,

fluorescence lifetime measurements, and studies in which the viscosity of the solution was varied enabled the mechanisms underlying these differing responses to be elucidated, which were shown to be restriction of rotation about the BODIPY-*meso* bond and anion binding-enhanced PET respectively.

The redox-active ferrocene motif incorporated into **2.Fc-XB/HB** allowed both to also function as electrochemical anion sensors. Importantly, the redox sensing capability of **2.Fc-HB** was combined with the ability of the BODIPY fluorescent reporter group to relay the oxidation state of the Fc moiety to allow the first example of spectroelectrochemical anion sensing – in effect electrochemical anion sensing at nanomolar concentrations. Notably, the unprecedented 'fluorescence CV' experiment, developed in Chapter Two, enabled the simultaneous measurement of the anion recognition optical response of the sensor in two different oxidation states and the electrochemical voltammetric response of the redox probe in a single, combined experiment.

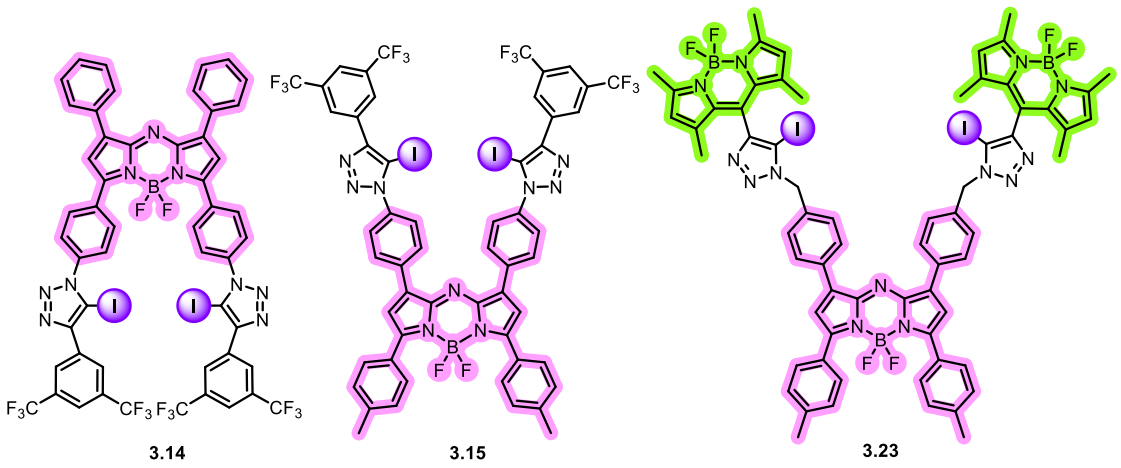


Fig. 5.2. The XB aza-BODIPY-based fluorescent anion sensors studied in Chapter Three.

Chapter Three presented three novel XB aza-BODIPY anion sensors, which facilitated XB-mediated anion sensing in the biologically-relevant NIR-1 window (Fig. 5.2).

The aza-BODIPY motif proved to be highly sensitive to halide anion binding, displaying quenching responses of up to 70%, whereas no emission response was observed upon addition of the oxo-anions HSO_4^- and $H_2PO_4^-$, highlighting the halide selectivity offered by XB donors. The connectivity of sensor **3.14** proved to be more potent than that of **3.15**, both in terms of anion binding affinity and the magnitude of emission response, which should inform the development of further biologically-relevant sensors based on the aza-BODIPY fluorophore.

The ratiometric mixed BODIPY/aza-BODIPY dyad compound **3.23** exhibited energy transfer between the peripheral BODIPY units and the central aza-BODIPY core, enabling the emission response of both fluorophores to anion binding to be simultaneously monitored *via* excitation at one wavelength. Characteristic emission response signatures were induced by each halide anion, allowing their identity as well as concentration to be determined. Calibration curves relating the chloride and bromide anion concentration to the ratio of BODIPY to aza-BODIPY emission intensity were constructed, which enabled **3.23** to act as a ratiometric sensor.

In addition to its anion sensing properties, receptor **3.14** was shown to act as a photosensitiser, efficiently producing singlet oxygen due to the presence of heavy iodine atoms in its structure. Importantly, anion binding-modulated singlet oxygen production was demonstrated, with utility in improving the selectivity of photodynamic therapy agents.

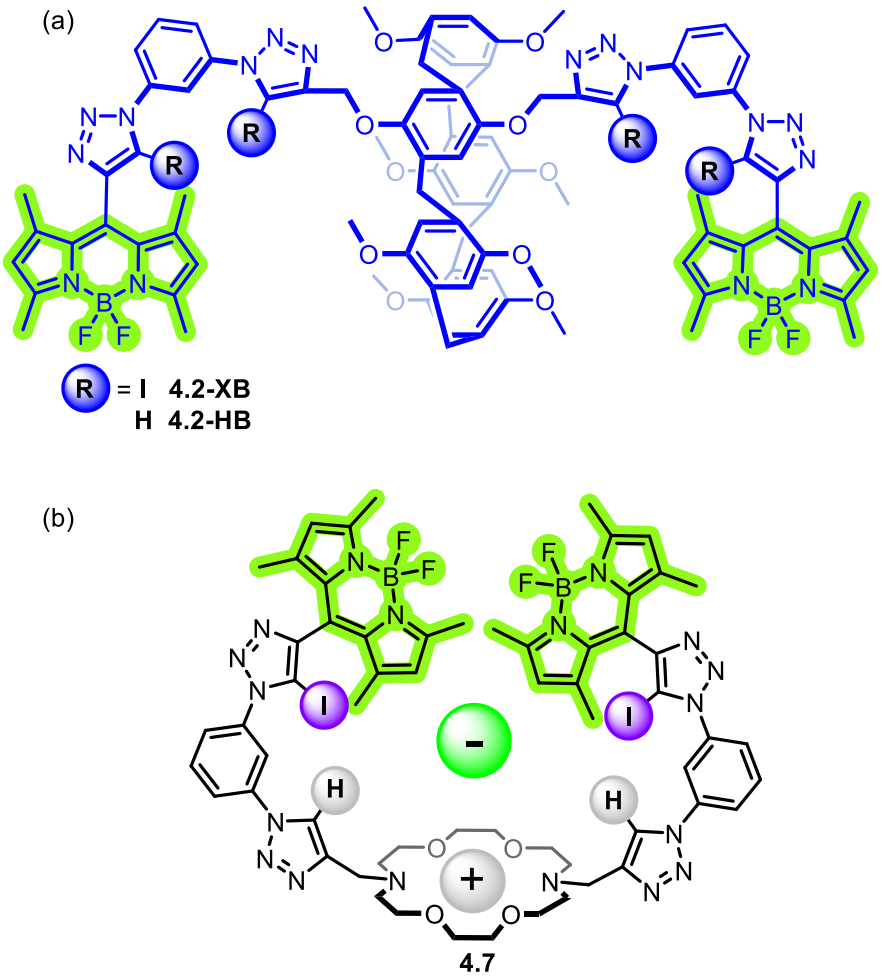


Fig. 5.3. The BODIPY-based fluorescent sensors studied in Chapter Four. (a) The P5A-based sensors for DCBs and CEES and (b) the diaza-18-crown-6 sensor for ion-pairs.

Chapter Four demonstrated the reliability and generalisability of the XB-BODIPY fragment developed in Chapter Two through its incorporation into pillar[5]arene and diaza-18-crown-6 macrocyclic structural frameworks to sense anions, neutral species and ion-pairs. Specifically, an XB BODIPY P5A-based sensor and its HB analogue were developed for the sensing of dicarboxylates and a chemical warfare agent simulant (Fig. 5.3a). The superior signal transduction capability of XB donors was again displayed, with **4.2-XB** demonstrating strong turn-on BODIPY emission responses to DCB binding in organic solvent, whereas **4.2-HB** remained unresponsive. In aqueous-containing media, both sensors exhibited quenching responses to DCB binding, highlighting the strong

influence of solvent on the behaviour of fluorescent sensors. The power of leveraging hydrophobic effects was highlighted, as, in the presence of water, both sensors displayed very strong affinity for hydrophobic guests – the XB sensor proved to be particularly potent with association constant values of 104,000 M^{-1} and 528,000 M^{-1} recorded for $^{-}OOC(CH_2)_{10}COO^{-}$ and the sulfur mustard simulant, CEES, respectively. In addition to their high affinities and low limits of detection for CEES, both **4.2-XB/HB** also displayed good selectivity over other CWA simulants and the non-toxic hydrolysis product of sulfur mustard, rendering them promising candidates for real-world sensing applications.

The same XB BODIPY fragment was also appended to a central diaza-18-crown-6 macrocycle for the sensing of ion-pairs (Fig. 5.3b). Receptor **4.7** exhibited the ability to selectively sense potassium cations over sodium cations, which was shown to be due to the size-dependent alkali metal cation binding mode adopted. Sensor **4.7** also displayed strong positive cooperativity in ion-pair sensing, with its apparent anion affinity increased 25-fold in the presence of a coordinating cation, such as K^{+}.

The ability of the diaza-crown ether motif to also recognise organic alkyl ammonium species was exploited to allow the selective detection of the HCl salt of the neuromodulator dopamine. The particular affinity for dopamine.HCl was shown to be due to the unique inter-ion HB interactions formed between the catechol-OH groups of the dopamine cation and co-bound chloride anion, which formed a guest binding pocket reminiscent of those found in nature.

A core theme illustrated by the work described in this thesis is the superiority of XB interactions over traditionally employed HB interactions in terms of anion binding, and also transduction of an anion binding event into a fluorescence response. The optical

sensing of not only anions but also neutral species using XB interactions has been demonstrated for the first time and it is hoped that this work will inspire efforts to continue to integrate XB donors into future sensors, despite the slightly increased synthetic difficulty that they present.

Another theme, demonstrated by the work in Chapter Two, is that predictable control over the direction of BODIPY emission enhancement/quenching sensing behaviour can be engineered in the design of anion sensors, although the work in Chapters Three and Four illustrated that the magnitude and direction of emission responses are also importantly dependent on the nature of the solvent and difficult to predict for novel and more complex fluorophores. *A priori* prediction of host emission responses to guest binding in a variety of solvents is an important problem to solve in the field of supramolecular sensing, as it would unlock the ability to design sensors targeted at applications requiring a particular turn-on/off response, such as biological imaging. Therefore, this is a potentially fruitful avenue of future research.

As illustrated by the spectroelectrochemical anion sensing, described in Chapter Two, and the anion binding-modulated photosensitising behaviour, described in Chapter Three, fluorescent sensors are often capable of much more than simply detecting their target guest optically. Therefore, the intersection of supramolecular chemistry with fluorescence is a fascinating area with much more untapped potential.

The K^+ over Na^+ selectivity displayed by sensor **4.7** and the 'finger-print' identification emission responses of ratiometric sensor **3.23** to halide anion binding points to a more general phenomenon, which is that optical sensors can offer selective sensing responses with modest underlying differences in guest affinity. This mode of selectivity,

which has previously been exploited by Anslyn,[1-2] Anzenbacher,[3-4] and Sessler,[5-6] amongst others,[7-8] continues to offer supramolecular chemists another tool in the pursuit of selectively sensing species which are highly similar to one another, and hence challenging to discriminate on the basis of molecular recognition alone, and is therefore also an interesting area for future research.

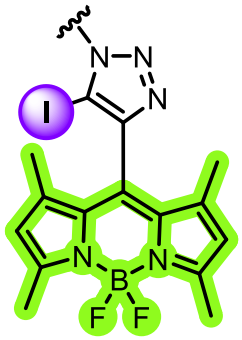


Fig. 5.4. The key XB BODIPY sensing fragment utilised throughout this thesis.

Finally, the generalisability of key sensing molecular fragments was demonstrated by the use of the XB BODIPY motif which was deployed in a variety of molecular environments across Chapters Two, Three and Four (Fig. 5.4). This points to the utility of developing simple model systems to assist in the development of more complex sensors. It is therefore hoped that the work described in this thesis may be of use to supramolecular chemists seeking to graft fluorescent sensors onto surfaces, which is a key step in pursuit of re-usable sensors capable of real-world deployment.

5.2 References for Chapter Five

1. J. J. Lavigne, E. V. Anslyn, *Angew. Chem. Int. Ed.* **2001**, *40*, 3118-3130.
2. H. A. Fargher, S. d'Oelsnitz, D. J. Diaz, E. V. Anslyn, *Anal. Sens.* **2023**, *3*, e202200095.
3. A. Radujević, A. Penavic, R. Z. Pavlović, J. D. Badjić, P. Anzenbacher, *Chem* **2022**, *8*, 2228-2244.
4. A. R. Sartori, A. Radujević, S. M. George, P. Anzenbacher, *Chem. Sci.* **2023**, *14*, 7545-7552.
5. J. Yoo, M.-S. Kim, S.-J. Hong, J. L. Sessler, C.-H. Lee, *J. Org. Chem.* **2009**, *74*, 1065-1069.
6. H. Miyaji, W. Sato, J. L. Sessler, *Angew Chem Int Ed Engl* **2000**, *39*, 1777-1780.
7. H. M. Tay, A. Docker, A. Taylor, P. D. Beer, *Chem. Eur. J.* **2024**.
8. M. Más-Montoya, D. Curiel, C. Ramírez de Arellano, A. Tárraga, P. Molina, *Eur. J. Org. Chem.* **2016**, *2016*, 3878-3883.

Chapter 6

Experimental Details

6 Experimental Details

6.1 General Information

6.1.1 Instruments and Reagents

Solvents and reagents were purchased from commercial suppliers and used as received. Dry solvents were obtained by purging with nitrogen and passing through a MBraun MPSP-800 column. Where indicated, solvents were further degassed by purging with N_2 for 15 minutes immediately prior to use. H_2O was deionised and micro-filtered using a Milli-Q® Millipore machine.

Triethylamine was distilled from, and stored over, potassium hydroxide. Tris[(1-benzyl-1*H*-1,2,3-triazol-4-yl)methyl]amine is abbreviated as TBTA.

50 mM HEPES buffer was prepared by dissolving HEPES (*N*-(2-hydroxyethyl)piperazine-*N*'-(2-ethanesulfonic acid)) in deionised water and then adjusting the pH to 8.0 by addition of small volumes of a 3 M NaOH solution.

Experiments were conducted at room temperature unless otherwise stated. Merck silica gel 60 was used for flash column chromatography. Neutral Brockman grade I activated alumina was purchased from Merck and used for purification as received. TBA salts were stored in vacuum desiccators prior to use. NMR spectra were either recorded on a Bruker Avance III HD Nanobay NMR spectrometer equipped with a 9.4 T magnet or a Bruker NEO 600 with broadband helium cryoprobe. Chemical shifts are quoted in parts per million relative to the residual solvent peak.

UV-vis and fluorescence measurements were carried out on a Horiba Duetta using quartz cuvettes with a path length of 10 mm. All fluorescence spectra were recorded with

5 nm excitation and emission slits in, at least, triplicate repeat measurements to ensure signal stability. Excitation wavelengths were as noted in the main text or 485 nm for BODIPY compounds and 600 nm for aza-BODIPY compounds. Spectroscopic grade solvents were used throughout for all optical studies.

Fluorescence lifetimes were measured on an Edinburgh Instruments FS5 spectrofluorometer operating Fluoracle® software, using time-correlated single photon counting (TCSPC) mode using a picosecond pulsed diode laser (EPL-475) as the excitation source. The detector was a R13456 PMT detector (200 – 950 nm spectral coverage, Hamamatsu). Measurements were conducted at 298 K.

6.1.2 General Method for Optical Titrations

Titration studies were carried out by titrating a 1 μM solution of the receptor with aliquots of a concentrated solution of the guest in the same receptor solution to ensure a constant receptor concentration. In a typical experiment, successive aliquots of a guest solution of appropriate concentration were added to 1.0 mL of the host solution. The cuvette was inverted to thoroughly mix the sample prior to each data collection. Changes in the optical spectra were fitted by a global fitting using either Bindfit or OriginPro,[1-2] with a 1:1 stoichiometric host-guest binding model used unless specified otherwise.

6.1.3 General Method for ^{1}H NMR Titrations

^{1}H NMR titrations were recorded on a Bruker Avance III NMR spectrometer equipped with a 11.75 T magnet at 298 K. Unless stated otherwise, titrations were carried out by successive addition of a 50 mM stock solution of the target guest to a 1 mM solution of host, such that 1.0 equivalent of guest corresponds to a 10.0 μL stock solution addition. The sample was thoroughly mixed by inversion of the NMR tube prior to each spectrum being

collected. 17 data points were collected, upon addition of 0.0, 0.2, 0.4, 0.6, 0.8, 1.0, 1.2, 1.4, 1.6, 1.8, 2.0, 2.5, 3.0, 4.0, 5.0, 7.0 and 10.0 equivalents of guest. All systems for which binding constants are quoted displayed fast NMR exchange at 298 K. The changes in chemical shift upon binding were fitted using Bindfit to a 1:1 stoichiometric binding model unless specified otherwise.[1]

6.2 Experimental Details for Chapter Two

6.2.1 Determination of Quantum Yields

Fluorescence quantum yields were determined according to established procedures reported by Resch-Genger and co-workers. Briefly, the quantum yield was calculated according to equation 6.1 relative to fluorescein in 0.1 M NaOH as standard (Φ_{St} = 0.89).[3]

$$\Phi = \Phi_{St} \frac{F_{BDP}}{F_{St}} \frac{f_{St}}{f_{BDP}} \frac{n_{BDP}^2}{n_{St}^2} \qquad \text{(Eqn. 6.1)}$$

Where F is the integral photon flux of the standard and the BODIPY receptor, Φ_{St} the quantum yield of the standard, n the refractive index of the solvent and $f = 1 - 10^{-A_{Exc}}$. With n_{BDP} (acetone) = 1.3586 and n_{St} (water) = 1.3300.

Identical measurement parameters were used for both the standard and receptor samples: λ_{Exc} = 465 nm, 5 nm emission and excitation slits, 20 accumulations. The emission was measured, and integrated, in the range between 475 – 850 nm. The absorbance at the excitation wavelength was kept around ≈ 0.1 for both the BODIPY samples and the standard. Both absorbance and emission were measured multiple times to ensure signal stability. All quantum yields were rounded to the nearest percent.

6.2.2 Electrochemical Measurements

All experiments were carried out with an Autolab Potentiostat (Metrohm) or a PalmSens4 Potentiostat with a three-electrode setup comprising a glassy carbon (GC) working electrode (3 mm, BASi), a Pt wire counter electrode and an Ag|$AgNO_3$ reference electrode (with an inner filling solution of 10 mM $AgNO_3$, 100 mM $TBAClO_4$ in ACN). Prior to each experiment the GC working electrode was mechanically polished with an alumina slurry (0.05 µm particle size), followed by sonication in EtOH : H_2O 1:1 (*v/v*). 100 mM $TBAPF_6$ or

100 mM $TBAClO_4$ were used as supporting electrolyte, as indicated. Cyclic voltammograms (CVs) were recorded using a step potential of 2.4 mV and at a scan rate of 100 mV/s, unless otherwise noted. Square wave voltammograms (SWVs) were recorded using a step potential of 2 mV, a 20 mV amplitude and at a frequency of 25 Hz. The receptors' half-wave potentials ($E_{1/2}$) were determined as the peak potential by SWV and were referenced to Fc as an internal standard.

Voltammetric titration experiments were carried at a constant receptor concentration of 0.1 mM or 0.25 mM, as indicated. In all cases the overall ionic strength was kept constant (at 100 mM) by titration of an initial host solution containing 100 mM $TBAClO_4$ with an anion solution in the same solvent system containing 100 mM TBA-anion. In select cases up to 200 μM aqueous $HClO_4$ was also added to the electrolyte system to stabilise the ferrocenium redox state, as required for spectroelectrochemical experiments.[4-5] All electrochemical titrations were followed by SWV.

6.2.3 Spectroelectrochemical Measurements

Spectroelectrochemical experiments were conducted in a standard quartz fluorescence cuvette (1 × 1 × 3 cm), using a 3D printed cap, which held another three-electrode setup (Pt grid working electrode, non-aqueous $Ag|AgNO_3$ reference electrode (as above), Pt wire counter electrode) in the solution but above the light path. The solution was stirred rapidly throughout measurements, using a stirrer bar below the light path (Fig. 2.27). The sample was excited at 485 nm, and the emission at 521 nm was continually monitored throughout all experiments. 'Fluorescence CV' scans and anion binding titrations were carried out at a scan rate of 0.75 mV/s. Fluorescence CV scans were conducted in ACN, containing 100 mM $TBAClO_4$, 200 μM $HClO_4$ and 0.02% H_2O. Data for fluorescence CV scans were smoothed using a 5-point weighted moving average method. $E_{1/2}$ values from fluorescence CVs were

obtained by finding the value of *E* at the midpoint between the minimum and maximum fluorescence intensities for the forward and backward scan and taking the arithmetic mean.

6.2.4 Gibbs Free Energy of Electron Transfer Calculations

As described in Chapter Two, the Gibbs free energy of electron transfer is calculated *via*:[6-8]

$$\Delta G_{\mathrm{ET}} = e\left[E_{\mathrm{Ox,Don}} - E_{\mathrm{Red,Acc}}\right] - E_{00} - \Delta G_{\mathrm{S}} \qquad \text{(Eqn. 6.2)}$$

Where, E_{Ox} and E_{Red} are the half-wave potentials of the donor (Fc) and acceptor (BODIPY), respectively, E_{00} is the photoexcitation energy for the BODIPY and ΔG_{S} is the coulombic energy of the charge separated state.

In the case of mirror image spectra, E_{00} of the BODIPY can be calculated from the midpoint between absorption and emission maxima *via* $E_{00} = \frac{h * c}{\lambda_{00}}$.[9-10] For **2.Fc-XB** and **2.Fc-HB** the midpoint between these spectra in acetone is 516.5 and 514 nm, respectively, which gives E_{00} of 2.40 and 2.41 eV, **2.Fc-XB** and **2.Fc-HB** respectively.

As shown in Chapter Two, ΔG_{ET} can be obtained in good approximation (without consideration of $\Delta \mathrm{G_S}$, *vide infra*):

$$\Delta G_{ET,XB} = e[0.097V - -1.400V] - 2.4\ eV - \Delta \mathrm{G_S} = \mathbf{-0.903\ eV} - \Delta \mathrm{G_S}$$

$$\Delta G_{ET,HB} = e[0.073V - -1.402V] - 2.41\ eV - \Delta \mathrm{G_S} = \mathbf{-0.935\ eV} - \Delta \mathrm{G_S}$$

These values confirm that in both cases electron transfer is thermodynamically exergonic and thus favourable.

ΔG_S, the coulombic energy of the charge separated state, can, for singly charged donor/acceptor (after electron transfer has occurred) be calculated *via*:

$$\Delta G_S = -\frac{e^2}{4\pi\varepsilon\varepsilon_0 R_{DA}} - \frac{e^2}{8\pi\varepsilon_0}\left(\frac{1}{r_D} + \frac{1}{r_A}\right)\left(\frac{1}{\varepsilon_{EC}} - \frac{1}{\varepsilon}\right) \text{ (Eqn. 6.3)}$$

where ε_{EC} is the dielectric constant of the solvent utilised for electrochemical experiments (in this case ACN), ε is the dielectric constant of the photophysical system, R_{DA} is the centre-to-centre distance between donor and acceptor and r_D and r_A are the radii of donor and acceptor respectively. R_{DA}, r_D and r_A are not directly available, such that ΔG_S can only be estimated using reasonably values of these parameters.

By setting with $\varepsilon = 21$ for acetone (as this was the solvent used for the anion titration experiments) and R_{DA} = 0.5 or 2 nm, the first term of Eqn. 6.3 can be approximated:

$$\Delta G_S = -\frac{e^2}{4\pi\varepsilon\varepsilon_0 R_{DA}} = -1.44 \times 10^{-9} eVm \times \frac{1}{\varepsilon R_{DA}}$$

For R_{DA} = 0.5 nm:

$$\Delta G_S = -0.137\ eV$$

For R_{DA} = 2 nm:

$$\Delta G_S = -0.034\ eV$$

In both cases the first term of Eqn. 6.3 is much smaller than the above-stated values for ΔG_{ET} and therefore has a negligible impact on the interpretation of the values given.

The second term of the Eqn. 6.3 can also be estimated using literature values of r_D = 0.175 nm and r_A = 0.434 nm as approximate radii of donor and acceptor, and ε = 37.5 for ACN.[7]

$$\Delta G_S = -\frac{e^2}{4\pi\varepsilon\varepsilon_0 R_{DA}} - \frac{e^2}{8\pi\varepsilon_0}\left(\frac{1}{r_D}+\frac{1}{r_A}\right)\left(\frac{1}{\varepsilon_{EC}}-\frac{1}{\varepsilon}\right) = -\frac{e^2}{4\pi\varepsilon\varepsilon_0 R_{DA}} + 0.121eV$$

This value is again much smaller than the first term of ΔG_{ET} (≈ –0.9 eV) and is also of opposite sign as the first term of ΔG_S, further reducing its influence on the overall value of ΔG_{ET} and therefore justifying neglecting it in the calculations and discussions of ΔG_{ET}.

6.2.5 Synthesis and Characterisation of Novel Compounds

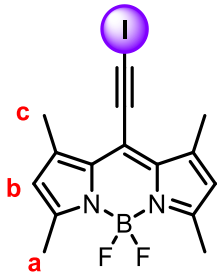
General Synthetic Procedure 2.1

$Cu(MeCN)_4PF_6$ (0.04 mmol) and TBTA (0.04 mmol) were dissolved in degassed DCM (≈ 2 mL) and left to stir for 10 minutes. The requisite alkyne precursor (**2.3** or **2.7**) (0.37 mmol) was added to the solution of the copper complex, followed by the bis-azide **2.1** (0.75 mmol). The resultant mixtures were left to stir until TLC analysis confirmed full consumption of the alkyne precursor. The crude reaction mixture was diluted with DCM (15 mL) and the organic layer washed with aqueous 0.01 M NH_4OH/EDTA solution (10 mL). The resultant aqueous layer was back extracted with DCM (2 × 10 mL) and the combined organic phases washed with water before they were dried over $MgSO_4$ and concentrated *in vacuo* to obtain the crude product mixture. The relevant products were isolated *via* silica-gel chromatography (DCM : EtOAc 95:5 (*v/v*)).

General Synthetic Procedure 2.2

$Cu(MeCN)_4PF_6$ (0.02 mmol) and TBTA (0.02 mmol) were dissolved in degassed DCM (≈ 1 mL) and left to stir for 10 minutes. The requisite alkyne precursor (**2.3**, **2.5**, **2.6**, ethynylferrocene, **2.7** or phenylacetylene) (0.15 mmol) was added to the solution of the copper complex, followed by the azide coupling partner (**2.4** or **2.8**) (0.15 mmol). The resultant mixtures were left to stir until TLC analysis confirmed full consumption of the alkyne precursor. The crude reaction mixture was diluted with DCM (15 mL) and the organic layer washed with aqueous 0.01 M NH_4OH/EDTA solution (10 mL). The resultant aqueous layer was back extracted with DCM (2 × 10 mL) and the combined organic phases washed with water before they were dried over $MgSO_4$ and concentrated *in vacuo* to obtain the crude product mixture. The relevant products were isolated *via* silica-gel chromatography (DCM : EtOAc 90:10 (*v/v*)).

8-(iodo)ethynyl-BODIPY 2.3



TMS protected 8-ethynyl-BODIPY (**2.2**)[11] (60 mg, 0.174 mmol, 1 equiv.) and AgF (22 mg, 0.174 mmol, 1 equiv.) were dissolved in dry degassed MeCN (3 mL). *N*-iodosuccinimide (NIS) (42 mg, 0.174 mmol, 1 equiv.) was added and the reaction mixture left to stir in darkness for 5 h. The mixture was filtered through a silica plug and the filtrate reduced *in vacuo*. The crude was dissolved in DCM (20 mL) and washed with H_2O (3 × 20 mL) before

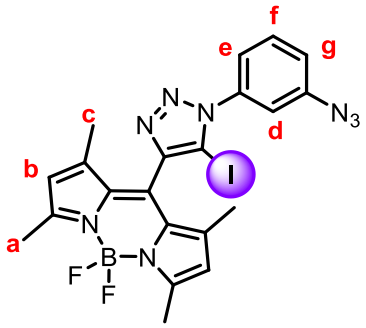
drying over $MgSO_4$. The solvent was removed *in vacuo* and the product was purified by column chromatography (EtOAc/hexanes) and isolated as a red powder (69 mg, 94%).

^{1}H NMR (500 MHz, $CDCl_3$) δ: 6.06 (s, 2H, H_b), 2.52 (s, 6H, H_c), 2.41 (s, 6H, H_a).

^{13}C NMR (151 MHz, $CDCl_3$) δ: 155.05, 142.21, 134.11, 121.07, 119.69, 90.49, 28.44, 15.35, 14.80.

HRMS – *unable to obtain due to decomposition*.

XB Synthon 2.4



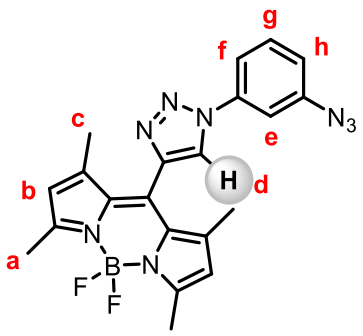
Synthon **2.4** was prepared from 1,3-diazidobenzene (**2.1**) and **2.3** according to General Synthetic Procedure 2.1, affording **2.4** in 40% yield.

^{1}H NMR (400 MHz, $CDCl_3$) δ: 7.60 (t, J = 8.1 Hz, 1H, H_f), 7.34 (dd, 1H, H_e), 7.30 (dd, 1H, H_g), 7.22 (t, J = 2.1 Hz, 1H, H_d), 6.05 (s, 2H, H_b), 2.58 (s, 6H, H_c). *H_a not observed as coincident with residual H_2O peak.*

^{13}C NMR (151 MHz, $CDCl_3$) δ: 157.43, 146.76, 142.27, 141.95, 137.66, 132.25, 130.85, 127.16, 122.10, 121.79, 120.83, 116.75, 82.39, 14.84, 13.84.

HRMS (ESI +ve) m/z: 559.0833, ([M+H]+, $C_{21}H_{19}BF_2IN_8$ requires 559.0835).

HB Synthon 2.8



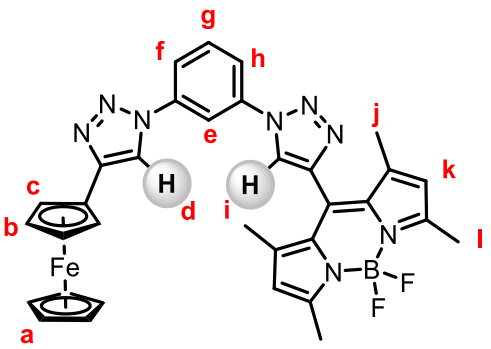
Synthon **2.8** was prepared from 1,3-diazidobenzene (**2.1**) and 8-ethynyl-BODIPY (**2.7**) according to General Synthetic Procedure 2.1, affording **2.8** in 42% yield.

^{1}H NMR (400 MHz, $CDCl_3$) δ: 8.04 (s, 1H, H_d), 7.60 – 7.48 (m, 3H, $H_{f,g,h}$), 7.21 – 7.14 (m, 1H, H_e), 6.02 (s, 2H, H_b), 2.56 (s, 6H, H_c), 1.54 (s, 6H, H_a).

^{13}C NMR (151 MHz, $CDCl_3$) δ: 157.17, 142.85, 142.58, 141.43, 137.92, 132.53, 131.48, 127.93, 121.89, 121.49, 119.69, 116.41, 111.46, 14.90, 14.61.

HRMS (ESI +ve) m/z: 433.1878, ([M+H]+, $C_{21}H_{20}BF_2N_8$ requires 433.1868).

2.Fc-HB



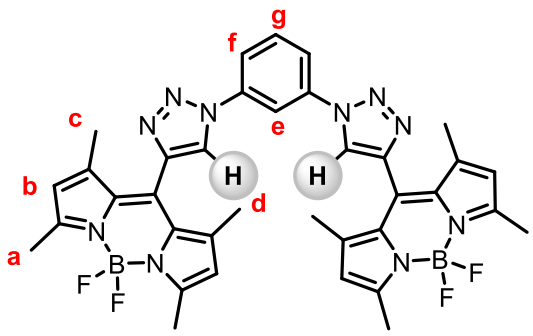
2.Fc-HB was prepared from **2.8** and ethynylferrocene according to General Synthetic Procedure 2.2, affording **2.Fc-HB** in 98% yield.

^{1}H NMR (600 MHz, DMSO-d_6) δ: 9.29 (s, 1H, H_i), 9.07 (s, 1H, H_d), 8.60 (t, J = 2.1 Hz, 1H, H_e), 8.13 (m, 2H, $H_{f,h}$), 7.90 (t, J = 8.2 Hz, 1H, H_g), 6.27 (s, 2H, H_k), 4.82 (t, J = 1.9 Hz, 2H, H_c), 4.38 (t, J = 1.9 Hz, 2H, H_b), 4.11 (s, 5H, H_a), 1.55 (s, 6H, H_l). *H_c not observed as coincident with residual DMSO peak.*

^{13}C NMR (151 MHz, DMSO-d_6) δ: 156.39, 147.03, 142.87, 139.64, 137.72, 137.28, 131.81, 131.58, 128.69, 124.02, 121.89, 119.98, 119.74, 118.68, 111.48, 74.96, 69.40, 69.38, 68.66, 66.50, 14.39, 14.00.

HRMS (ESI +ve) m/z: 643.1987, ([M+H]+, $C_{33}H_{30}BF_2FeN_8$ requires 643.1998).

2.BDP-HB



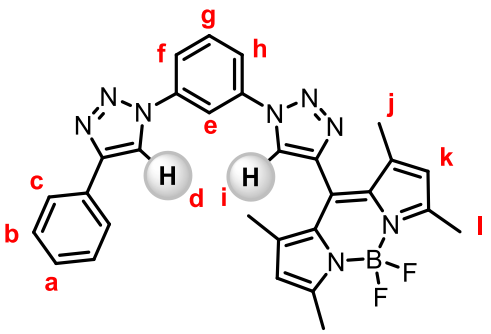
2.BDP-HB was prepared from **2.8** and 8-ethynyl-BODIPY (**2.7**) according to General Synthetic Procedure 2.2, affording **2.BDP-HB** in 86% yield.

^{1}H NMR (600 MHz, DMSO-d_6) δ: 9.29 (s, 2H, H_d), 8.69 (t, J = 2.1 Hz, 1H, H_e), 8.18 (dd, J = 8.2, 2.1 Hz, 2H, H_f), 7.93 (t, J = 8.2 Hz, 1H, H_g), 6.26 (d, J = 1.1 Hz, 4H, H_b), 2.48 (s, 12H, H_c), 1.54 (s, 12H, H_a).

^{13}C NMR (151 MHz, DMSO-d_6) δ: 156.39, 142.86, 139.64, 137.37, 132.02, 131.56, 128.62, 124.06, 121.88, 120.46, 112.10, 14.38, 13.96.

HRMS (ESI +ve) m/z: 703.3007, ([M+H]+, $C_{36}H_{33}B_2F_4N_{10}$ requires 703.3017).

2.Ph-HB



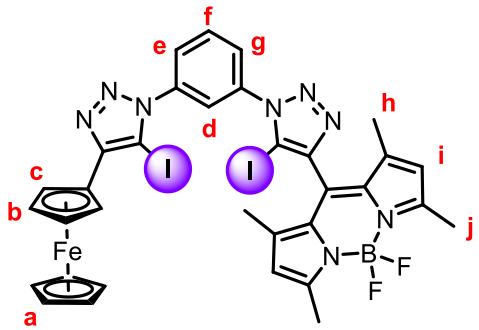
2.Ph-HB was prepared from **2.8** and phenylacetylene according to General Synthetic Procedure 2.2, affording **2.Ph-HB** in 99% yield.

^{1}H NMR (400 MHz, $CDCl_3$) δ: 8.40 (t, J = 2.1 Hz, 1H, H_e), 8.34 (s, 1H, H_i), 8.18 (s, 1H, H_d), 8.00 – 7.85 (m, 4H, $H_{b,c}$), 7.78 (t, J = 8.1 Hz, 1H, H_g), 7.53 – 7.44 (m, 2H, $H_{f,h}$), 7.44 – 7.36 (m, 1H), 6.02 (s, 2H, H_k), 2.57 (s, 6H, H_j), 1.56 (s, 6H, H_l).

^{13}C NMR (151 MHz, $CDCl_3$) δ: 157.26, 149.20, 142.79, 141.73, 138.52, 137.85, 132.51, 131.79, 129.87, 129.20, 128.97, 127.67, 126.10, 121.94, 121.61, 120.57, 119.94, 117.53, 112.43, 14.90, 14.65.

HRMS (ESI +ve) m/z: 557.2177, ([M+Na]+, $C_{29}H_{25}BF_2N_8Na$ requires 557.2156).

2.Fc-XB



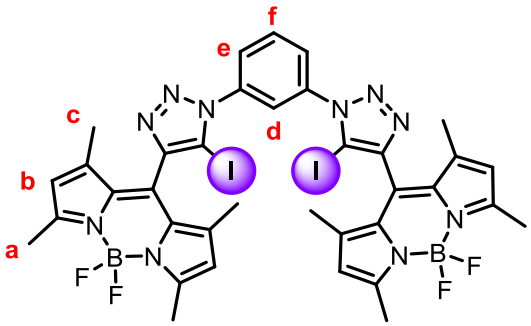
2.Fc-XB was prepared from **2.4** and **2.5** according to General Synthetic Procedure 2.2, affording **BDP-Fc•XB** in 81% yield.

^{1}H NMR (600 MHz, $CDCl_3$) δ: 7.91 (t, J = 2.0 Hz, 1H, H_d), 7.89 – 7.80 (m, 3H, $H_{e,f,g}$), 6.05 (s, 2H, H_i), 5.09 (t, J = 1.9 Hz, 2H, H_c), 4.41 (t, J = 1.9 Hz, 2H, H_b), 4.20 (s, 5H, H_a), 2.59 (s, 6H, H_h), 1.54 (s, 6H, H_j).

^{13}C NMR (151 MHz, $CDCl_3$) δ: 157.89, 151.58, 147.44, 142.58, 138.19, 137.51, 132.59, 130.91, 128.48, 127.45, 127.30, 124.15, 122.20, 82.84, 75.39, 74.44, 69.98, 69.52, 67.83, 15.20, 14.27.

HRMS (ESI +ve) m/z: 894.9925, ([M+H]+, $C_{33}H_{28}BF_2FeI_2N_8$ requires 894.9931).

2.BDP-XB



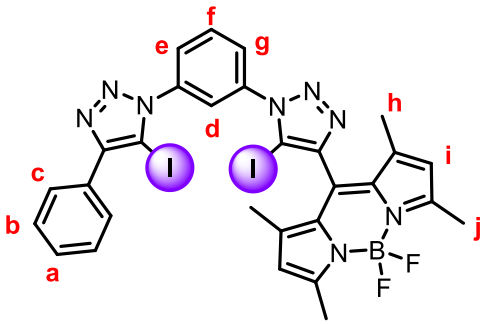
2.BDP-XB was prepared from **2.4** and **2.3** according to General Synthetic Procedure 2.2, affording **2.BDP-XB** in 74% yield.

^{1}H NMR (400 MHz, $CDCl_3$) δ: 8.00 – 7.91 (m, 1H, H_d), 7.88 (m, 3H, $H_{e,f}$), 6.06 (s, 4H, H_b), 2.59 (s, 12H, H_c), 1.58 (s, 12H, H_a).

^{13}C NMR (151 MHz, $CDCl_3$) δ: 157.79, 147.44, 142.28, 137.58, 132.35, 131.00, 127.63, 126.88, 123.24, 122.04, 82.53, 15.00, 14.08.

HRMS (ESI +ve) m/z: 957.1100, ([M+H]+, $C_{36}H_{33}B_2F_4I_2N_{10}$ requires 957.1107).

2.Ph-XB



2.Ph-XB was prepared from **2.4** and **2.6** according to General Synthetic Procedure 2.2, affording **2.Ph-XB** in 93% yield.

^{1}H NMR (400 MHz, $CDCl_3$) δ: 8.04 – 7.93 (d, 2H, H_c), 7.93 – 7.80 (m, 4H, $H_{d,e,f,g}$), 7.57 – 7.42 (m, 3H, $H_{a,b}$), 6.05 (s, 2H, H_i), 2.59 (s, 6H, H_h), 1.57 (s, 6H, H_j).

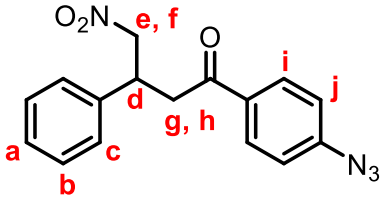
^{13}C NMR (151 MHz, $CDCl_3$) δ: 157.69, 151.27, 147.23, 142.37, 138.06, 137.34, 132.37, 130.80, 129.78, 129.24, 128.87, 128.48, 127.96, 127.48, 127.06, 124.18, 122.01, 82.65, 77.57, 14.99, 14.04.

HRMS (ESI +ve) m/z: 787.0272, ([M+H]+, $C_{29}H_{24}BF_2I_2N_8$ requires 787.0273).

6.3 Experimental Details for Chapter Three

6.3.1 Synthesis and Characterisation of Novel Compounds

Compound 3.3



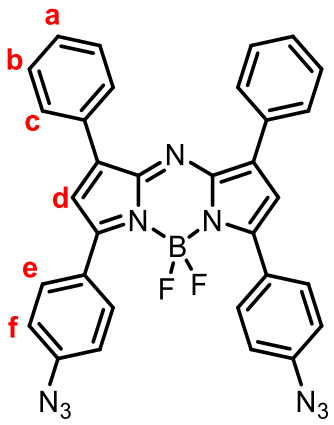
Compound **3.2**[12] (1.29 g, 5.18 mmol), $MeNO_2$ (1.4 mL, 26 mmol) and TEA (1 mL) were dissolved in EtOH (5 mL) and the mixture stirred at reflux overnight. The reaction mixture was allowed to cool, and then was acidified with HCl (2 M) and diluted with distilled H_2O (10 mL). The aqueous mixture was extracted with EtOAc (3 × 15 mL) and the combined organic layers were dried over $MgSO_4$ and filtered. The solvent was removed *in vacuo* to give the crude product, which was purified by flash column chromatography (Hexane : EtOAc 85:15 (*v/v*)). Compound **3.3** was isolated as thick yellow oil (1.14 g, 71%).

^{1}H NMR (400 MHz, $CDCl_3$) δ: 7.96 – 7.88 (m, $2H_i$), 7.38 – 7.26 (m, $5H_{a,b,c}$), 7.09 – 7.05 (m, $2H_j$), 4.83 (dd, J = 12.5, 6.7 Hz, $1H_e$), 4.69 (dd, J = 12.5, 7.8 Hz, $1H_f$), 4.21 (m, $1H_d$), 3.50 – 3.34 (m, $2H_{g,h}$).

^{13}C NMR (101 MHz, $CDCl_3$) δ: 195.42, 145.59, 139.17, 133.15, 130.16, 129.26, 128.09, 127.59, 119.27, 79.69, 41.51, 39.48.

HRMS (ESI +ve) m/z: 333.0955, ($[M+Na]^+$, $C_{16}H_{14}O_3N_4Na$ requires 333.0958).

Compound 3.4



Compound **3.5** was prepared *via* a modified literature procedure.[13] Compound **3.3** (300 mg, 0.97 mmol) and NH_4OAc (2.61 g, 34 mmol) were suspended in *n*-BuOH (7 mL) and stirred at 120°C for 24 h. The solution was cooled to 0°C and diluted with hexane (7 mL). The solution was filtered, and the solid washed with water and minimum cold EtOH to yield the aza-DIPY intermediate **3.4** as a blue solid. Without further purification, the aza-DIPY intermediate **3.4** was dissolved in dry DCM (15 mL) and treated with triethylamine (0.52 mL, 3.7 mmol) and $BF_3{\cdot}OEt_2$ (0.64 mL, 5.18 mmol) and stirred under N_2 overnight. The reaction mixture was then diluted with DCM (50 mL) and washed with water (3 × 20 mL) and 1 M NaOH (20 mL). The organic layer was dried over $MgSO_4$, filtered and the solvent removed *in vacuo*. The crude product was purified by flash column chromatography (DCM : Hexane : Toluene 2:2:1 (*v*/*v*)) to yield compound **3.5** as a green solid (50 mg, 18% over two steps).

^{1}H NMR (400 MHz, $CDCl_3$) δ: 8.14 – 8.02 (m, $8H_{e,f}$), 7.47 (m, $6H_{a,b}$), 7.21 – 7.11 (m, $4H_c$), 7.05 (s, $2H_d$).

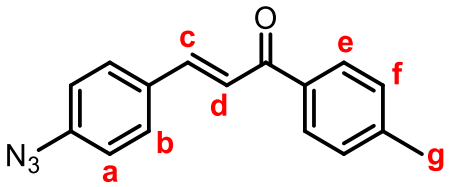
^{13}C NMR (151 MHz, $CDCl_3$) δ: 158.12, 145.85, 144.25, 142.96, 132.36, 131.54, 129.74, 129.52, 128.81, 128.26, 119.50, 118.99.

^{19}F NMR (377 MHz, $CDCl_3$) δ: -130.99 – -132.15 (m).

^{11}B NMR (128 MHz, $CDCl_3$) δ: 0.88 (t, J = 36.6 Hz).

HRMS (ESI +ve) m/z: 580.1972, ($[M+H]^+$, $C_{32}H_{21}N_9BF_2$ requires 580.1979).

Compound 3.7



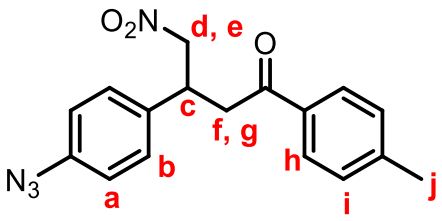
4-azidobenzaldehyde[14] (1.3 g, 8.84 mmol) and 4-methylacetophenone (1.16 mL, 8.84 mL) were dissolved in ethanol (10 mL) and cooled to 0°C. 2.5 mL of 50% (w/w) aqueous KOH was added and the mixture left to stir overnight in the dark. The solution was neutralized with HCl and diluted with H_2O (20 mL), then filtered. The solid was recrystallized from EtOH to yield compound **3.7** as a yellow solid (1.7 g, 73%).

^{1}H NMR (400 MHz, $CDCl_3$) δ: 7.97 – 7.90 (m, $2H_e$), 7.77 (d, J = 15.7 Hz, $1H_c$), 7.68 – 7.60 (m, $2H_b$), 7.49 (d, J = 15.7 Hz, $1H_d$), 7.34 – 7.28 (m, $2H_f$), 7.11 – 7.03 (m, $2H_a$), 2.44 (s, $3H_g$).

^{13}C NMR (101 MHz, $CDCl_3$) δ: 189.81, 143.72, 143.19, 142.07, 135.62, 131.86, 129.98, 129.37, 128.64, 121.59, 119.55, 21.70.

HRMS (ESI +ve) m/z: 264.1132, ($[M+H]^+$, $C_{16}H_{14}ON_3$ requires 264.1131).

Compound 3.8



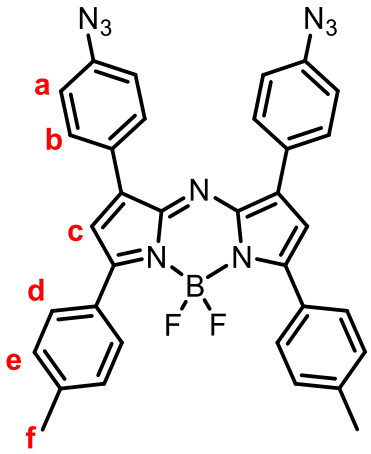
Compound **3.7** (1.7 g, 6.46 mmol), triethylamine (4.5 mL, 32.31 mmol) and nitromethane (1.75 mL, 32.31 mmol) were dissolved in EtOH (75 mL) and heated at reflux overnight. The solution was allowed to cool, and the solvent removed *in vacuo*. The residue was dissolved in DCM (50 mL) and washed with 1 M HCl (20 mL) and brine (2 × 20 mL). The organic layer was dried over $MgSO_4$ and filtered, and the solvent was removed *in vacuo*. The crude mixture was purified by flash column chromatography (Hexane : EtOAc 85:15 (*v/v*)) to yield compound **3.8** as a thick orange oil (1.3 g, 62%).

^{1}H NMR (400 MHz, $CDCl_3$) δ: 7.88 – 7.75 (m, $2H_h$), 7.29 – 7.22 (obscured by residual solvent peak) (m, $4H_{a,b}$), 7.01 – 6.95 (m, $2H_i$), 4.81 (dd, J = 12.5, 6.4 Hz, $1H_d$), 4.65 (dd, J = 12.5, 8.2 Hz, $1H_e$), 4.20 (m, $1H_c$), 3.48 – 3.32 (m, $2H_{f,g}$), 2.41 (s, $3H_j$).

^{13}C NMR (101 MHz, $CDCl_3$) δ: 196.35, 144.79, 139.78, 135.95, 133.98, 129.61, 129.09, 128.28, 119.78, 79.70, 41.41, 38.97, 21.83.

HRMS (ESI +ve) m/z: 347.1114, ($[M+Na]^+$, $C_{17}H_{16}O_3N_4Na$ requires 347.1115).

Compound 3.10



Compound **3.8** (750 mg, 2.31 mmol) was dissolved in *n*-BuOH (18 mL) and NH_4OAc (4.45 g, 58 mmol) was added. The suspension was heated at reflux for 24 h and then allowed to cool. The solution was diluted with hexane (5 mL), cooled to 0°C and filtered. The solid was washed with water and minimum cold ethanol to yield the aza-DIPY intermediate **3.9** as a blue solid. Without further purification, the aza-DIPY intermediate **3.9** was dissolved in dry DCM (25 mL) and treated with triethylamine (0.77 mL, 5.5 mmol) and $BF_3{\cdot}OEt_2$ (0.95 mL, 7.7 mmol) and stirred under N_2 overnight. The solvent was then removed *in vacuo* and the residue washed with copious H_2O to remove excess $BF_3{\cdot}OEt_2$. The solid was then dissolved in DCM (50 mL) and washed with 1 M NaOH (3 × 20 mL) and H_2O (20 mL). The organic layer was dried over $MgSO_4$, filtered and the solvent removed *in vacuo*. The crude product was purified by flash column chromatography (Hexane : DCM 3:2 (*v/v*)) to yield compound **3.10** as a red-blue solid (336 mg, 48% over two steps).

^{1}H NMR (400 MHz, $CDCl_3$) δ: 8.05 (d, J = 8.5 Hz, $4H_d$), 7.96 (d, J = 8.0 Hz, $4H_b$), 7.30 (d, J = 8.0 Hz, $4H_a$), 7.12 (d, J = 8.5 Hz, $4H_e$), 6.99 (s, $2H_c$), 2.43 (s, $6H_f$).

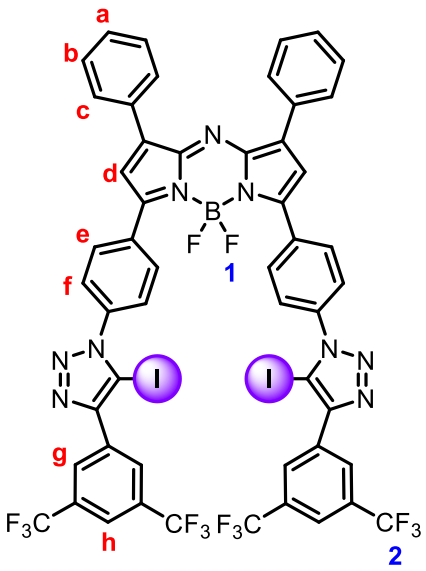
^{13}C NMR (151 MHz, $CDCl_3$) δ: 159.81, 145.65, 142.81, 141.79, 141.32, 132.37, 130.85, 129.77, 129.60, 129.45, 129.80, 119.46, 21.81.

^{19}F NMR (377 MHz, $CDCl_3$) δ: -131.36 – -131.61 (m).

^{11}B NMR (128 MHz, $CDCl_3$) δ: 0.95 (t, J = 38.0 Hz).

HRMS (ESI +ve) m/z: 608.2288, ($[M+H]^+$, $C_{34}H_{25}N_9BF_2$ requires 608.2293).

Sensor 3.14



Compound **3.5** (45 mg, 0.07 mmol), 1-(iodoethynyl)-3,5-bis(trifluoromethyl)benzene[15] **(3.13)** (71 mg, 0.173 mmol), $[Cu(CH_3CN)_4]PF_6$ (7 mg, 0.014 mmol) and TBTA (9 mg, 0.014 mmol) were added to a microwave vial, which was flushed with N_2 for 10 minutes. Dry DCM (min) was added, and the mixture stirred at room temperature until TLC indicated consumption of the azide starting material. The reaction mixture was diluted with DCM (20 mL) and washed with 0.1 M EDTA dissolved in aqueous 1 M NH_4OH (10 mL) followed by water (10 ml). The organic phase was dried over $MgSO_4$, filtered, concentrated *in vacuo* and purified by flash column chromatography (DCM : Hexane 1:1 (*v/v*) to DCM) followed

by preparative TLC (DCM : Hexane : Acetone 59:39:2 (*v/v*)) to yield sensor **3.14** as a blue solid (37 mg, 41%).

^{1}H NMR (400 MHz, $CDCl_3$) δ: 8.56 (s, $4H_g$), 8.32 (d, J = 8.2 Hz, $4H_f$), 8.11 (d, J = 6.6 Hz, $4H_c$), 7.96 (s, $2H_h$), 7.77 (d, J = 8.2 Hz, $4H_e$), 7.51 (m, $6H_{a,b}$), 7.17 (s, $2H_d$).

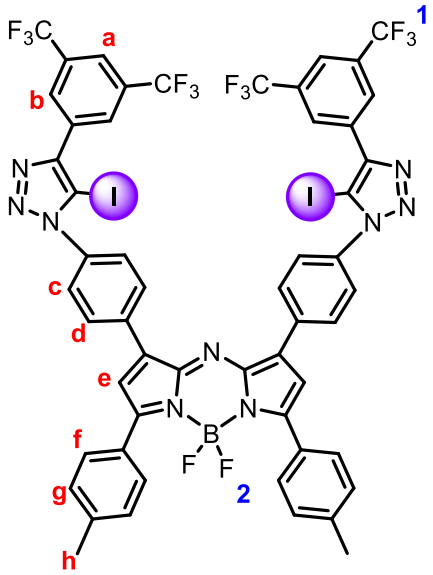
^{19}F NMR (377 MHz, $CDCl_3$) δ: -62.92(s, $12F_2$), -130.68 (m, $2F_1$).

^{11}B NMR (128 MHz, $CDCl_3$) δ: 0.98 (t, J = 39.1 Hz).

Extremely low solubility prevented characterization by ^{13}C NMR.

HRMS (ESI -ve) m/z: 1307.0226, ($[M-H]^-$, $C_{52}H_{26}N_9BF_{14}I_2$ requires 1307.0284).

Sensor 3.15



Compound **3.10** (45 mg, 0.07 mmol), 1-(iodoethynyl)-3,5-bis(trifluoromethyl)benzene[15] (**3.13**) (71 mg, 0.173 mmol), $Cu(CH_3CN)_4PF_6$ (7 mg, 0.014 mmol) and TBTA (9 mg, 0.014 mmol) were added to a microwave vial, which was flushed with N_2 for 10 minutes. Dry

DCM (min) was added, and the mixture stirred at room temperature until TLC indicated consumption of the azide starting material. The reaction mixture was diluted with DCM (20 mL) and washed with 0.1 M EDTA dissolved in aqueous 1 M NH_4OH (10 mL) followed by water (10 ml). The organic phase was dried over $MgSO_4$, filtered, concentrated *in vacuo* and purified by flash column chromatography (Toluene : EtOAc 199:1 (*v/v*)) to yield sensor **3.15** as a green solid (52 mg, 56%).

^{1}H NMR (400 MHz, $CDCl_3$) δ: 8.58 (s, $4H_b$), 8.22 (d, J = 8.1 Hz, $4H_f$), 8.03 (d, J = 8.0 Hz, $4H_d$), 7.96 (s, $2H_a$), 7.73 (d, J = 8.0 Hz, $4H_c$), 7.35 (d, J = 8.1 Hz, $4H_g$), 7.17 (s, $2H_e$), 2.46 (s, $6H_h$).

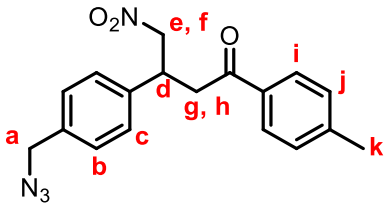
^{19}F NMR (377 MHz, $CDCl_3$) δ: -63.02 (s, $12F_1$), -132.04 (m, $2F_2$).

^{11}B NMR (128 MHz, $CDCl_3$) δ: 1.08 (t, J = 36.0 Hz).

Extremely low solubility prevented characterization by ^{13}C NMR.

HRMS (ESI -ve) m/z: 1335.0542, ($[M-H]^-$, $C_{54}H_{30}N_9BF_{14}I_2$ requires 1335.0597).

Compound 3.20



Compound **3.18** (2.10 g, 6.7 mmol) was dissolved in DCM (25 mL) and cooled to 0°C. $SOCl_2$ (1.46 mL, 20.1 mmol) was added to the stirred solution dropwise and the mixture allowed to stir under N_2. After 1 h, the mixture was diluted with DCM (40 mL) and washed with water (3 × 20 mL). The organic layer was dried over $MgSO_4$ and filtered. The solvent was removed *in vacuo* to yield the crude product containing **3.19** as an inseparable mixture.

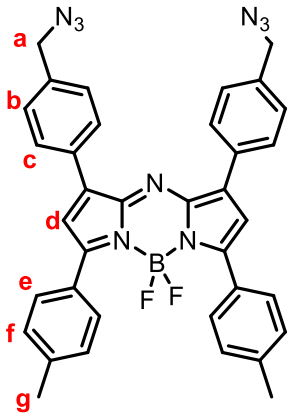
This crude material was redissolved in DMF (8 mL), to which NaN_3 (1.8 g, 33.5 mmol) and NaI (spatula tip) were added. The suspension was allowed to stir overnight. The mixture was diluted with water (20 mL) and the aqueous layer extracted with EtOAc (3 × 30 mL). The combined organic fractions were washed with brine (3 × 20 mL), dried over $MgSO_4$ and filtered. The solvent was removed *in vacuo* and the crude product was purified by flash column chromatography (Hexane : DCM : EtOAc 50:47:3 (*v/v*)) to give compound **3.20** as a thick yellow oil (0.87 g, 38% over two steps).

^{1}H NMR (400 MHz, $CDCl_3$) δ: 7.87 – 7.78 (m, $2H_j$), 7.35 – 7.22 (m, $6H_{b,c,i}$), 4.84 (dd, J = 12.6, 6.4 Hz, $1H_e$), 4.68 (dd, J = 12.6, 8.2 Hz, $1H_f$), 4.32 (s, $2H_a$), 4.24 (m, $1H_d$), 3.50 – 3.32 (m, $2H_{g,h}$), 2.41 (s, $3H_k$).

^{13}C NMR (151 MHz, $CDCl_3$) δ: 196.42, 144.73, 139.51, 135.28, 134.01, 129.58, 128.95, 128.29, 128.12, 79.58, 54.48, 41.44, 39.19, 21.81.

HRMS (ESI +ve) m/z: 312.1268, ($[M+Na]^+$, $C_{18}H_{18}N_4O_3Na$ requires 361.1271)

Compound 3.22



Compound **3.20** (150 mg, 0.44 mmol) was dissolved in *n*-BuOH (4.1 mL) and NH_4OAc (850 mg, 11 mmol) was added. The suspension was heated at reflux for 24 h and then allowed

to cool. The solution was diluted with hexane (5 mL) and filtered. The solid was washed with water and minimum cold ethanol to yield the aza-DIPY intermediate **3.21** as a blue solid. Without further purification, the aza-DIPY intermediate **3.21** was dissolved in dry DCM (3 mL) and treated with triethylamine (0.1 mL, 0.55 mmol) and $BF_3{\cdot}OEt_2$ (0.1 mL, 0.77 mmol) and stirred under N_2 overnight. The reaction mixture was then diluted with DCM (20 mL) and washed with water (3 × 10 mL) and 1M NaOH (10 mL). The organic layer was dried over $MgSO_4$, filtered and the solvent removed *in vacuo*. The crude product was purified by flash column chromatography (Hexane : DCM 3:2 (*v/v*)) to yield the aza-BODIPY azide as a green solid (40 mg, 14% over two steps).

^{1}H NMR (400 MHz, $CDCl_3$) δ: 8.10 – 8.03 (m, $4H_e$), 7.97 (d, J = 8.0 Hz, $4H_c$), 7.45 – 7.39 (m, $4H_b$), 7.30 (d, J = 8.0 Hz, $4H_f$), 7.05 (s, 2H), 4.43 (s, $4H_a$), 2.43 (s, $6H_g$).

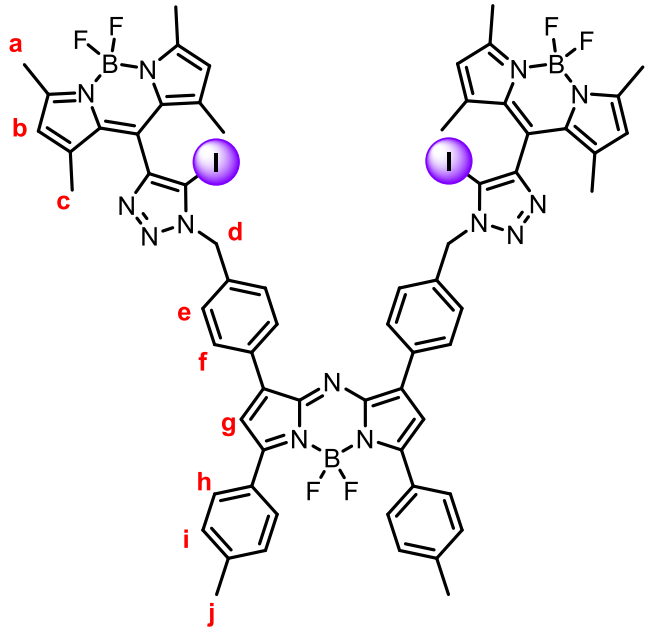
^{13}C NMR (151 MHz, $CDCl_3$) δ: 159.45, 145.53, 143.04, 141.74, 136.61, 132.42, 129.71, 129.68, 129.50, 128.73, 128.39, 119.12, 54.54, 21.67.

^{19}F NMR (377 MHz, $CDCl_3$) δ: -127.69 – -138.69 (m).

^{11}B NMR (128 MHz, $CDCl_3$) δ: 0.93 (t, J = 44.0 Hz).

HRMS (ESI +ve) m/z: 636.2597, ($[M+H]^+$, $C_{36}H_{29}BF_2N_9$ requires 636.2606)

Sensor 3.23



Compound **3.22** (20 mg, 0.03 mmol), iodoalkyne **2.3** (31 mg, 0.08 mmol), $Cu(CH_3CN)_4PF_6$ (3 mg, 0.01 mmol) and TBTA (5 mg, 0.01 mmol) were added to a microwave vial, which was flushed with N_2 for 10 minutes. Dry DCM (min) was added, and the mixture stirred at room temperature until TLC indicated consumption of the azide starting material. The reaction mixture was diluted with DCM (20 mL) and washed with 0.1 M EDTA dissolved in aqueous 1 M NH_4OH (10 mL) followed by water (10 ml). The organic phase was dried over $MgSO_4$, filtered, concentrated *in vacuo* and purified by repeated preparative thin layer chromatography (Toluene : $CHCl_3$: EtOAc 50:50:3 (*v/v*)) to yield sensor **3.22** as a red solid (3 mg, 7%).

^{1}H NMR (500 MHz, $CDCl_3$) δ: 8.00 (d, J = 8.2 Hz, $2H_e$), 7.98 – 7.95 (d, J=8.0 Hz, $2H_f$), 7.48 (d, J = 8.2 Hz, $2H_f$), 7.31 (d, J = 8.0 Hz, $2H_i$), 7.05 (s, $2H_g$), 5.95 (s, $4H_b$), 5.70 (s, $4H_d$), 2.54 (s, $6H_j$), 2.43 (s, $6H_c$), 1.25 (s, $6H_a$).

^{19}F NMR (377 MHz, $CDCl_3$) δ: -131.71 – -132.01 (m), -145.69 – -146.73 (m).

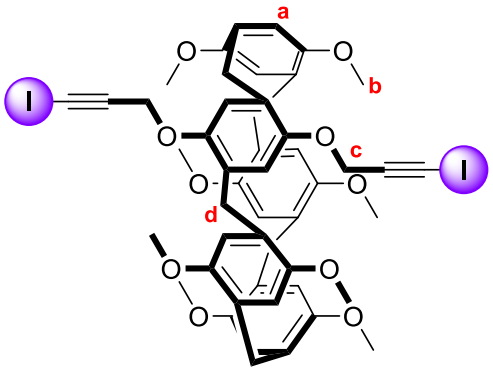
Extremely low solubility prevented characterization by ^{13}C NMR.

HRMS (ESI +ve) m/z: 1432.3104, ($[M+H]^+$, $C_{66}H_{57}B_3F_6I_2N_{13}$ requires 1432.3127)

6.4 Experimental Details for Chapter Four

6.4.1 Synthesis and Characterisation of Novel Compounds

Compound 4.1-XB



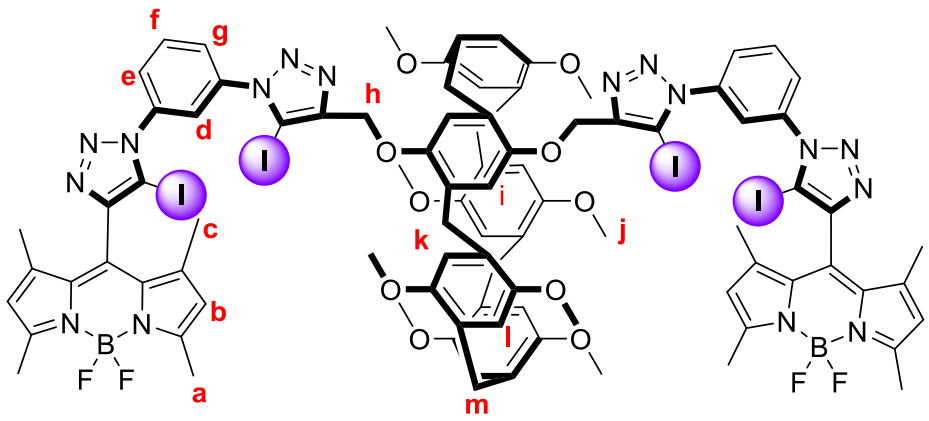
4.1-HB (170.0 mg, 0.313 mmol) and catalytic CuI (5.9 mg, 0.031 mmol) were dissolved in dry THF (2 mL). *N*-iodomorpholine hydriodide (420 mg, 1.235 mmol) was added, and the mixture stirred at room temperature, under exclusion of light, for 3 h, after which only one spot was visible by TLC. The reaction mixture was diluted with DCM (50 mL), and poured onto a saturated DCM pad of neutral alumina. The pad was eluted with DCM until the solution ran clear and the organic layer decolourised with saturated $Na_2S_2O_3$ (aq.) (25 mL), and washed with H_2O (3 × 100 mL). The organic layer was dried over $MgSO_4$ and the volatiles removed *in vacuo*. The crude product was dry-loaded onto SiO_2 and eluted with hexane : EtOAc 9:1 (*v/v*) to afford **4.1-XB** as an off-white solid. The product was estimated by ^1H NMR to be 66% pure, with the contaminant identified as non-functionalised *per*-methoxypillar[5]arene, residual from the synthesis of **4.1-XB**. As the side product would not react in the subsequent step, **4.1-XB** was used without further purification. Yield: 329.1 mg (66%).

^{1}H NMR (400 MHz, $CDCl_3$) *δ*: 6.89 6.88 6.85 6.80 6.76 (5 s, 2H each, H_a), 4.79 (s, 4 H, H_c), 3.72 (m, 10H, H_d), 3.69-3.61 (m, 24H, H_b).

^{13}C NMR (151 MHz, $CDCl_3$) *δ*: 150.6, 150.4, 150.3, 148.7, 129.4, 128.7, 128.0, 127.7, 127.6, 116.2, 114.3, 113.8, 113.7, 113.4, 89.5, 57.7, 55.8, 55.7, 55.6, 55.5, 29.8, 29.7, 29.6, 29.0. Iodoalkyne environment is not observed, due to it likely being coincident with the $CDCl_3$ solvent resonance.

HRMS: m/z calculated for $[C_{49}H_{48}I_2O_{10}Na]^+$, $[M+Na]^+$: 1073.1229, found: 1073.1272.

Sensor 4.2-XB



$[Cu(MeCN)_4]PF_6$ (5.6 mg, 0.015 mmol) and TBTA (8.0 mg, 0.015 mmol) were placed in a 5 mL microwave vial and degassed for 10 minutes. The solids were dissolved in the minimum amount of degassed dry DCM (3 mL) and stirred at room temperature for 15 min. XB BODIPY synthon **2.4** (40 mg, 0.072 mmol) and P5A bis-alkyne **4.1-XB** (18.9 mg, 0.018 mmol) were dissolved in the minimum amount of degassed dry DCM (2 mL) and the resulting solution added to the pre-complexed Cu^{I}/TBTA solution. The resulting solution was stirred at room temperature, under exclusion of light, for 12 h, after which the reaction mixture was diluted with DCM (15 mL) and washed with NH_4OH/EDTA (aq.) (2 ×

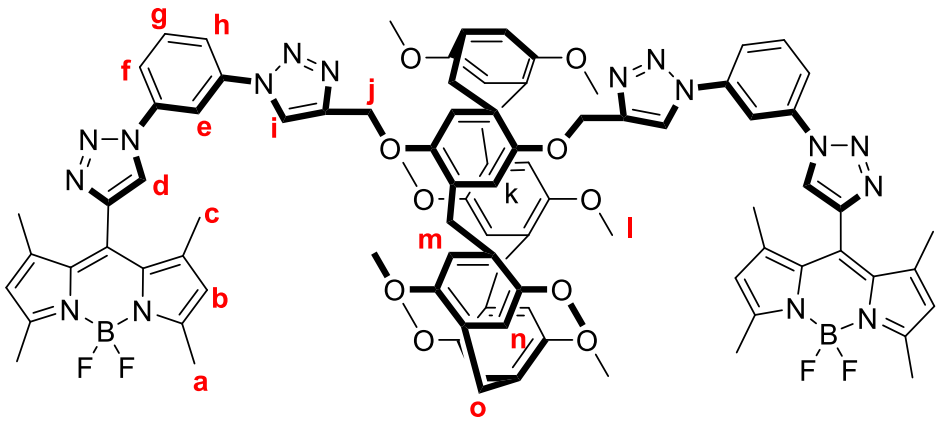
20 mL) and H_2O (20 mL). All aqueous layers were back-extracted with DCM (10 mL) and the combined organic layers were dried over $MgSO_4$ and the volatiles removed *in vacuo*. **4.2-XB** was obtained by column chromatography of the resulting crude solid in DCM : acetone mixtures graded from 100:0 to 97:3 (*v/v*), as a purple solid. Yield 28.0 mg (72%).

^{1}H NMR (400 MHz, Acetone-d_6) δ: 8.17 (broad s, 2H, H_f), 8.08 (app. s, 6H, $H_{d,e,g}$), 7.23 (s, 2H, H_i), 6.91-6.86 (m, 8H, H_l), 6.23 (s, 4H, H_b), 5.16 (app. q, 4H, H_h), 3.81-3.64 (m, 34H, $H_{j,k,m}$), 2.55 (s, 12H, H_c), 1.64 (s, 12H, H_a).

^{13}C NMR (151 MHz, Acetone-d_6) δ: 157.2, 150.5, 150.5, 150.4, 150.4, 150.0, 148.8, 146.4, 142.7, 138.1, 137.5, 132.1, 131.1, 129.4, 128.4, 128.3, 128.2, 128.2, 128.1, 128.0, 127.8, 124.3, 121.8, 121.8, 115.9, 113.7, 113.5, 113.4, 85.2, 83.5, 62.7, 55.3, 55.1, 55.1, 55.0, 13.9, 13.2 ppm.

HRMS: m/z calculated for $[C_{91}H_{85}B_2F_4I_4N_{16}O_{10}]^+$, $[M+H]^+$: 2167.2930, found: 2167.2886.

Sensor 4.2-HB



$[Cu(MeCN)_4]PF_6$ (5.0 mg, 0.013 mmol) and TBTA (7.1 mg, 0.013 mmol) were placed in a 5 mL microwave vial and degassed for 10 minutes. The solids were dissolved in the

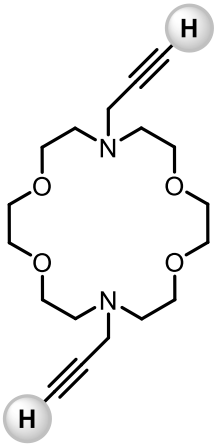
minimum amount of degassed dry DCM (3 mL) and stirred at room temperature for 15 min. HB BODIPY synthon **2.8** (25.0 mg, 0.058 mmol) and P5A bis-alkyne **4.1-HB** (12.0 mg, 0.015 mmol) were dissolved in the minimum amount of degassed dry DCM (2 mL) and the resulting solution added to the pre-complexed Cu^{I}/TBTA solution. The resulting solution was stirred at room temperature for 12 h, after which the reaction mixture was diluted with DCM (15 mL) and washed with NH_4OH/EDTA (aq.) (2 × 20 mL) and H_2O (20 mL). All aqueous layers were back-extracted with DCM (10 mL) and the combined organic layers were dried over $MgSO_4$ and the volatiles removed *in vacuo*. **4.2-HB** was obtained by column chromatography of the resulting crude solid in DCM : acetone mixtures graded from 100:0 to 97:3 (*v/v*), as a purple solid. Yield 24.2 mg (46%).

^{1}H NMR (400 MHz, Acetone-d_6) δ: 9.08 8.96 (2s, 2H each, $H_{d,i}$), 8.64 (t, J = 2.1 Hz, 2H, H_e), 8.17 (m, 4H, $H_{f,h}$), 7.94 (t, J = 8.2 Hz, H_g), 7.13 (s, 2H, H_k), 6.87-6.84 (m, 8H, H_n), 6.18 (broad s, 4H, H_b), 5.20 (m, 4H, H_j), 3.76-3.59 (m, 34H, $H_{l,o}$), 2.53 (s, 12H, H_c),1.62 (s, 12H, H_a).

^{13}C NMR (151 MHz, Acetone-d_6) δ: 156.6, 150.5, 150.5, 150.5,149.8,145.7, 143.1, 140.6, 138.4, 138.1, 132.2, 131.7, 129.2, 128.9, 128.8, 128.2, 128.2, 128.1, 128.1, 128.1, 128.0, 127.9, 127.7, 123.4, 122.0, 120.1, 115.1, 113.7, 113.5, 113.4, 112.2, 75.4, 62.2, 55.1, 55.1, 55.1, 55.0, 13.6, 12.9.

HRMS: m/z calculated for $[C_{91}H_{89}B_2F_4N_{16}O_{10}]^+$, $[M+H]^+$: 1663.7064, found: 1663.7053.

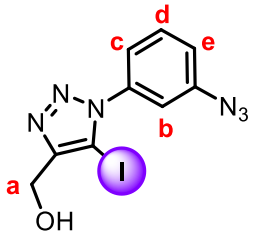
Compound 4.3-HB



Diaza-18-crown-6 (Kryptofix® 22) (500 mg, 1.9 mmol) was dissolved in 20 mL DCM : MeOH 1:1 (*v/v*). Propargyl bromide (80 wt % in toluene) (0.5 mL, 5.1 mmol, 2.5 eq) and K_2CO_3 (1.3 g, 5 eq) were added and the mixture was left to stir overnight at room temperature. The mixture was filtered and the solvent removed *in vacuo*. The residue was redissolved in DCM (20 mL) and washed with H_2O (3 × 10 mL). The crude was purified by alumina column chromatography (DCM:MeOH 99:1) to give compound **4.3-HB** as a colourless wax in 76% yield.

^{1}H and ^{13}C NMR characterisation were consistent with previous reports.[16-17]

XB Synthon 4.4

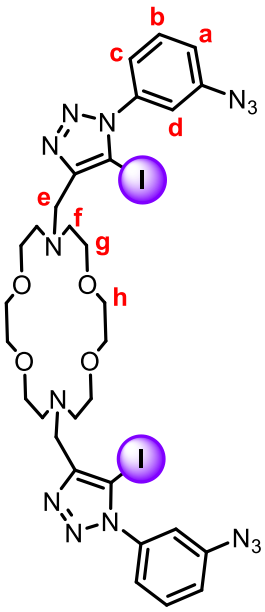


$[Cu(MeCN)_4]PF_6$ (16.0 mg, 0.042 mmol) and TBTA (22.0 mg, 0.042 mmol) were placed in a 5 mL microwave vial and degassed for 10 minutes. The solids were dissolved in the

minimum amount of degassed dry DCM (4 mL) and stirred at room temperature for 15 min. Azide synthon **2.1** (120.0 mg, 0.75 mmol) and 3-iodo-2-propyn-1-ol[18] (45.0 mg, 0.25 mmol) were dissolved in the minimum amount of degassed dry DCM (8 mL) and the resulting solution added to the pre-complexed Cu^{I}/TBTA solution. The resulting solution was stirred at room temperature for 12 h, after which the reaction mixture was diluted with DCM (30 mL) and washed with NH_4OH/EDTA (aq.) (2 × 30 mL) and H_2O (30 mL). All aqueous layers were back-extracted with DCM (20 mL) and the combined organic layers were dried over $MgSO_4$ and the volatiles removed *in vacuo*. **4.4** was obtained by column chromatography of the resulting crude solid in DCM : EtOAc mixtures graded from 100:0 to 90:10 (*v/v*), as a white solid. Yield 78 mg (91%).

^{1}H NMR (400 MHz, $CDCl_3$) δ: 7.60 – 7.51 (t, J = 7.9 Hz, $1H_d$), 7.32 (ddd, J = 7.9, 1.9, 1.0 Hz, $1H_c$), 7.25 – 7.19 (m, $2H_{b,e}$), 4.83 (s, $2H_a$).

Compound 4.6



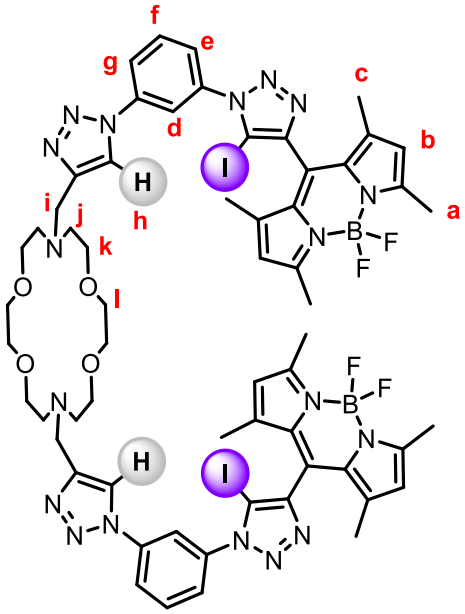
Compound **4.4** (48 mg, 0.14 mmol) was dissolved in DCM (15 mL) and cooled to 0° C in an ice bath. Methanesulfonyl chloride (40 µL, 0.21 mmol) was added slowly and the reaction mixture stirred at 0° C for 30 minutes. An aqueous solution of saturated sodium bicarbonate was added. The organic layer was washed with H_2O (2 × 30 mL). The combined organic layers were dried over $MgSO_4$ and the volatiles removed *in vacuo* to give the intermediate **4.5** as a crude mixture. This crude mixture containing intermediate **4.5** was dissolved in DMF (10 mL), to which K_2CO_3 (23 mg, 0.17 mmol) and diaza-18-crown-6 (Kryptofix® 22) (16 mg, 0.06 mmol) was added. The solution was heated to 50° C and stirred overnight. The solution was cooled, diluted with H_2O (20 mL) and extracted with DCM (3 × 30 mL). The combined organic layers were washed with aqueous LiCl (5%) (20 mL) and water (2 × 20 mL). The organic layer was dried over $MgSO_4$ and the volatiles removed *in vacuo.* The resulting crude solid was purified by alumina column chromatography, using DCM : MeOH mixtures graded from 100:0 to 98:2 (*v/v*), to give **4.6** as a white solid (29 mg, 53%).

^{1}H NMR (600 MHz, $CDCl_3$) δ: 7.53 (m, $2H_b$), 7.32 (m, $2H_c$), 7.23 – 7.18 (m, $4H_{a,d}$), 3.90 (s, $4H_e$), 3.71 (t, J = 5.7 Hz, $8H_f$), 3.65 (s, $8H_h$), 2.95 (t, J = 5.7 Hz, $8H_g$).

^{13}C NMR (151 MHz, $CDCl_3$) δ: 149.50, 141.54, 138.18, 130.53, 122.36, 120.41, 116.91, 81.24, 70.71, 69.85, 53.52, 49.77.

HRMS m/z calculated for $[C_{30}H_{37}I_2N_{14}O_4]^+$, $[M+H]^+$: 911.1206, found: 911.1229.

Sensor 4.7



Compound **4.3-HB** (17 mg, 0.05 mmol) was dissolved in dry DCM (6 mL) and the XB synthon, **2.3**, (60 mg, 0.11 mmol, 2.1 eq), $[Cu(CH_3CN)_4]PF_6$ (4 mg, 0.01 mmol, 0.2 eq) and TBTA (6 mg, 0.01 mmol, 0.2 eq) were added. The mixture was left to stir under N_2 overnight at room temperature in the dark. The reaction mixture was diluted with DCM (15 mL) and washed with NH_4OH/EDTA (aq.) (2 × 20 mL) and H_2O (20 mL). The combined organic layers were dried over $MgSO_4$ and the volatiles removed *in vacuo*. The crude residue was purified by alumina column chromatography (DCM : MeOH 98:2 (*v*/*v*)). Following purification by

chromatography, the solvent was removed *in vacuo* and the solid redissolved in DCM (20 mL), which was washed with water (3 × 10 mL) to remove any residual salts from the alumina. The product, **4.7**, was obtained as a pink solid in 41% yield.

^{1}H NMR: (500 MHz, Acetone-d_6) δ: 8.68 (s, $2H_h$), 8.30 (s, $2H_d$), 8.23 (d, J = 8.1 Hz, $2H_e$), 7.91 (t, J = 8.1 Hz, $2H_f$), 7.79 (d, J = 8.0 Hz, $2H_g$), 6.21 (s, $4H_b$), 3.91 (s, $4H_i$), 3.63 (t, J = 5.6 Hz, $8H_j$), 3.60 (s, $8H_l$), 2.78 (t, J = 5.6 Hz, $8H_k$), 2.54 (s, $12H_c$), 1.62 (s, $12H_a$).

^{13}C NMR: (126 MHz, Acetone-d_6) δ: 158.19, 147.26, 143.71, 139.26, 138.81, 133.10, 132.23, 129.44, 126.87, 122.77, 122.63, 118.67, 71.41, 70.74, 55.15, 51.13, 14.91, 14.25. (3 aromatic peaks are coincident).

HRMS: m/z calculated for $[C_{60}H_{66}B_2F_4I_2N_{18}O_4Na]^+$, $[M+Na]^+$: 1477.3624, found: 1477.3620.

6.5 References for Chapter Six

1. *Bindfit v0.5*, http://app.supramolecular.org/bindfit/. (accessed periodically and repeatedly).
2. Origin Corporation, *OriginPro*, **2023**.
3. C. Würth, M. Grabolle, J. Pauli, M. Spieles, U. Resch-Genger, *Nat. Protoc.* **2013**, *8*, 1535-1550.
4. R. Hein, X. Li, P. D. Beer, J. J. Davis, *Chem. Sci.* **2021**, *12*, 2433-2440.
5. S. C. Patrick, R. Hein, M. Sharafeldin, X. Li, P. D. Beer, J. J. Davis, *Chem. Eur. J.* **2021**, *27*, 17700-17706.
6. J. Ding, K. Feng, C.-H. Tung, L.-Z. Wu, *J. Phys. Chem. C* **2011**, *115*, 833-839.
7. X. Wu, W. Wu, X. Cui, J. Zhao, M. Wu, *J. Mater. Chem. C* **2016**, *4*, 2843-2853.
8. Y. V. Zatsikha, T. S. Blesener, A. J. King, A. T. Healy, P. C. Goff, N. O. Didukh, D. A. Blank, Y. P. Kovtun, V. N. Nemykin, *J. Phys. Chem. B* **2020**, *125*, 360-371.
9. K. Vandewal, J. Benduhn, V. C. Nikolis, *Sustain. Energy Fuels* **2018**, *2*, 538-544.
10. R. Marcus, *J. Phys. Chem.* **1989**, *93*, 3078-3086.
11. M. Albrecht, A. Lippach, M. P. Exner, J. Jerbi, M. Springborg, N. Budisa, G. Wenz, *Org. Biomol. Chem.* **2015**, *13*, 6728-6736.
12. A. Zarghi, T. Zebardast, F. Hakimion, F. H. Shirazi, P. N. Praveen Rao, E. E. Knaus, *Biorg. Med. Chem.* **2006**, *14*, 7044-7050.
13. S. Kumar, K. G. Thorat, M. Ravikanth, *J. Org. Chem.* **2017**, *82*, 6568-6577.
14. A. Kafle, S. Yossef, S. T. Handy, *Tetrahedron Lett.* **2020**, *61*, 151899.
15. M. Kaasik, S. Kaabel, K. Kriis, I. Järving, R. Aav, K. Rissanen, T. Kanger, *Chem. Eur. J.* **2017**, *23*, 7337-7344.
16. K. A. Arnold, A. M. Viscariello, M. Kim, R. D. Gandour, F. R. Fronczek, G. W. Gokel, *Tetrahedron Lett.* **1988**, *29*, 3025-3028.
17. J. Hu, G. W. Gokel, *Chem. Commun.* **2003**, 2536.
18. E. Jahnke, J. Weiss, S. Neuhaus, T. N. Hoheisel, H. Frauenrath, *Chem. Eur. J.* **2009**, *15*, 388-404.